Katherine Aurand

Enhanced oil recovery using silica nanoparticles

An experimental evaluation of oil production, recovery mechanisms and nanofluid stability

Doctoral thesis

Katherine Aurand

NTNU
Norwegian University of Science and Technology
Thesis for the Degree of
Philosophiae Doctor
Faculty of Engineering
Department of Geoscience and Petroleum

NTNU
Norwegian University of
Science and Technology

NTNU
Norwegian University of
Science and Technology

NTNU

Katherine Aurand

Enhanced oil recovery using silica nanoparticles

An experimental evaluation of oil production, recovery mechanisms and nanofluid stability

Thesis for the Degree of Philosophiae Doctor

Trondheim, December 2017

Norwegian University of Science and Technology
Faculty of Engineering
Department of Geoscience and Petroleum

NTNU

Norwegian University of
Science and Technology

Abstract

Water flooding additives can increase oil production from existing reservoirs, helping to meet the world's growing energy demand. Hydrophilic silica nanoparticles are promising additives due to their large surface area and small size. Experimental methods are used to evaluate nanofluid stability, determine oil production via core flooding and investigate the enhanced oil recovery (EOR) mechanisms.

Nanofluids are created by dispersing nanoparticles in synthetic sea water (SSW). The nanofluids are injected through Berea sandstone cores filled with crude oil to determine how they react in a typical petroleum reservoir. Twenty-seven unique core flooding configurations are evaluated. Interfacial tension experiments, contact angle measurements and glass micromodel flooding tests are used to investigate the nanoparticles' EOR mechanisms.

Nanofluid stability is defined here as a nanofluid dispersion having a nanoparticle size distribution curve that maintains its original unimodal form and mean nanoparticle size from the initial measurement at time = 0. The six commercially available silica nanoparticles tested in this thesis are unstable in SSW but increased oil production by 2% to 12% of the original oil in place (OOIP). This finding prompted Evonik Industries, the nanoparticle supplier, to develop patent-pending nanoparticle surface treatments. The three most promising unmodified nanoparticles are modified by silanization. They are stable in SSW at 20°C but not at the reservoir temperature (60°C). Two further surface modifications are created for the nanoparticle with the largest surface area. This resulted in SSW stability at 60°C. However, the surface-modified nanoparticles do not produce significant amounts of oil (< 4% OOIP) during the first five pore volumes of nanofluid flooding.

The driving EOR mechanism from the unmodified nanoparticle flooding appears to be microscopic flow diversion because of nanoparticle agglomeration and retention. The silanized nanoparticles have delayed oil production, and the mechanism is likely in-situ generation of oil-in-water emulsions. Interfacial tension reduction is likely not a dominating EOR mechanism for any of the nanoparticles. Wettability alteration could be affecting some systems with aged cores, but not to the extent needed to produce significant oil. Over 95% of the unmodified nanoparticles are retained in the core plugs, but it appears that most of the surface-modified nanoparticles can propagate through the core plugs. Future research should focus on the nanoparticle surface chemistry and its effect on EOR mechanisms and hence oil production.

Preface

This thesis is submitted to the Norwegian University of Science and Technology (NTNU) for partial fulfilment of the requirements for the degree of philosophiae doctor.

The work presented in this thesis was conducted at the Department of Geoscience and Petroleum, NTNU, Trondheim. Dr. Sigve Hovda was the main supervisor. Dr. Jan Åge Stensen from SINTEF Petroleum was the co-supervisor.

The research was funded by NTNU, with additional financial support from Evonik Industries for hiring master students to assist with some of the core flooding tests presented in Parts 3 and 4. The micromodel experiments were conducted by the author at the Statoil Research Center – Rotvoll, Trondheim.

Acknowledgements

The elusive PhD. A rocky road riddled with dead-ends, often skimming the precipice of self-doubt. You do not always know which path you should take, let alone where you are headed. Laced with seemingly Sisyphean tasks, the only momentum forward is often fueled by caffeine and the fear of quitting after already making it so far. But just like Frodo had Sam, Sherlock had Watson, and Kuzco had Pacha, the lesson learned is that difficult quests have a better chance of success when you do not fly solo. I am therefore very thankful to have so many people support me along my journey.

Thank you to my advisor Dr. Sigve Hovda, NTNU, for jumping in to this topic. I am thankful that you helped me set boundaries with the lab work and focus on writing this past year. I would likely still be wandering in the lab if not for your encouragement. Thank you to Dr. Jan Åge Stensen, my co-advisor at SINTEF Petroleum, for your detailed editing and advice. I appreciate that you always made time to help me find answers to my many questions. A special thanks to Dr. Cathrine Ringstad, SINTEF Petroleum, for providing detailed feedback that had a significant impact on the final version of the thesis. You have been a great source of encouragement throughout this journey.

Thank you to Professor Ole Torsæter, NTNU, for laying the groundwork for this research and directing me into this field. I appreciate the financial support and the nanoparticle-EOR laboratory space. Thank you to Professor Jon Kleppe, NTNU, for introducing me to the opportunities at the department and for your support throughout the initial stages of the PhD.

A special thank you to Drs. Ulrich Fischer, Wolfgang Lortz, Cornel Venzago, and Maximilian Cornelius at Evonik Industries. Your ideas and advice have greatly enriched this research project. I appreciate the opportunity to test your novel nanoparticles and the financial support which allowed master students to become involved in this exciting research.

I appreciate the questions and critiques from many engineers at Statoil that helped direct the research. A special acknowledgement goes to Berit Robøle for facilitating discussions. Thank you to Espen Kowalewski for coordinating the micromodel experiments and Ann Lisbeth Bye for providing laboratory assistance at Statoil.

Core flooding experiments can sometimes feel cursed with misfortune. Whether it is a sudden leak in the tubing or a broken pump (or five), it is quickly demotivating to have only one unusable experiment to show for many hours of work. Thankfully, I had a wonderful team of master students to assist me in the lab. Their support is what kept me pushing forward.

Thank you to Gunnar Sie Dahle for helping me troubleshoot the experiments and lay the groundwork for this research. I sincerely appreciate your contributions to the Part 1 core flooding experiments and related nanofluid tests. Thank you to Helene Virkesdal Daae for your help with the Part 2 core flooding experiments and related nanofluid tests. It was wonderful

having you in the lab. A special thank you to Reidun Cecilie Aadland, for contributing to the Part 2 tests and continuing to work alongside me as a fellow PhD candidate thereafter. I am very thankful to have your friendship and companionship through this difficult journey.

Thank you to Marthe Bodahl Lunde, Hanne Gjerstad Folde, Bendik Helgestad, Victoria Flatås, Erik Norrud Pollen, Kolbjørn Stenvold, Jon Steinar Folstad and Tonje Løland Bjerga, the team of master students hired on for Parts 3 and 4 of the research project. I am grateful to have had your assistance and company in the lab. It would not have been as fun without you.

Thank you to the technical team that keeps the reservoir lab running: Roger Overå, Terje Bjerkan, Håkon Myhren, Steffen Wærnes Moen, Noralf Vedvik and Dr. Georg Voss. Thank you to Karoline Oen and Magnus Lunde for your assistance with and ideas for the lab component of the core analysis course that subsequently helped the research project.

Thank you to Dr. Narjes Jafariesfad for being the best officemate I could ask for. I will miss our many coffee breaks together where we shared ideas and advice for getting through the PhD. Also, thank you to the many other colleagues and fellow PhD candidates at the department for providing support and encouragement. I also appreciate the opportunity to be involved with the NTNU Forsker Grand Prix group to improve my scientific communication skills.

The PhD is just a small part of my life, and I sincerely appreciate the support of my friends and especially my family. Thank you to my parents-in-law and other Norwegian family for your continual support. Thank you to my loving parents and siblings. I would not have gotten this far without you.

And finally, a special thank you to Jacqueline Reyno for always taking my calls and providing sage wisdom. Our rock-solid friendship is what keeps me grounded.

Most importantly, *tusen hjertelig takk* to my wonderful husband Ivar Hellzén Melby for providing unfailing support and encouragement. You have helped me carry the burden of the PhD without protest, and I know you are just as glad as I am that this journey has finally come to an end.

The acknowledgements would not be complete without mentioning Finley, you furry fluff ball, for always greeting me with a wagging tail and a desire to frolic in the forest. You have ensured that I remain happy and healthy throughout this journey, snow or shine, thanks to your philosophy of *ut på tur, aldri sur.* I would be literally rolling out of here if not for you.

Table of Contents

List of figures

List of tables

Abbreviations and nomenclature

	Description	Units
A	Cross-sectional area of the core plug	cm^2
AERODISP®	Aqueous dispersions of hydrophilic fumed silica (AEROSIL®) produced by Evonik Industries	
AEROSIL®	Hydrophilic fumed silica produced by Evonik Industries	
°API	American Petroleum Institute gravity	
ASP	Alkaline surfactant polymer	
atm	atmospheres	
BET	Brunauer-Emmett-Teller theory	
Cnp	Colloidal nanoparticle	
Cnp_1	Colloidal nanoparticle with a surface area of 65 m^2/g	
Cnp_2	Colloidal nanoparticle with a surface area of 150 m^2/g	
Cnp_3	Colloidal nanoparticle with a surface area of 350 m^2/g	
cP	Centipoise	
Cryo-SEM	Cryogenic scanning electron microscope	
CT	Computed tomography	
D_{avg}	Average particle diameter (z-average from cumulants analysis)	nm
DLS	Dynamic light scattering	
DLVO	Derjaguin-Landau-Verwey-Overbeak theory	
dP	Differential pressure across the core plug (see also ΔP)	bar, atm
dP_{avg}	Average differential pressure	bar
dP_{max}	Maximum differential pressure	bar
E_D	Microscopic displacement efficiency	
EDL	Electrical double layer	
EOR	Enhanced oil recovery	
E_V	Macroscopic displacement efficiency	
HMDS	Hexamethyldisilazane	
I_{AH}	Amott-Harvey wettability index	
ICP-EOS	Inductively coupled plasma optical emission spectrometry	
IFT	Interfacial tension (see also σ)	mN/m
I_o	Wettablity index to oil	
I_w	Wettability index to water	
k	Permeability	mD

	Description	Units
k_{abs}	Absolute permeability	mD
k_e	Effective permeability	mD
k_{eo}	Effective permeability for the oil phase	mD
k_{ew}	Effective permeability for the water phase	mD
k_r	Relative permeability	
k_{ref}	Reference permeability	
k_{ro}	Relative permeability for the oil phase	
k_{rw}	Relative permeability for the water phase	
L	Length of the core plug	cm
M	Mobility ratio	
mD	MilliDarcy	
MD	Molecular dynamics simulations	
mV	Millivolts	
n	Number of measurements or tests	
Nanofluid	Nanoparticles dispersed in a fluid	
Nanofluid flooding	Flooding with a nanofluid; also referred to as *nano flooding*	
N_c	Capillary number	
NCS	Norwegian Continental Shelf	
NIBS	Non-invasive backscatter	
NF	Nanofluid flooding	
NF-Q_{high}	Nanofluid flooding at an injection rate of 3.0 ml/min	
NF-Q_{low}	Nanofluid flooding at an injection rate of 0.3 ml/min	
Nsp	Nano-structured particles	
Nsp_1a	Unmodified nano-structured particle with a surface area of 130 m^2/g	
Nsp_1b	Silanized nano-structured particle based on Nsp_1a	
Nsp_2a	Unmodified nano-structured particle with a surface area of 200 m^2/g	
Nsp_2b	Silanized nano-structured particle based on Nsp_2a	
Nsp_3a	Unmodified nano-structured particle with a surface area of 300 m^2/g	
Nsp_3b	Silanized nano-structured particle based on Nsp_3a	
Nsp_3c	PEG-modified nano-structured particle based on Nsp_3a	
Nsp_3d	Epoxy-modified nano-structured particle based on Nsp_3a	

	Description	Units
NTNU	Norwegian University of Science and Technology	
OOIP	Original oil in place (see also % OOIP)	ml
o/w	Oil-in-water emulsion	
P_c	Capillary pressure	bar, atm
PdI	Polydispersity index	
PEG	Polyethylene glycol (refers to the nanoparticle surface modification by polyethylene terminated silane groups)	
ppm	Parts per million	
PSD	Particle size distribution	nm
PTFE	Polytetrafluoroethylene	
PV	Pore volume	ml
PVP	Polyvinylpurrolidone	
q	Volumetric flow rate	ml/min
Q	Volumetric flow rate	ml/min
Q_{inj}	Injection rate	ml/min
r	Radius	cm
RF	Recovery factor	% OOIP
rpm	Rotations per minute	
SARA	Crude oil analysis determining the composition of saturates, aromatics, resins and asphaltenes	
SEM	Scanning electron microscope	
S_g	Gas saturation	
S_o	Oil saturation	
S_{oi}	Initial oil saturation	
S_{or}	Residual oil saturation	
SPE	Society of Petroleum Engineers	
SSW	Synthetic sea water	
S_{wi}	Initial water saturation	
S_{wir}	Irreducible water saturation	
t = 0	Start time	
TAN	Total acid number	
TBN	Total base number	
TDS	Total dissolved solids	
Temp.	Temperature	°C
USBM	U.S. Bureau of Mines	

	Description	Units
v	Velocity	cm/sec; m/day
V_A	van der Waals attractive force	joules
V_b	Bulk volume	ml; cm^3
V_g	Volume of gas	ml
V_o	Volume of oil	ml
$\sum V_o$	Total volume of oil produced	ml
V_R	Electrostatic repulsion	joules
V_T	Net inter-particle interaction energy	joules
V_w	Volume of water	ml
WF	Water flooding	
WF-Q_{high}	Water flooding at an injection rate of 3.0 ml/min	
WF-Q_{low}	Water flooding at an injection rate of 0.3 ml/min	
WI	Wettability index	
wt%	Weight percent	
w/o	Water-in-oil emulsion	
XDLVO	Extended DLVO theory	
XRD	X-ray diffraction	
y	Distance from a particle	nm
ΔP	Differential pressure over the core plug (see also dP)	bar; atm
δ	Thickness of the electrical double layer	nm; m
Θ	Contact angle	degrees
Θ_{ow}	Contact angle between the oil and water phase	degrees
λ	Debye screening length	nm; m
μ	Fluid viscosity (dynamic viscosity)	cP
μ_o	Oil viscosity (dynamic viscosity)	cP
μ_w	Water viscosity (dynamic viscosity)	cP
ρ	Density	g/cm^3
σ	Interfacial tension (see also IFT)	mN/m
σ_{ow}	Interfacial tension between oil and water	mN/m
σ_{so}	Interfacial tension between a solid and oil	mN/m
σ_{sw}	Interfacial tension between a solid and water	mN/m
Φ_e	Effective porosity	%
% OOIP	The percentage of the oil in place that has been produced	

1 Introduction

1.1 Motivation

The U.S. Energy Information Administration (2016) estimates that worldwide consumption of petroleum and other liquid fuels will increase from 90 million barrels per day in 2012 to 121 million barrels per day by 2040 due to population growth and industrialization. The increased petroleum demand must be met by finding new oilfields and/or extending the life of existing oilfields. New oilfields are becoming increasingly difficult to find. The consensus in the petroleum industry is that most of the large, easily harvestable reservoirs have been discovered. The remaining undiscovered reserves are either in harsh environments (i.e. the Arctic) or are energy-intensive to extract (i.e. tar sands) (Muggeridge et al., 2014). The petroleum industry is therefore interested in new methods that extract more oil from existing reservoirs.

An estimated 65% of oil cannot be extracted from reservoirs currently in production (Thomas, 2013). This is because the technology to extract the remaining oil does not exist or is uneconomical with the current oil price. If the worldwide ultimate recovery is increased from 35% to 45%, an estimated one trillion barrels of oil can be produced from existing fields (Thomas, 2013). That would be enough oil to supply the entire world for over 30 years assuming the worldwide consumption of 90 million barrels per day (consumption estimate for 2012).

The Norwegian Petroleum Directorate (2014a) estimates that 50% of the oil on the Norwegian Continental Shelf (NCS) will remain in the reservoirs at field end-of-life according to current production plans. Many of the reservoirs on the NCS already employ water flooding (the process of injecting water into the reservoir to displace oil) to maintain the reservoir pressure (Norwegian Petroleum Directorate, 2014b). This traditional water flooding can be chemically altered to perform a more efficient oil displacement, thereby extending the production life of existing reservoirs. Employing an enhanced oil recovery (EOR) production method would increase oil recovery using mechanisms other than pressure maintenance.

This thesis investigates the potential of adding silica nanoparticles to traditional water flooding operations to harvest more of the oil trapped inside existing reservoirs. The technique investigated in this thesis can therefore be labeled as nanoparticle-enhanced water flooding or

nanoparticle-EOR. One of the goals was to develop a method that uses existing water flooding injection procedures and infrastructure so that the threshold for adopting the technology is minimized. Three main arguments for using nanoparticles as water flooding EOR additives are synthesized from Sun et al. (2017) and papers referenced therein:

1. Nanoparticles have a large surface area to volume ratio and therefore a large chemical reactivity. This means that a smaller concentration can be used to induce enhanced oil recovery. This translates into lower costs and better logistics, as a smaller volume is needed for transport and platform storage compared to other additives.

2. Nanoparticles are small enough to pass through the reservoir's pore network. They might even be able to penetrate nanoscale pores that other additives cannot access.

3. Many nanoparticles have passed ecotoxicity tests, rendering them more likely to be approved for field applications. This is a challenge with chemical flooding techniques on the NCS. Certain titanium dioxide and silica nanoparticles are already used as food additives (E171 and E551, respectively), although there is ongoing research as to how injection affects the gastrointestinal system (Peters et al., 2012; Weir et al., 2012). Silica nanoparticles specifically are often heralded as the "environmentally-friendly" EOR additive (Sun et al., 2017), although any surface modified nanoparticle would need to undergo new ecotoxicity tests.

1.2 Problem formulation

This study experimentally investigates the conditions needed for silica nanoparticles to enhance oil recovery to determine what further information needs to be gathered before they can be applied commercially. Because the most feasible situation under which this technology would be applied is after water-flooded reservoirs have reached maturity, the nanoparticle flooding investigated here is conducted as post- water flooding (tertiary) recovery.

The three research objectives are therefore:

> **O1:** Identify or develop a nanoparticle that can be dispersed in sea water and therefore applied in offshore oilfields.

> **O2:** Investigate the potential of nanoparticles as a tertiary EOR agent added to water flooding.

> **O3:** Determine how the nanoparticles affect the oil production.

Nanoparticles are viable EOR candidates if they meet the following criteria:

1. **The nanoparticles are stable in sea water at a temperature of at least 60°C for at least four months.** Sea water is the most common injection liquid for offshore fields. Oil is formed when kerogen temperature reaches 60° to 120°C (Norwegian Petroleum Directorate, 2014a). Most petroleum reservoirs on the Norwegian Continental Shelf are hotter than 60°C, but nanoparticle stability at 60°C would be applicable for some of the shallower reservoirs. Nanofluid stability is defined here as a nanofluid dispersion having a nanoparticle size distribution curve that maintains its original unimodal form and mean nanoparticle size from the initial measurement at time = 0. This is investigated by evaluating the nanofluids' particle size distribution curves.

2. **During core flooding tests, oil should be produced from the core outlet within the first 0.6 pore volumes (PV) of nanoparticle flooding or the oil recovery should be at least 5% of the original oil in place (OOIP) after 1 PV of nanoparticle flooding (Hamon, 2015).** Oil production needs to occur as quickly as possible after EOR implementation to produce the most economical results. The main questions posed here are how much oil can be recovered and when. This is addressed by analyzing oil curves recovery produced from core flooding tests.

3. **The EOR mechanisms are understood and related to relevant reservoir properties.** Because each petroleum reservoir has unique characteristics, it is important to know *why* oil is produced (or not produced) from a core flooding test. By knowing how the EOR fluid interacts with various reservoir parameters, an evaluation framework can be

established whereby the most effective EOR technique can be chosen for each field. The main question posed here is how or why is the oil produced. This is investigated by comparing data to conceptual models of EOR mechanisms like wettability alteration and interfacial tension reduction.

1.3 Research rationale

Previous studies at the Norwegian University of Science and Technology (NTNU) have shown that commercially available hydrophilic silica nanoparticles can increase the recovery factor by up to 15% of the original oil in place (Hendraningrat et al., 2013b, 2013c, 2013d, Hendraningrat and Torsæter, 2014a, 2015a, 2016, Li et al., 2013, 2015). They tested nanoparticle concentrations ranging from 0.01 to 0.1 wt%. Most experiments were conducted at 0.05 wt% because this concentration yielded the highest tertiary recovery factor (Hendraningrat et al., 2013c). Not all experiments were published with differential pressure profiles, and those experiments that did include the profiles showed an increase in differential pressure throughout the tertiary nanoparticle flooding (Hendraningrat et al., 2013b; Hendraningrat and Torsæter, 2014a, 2015a, 2016; Li et al., 2015). This was attributed to nanoparticle adsorption to the rock surface and/or nanoparticle agglomeration, both of which would result in subsequent permeability impairment. Wettability alteration and occasionally interfacial tension reduction are put forth as the EOR mechanisms for all core flooding tests (Hendraningrat et al., 2013c; Hendraningrat and Torsæter, 2014a, 2014b; Li et al., 2015; Li and Torsæter, 2015). Only Li et al. (2015) acknowledged that the increase in differential pressure throughout the nanoparticle flooding could be an EOR mechanism, albeit an uncontrollable one.

Previous NTNU studies did not investigate nanoparticles dispersed in synthetic sea water. All experiments used 3 wt% NaCl as the dispersing fluid with the exception of Hendraningrat and Torsæter (2016). That study investigated the effect of the dispersing fluid's water chemistry on the tertiary recovery factor and contact angle for nanoparticles dispersed at 0.05 wt%. The following dispersing solutions with divalent cations (Ca^{2+} and Mg^{2+}) were among those tested: 2.7 wt% NaCl + 0.57 wt% $CaCl_2 \cdot 2H_2O$ and 2.7 wt% NaCl + 1.01 wt% $MgCl_2 \cdot 6H_2O$. This preliminary study showed that water chemistry affects the recovery factor and wettability, but the results are inconsistent. The Mg^{2+} solution, when combined with the silica nanoparticles,

produced a significant amount of oil in the tertiary phase (13%), but there was no effect on wettability. This scenario had the greatest increase in differential pressure throughout the nanoparticle flooding. Conversely, the Ca^{2+} nanofluid produced the same amount of oil during the nanoparticle flooding as the 3 wt% NaCl nanofluid (3%) even though it had the greatest reduction in contact angle (-10°).

These previous studies produced the following motivations for embarking upon the initial experiments: The nanoparticles must be dispersed in synthetic sea water to assess their performance in a real-world application. There is an increase in differential pressure throughout most of the aforementioned nanoparticle flooding cases (Hendraningrat et al., 2013a, 2013b, Hendraningrat and Torsæter, 2014a, 2015a, 2015a; Li et al., 2015; Li and Torsæter, 2014, 2015). This could be the primary reason why EOR takes place. Therefore, various nanoparticle surface areas (and hence various chemical reactivity strengths) are tested and compared. The reasoning behind the proposed nanoparticle EOR mechanisms is unclear because experiments produce conflicting results. For example, the nanoparticle types and concentrations having the largest decrease in contact angle and/or the largest increase in the wettability index do not correspond to the largest tertiary recovery factors (Hendraningrat et al., 2013c; Hendraningrat and Torsæter, 2016). Additionally, the interfacial tension reduction is not of orders of magnitude, which is the conventional benchmark by which to assess if it is a primary EOR mechanism (Hamon, 2015; Hendraningrat et al., 2013b; Hendraningrat and Torsæter, 2015a). Therefore, additional contact angle and interfacial tension experiments are conducted.

Subsequent investigations focusing on nanoparticles modified for improved stability are conducted in a similar manner, with the same rationale for determining whether the nanoparticles are viable EOR candidates. The EOR mechanism(s) dominating each core flooding system are proposed.

The research questions are therefore:

RQ1: Are the nanoparticles stable in synthetic sea water?

RQ2: Do the nanoparticles increase the oil recovery?

RQ3: What are the EOR mechanisms contributing to nanoparticle-induced oil recovery?

1.4 Contributions and scope

The primary contributions are as follows:

C1: The commercially available silica nanoparticles from Evonik Industries are unstable in synthetic sea water. This finding prompted the company to develop new nanoparticle surface treatments that were subsequently tested in this thesis. Stable products are identified.

C2: To determine if nanoparticles increased oil recovery, 27 unique core flooding configurations were conducted. Seven of the test configurations were repeated, resulting in 35 total core flooding tests for evaluating the tertiary flooding potential of nanoparticles.

C3: Interfacial tension experiments, contact angle measurements and glass micromodel flooding tests are used to explore the nanoparticles' EOR mechanisms.

C4: Additional analysis of the core flooding tests provides information about the EOR mechanisms and nanoparticle transport through the core plug. This analysis varied per the core flooding configuration. Investigated factors include relative permeability estimation, differential pressure changes throughout the core flooding and nanoparticle concentration and particle size distribution in the nanofluid effluent.

The scope of the thesis is summarized in Table 1.1.

Table 1.1. Thesis scope.

Objective	Research question	Contribution	Experimental method
O1	RQ1	C1	Nanoparticle size distribution
O2	RQ2	C2	Core flooding tests
O3	RQ3	C3	• Interfacial tension tests • Contact angle measurements
		&	• Micromodel flooding
		C4	From core flooding tests: • Differential pressure patterns • Visual observation of effluent • Effluent nanoparticle concentration • Effluent nanoparticle size distribution • Relative permeability

1.5 Thesis structure

The structure of the thesis is as follows:

Chapter 1: The motivation for studying the potential of nanoparticles as EOR agents is given. The problem statement and research rationale are presented together with the thesis structure.

Chapter 2: An overview of EOR theory and methods is provided for context. This is followed by a discussion specifically about nanoparticles for EOR in four sections: terminology, nanofluid stability, oil production and EOR mechanisms. The nanoparticle terminology is introduced to provide consistency. The nanofluid stability, oil production and EOR mechanisms are each presented with the following sections: general theory and rationale behind each criterion, appropriate laboratory methods used for evaluation and previous experimental results from literature. Focus is placed on studies that have investigated pure silica nanoparticles without additional additives. The EOR mechanisms section is subdivided into fluid-fluid interactions, fluid-rock interactions and mechanical displacement.

Chapter 3: The experimental materials and their properties are defined. Five fluids (crude oil, n-decane, formation water, synthetic sea water (SSW) and nanofluids) are described. The core plugs and micromodel porous media are described.

Chapter 4: The experimental methods are described. The methods are presented in order of the results: nanofluid stability, interfacial tension, contact angle, core flooding and micromodel flooding.

Chapter 5: The results from the experimental investigation are presented including objectives for the experiments, detailed procedures where appropriate and a summary of the results. The four parts used to evaluate the core flooding were decided chronologically based upon nanoparticle surface development.

Chapter 6: The discussion follows the order of the research questions. First, the nanofluid stability is discussed. This is followed by analysis of the core flooding tests and their subsequent oil production. The potential EOR mechanisms are then discussed based on the following classifications: fluid-fluid interactions (primarily interfacial tension reduction and in-situ emulsion generation), fluid-rock interactions (primarily wettability alteration) and mechanical displacement (flow diversion).

Chapter 7: The conclusions from the experiments are provided, followed by recommendations for future work and nanoparticle development.

2 Enhanced oil recovery (EOR) fundamentals

The purpose of Chapter 2 is to provide background information about nanoparticle-EOR so the reader can readily evaluate the thesis results. Typical petroleum production methods are presented to describe what has happened in a mature reservoir prior to potential nanoparticle-EOR implementation. This is followed by fundamental topics associated with the thesis research questions as shown in Table 2.1.

Table 2.1. Chapter 2 topic outline.

Research question	Topic (section location)
Enhanced oil recovery (EOR) background	• Two-phase flow in porous media (2.1.1) • Reservoir history (2.1.2) • Reservoir production methods (2.1.3) • EOR methods (2.2.1)
RQ1: Are the nanoparticles stable in synthetic sea water?	• Terminology (2.3.1) • Fluid stability (2.3.2)
RQ2: Do the nanoparticles increase the oil recovery?	• EOR assessment by core flooding (2.2.2) • Oil production (2.3.3)
RQ3: What are the EOR mechanisms contributing to nanoparticle-induced oil recovery?	• Fluid-fluid interactions (2.3.4.1) • Fluid-rock interactions (2.3.4.2) • Mechanical displacement (2.3.4.3)

2.1 Reservoir background

Petroleum fluids reside in the pore space in reservoir rocks. The volume of the connected pore space is called the pore volume (PV). It is a product of the total reservoir (bulk) volume (V_b) and the effective porosity of the rock (Φ_e). The ratio between the volume of oil (V_o), gas (V_g) or water (V_w) and the pore volume is called the oil saturation (S_o), gas saturation (S_g) or water saturation (S_w), respectively (Eq. 2.1):

$$S_o = \frac{V_o}{PV}; \;\; S_g = \frac{V_g}{PV}; \;\; S_w = \frac{V_w}{PV} \qquad \text{(Eq. 2.1)}$$

The sum of the saturations should be unity if the pore space is completely filled with fluid. Because gas production was not a focus of this research and gas saturation was therefore not

included in the experiments, the remainder of the thesis will consider that only oil and water are present in the pore space as immiscible fluids.

2.1.1 Two-phase flow in porous media

The oil must be able to flow through the reservoir rock. The ability of a reservoir to transmit fluids is defined as its permeability. Permeability can be mathematically expressed by the generalized equation of Darcy's Law (Eq. 2.2):

$$\frac{q}{A} = \frac{k}{\mu} \frac{\Delta P}{L}$$
(Eq. 2.2)

This relationship describes the movement of a single fluid through a porous medium, where q is the volumetric flow rate (cm^3/sec), A is the cross-sectional area of the porous medium (cm^2), k is the absolute permeability (Darcy), ΔP is the pressure drop per unit length (atm), μ is the fluid viscosity (cP) and L is the unit length (cm). The permeability of a reservoir is typically expressed in *milli*darcy (mD) because the permeability values are so small (Dandekar, 2013).

Henry Darcy first developed a form of Eq. 2.2 based upon experiments conducted in sand packs that were 100% saturated with water. It was later discovered that his work could be extrapolated to other fluids by incorporating the fluid's viscosity as seen above. It is important to note that Darcy's equation is valid under the following assumptions (Dandekar, 2013):

- The flow is horizontal, steady state and laminar.
- The porous medium is 100% saturated with the flowing fluid (single-phase flow).
- The flowing fluid is incompressible and unreactive with the porous medium.
- The measurement is conducted under isothermal conditions (changes in temperature causes changes in viscosity).

As previously mentioned, the reservoir rocks are saturated with at least two fluids. This already invalidates an assumption behind Darcy's Law. Nevertheless, the concept of relative permeability has been developed to attempt to account for having more than one fluid in the pore space. Relative permeability (k_r) is defined as the ratio of effective permeability (k_e) to a

reference permeability (k_{ref}) as shown in Eq. 2.3 for oil and water (subscripts $_o$ and $_w$, respectively) (Dandekar, 2013):

$$k_{ro} = \frac{k_{eo}}{k_{ref}}; \quad k_{rw} = \frac{k_{ew}}{k_{ref}} \qquad \text{(Eq. 2.3)}$$

The effective permeability is measured using Darcy's Law much like absolute permeability. The effective permeability of a fluid will increase as its saturation in the porous medium increases. Therefore, relative permeability changes as a function of fluid saturation.

In addition to fluid saturation, effective permeability is a function of the following: pore size, pore size distribution, wettability and the porous medium's saturation history (Standing, 1975). One way to measure effective permeability is to apply Darcy's Law for a given fluid when its saturation in the porous medium is stable and known. For example, the effective permeability of water at the residual oil saturation (S_{or}) can be measured from the flow rate and pressure drop across the core. This is because the fluid saturations are stable at S_{or}, and the recorded data is only a function of water flux.

The reference permeability is a base value by which the effective permeability is normalized. The two most common values are absolute permeability (K_{abs}) and effective oil (hydrocarbon) permeability at irreducible water saturation (S_{wir}) (Standing, 1975). The absolute permeability will be used at the reference permeability throughout this thesis.

When a fluid is injected into a porous medium, the main forces at the pore scale are viscous (driving) and capillary (resistant) forces, both of which are dependent upon the pore radius. The viscous forces are the product of the liquid's dynamic viscosity (μ) and its velocity (v). The capillary forces can be described by capillary pressure (P_c) in Eq. 2.4 (Lake, 1989):

$$P_c = \frac{2\sigma \cos \theta}{r} \qquad \text{(Eq. 2.4)}$$

The capillary forces are therefore a function of the interfacial tension between the fluids (σ), the wettability of the rock (expressed by the contact angle, Θ) and the pore diameter (r). The interfacial tension and wettability are described in more detail in sections 2.3.4.1 and 2.3.4.2, respectively.

The ratio of viscous to capillary forces is described by the capillary number (N_c) in Eq. 2.5 (Lake, 1989):

$$N_c = \frac{\mu_w \, v_o}{\sigma_{ow}}$$

(Eq. 2.5)

Flow in a porous medium is dominated by capillary forces if the capillary number is low and is dominated by viscous forces if the capillary number is high. Increasing the capillary number results in oil mobilization and production. This can be achieved by increasing the viscosity of the aqueous phase or the velocity of the oleic phase or by decreasing the interfacial tension. According to Lake (1989), the capillary number for waterflooding in sandstones is typically between 10^{-7} and 10^{-5}. The critical capillary number, whereby residual oil saturation begins to decrease, varies from 10^{-5} to 10^{-4}.

2.1.2 Reservoir history

The pore space in a reservoir was initially saturated with water. As kerogen in underlying source rocks was heated, it produced hydrocarbons that migrated upwards until trapped in a reservoir. The initial saturation distribution of the oil, gas, and water in the reservoir pore space is due to a balance between gravitational forces and capillary forces (Dandekar, 2013). The gravity segregation in the reservoir is due to differences in fluid density. The capillary forces prevent a displacement of indigenous reservoir water. This is why reservoirs include initial water saturation (S_{wi}), which is the ratio of the volume of water initially in the reservoir to the pore volume (Dandekar, 2013). This naturally occurring water is often called formation or connate water.

2.1.3 Reservoir production methods

When a production well is drilled, the resulting pressure gradient in the reservoir allows oil to be produced. This is called *primary production.* The pressure in the pore space decreases as oil is removed from the reservoir (Muggeridge et al., 2014). Therefore, water (or sometimes gas) is often injected into the reservoir through *injection wells* to maintain the pressure gradient.

This injection of water or gas for pressure maintenance is called *secondary recovery*. It works by physically displacing the oil and filling the pore space that would be otherwise empty (Muggeridge et al., 2014). The water and gas injection processes are referred to as *water flooding* and *gas flooding* respectively.

The effectiveness of water and gas flooding is affected by the physical spacing between the injection and production wells and is termed *macroscopic displacement efficiency*. The oil that is left behind is called *mobile oil* because it can theoretically be produced by adding additional wells or by increasing the duration of water or gas injection (Norwegian Petroleum Directorate, 2014b).

The effectiveness of water and gas flooding is also affected by the physical and chemical properties of the reservoir rock and fluids with which it has already come into contact. This is described by its *microscopic sweep efficiency*. This residual oil that is left behind is called *immobile oil* because it cannot be mobilized despite additional injection of water or gas (Norwegian Petroleum Directorate, 2014b).

Water or gas flooding can be used to increase oil production by exploiting mechanisms other than pressure maintenance (Lake, 1989). This approach is called *enhanced oil recovery* (EOR) and also includes any modification of water or gas flooding (like adding chemicals to the water). EOR methods can be implemented from the beginning of field production or employed after water or gas flooding has already taken place. Therefore, EOR is often referred to as *tertiary recovery* (Taber et al., 1997). In this thesis, tertiary recovery refers only to oil produced by EOR techniques employed *after* water flooding.

2.2 **EOR theory**

The goal of EOR is to achieve a high ultimate recovery factor, thereby decreasing the saturation of the oil remaining in the reservoir. The recovery factor (RF) is a product of the volumetric sweep efficiency (E_v) and the displacement efficiency (E_D) as shown in Eq. 2.6 (Lake, 1989).

$$RF = E_V \times E_D$$

(Eq. 2.6)

E_v is a ratio of the volume of oil contacted by the injection fluid to the volume of oil originally in the reservoir. It is a function of injection duration, fluid viscosities, well arrangements, reservoir heterogeneity, and gravity and capillary forces (Lake, 1989). E_v is a product of the areal and vertical sweep efficiency (Lake, 1989). For example, water flooding will not be efficiently sweeping through zones of ultra-low permeability (poor vertical displacement) or where injection wells are not present (poor areal displacement) (Smalley et al., 2009).

E_D is the ratio of the volume of oil displaced or produced to the volume of oil contacted with the injection fluid. It is a function of injection time, fluid viscosity, relative permeability and capillary pressure (Lake, 1989). E_D can vary from < 20% for primary recovery methods to 50 to 80% for high-quality water flooding (Smalley et al., 2009). E_D is also inversely proportional to the mobility ratio (M) between the injected fluid and the oil in the reservoir. The mobility ratio can be decreased, and hence the displacement efficiency increased, by increasing the viscosity of the injected water or decreasing the oil viscosity as shown in Eq. 2.7 (Dake, 1998):

$$M = \frac{mobility\ of\ the\ displacing\ fluid}{mobility\ of\ the\ displaced\ fluid} = \frac{\left(k_{rw}/\mu_w\right)}{\left(k_{ro}/\mu_o\right)} \qquad \text{(Eq. 2.7)}$$

Based on the definitions of volumetric sweep efficiency and displacement efficiency, the recovery factor can also be defined as the ratio of the volume of oil produced ($\sum V_o$) to the volume of oil originally in place (OOIP) as shown in Eq. 2.8:

$$RF = \frac{\Sigma V_o}{OOIP} = \left(\frac{(S_{oi} - S_{or})}{S_{oi}}\right) \qquad \text{(Eq. 2.8)}$$

Oil production can also be described by the change in oil saturation (Morrow, 1990) as shown in Eq. 2.8 where S_{oi} is the initial oil saturation in the reservoir and S_{or} is the residual (remaining) oil saturation in the reservoir. These are the common definitions for oil recovery reported from core flooding tests. The oil recovery is commonly expressed as a percentage instead of a fraction, with 100% meaning that all the oil has been produced from the reservoir.

The ultimate goal is to continue economical production until a recovery factor of 100% is obtained. Based on the discussion presented in Muggeridge et al. (2014), this is theoretically possible but practically unattainable. In addition to the physical challenges associated with achieving complete oil recovery, there is an economic factor to consider. Smalley et al. (2009) introduced an economic efficiency or cut-off efficiency, E_C, as an additional factor to Eq. 2.6. E_C is the fraction of oil that can be produced before the water-to-oil production ratio is too high to be economical. This is because oil production tends to "tail off", where small volumes of oil can continue to be produced but only with large volumes of water injection and concurrent water production (Smalley et al., 2009). Oil production is therefore stopped before the ultimate oil recovery is reached. Although EOR methods primarily focus on increasing E_V and E_D, they must also take into account E_C (Muggeridge et al., 2014).

2.2.1 EOR methods

Lake (1989) divides EOR methods into three groups: thermal, chemical, and solvent. Their applicability to a reservoir is primarily based upon the crude oil's density represented by the °API index, where a large API represents dense (heavy) oil (Figure 2-1). Thermal methods include in-situ combustion and steam injection to decrease the viscosity of the heavy crude oil (Taber et al., 1997). Chemical methods encompass any technique whereby additives are added to water flooding to increase oil production. This includes but is not limited to the following techniques: polymer flooding, alkaline surfactant polymer (ASP) flooding, low-salinity water injection, smart water injection, and nanoparticle flooding. The application of chemical EOR methods is highly dependent upon the oil price and, to a lesser extent, the cost of the chemical being used (Alvarado and Manrique, 2010). Solvent methods include CO_2 or hydrocarbon gas injection to approach miscibility with the crude oil (Taber et al., 1997).
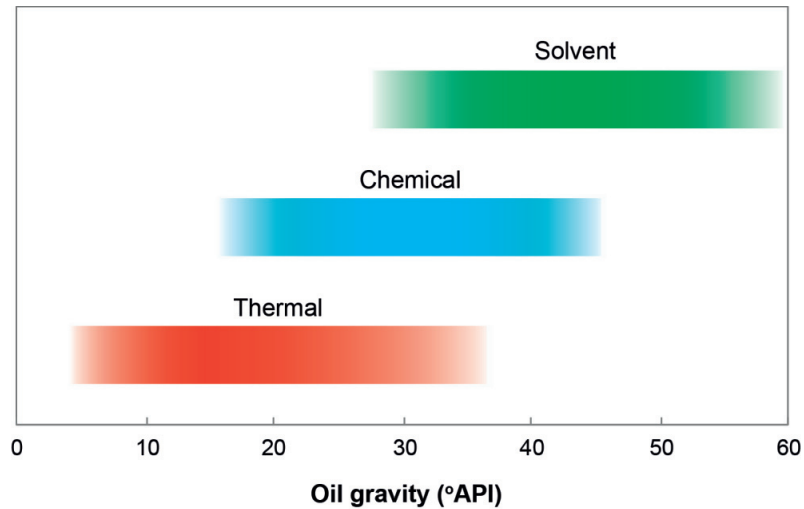
Figure 2-1. Optimal oil gravity (expressed in °API) for application of EOR techniques. Figure modified from Taber et al. (1997).

The implementation of EOR techniques for producing immobile oil is hindered by not only economics but also by infeasibility and knowledge gaps. In reservoirs where heavy oil is not present, energy-intensive thermal methods are typically not appropriate. If a large quantity of gas is not easily available, solvent methods are not feasible. For chemical flooding techniques, the concentration of the chemical needed to produce economic recovery can be so great that it is not feasible to transport and store such a large volume, especially for offshore platforms. Additionally, many of the chemical flooding mechanisms are either not well known or debated. Chemical flooding is the least applied of the three EOR types (Alvarado and Manrique, 2010), but that is where the majority of the research activity is happening. This is because of the potential of using chemical flooding for a large variety of reservoir conditions.

According to an interpretation of Taber et al. (1997), the following questions should be addressed when selecting an EOR method: 1) What method is most appropriate for the oil properties and reservoir characteristics for the oilfield in question? 2) How does the method compare with traditional water flooding? and 3) Is it economical?

To answer the first question, the reader is directed to literature reviews such as Table 3 in Taber et al. (1997). Although the article is 20 years old and does not include some of the newer EOR methods, they provide an excellent framework for screening criteria. This includes investigation of oil properties such as density, viscosity and composition and reservoir characteristics such as oil saturation, formation type, permeability and temperature. By relating a new EOR method to these parameters, appropriate oilfields can be identified for applying the technology. An understanding of EOR mechanisms leading to incremental oil production and how they are affected by changing these parameters

Comparison with traditional water flooding helps to assess at what point it is appropriate to apply the EOR method. Some EOR techniques, such as steam or polymer flooding, produce highest ultimate recovery rates when employed from the very beginning of field production (Taber et al., 1997). Otherwise, most EOR techniques are applied in mature, water flooded fields. The reader is directed to Muggeridge et al. (2014) for a comparison of the most common EOR methods to water flooding on both a microscopic and macroscopic scale. They also present limitations of these EOR methods.

Finally, an economic assessment needs to be conducted, where the profit from the produced oil is compared to the expenditure of implementing EOR (Muggeridge et al., 2014; Taber et al., 1997). Because the volumes and thereby amount of money involved is so large, field investigations are typically not conducted until positive results have been replicated and understood in a laboratory setting.

2.2.2 EOR assessment by core flooding

Chemical EOR methods are screened by injecting the EOR fluid through a cylindrical rock core saturated with reservoir fluids. The oil production is then plotted over time. This procedure is referred to as *core flooding*. Because each core has different physical properties leading to variations in pore volume, the duration of fluid injection is normalized as *pore volumes (PV) flooded* to better compare different core tests. Upscaling core flooding results for application in reservoir simulations introduces several errors. This is beyond the scope of this thesis and is not discussed here.

EOR methods are typically tested via tertiary flooding. The goals for this are twofold. 1) Mature, water flooded fields are the typical targets for EOR; 2) If secondary flooding is used for the comparison, two nearly identical cores must be used to compare water flooding results to the EOR results (Hamon, 2015). No two cores have the exact same geometry and mineralogical distribution, introducing additional unknowns to the system. The original core can typically not be re-used, especially if crude oil is being used, because of the difficulty of removing all the oil components from the core without harming the original state. Additionally, cores are rarely re-used for EOR tests because the EOR method could alter the physical and/or chemical state of the original core.

If tertiary flooding is used, care must be taken that the ultimate recovery factor has indeed been reached with water flooding prior to initiation of tertiary EOR flooding. This means a criterion should be established such that EOR injection begins only after water flooding has not produced oil for a certain amount of pore volumes. Then it can be reasonably assumed that any additional oil produced when EOR flooding is initiated is a result of the EOR technique itself and not just an artifact of additional flooding time.

The goal with employing EOR is to produce as much oil as possible as quickly as possible. In technical terms, this means the goal is as large a recovery factor (RF) as possible within as few pore volumes (PV) of injection as possible. Hamon (2015) presented sensible criteria for evaluating whether tertiary flooding in the laboratory provides "realistic, positive results" for the EOR method. These criteria are that the initial oil bank should appear after the EOR fluid has been injected for 0.5 to 0.6 PV *or* that an oil recovery of at least 5% OOIP is achieved within the first pore volume of injection. These are used as criteria throughout this thesis.

A sample oil recovery curve from a core flood with a successful tertiary EOR flood is shown in Figure 2-2. Water flooding fails to produce more oil after prolonged injection. If the EOR fluid is injected after the water flooding fails to produce additional oil for 1 PV, the ultimate recovery factor increases. This additional oil produced from the EOR flood is called *incremental oil*. It is defined as the difference between the amount of oil recovered with the EOR flood and the amount of oil that would have been recovered if the EOR flood was not applied (Lake, 1989). There should also be a slight delay in the oil production as the EOR fluid mobilizes the oil in the core.
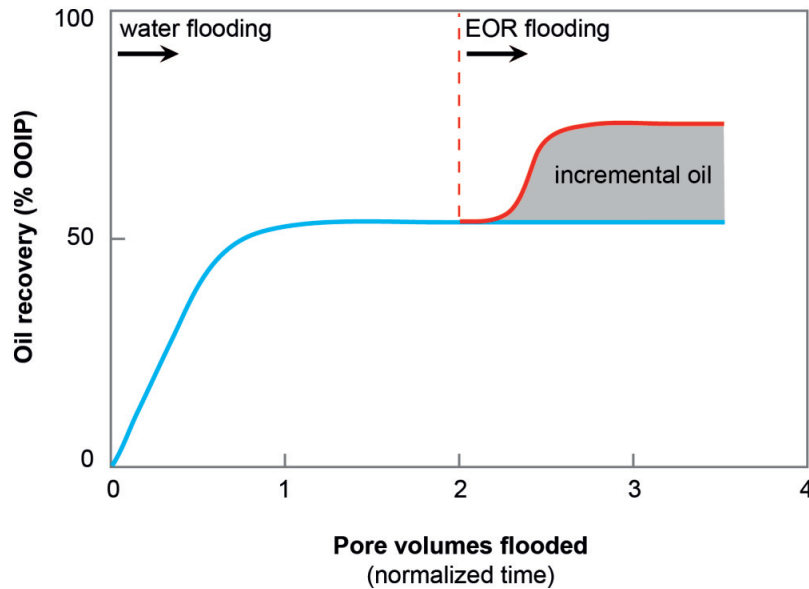
Figure 2-2. Oil recovery curve showing a positive response from tertiary EOR flooding in a core flooding test. Figure modified from Prats (1982).

2.3 Nanoparticles for EOR

It appears that the first published study specifically investigating the potential of hydrophilic nanoparticles as an EOR agent was conducted by Ju et al. in 2006. This computer simulation was spurred by their previous experimental work that concluded hydrophobic nanoscale polysilicon materials could change the wettability of porous surfaces (Ju et al., 2002). These early studies drew from reservoir fines migration concepts.

The number of studies on the application of nanotechnology in the petroleum sector has greatly increased since 2010 according to Bera and Belhaj (2016). The majority of the research is experimental (Bera and Belhaj, 2016). However, studies have investigated the potential of nanoparticle-EOR using molecular dynamic (MD) simulations (Miranda et al., 2012; Wu et al., 2012) or core-scale effects (Ju et al., 2006).

Papers by Fletcher and Davis (2010) and Bennetzen and Mogensen (2014) provide general frameworks exhibiting how nanoparticles can be applied to EOR. Recent review papers take

different approaches. Negin et al. (2016) presents background on silica nanoparticles for EOR. Bera and Belhaj (2016) and Sun et al. (2017) provide comprehensive discussions and comparisons of experimental nanoparticle research and proposed EOR mechanisms.

It appears that silica nanoparticles are the most commonly researched nanoparticle type for EOR applications according to the literature cited in Bera and Belhaj (2016) and Sun et al. (2017). This could be because the initial focus on silica nanoparticles led to positive results, leading to further excitement on the topic. Metal oxides such as titanium dioxide, aluminum dioxide and iron oxide have also been presented in literature (Alomair et al., 2014; Hendraningrat and Torsæter, 2015b; Ogolo et al., 2012; Ragab et al., 2015) but will not be discussed. Although hydrophobic or partially hydrophobic nanoparticles have also been investigated for EOR (Ogolo et al., 2012; Roustaei et al., 2013), focus in this thesis is given to *hydrophilic* silica nanoparticles which can therefore be dispersed in traditional water flooding fluids.

Silica nanoparticles can also be added to polymer flooding (typically polyacrylamide: Cheraghian, 2016; Maghzi et al., 2013; Yousefvand and Jafari, 2015) or surfactant flooding (typically sodium dodecyl sulfate: Rahimi and Adibifard, 2015; Zargartalebi et al., 2015). This can be termed *nanoparticle-assisted flooding*. The following literature review focuses on studies that have investigated the use of silica nanoparticles as stand-alone EOR additives to provide context for the silica nanoparticles investigated in this thesis.

2.3.1 Terminology

A particle is considered in the *nano* domain when it is smaller than 100 nm (1×10^{-7} meters) in at least one dimension (Arce, 2010). Nanoparticles can consist of the following components: primary particles, aggregates and agglomerates (Figure 2-3). Primary particles are the smallest individual components of the nanoparticle mixture. The primary particles' attraction to each other causes aggregates to form. This constitutes the true structure of the nanoparticles. The term *aggregate* is therefore used in this thesis to describe binding of the primary particles to form nano-structures. The term *agglomerate* is used in this thesis to describe an assemblage of nanoparticles or aggregates (as proposed by Nichols et al., 2002).
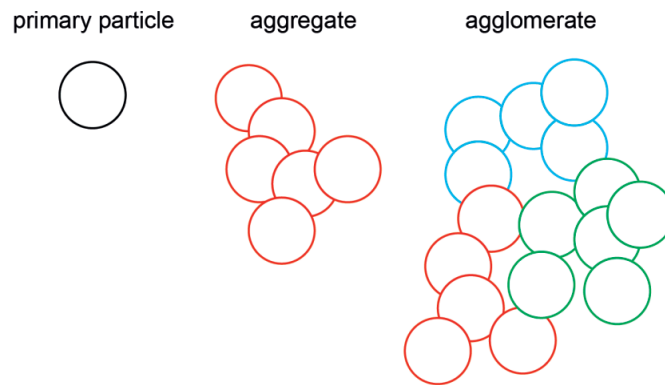
Figure 2-3. Illustration of the terms primary particle, aggregate and agglomerate used throughout this thesis.

The primary particles are often identified as "hypothetical particles" with the assumption that they are spherical particles making up the aggregate shape (Evonik Industries, 2015). This is exemplified in Figure 2-4, where an image of an aggregate structure has been taken with a scanning electron microscope (SEM). The aggregates can join to form agglomerates. The aggregates are not fused together but are rather held together by weak interactions such as van der Waals forces or hydrogen bonds (Evonik, 2015). Examples of the agglomerates (Figure 2-4A) and an aggregate (Figure 2-4B) are shown for Evonik Industry's AEROSIL® 200 silica nanoparticle product used in this thesis ("200" means it has a specific surface area of 200 m^2/g).

A)

B)
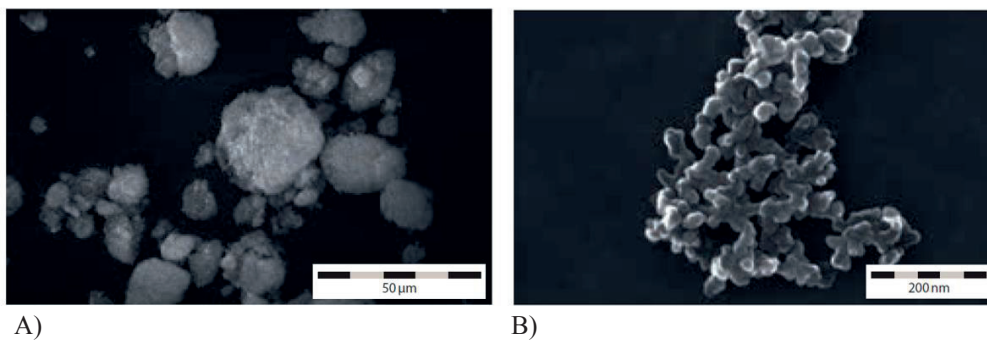
Figure 2-4. SEM images for AEROSIL® 200 (Nsp_2a) used with permission from Evonik Industries (2015). A) Agglomerates of the silica particles. B) A nano-structured particle (aggregate). Primary particles are clearly visible but are fused together and cannot be separated.

Silica nanoparticles can be produced via a wet-chemical process or a fumed/thermal process. *Colloidal silica nanoparticles* (Cnp) used in this thesis were produced by the wet-chemical method, while *fumed silica nano-structured particles* (Nsp) were created via flame hydrolysis. The reader is directed to the technical report by Evonik Industries (Evonik Industries, 2015) for details about the manufacturing processes and their effects on the nanoparticle products.

Although some of the nano-structured particles have aggregate sizes larger than the defined range for the nanoscale, both Nsp and Cnp are collectively referred to as simply *nanoparticles* or by their abbreviations *Cnp* and *Nsp* throughout this thesis.

The term *nanofluid* refers to a solution where nanoparticles are suspended at a specific concentration in a dispersing fluid. The dispersing fluid is typically a saline aqueous solution for enhanced oil recovery purposes. This is practical, as the nanoparticles need a medium by which to be injected and transported through the reservoir. An aqueous solution is cheap and, in the case of reservoirs already employing water flooding, already available and in use.

2.3.2 Nanofluid stability

The nanoparticles in the dispersing fluid need to be resistant to agglomeration. Otherwise, they can begin to form larger structures which then negate their advantageous properties such as nanoscale-size and large surface reactivity. In extreme cases, the agglomerates can become so large that they begin to block pore throats, decreasing reservoir permeability. Nanoparticle agglomeration is undesirable because it limits nanoparticle propagation in the reservoir.

2.3.2.1 Nanofluid stability criteria

The nanoparticles intended for EOR use must be dispersed in a complex saline solution to work properly in a petroleum reservoir, as sea water and recycled formation water are the most common injection fluids offshore. As will be discussed in *stabilization theory* below, nanoparticle agglomeration increases with increasing ionic strength (Hotze et al., 2010; Metin et al., 2010). The challenge associated with preventing nanoparticle agglomeration in sea water

could be why most silica nanoparticle EOR research continues to use fresh water or a simple saltwater with Na^+ as the only cation in solution as is described in Section 2.3.3.

The nanofluid stability must withstand the reservoir's increased temperature and pressure throughout the reservoir travel time. The rate of particle agglomeration increases as temperature is increased (Ghosh et al., 2006; Metin et al., 2010). Agglomeration also increases as pressure is increased (Ghosh et al., 2006). Reservoir temperature is at least 60°C on the NCS (Norwegian Petroleum Directorate, 2014a).

The reservoir travel time is a function of the distance between the injection and production wells and the injection velocity. Typical field injection velocities range from 1 ft/day ($\approx$ 0.30 m/day) (McPhee and Arthur, 1994) to 3 ft/day ($\approx$0.91 m/day) (Zhang and Morrow, 2006). This means that the water and oil move through the reservoir at a rate of at least 110 m/year. Given a distance of 100 to 300 m between the injection and production wells offshore (Han et al., 1999), reservoir travel time can be one to three years.

The effect of ionic strength, temperature and pressure on nanofluid stabilization can be measured by analyzing the particle size distribution (PSD) in the fluid. The PSD should be measured over time to determine the nanofluid's durability. The most reliable methods for detecting particle agglomeration are light scattering techniques, which non-invasively measure the PSD in a fluid (Moore et al., 2015).

2.3.2.2 Particle stabilization theory

Nanoparticle stability in an aqueous solution is dependent upon the balance between inter-particle attractive and repulsive forces. Derjaguin-Landau-Verwey-Overbeak (DLVO) theory (Derjaguin and Landau, 1941; Verwey et al., 1948) describes the short-range thermodynamic interactions that dictate whether colliding particles are attached to or repelled from each other (Hotze et al., 2010). DLVO theory states that only two forces determine the interaction between two particles: the attractive van der Waals force (V_A) and the electrostatic repulsion (V_R) (Hotze et al., 2010). The net interaction energy (V_T) between two particles is a sum of V_A and V_R. This

potential energy, or interaction potential, between two particles is a function of their distance from each other.

The van der Waals dispersion force arises from the interactions between permanent, instantaneous or induced dipoles (Moore et al., 2015). These interactions are typically attractive for particles in aqueous environments and are unaffected by changes in solution chemistry (Chen et al., 2010). The van der Waals forces are primarily active from a distance of 10 nm and less (Sparreboom et al., 2009).

The electrostatic repulsion force is a function of the nanoparticles' surface charge and the ionic strength of the surrounding fluid (Hotze et al., 2010). It is in effect about as far as the particle's electrical double layer (EDL) extends, which is typically from 1 to 100 nm (Eijkel and Berg, 2005). Because the EDL, and hence V_R, is strongly affected by solution chemistry, it is explained in more detail below:

The silica nanoparticles used in this thesis have a negatively charged surface. The positively charged ions in the dispersing solution are then called *counter-ions*, while the negatively charged ions in the dispersing solution are called *simil-ions*. Each nanoparticle will have a dense layer of counter-ions on its surface due to its counter-charge attraction. This dense layer of counter-ions is called the Stern layer as depicted in Figure 2-5 (Moore et al., 2015). The Stern layer would be a thicker layer of counter-ions if not for Brownian motion, which partially overcomes the electrostatic attractions and causes the formation of a diffuse layer of counter-ions. The counter-ions therefore decrease in occurrence as a function of increased distance from the nanoparticle. This outer cloud of ions, where the counter-ions still outnumber the simil-ions, is called the Gouy-Chapman layer (or simply the diffuse layer). It extends to some finite distance where electro-neutrality is reached (Faust and Aly, 1998). The potential gradient over the diffuse layer is called the zeta potential. The EDL describes both the Stern layer and the electrically-charged diffuse layer.
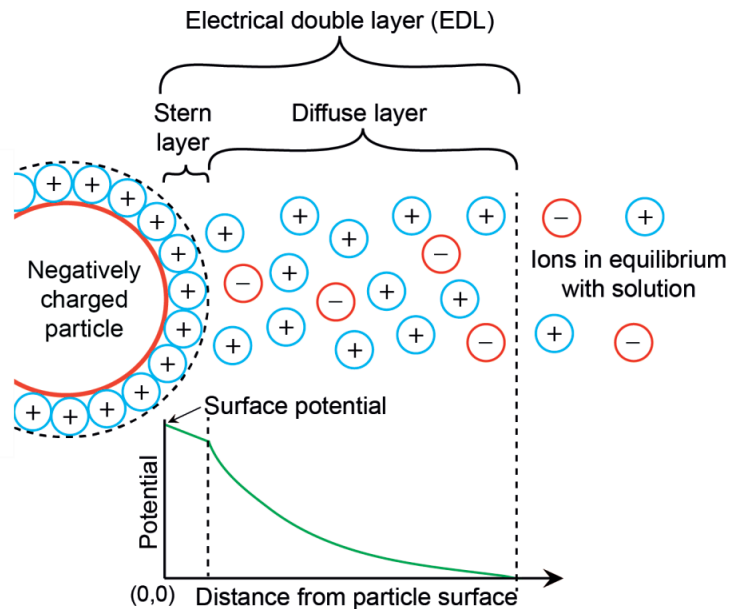
Figure 2-5. Illustration of the electrical double layer (EDL). Figure modified from Malvern Instruments (2017).

The larger the EDL, the larger the "buffer" zone by which the nanoparticles maintain a distance from each other. The EDL can be modeled as a function of distance from the nanoparticle (Figure 2-6). For spherical nanoparticles in an aqueous solution, the EDL thickness (δ) can be calculated by the derivation of the Poisson-Boltzmann equation (refer to Faust and Aly, 1998).

The EDL can be compressed, or shortened, by increasing the ionic strength of the solution (Figure 2-6). This is done by increasing the concentration of ions in the solution or by adding ions with higher valence numbers, such as divalent and trivalent ions, to the solution. The potential in the EDL decreases as a function of $\exp(-y/\lambda)$, where y is the distance from the particle and λ is the Debye screening length. The Debye screening length is inversely proportional to the square root of the ionic strength (Sparreboom et al., 2009). Therefore, an increase in the ionic concentration of the solution will result in a higher propensity of nanoparticle agglomeration (Cebrián et al., 2011).
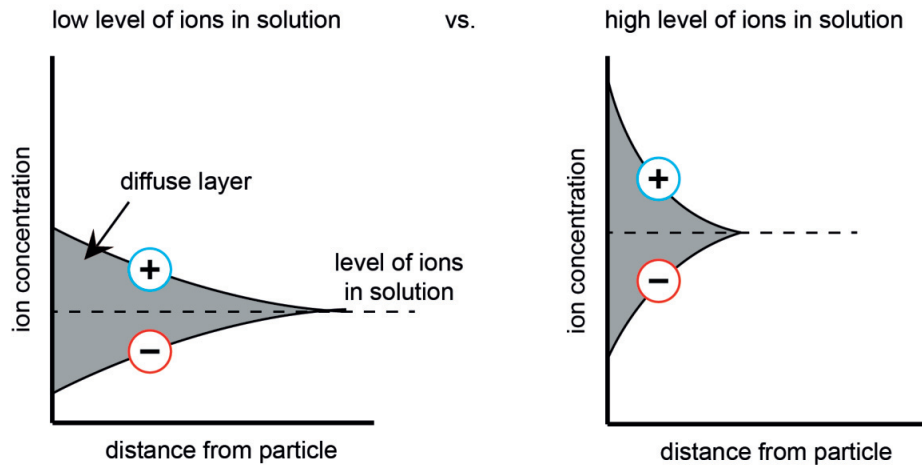
Figure 2-6. The variation of ion density in the diffuse layer (outer part of the EDL). When more ions are in the solution, the point of ionic equilibrium is reached as a shorter distance from the particle surface. The shaded area represents the net charge density of the diffuse layer. Figure modified from Ravina and Moramarco (1993).

Returning to DLVO theory, the net interaction energy between two particles can be plotted as the sum of the van der Waals attraction and electrostatic repulsion (Figure 2-7). The positive area under the curve is the energy barrier that the particles need to overcome in order to agglomerate. If their net attraction manages to overcome the energy barrier, it enters the energy trap where the particles are then agglomerated. The higher the energy barrier, the more resistant the particles are to agglomeration. This is because more energy is needed for the particles to physically approach each other and enter the energy trap. If the EDL is compressed, V_R decreases, causing a decrease in the energy barrier. Therefore, increasing the ionic strength leads to increased nanoparticle agglomeration. This has been confirmed experimentally by Metin et al. (2010), who concluded that amongst Na^+, Ca^{2+}, Ba^{2+} and Mg^{2+} cations, the sodium had a much smaller destabilizing effect for silica nanoparticles than the divalent cations. They also concluded that ionic strength affects silica nanoparticle stability more than changes in pH (Metin et al., 2010).
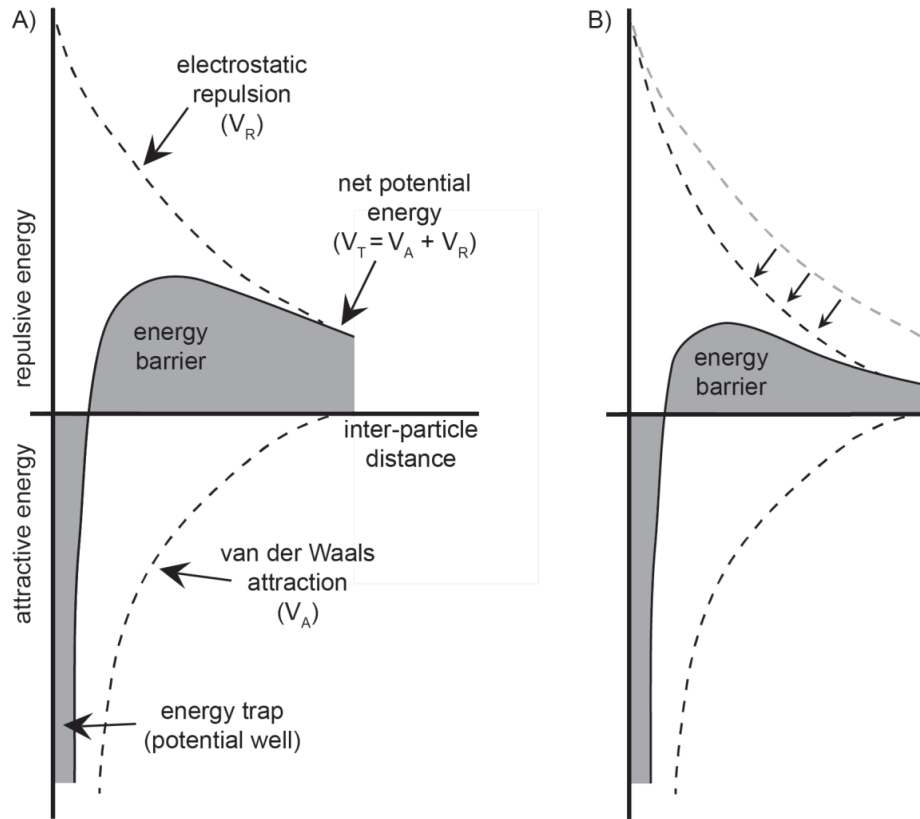
Figure 2-7. Depiction of DLVO theory. A) The net interaction (V_T) of two particles is a sum of the van der Waals attraction (V_A) and the electrostatic repulsion (V_R). B) Compression of the EDL decreases V_R and lowers the energy barrier. This results in a lower threshold for agglomeration. Figure modified from Ravina and Moramarco (1993) and Hotze et al. (2010).

Because there are many more inter-particle forces than van der Waals and electrostatic repulsion, additions to the DLVO theory have been made based upon the types of particles considered. These additional force interactions include magnetic attraction, polar interactions, osmotic repulsion, elastic-steric repulsion and bridging attraction (see Hotze et al., 2010, for an overview). When one or more of these forces is considered with the classic DLVO theory, it is called the extended DLVO theory or XDLVO (Hotze et al., 2010). The polar force of hydrophobic attraction would be of most interest for this thesis, as it has an interaction range of

27

up to 100 nm and is much stronger than van der Waals attraction at short distances (Sparreboom et al., 2009).

In addition to not considering all relevant inter-particle forces, the nanoparticle dispersions in this thesis violate some assumptions upon which the DLVO theory is based. The DLVO theory was developed for larger colloidal particles with easily defined geometries (spheres). At very small diameters, spherical nanoparticles have curvature that is too great to assume that a flat surface tangential to the sphere covers a substantial area of the particle (Hotze et al., 2010). Anisometric geometries, such as those exhibited by the dendritic nano-structured particles, bring about complexities in modeling intermolecular forces. The orientation of the particle and distance to protruding limbs will render the linear force calculation between two distinct particles incomplete and thus invalid. The reader is directed to the article by Hotze et al. (2010) for a detailed review of nanoparticle aggregation and conflicts with DLVO theory. Additionally, Wang et al. (2012) show how DLVO calculations fail to adequately predict and describe experimentally-observed retention of 8 nm silica nanoparticles in porous media.

2.3.2.3 Improving nanofluid stability

The simplest way to improve nanoparticle stability is to decrease the ionic strength of the aqueous solution. However, because an objective of this thesis is to disperse the nanoparticles in sea water, stabilization efforts must focus on the nanoparticles themselves if unstable nanofluids are identified.

Steric stabilization is the most common approach for improving particle stability in suspension (Moore et al., 2015). It occurs when hydrophilic macromolecules coat the nanoparticles, shielding the nanoparticles from interaction (Cebrián et al., 2011; Moore et al., 2015). Thus, applying a neutral polymer, such as polyethylene glycol (PEG) or polyvinylpurrolidone (PVP), or a non-ionic surfactant has been shown to improve particle stability (see the review by Moore et al., 2015).

2.3.3 Oil production

It is difficult to determine how effective silica nanoparticles are for enhancing oil recovery due to the variability of core flooding results reported in the literature. That is why it is a focus in this thesis. In some studies, little to no oil is produced within the first pore volume of nanofluid flooding as tertiary flooding (Alomair et al., 2014; Hendraningrat et al., 2013b, 2013d; Youssif et al., 2017). Skauge et al. (2010) showed that their nano-sized silica particles propagated through water-wet Berea sandstone cores but did not mobilize oil. Conversely, some studies have produced an oil recovery of greater than 10% OOIP (Roustaei and Bagherzadeh, 2015), with El-Diasty (2015) even reporting an oil recovery of greater than 30% OOIP for one of their silica nanoparticle systems.

The challenge with comparing the experimental studies that have investigated the potential of silica nanoparticles for EOR is that no two research groups use the same materials. The same nanoparticles are rarely used, and many have their own in-house blend (Ragab et al., 2015; Tarek and El-Banbi, 2015). The large variation in the fluid composition used for nanoparticle dispersion further complicates comparisons. The dispersing fluid composition ranges from distilled water (Ogolo et al., 2012) to 5 wt% NaCl (Roustaei and Bagherzadeh, 2015) to filtered formation water (Alomair et al., 2014). Stabilizers such as PVP have also been added to the nanofluid (Hendraningrat and Zhang, 2015).

The nanoparticle concentration is often a varied parameter within the study itself and varies from 0.01 wt% to at least 3 wt% (El-Diasty, 2015). Nanoparticle concentration tests produce different results depending on the silica nanoparticle in use. For example, Youssif et al. (2017) concluded that 0.1 wt% was the optimum concentration for EOR when compared with 0.01, 0.05, 0.2 and 0.5 wt%. Conversely, Hendraningrat et al. (2013c) concluded that 0.05 wt% was the optimum concentration for EOR when compared with a range of concentrations from 0.01 to 0.10 wt%. Both studies used 3 wt% NaCl as the dispersing fluid, sandstone cores for the porous media, and a light crude oil.

The oil used for the experiments also varies – anything from an unspecified mineral oil (El-Diasty, 2015; Tarek and El-Banbi, 2015) to a heavy crude oil (Alomair et al., 2014; Cheraghian, 2016) has been used. The composition of the oil will affect how the nanofluid reacts with the residual oil.

The type of porous media varies not just in mineralogy but also in physical properties such as size, porosity and permeability. Tests conducted with sandstone cores are the focus of this thesis, but nanofluid flooding in carbonate cores has been shown to produce immediate and significant (> 9 % OOIP) oil recovery using silica nanoparticles (Roustaei and Bagherzadeh, 2015).

The core flooding injection scheme itself varies in injection rate, volume of fluids flooded and water flooding procedure. Many studies conduct nanofluid flooding without prior water flooding (a process that will be called secondary flooding throughout this thesis). Most of these studies using secondary nanofluid flooding schemes compare the total nanofluid flooding oil recovery to only one water flooding test (Alomair et al., 2014; El-Diasty, 2015; Ogolo et al., 2012; Ragab et al., 2015). Those studies cannot be directly compared to the results from core flooding tests where nanofluid flooding has been conducted after water flooding (a process called tertiary flooding throughout this thesis).

As can be seen, the large variation in many variables makes it nearly impossible to directly compare core flooding results from different research groups. In addition, most of these studies are published in Society of Petroleum Engineers (SPE) conference papers, where typically only the abstract is reviewed and approved. This is why many of the studies have missing information that is critical for comparison such as the composition of the dispersing fluid (El-Diasty, 2015), graphs of the oil recovery curves (Ogolo et al., 2012) or injection rate (Ragab and Hannora, 2015; Ragab et al., 2015).

The core flooding tests that have specifically used silica nanoparticles without any additives have been gathered from literature. Literature selection criteria also included using sandstone (sst) or sand as the porous medium and an aqueous fluid as the nanofluid dispersing phase. Detailed information and references for the core flooding tests can be found in Appendix A. The results are divided into those that investigated nanofluid flooding as a secondary injection scheme (Figure 2-8) and those that used a tertiary flooding scheme (Figure 2-9). The oil recovery (calculated as % OOIP) is compared to the nanoparticle size and concentration. A negative oil recovery for some secondary core flooding tests is a result of the nanofluid flooding producing a smaller total oil recovery that the water flooding test with which it is compared. Some tests, such as those from El-Diasty (2015) and Ragab and Hannora (2015), display a

correlation between nanoparticle size and secondary oil recovery, where smaller nanoparticles produce more oil (Figure 2-8A). There is otherwise no clear correlation between oil recovery and nanoparticle size or oil recovery and nanoparticle concentration when comparing literature studies without considering other variables such as flooding scheme and oil type. For example, Hendraningrat et al. (2013c) observed a correlation between nanoparticle concentration and oil recovery that is not visible in Figure 2-9B. Additional tests by Skauge et al. (2010) showed that no oil was produced when silica nanoparticles dispersed in 0.5 wt% NaCl were flooded through Berea sandstone cores as a tertiary process.
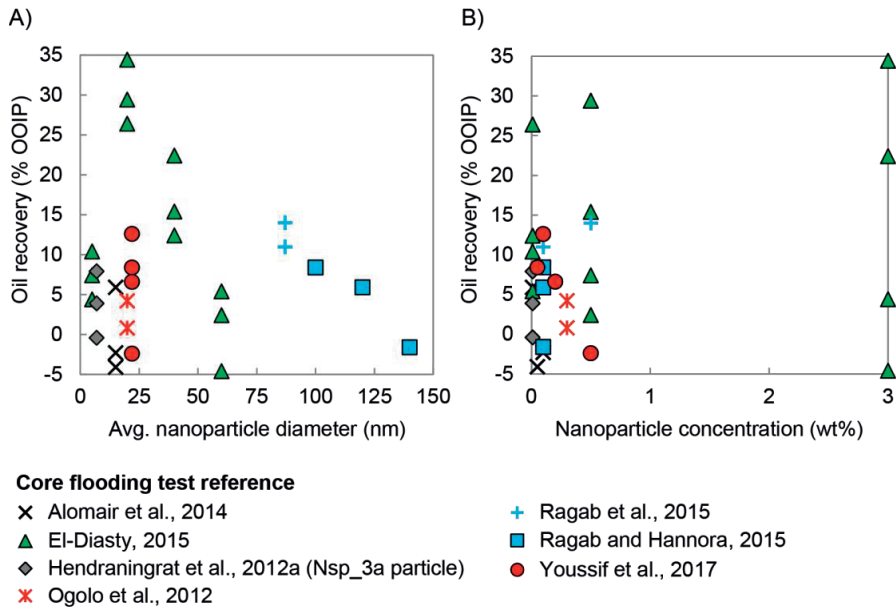
Figure 2-8. Comparison of secondary nanofluid flooding tests from literature. A) Oil recovery vs. nanoparticle diameter. B) Oil recovery vs. nanoparticle concentration in the nanofluid.
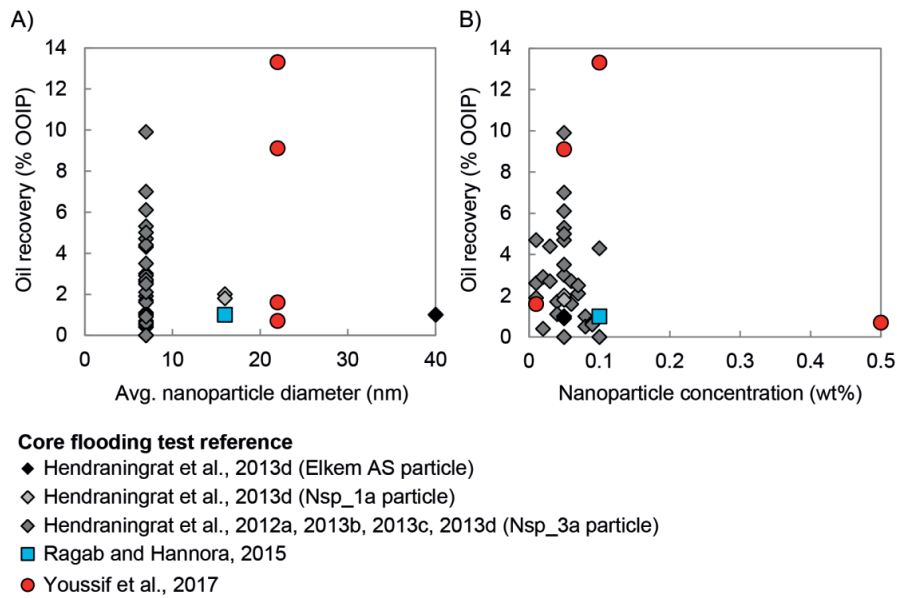
Figure 2-9. Comparison of tertiary nanofluid flooding tests from literature. A) Oil recovery vs. nanoparticle diameter. B) Oil recovery vs. nanoparticle concentration in the nanofluid.

2.3.4 EOR mechanisms

The goal of nanoparticle EOR is primarily focused on producing immobile oil from the reservoir. This is done by mobilizing and coalescing oil ganglia. The EOR mechanisms contributing to the success of chemical EOR flooding can be divided into the following classifications: fluid-fluid interactions (interfacial tension reduction and in-situ emulsification), fluid-rock interactions (wettability alteration) and mechanical displacement (improved sweep efficiency). These mechanisms are summarized in Table 2.2.

Table 2.2. Summary of EOR mechanisms.

EOR mechanism	How it improves oil recovery
Interfacial tension (IFT)	A reduction in IFT reduces capillary trapping, allowing the oil to flow through the reservoir more easily. It needs to be in the order of 10^{-3} mN/m to significantly contribute to EOR (Sheng, 2015).
In-situ emulsification	Emulsification leads to an increase in viscosity for the displacing phase (oil-in-water emulsion) or a decrease in viscosity for the displaced phase (water-in-oil emulsion). Both scenarios decrease the mobility ratio, which means that the injected water is displacing the oil in the reservoir more efficiently.
Wettability alteration	Wettability alteration towards a water-wet state causes oil droplets to be released from the rock surface.
Mechanical displacement	When highly permeable pore channels are blocked by particles or gels, microscopic flow diversion occurs, displacing oil from channels not previously penetrated by water flooding.

In addition to EOR mechanisms, it is important to investigate nanoparticle transport. The adsorptive behavior of the nanoparticles is important to determine the necessary injection concentration to ensure that enough particles propagate throughout the flooding section (T. Zhang et al., 2014). Increasing the nanoparticle concentration or decreasing the injection rate leads to more nanoparticle adsorption in porous media (T. Zhang et al., 2014).

2.3.4.1 Fluid – fluid interactions

The primary fluid-fluid interaction leading to increased oil recovery is interfacial tension reduction. Spontaneous, in-situ emulsion generation is a rarer phenomenon that also exploits fluid-fluid interaction for EOR.

Theory. Interfacial tension (IFT or σ) is the boundary force between two immiscible fluids, such as water and oil (Dandekar, 2013). IFT is defined as energy per unit area (J/m^2), but it is most commonly expressed as force per unit length (N/m). At the small interfacial tension values

measured in oil-water systems, interfacial tension is measured as mN/m, which is equivalent to dynes/cm (Dandekar, 2013).

Interfacial tension for traditional crude oil / sea water systems is typically between 20 to 30 mN/m (Dandekar, 2013; Sheng, 2015). If the interfacial tension is decreased to the order of 10^{-3} mN/m, the capillary number can be increased by 1000 times (Sheng, 2015). Oil droplets can then flow through the pore network easier because of the reduction in capillary trapping (Sheng, 2015). A reduction in interfacial tension also allows the droplets to deform more readily, allowing them to be pushed through narrow pore throats. However, this typically must be accompanied with an increase in the viscosity of the displacing fluid for production to occur.

Interfacial tension can be decreased by adding molecules such as surfactants to the aqueous phase. Surfactants have a hydrophilic "head" and a hydrophobic "tail" (Frijters et al., 2012). This causes them to be attracted to the water-oil interface and exist in both phases simultaneously (Figure 2-10). This accumulation at the interface lowers interfacial tension by decreasing the force imbalance at the interface (Frijters et al., 2012). If nanoparticles are constructed as Janus particles with shells that are half hydrophilic and half hydrophobic, then they also can decrease the interfacial tension (Binks and Fletcher, 2001).
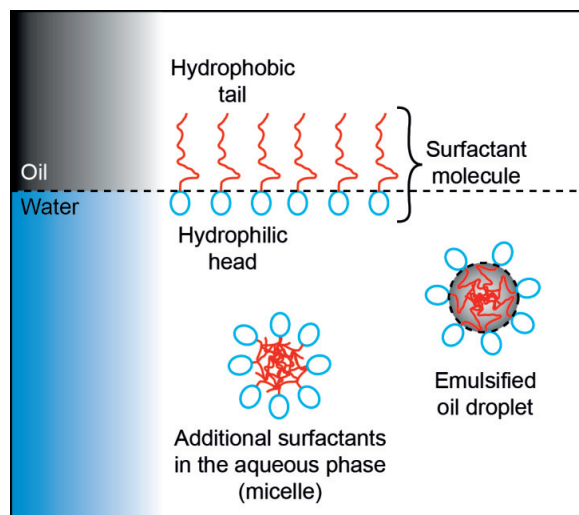
Figure 2-10. Surfactants straddle the oil-water interface, thereby reducing interfacial tension. Additional surfactant micelles are in the aqueous phase and can help stablize emulsified oil droplets. Illustration modified from Eykens et al. (2017).

The wettability or hydrophilicity of silica nanoparticles is dependent upon the amount of silanol (SiOH) groups at the surface (Binks and Lumsdon, 2000). If the number of surface silanol groups are reduced, the surface becomes less hydrophilic. The particle surface is important because particles with intermediate hydrophobicity stabilize emulsions, while particles with strong hydrophilicity or hydrophilicity result in unstable emulsions which coalesce (Binks and Lumsdon, 2000). Specifically in crude oil systems, particles can react with asphaltenes in the oil phase, thereby stabilizing oil-in-water emulsions (Sullivan and Kilpatrick, 2002). Hannisdal et al. (2006) showed that asphaltenes, and to a lesser extent resins, in the crude oil contribute to particle stabilization of oil in water emulsions due to their reactivity with the particles at the interface. Emulsion stability has been shown to increase with increasing particle concentration and increasing asphaltene-particle interaction (Sullivan and Kilpatrick, 2002). The droplet size decreases with increasing nanoparticle concentration (Zhang et al., 2010).

IFT measurements. The pendant drop method is the most common way to measure interfacial tension in the petroleum industry (McPhee et al., 2015). It evaluates the drop shape using the Young-Laplace equation and then incorporates the density of the phases to calculate the IFT (McPhee et al., 2015). The spinning-drop tensiometer is another drop shape analysis method that has recently gained popularity due to its ability to measure ultra-low IFT values. However, if particles are in the solution, as is the case with nanofluids, the rotational speeds could centrifuge out the particles. This means they would not be allowed to interact with the oil interface. Additional IFT methods employing force tensiometry include the Du Noüy ring and Wilhelmy plate (McPhee et al., 2015, presents the advantages and disadvantages of using these methods).

IFT literature results. The interfacial tension experiments in literature can be summarized thus: there is a reduction in interfacial tension when nanoparticles are added to the solution (Alomair et al., 2014; Ragab et al., 2015; Roustaei and Bagherzadeh, 2015), but the reduction is not on the order of magnitude at which surfactants alter the system (10^{-3} mN/m) (Sheng, 2015).

Three of the nanoparticles investigated in this thesis were previously tested for IFT at NTNU as nanofluids produced with 3 wt% NaCl as the dispersing fluid instead of SSW. These three nanoparticles are two nano-structured particles (Nsp_1a and Nsp_3a) and one colloidal nanoparticle (Cnp_1). All experiments in the literature were conducted at ambient conditions unless otherwise specified (Table 2.3). Three different oils were tested: an unspecified synthetic oil and two light crude oils from the North Sea with different compositions (crude oil 1 and 2). These are different from the medium crude oil tested in this thesis. The base system values refer to the interfacial tension between the oil phase and the 3 wt% NaCl without nanoparticles. Note that none of the articles replicated the IFT tests, so there are no error margins available. The tests conducted with the pendant drop method have IFT values that are significantly greater than the tests conducted with the spinning drop method. No explanation was given in the articles for this.

Table 2.3. Summary of interfacial tension experiments conducted at NTNU with silica nanoparticles dispersed in 3 wt% NaCl. IFT tests conducted without nanoparticles in the aqueous phase (base system) are highlighted in blue.

Nanoparticle type	Method	Oil phase	Temp. (°C)	Nanoparticle concentration (wt%)	IFT (mN/m)
Nsp_1a[1]	Pendent drop	Synthetic oil	22	0	65.41
				0.1	51.68
				0.5	31.03
				1.0	27.67
Nsp_3a[2]	Spinning drop	Synthetic oil	22	0	14.7
				0.01	9.3
				0.05	5.2
Nsp_3a[3]	Spinning drop	Crude oil 1	22	0	19.2
				0.01	10.9
				0.05	7.9*
Nsp_3a[4]	Spinning drop	Crude oil 1	22	0	19.2
				0.05	16.9*
			35	0	12.57
				0.05	15.60
			50	0	12.14
				0.05	12.80
Nsp_3a + PVP[5]	Spinning drop	Crude oil 1	22	0 + PVP‡	15.67
				0.05 + PVP‡	14.5†
				0.1 + PVP‡	15†
Nsp_3a[6]	Spinning drop	Crude oil 2	22	0	20†
				0.05	12†
				0.1	10†
Cnp_3[6]	Spinning drop	Crude oil 2	22	0.05	4.5†
				0.1	3†
				0.5	1†

*These two tests use the same materials and methods but produced different results. An explanation was not provided in the literature.
†Actual values not presented in literature. Values displayed here are interpretations from graphs.
‡ PVP (polyvinylpurrolidone) was added to the nanofluid as a stabilizer.

[1] Hendraningrat et al. (2012b)
[2] Hendraningrat et al. (2012a)
[3] Hendraningrat et al. (2013e)
[4] Hendraningrat and Torsæter (2014a)
[5] Hendraningrat and Torsæter (2014b)
[6] Li and Torsæter (2014)

All the systems except the ones with PVP as a stabilizer show that IFT decreases with increasing nanoparticle concentration at ambient temperature. IFT was shown to decrease with increasing temperature (Hendraningrat and Torsæter, 2014a). The composition of the oil phase affects the

IFT results. The colloidal nanoparticle (Cnp_1) lowers IFT more than the nano-structured particles (Nsp_1a and Nsp_3a) and is thus the most promising for EOR. However, the IFT values from the colloidal nanoparticle tests are not in the 10^{-3} mN/m range.

Emulsion theory. In-situ emulsification decreases the viscosity of the oil phase for water-in-oil (w/o) emulsions or increases the viscosity of the aqueous phase for oil-in-water (o/w) emulsions. Either of these emulsion conditions leads to a more favorable mobility ratio. Emulsions can be induced via chemical components such as certain surfactants or nanoparticles. Emulsification is dependent upon the shear rate. Droplets in the emulsion coalesce if they are not thermodynamically stable. Emulsions generated in-situ must be able to be easily separated in production facilities. If emulsification is occurring within the core, large emulsion droplets can block pore throats, resulting in entrainment and differential pressure increase (Rezaei and Firoozabadi, 2014).

In-situ emulsion generation can be evaluated by a qualitative analysis of the core flooding effluent. There should also be an associated increase in differential pressure compared to a system without emulsion generation because of the viscosity increase and effective permeability decrease of the aqueous phase. Micromodel tests can also provide visual evidence for in-situ emulsion generation.

Methods for testing emulsions. Micromodels are used to better understand the flow paths and oil saturation changes from the injection of nanofluids. Micromodel and emulsion studies can be conducted to answer the following questions:

- Where does the oil saturation change during nanofluid flooding? (quantify and define)
- How and where does emulsion generation begin to form?

Other groups have investigated the chemical properties of nanoparticles and their effect on emulsion generation and stabilization. In porous media, micro-emulsions form at the oil/water interface, while macro-emulsions form by snap-off or coalescence of micro-emulsions (Rezaei

and Firoozabadi, 2014). The intensity of oil and water mixing in the core is higher at higher injection rates, potentially creating more opportunities for emulsions to occur (Rezaei and Firoozabadi, 2014).

Emulsion literature results. Yuan et al. (2015) conducted experiments in a high temperature and high saline system that showed a positive correlation between surfactant concentration and emulsification strength. They concluded that a balance between interfacial tension reduction and   emulsification strength is important for sustainable oil production.

Wasan et al. (1978) conducted core flooding tests to investigate the recovery factor of emulsion systems. The highest tertiary recovery was achieved for emulsion systems having the fastest coalescence rates (in other words, the least stable emulsions). They concluded that systems with relatively stable emulsions have poor coalescence rates and thus poor oil recovery.

In-situ emulsion generation has been shown with micromodel experiments conducted at NTNU. Li et al. (2013) tested Nsp_3a in water-wet glass micromodels at 0.01, 0.5 and 0.1 wt% with crude oil 2. The procedure was to water flood at 0.1 ml/min until no oil was produced, then increase the injection rate to 0.2 ml/min until no additional oil was produced. This was followed by nanofluid flooding at 0.1 ml/min until no oil was produced followed by injection at 0.2 ml/min until S_{or} was reached. Flooding took place as long as there was no visible change in oil saturation. They concluded that at the low nanoparticle concentration (0.01 wt%), the injection rate was the primary factor affecting the recovery factor. The differential pressure across the micromodel increased during the nanoparticle injection for all three concentrations. The rate of increase and final differential pressure was positively correlated with the nanoparticle concentration. They did not calculate the final saturation distributions, but they did present pictures of "selected areas of interest" to show how the oil droplets moved over time. The 0.1 wt% nanofluid caused the oil to break into smaller, rounded droplets. This was interpreted as o/w emulsion generation. This is shown in Figure 2-11, but note that no physical scale was given in the article and the sample picture location on the micromodel was not identified.
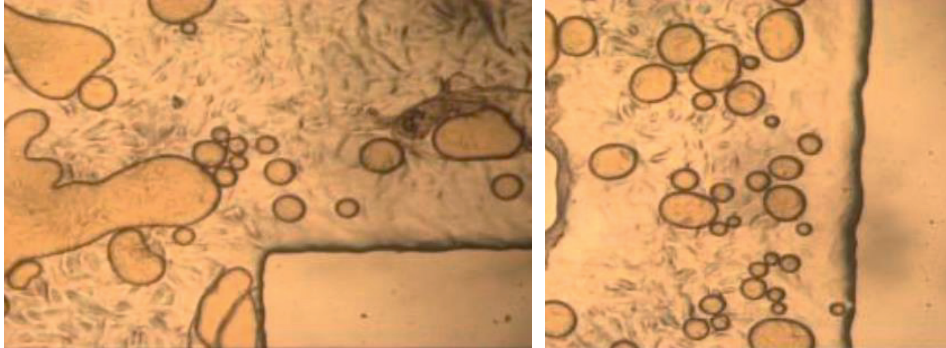
Figure 2-11. Light crude oil (darker droplets) in 0.1 wt% Nsp_3a nanofluid in a water-wet, glass micromodel. These images were interpreted as oil-in-water (o/w) emulsions generated during nanofluid flooding. Figure from Li et al. (2013).

Li and Torsæter (2014) investigated Nsp_3a at 0.05 and 0.1 wt% and a colloidal nanoparticle at 0.05, 0.1 and 0.5 wt% dispersed in 3 wt% NaCl brine. Crude oil 2 was used. Water flooding was conducted at 0.02 ml/min and then 0.04 ml/min until no more oil was produced. Nanofluid flooding was conducted using the same procedure. They did not quantify the volume of oil produced. Their conclusions were that all scenarios increase oil recovery. They conjectured that IFT reduction and emulsification generation were the EOR mechanisms for all systems. The Nsp_3a emulsions were o/w while the colloidal nanoparticle emulsions were w/o. They concluded that for both types of nanoparticles, the emulsions were formed in the 0.5 wt% concentrations at the 0.4 ml/min flow rate. However, there was no 0.5 wt% case for Nsp_3a. Additionally, two of the pictures they present to back-up the o/w emulsions for Nsp_3a appear to be the same pictures as presented in Li et al. (2013) for a 0.1 wt% system flooded at 0.1 and 0.2 ml/min.

2.3.4.2 Fluid – rock interactions

The primary fluid-rock interaction leading to increased oil recovery is wettability alteration, whose goal is typically to change the rock surface from an oil-wet state towards a neutral or water-wet state. It is also dependent upon the fluid-fluid interactions such as interfacial tension as shown below.

Wettability theory. Alteration towards the water-wet condition releases oil droplets and oil films from the rock surface. This leads to reduction in residual oil saturation (Sheng, 2015). Wettability alteration is typically targeted towards carbonate reservoirs, which are generally more oil-wet than siliceous reservoirs.

Wettability describes the forces that are active at the interface between the fluids and the rock surface. Wettability is the relative ability of a fluid to spread on a solid surface in the presence of another fluid (Dandekar, 2013). It affects the capillary pressure and relative permeability of the fluids in the reservoir. Young's equation (Eq. 2.9) describes the relationship between interfacial tensions and a contact angle resulting from mechanical equilibrium, where θ_{ow} is the oil-water contact angle measured in the aqueous phase, σ_{so} is the interfacial tension at the solid-oil interface, σ_{sw} is the interfacial tension at the solid-water interface and σ_{ow} is the interfacial tension at the oil-water interface (Figure 2-12):

$$\cos \theta_{ow} = \frac{\sigma_{so} - \sigma_{sw}}{\sigma_{ow}} \qquad \text{(Eq. 2.9)}$$
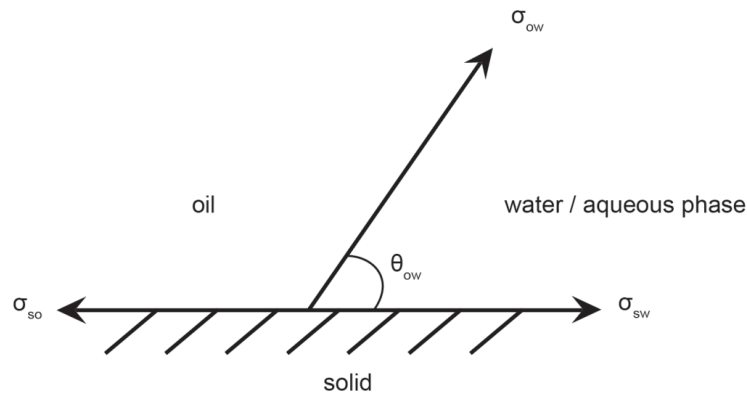
Figure 2-12. Relationship between the three interfacial tension forces. This results in the contact angle that described the wettability of the system. Illustration modified from Benner et al. (1938)

Wettability in a petroleum reservoir is an equilibrium condition between the water, oil and rock surface. Therefore, the water chemistry, oil composition and mineralogy need to be considered to understand the natural wettability condition. Buckley et al. (1998) concluded that there are four main categories of crude oil / brine / rock interactions. They are polar interactions, surface precipitation, acid/base interactions and ion-binding. The mineralogy of the reservoir affects the wettability. The quartz in sandstone is preferentially water-wet because it is negatively charged, while limestone has a net positive charge and is preferentially oil-wet (Kanicky et al., 2001).

The two wettability end-points are oil-wet and water-wet systems. In between is the mixed-wet condition and occurs when some rock surfaces are water-wet while the other rock surfaces are oil-wet. This arises when the mineralogy is diverse i.e. a sandstone containing water-wet quartz grains and oil-wet clay particles. Neutral wet minerals and systems are those that have no preference to water or oil coatings.

The wettability concept affects the saturation distribution in the reservoir. It also affects how water will displace oil during water flooding (Figure 2-13). Strongly water-wet reservoirs leave behind oil ganglia in pore spaces, while strongly oil-wet reservoirs leave behind oil films on the rock grains.
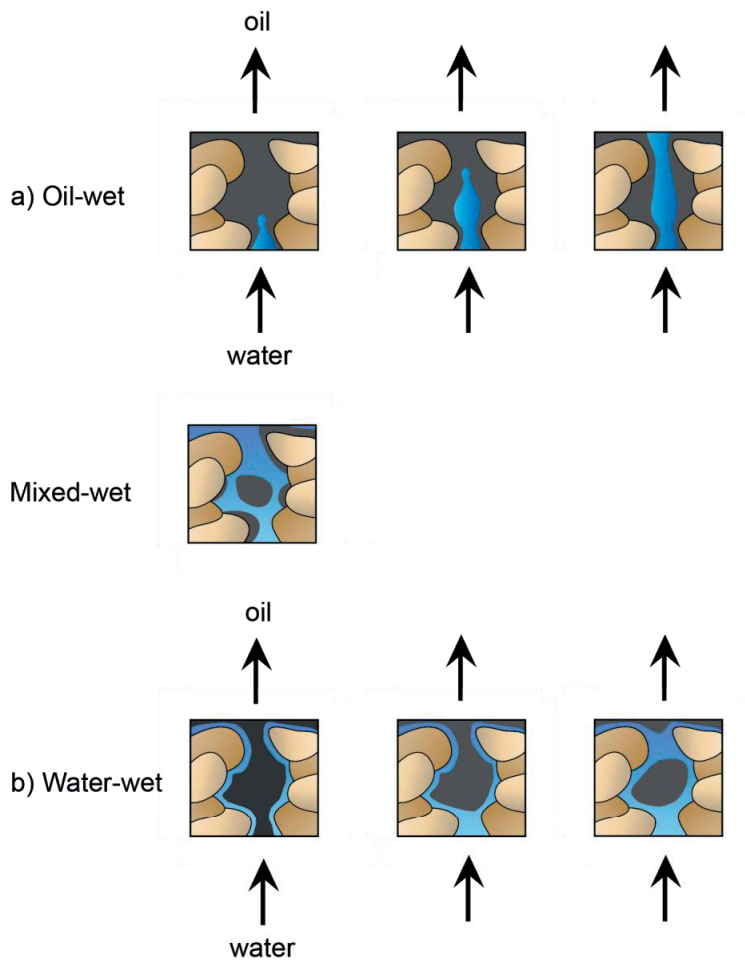
Figure 2-13. Illustration of wetting regimes in the reservoir. Water displacing oil from a pore throat during water flooding for a) a strongly oil-wet reservoir and b) a strongly water-wet reservoir. Figure modified from Abdallah et al. (2007) and Raza et al. (1968).

Wettability alteration can be performed by adding components to the aqueous phase that preferentially coat the rock surfaces. This allows the oil droplets to be released from the rock. If the adsorption is not easily reversible, the chemical forms a coating that prevents additional oil droplets from adhering to the rock. If the released oil droplets constantly adhere to fresh oil-wet surfaces downstream, a lot of energy would be required to continuously dislodge the droplet all the way to the production well.

43

Contact angle measurements. Wettability can quickly be determined for a solid plate using the contact angle method. This is done by placing a droplet of one type of immiscible liquid (typically oil) on a polished rock surface immersed in the other immiscible liquid (typically the aqueous fluid). The contact angle is always measured in the aqueous phase Figure 2-14. A contact angle of 0° means that the system is completely water-wet. A contact angle of 180° means that the system is completely oil-wet. All systems fall between these two endpoints. If the contact angle is around 90°, the system is described as neutral-wet, meaning it has no preference as to whether it is coated with the oil or the aqueous phase. The contact angle can be measured over time to see how the EOR fluid reacts with the solid.
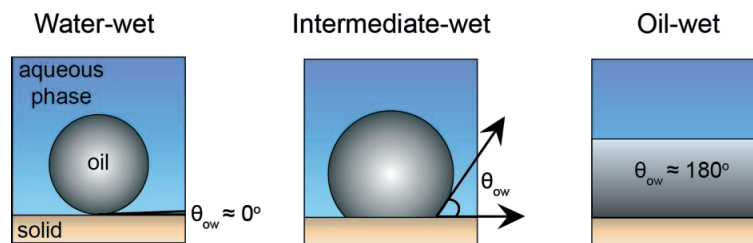
Figure 2-14. Wettability conditions and their associated contact angle value. Figure modified from Abdallah et al. (2007).

Wettability can be measured with an entire core plug by employing the Amott wettability test (Amott, 1959) or the U.S. Bureau of Mines (USBM) method (Donaldson et al., 1969). A petroleum system is typically described according to the wettability index (WI). For the Amott-Harvey index, I_{AH}, this is calculated as the difference between the wettability index to water, I_w, and the wettability index to oil, I_o. The water and oil wettability indexes are the ratios of the saturation changes during spontaneous imbibition or drainage to the total saturation change during both forced and spontaneous imbibition or drainage (Morrow, 1990). As shown in Table 2.4, Cuiec (1984) created a classification to describe the wettability of a system based on the wettability index.

Table 2.4. Wettability descriptions and their accompanying experimental values.

Wettability description	Water-wet	Intermediate wet			Oil-wet
		Slightly water-wet	Neutral	Slightly oil-wet	
Contact angle values[1]	0° to 60°	60° to 75°	75° to 105°	105° to 120°	120° to 180°
Wettability Index[2]	+0.3 to +1.0	+0.1 to +0.3	-0.1 to +0.1	-0.1 to -0.3	-0.3 to -1.0

[1]Values interpreted from Anderson (1987); [2]Values from Cuiec (1984)

Craig (1971) developed widely accepted general relationships between wettability and selected reservoir properties:

- Initial water saturation (S_{wi}) is typically greater than 20 to 25% for water-wet reservoirs and generally less than 15% (and frequently less than 10%) for oil-wet reservoirs.
- Oil and water relative permeabilities (k_{ro} and k_{rw}) are equal when the water saturation is greater than 50% for water-wet reservoirs or when the water saturation is less than 50% for oil-wet reservoirs.
- Relative permeability to water (k_{rw}) at maximum water saturation (equivalent to 1 - S_{or}) is typically less than 30% for water-wet reservoirs and greater than 50% for oil-wet reservoirs.

A trend has developed in the literature where the highest water flooding recovery factors occur at intermediate-wet and mixed-wet conditions (Morrow, 1990). Rao et al. (1992) investigated this relationship with a series of core flooding tests. The recovery factors decrease at the two extremes of the wettability index.

The relative permeability of a core can be determined and then correlated to its corresponding wettability following Craig's (1971) recommendations posed above.

Initial wettability of core plugs depends upon the saturation and distribution of the oil and brine phases during aging (Tang and Morrow, 1997). For systems with crude oil, wetting alteration factors including the temperature and duration of aging, brine, oil and rock compositions and initial water saturation (Buckley, 1995; Jadhunandan and Morrow, 1995; Tang and Morrow, 1997; Zhou et al., 1996).

Altering original core wettability by "aging". Crude oils can alter strongly water-wet core plugs, such as Berea sandstone, towards weakly water-wet or neutral wettability (Jia et al., 1991). To alter this initial wettability, the cores are saturated with crude oil and placed in an oven for a specified length of time to allow crude oil components to react with the mineral surface. This process is called "aging". Polar compounds adsorb unto the rock, exposing their hydrocarbon tail and therefore rendering the surface oil-wet (Anderson, 1986). The polar compounds and organic matter in the crude oil can alter wettability by adsorption and deposition, respectively (Anderson, 1986). Silica, the main component in the Berea sandstone core plugs, normally has a surface that is negatively charged and weakly acidic in water at a neutral pH (Anderson, 1986). Therefore, sandstone wettability will typically be more affected by organic bases (Anderson, 1986).

Aging for about six weeks at reservoir temperature is the most common method, as that is the length of time for wetting equilibrium to take place, although many tests have restored the wettability within one week of aging (see discussion by Anderson (1986)). Saturating the core directly with crude oil (no initial water saturation) can speed up the wettability equilibrium time because there are no water films that the polar components must diffuse across to reach the rock surface (Cuiec, 1977), although this approach is typically advised against because it is not representative of the fluid distribution in a reservoir (Anderson, 1986). However, having no initial water saturation in the core prior to aging ensures a consistent starting point when comparing different core flooding tests and was therefore used for all aged cores in this thesis. Relatively consistent initial water saturations can also be established by slowly controlling drainage with the porous plate method, but this takes many weeks or months and the equipment was not available for this thesis.

Literature results. The contact angle experiments from NTNU can be summarized thus: the addition of nanoparticles to the aqueous solution decreased the contact angle, rendering the solid more water-wet. This happened no matter the initial wettability or material of the solid, type of oil, type of base fluid, nanoparticle type or concentration or equilibrium time.

Hendraningrat et al., 2013e) measured the contact angle of Nsp_3a at 0.01, 0.05 and 0.1 wt% concentrations against a droplet of crude oil. A polished synthetic silica surface was used for

the solid. The base value was 54°. The contact angle decreased as nanoparticle concentration increased. The contact angle was 22° for the highest nanoparticle concentration of 0.1 wt%. Hendraningrat et al. (2013c) measured Nsp_3a at the remaining concentrations between 0.01 and 0.1 wt% at 0.01 increments. The results followed the trend where contact angle decreased with increased nanoparticle concentration. This suggests that the nanoparticles render the silica surface more water-wet. Hendraningrat et al. (2013d) tested Nsp_1a at 0.05 wt% and obtained a contact angle of 31.18°. This is similar to the contact angle for Nsp_3a at 0.05 wt%, which was 31°. Hendraningrat and Torsæter (2014a) measured the contact angle of Nsp_3a at 0.05 wt% in crude oil on both a water-wet and an oil-wet quartz plate. The nanoparticles decreased the contact angle for both scenarios. The water-wet case was decreased from 39° to 26°, and the oil-wet case was decreased from 131° to 112°.

(Li and Torsæter, 2015) conducted Amott tests using Nsp_3a and Cnp_3 in concentrations of 0.05 wt%, 0.2 wt% and 0.5 wt% in 3 wt% NaCl. The initial core plug condition was intermediate-wet (aged) Berea sandstone. They concluded that all nanofluids altered the wettability towards water-wet.

Contact angle measurements for carbonate systems show the nanofluid altering the system from strongly oil-wet to water-wet (Roustaei and Bagherzadeh, 2015). The greatest change in contact angle occurred with the highest concentration of nanoparticle tested (about 50° for 0.6 wt%). Roustaei and Bagherzadeh (2015) attribute this to adsorption of the hydrophilic nanoparticles on the carbonate surface.

Structural disjoining pressure. The structural disjoining pressure model presented by Wasan and Nikolov (2003) and further investigated by Chengara et al. (2004) has been cited as the primary recovery mechanism in many core flooding studies (see Bera and Belhaj, 2016; Hendraningrat et al., 2013d; McElfresh et al., 2012; Sun et al., 2017). It is presented here to explain the EOR mechanism of wettability alteration, especially towards the water-wet endpoint. However, this model has a major pitfall, which is discussed after the theoretical background.

The structural disjoining pressure theory results in oil production by improving the removal of discontinuous phases, such as crude oil, from the mineral surface. This is essentially an alteration of wettability. The triangular area where the aqueous solution is present in the three-phase contact zone is called the "wedge film". Nanoparticles diffuse into the wedge film and self-assemble (Wasan and Nikolov, 2003). Additional nanoparticles dispersed in the bulk aqueous solution will exert pressure on the wedge film due to electrostatic repulsion and Brownian motion (McElfresh et al., 2012). This causes an increase in the structural disjoining pressure that moves the oil-water interface in towards the center of the droplet, effectively "scraping" the oil from the substrate as shown in Figure 2-15 (Wasan and Nikolov, 2003).
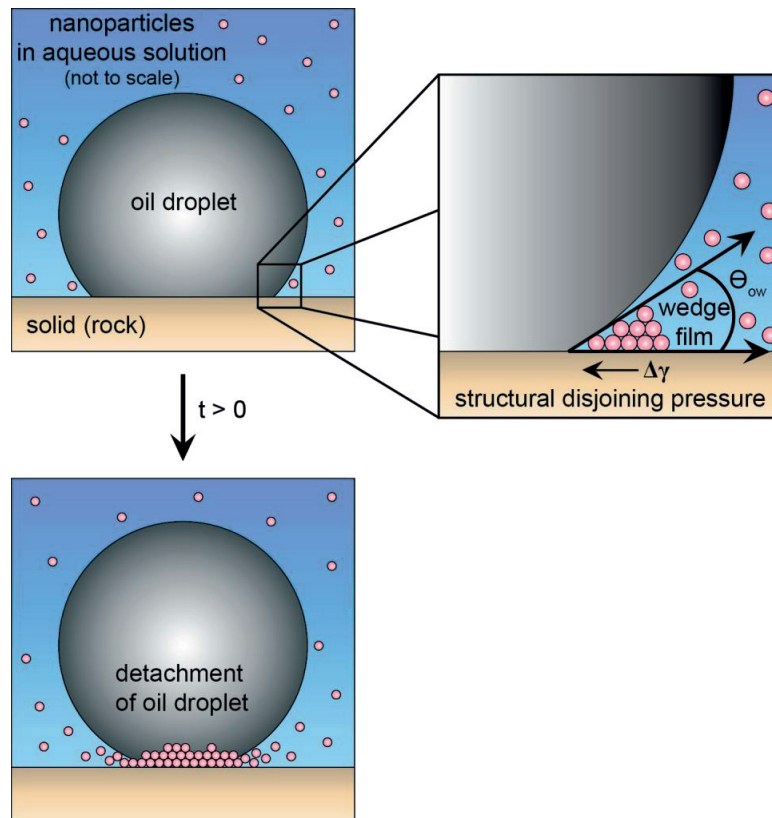
Figure 2-15. Illustration showing how disjoining pressure causes removal of the oil droplet in a three-phase contact region due to self-assembly of miscelles (nanoparticles) in the wedge film. Illustration modified from Wasan and Nikolov (2003).

Wasan and Nikolov (2003) conducted the experiments used to establish the application of structural disjoining pressure for the removal of oil droplets from a substrate. This was demonstrated experimentally with crude oil, Berea sandstone and two types of nanofluids by H. Zhang et al. (2014). Smaller particles will produce greater structural disjoining pressure than larger counterparts because of their ability to form ordered structures in the wedge film (Kondiparty et al., 2011). This is especially true at large contact angles (measured in the aqueous phase), where confinement size is too large for the particles to form ordered structures (Kondiparty et al., 2011). Spreading of the nanofluid film on a more oil-wet surface can be increased by decreasing particle size and increasing particle concentration (Kondiparty et al., 2011). With an increase in salt and subsequent shrinkage of the EDL, the magnitude of the structural disjoining pressure decreases (Kondiparty et al., 2011; Wasan and Nikolov, 2003). The structural disjoining pressure also decreases with an increase in nanoparticle polydispersity (Kondiparty et al., 2011).

What the petroleum literature fails to note is that the original proponents' use of the term "aqueous nanofluids" primarily refers to "micellar solution" as specifically noted in Chengara et al. (2004). To emphasize that the original structural disjoining pressure papers do not actually refer to solid nanoparticles, the following sentence from the conclusion by Chengara et al. (2004) is repeated here (emphasis added): "The disjoining pressure arises from the fact that *surfactant* used in the detergent formulation aggregate into *micelles* which then arrange themselves in well-ordered layers in the wedge between the oil drop and the [sic] surface." Additionally, the original experiments by Wasan and Nikolov (2003) were conducted with sodium lauryl sulphate, an anionic surfactant, in the aqueous phase. One experiment did not have surfactants in the aqueous phase but instead used charged latex spheres that were 1.01 μm in diameter, which is still much larger than the nanoparticles used in the core flooding literature. Additionally, this surfactant-free experiment was conducted for observing the structural disjoining pressure detachment of an air droplet, not an oil droplet, from a glass surface. Is it appropriate to extrapolate this theory for solid silica nanoparticles without surfactant additives? This is a question that is not thoroughly addressed in core flooding literature, and the effect of surface charges on the development of the structural disjoining pressure needs to be included in the discussion.

2.3.4.3 Mechanical displacement

The final mechanism discussed here is a more efficient mechanical displacement of the oil. Most of the petroleum literature on this topic focuses on polymer flooding, which increases the viscosity of the injection fluid, thereby creating a more favorable mobility ratio (Muggeridge et al., 2014). Polymer flooding does not necessarily lower the residual oil saturation when compared to traditional water flooding, but is instead used to improve macroscopic sweep efficiency and displace oil in low permeability zones (Huh and Pope, 2008).

Spildo et al. (2009) proposed that microscopic flow diversion can occur based on their experiments with colloidal dispersion gels. Microscopic flow diversion can be accomplished by physically rerouting the injection fluid into previously un-swept pore channels at the microscopic level. For water flooding additives that do not have the same shear-thinning properties of polymers and therefore do not significantly increase the injection fluid viscosity with increased shear rate, retention of the particles is what leads to blocking and subsequent rerouting. Retention occurs by either adsorption of the particles to the rock surface or particle entrapment (Huh et al., 1990). This microscopic diversion by retention will likely produce the most incremental oil from porous media with the most heterogeneous pore size distribution (Spildo et al., 2009). This is because the narrow throats can be plugged and then the injection fluid can be more easily rerouted through the larger channels outside the main flow path.

Particle entrapment occurs by s*training* if the particle diameter is larger than the pore diameter or by *log-jamming* if the particle diameter is smaller than the pore diameter (Bolandtaba et al., 2009). Straining therefore causes nanoparticles to physically plug the previously swept channels. Because nanoparticles, by definition, are less than 100 nm in diameter, and pore channels are typically at the micrometer range, this mechanism should not be contributing to EOR oil production except for very low permeability cores with especially narrow pore throats.

Log-jamming occurs when particles that would typically flow through a pore throat on their own accumulate at a pore throat entrance, thereby blocking the channel and forcing the injection fluid to find a new path. This occurs when nanoparticles agglomerate in-situ and therefore become larger than the pore itself. This can also occur because pore channel constriction will cause an increase in fluid velocity, whereby the water molecules could flow faster than the

nanoparticles in solution, resulting in an accumulation of the nanoparticles at the channel entrance (Sun et al., 2017). The log-jamming process is illustrated in Figure 2-16.
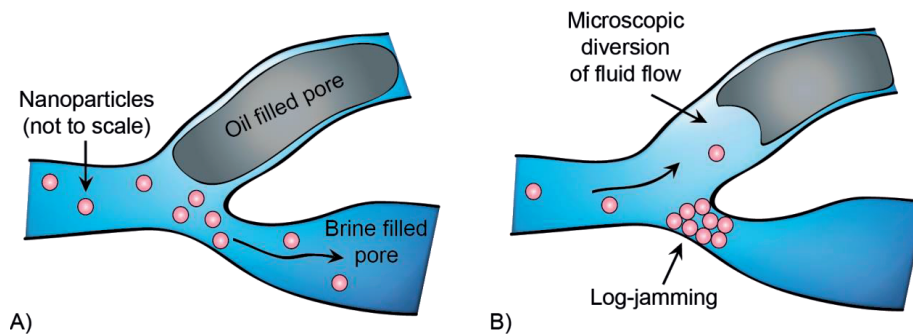
Figure 2-16. An interpretation of the log-jamming mechanical mechanism leading to microscopic diversion of the fluid flow and subsequent additional oil recovery. A) The nanofluid initially flows along the path of least resistance. Oil in untouched pores provides resistance to brine and nanofluid sweeps because of its higher fluid viscosity. B) Eventually, the silica particles may block a previously available pore throat. This is especially likely if there is a constriction in the pore diameter, causing the particles to crowd together as they attempt to squeeze through the opening. This could lead to nanoparticles creating a relatively impassable wall via a process called "log-jamming". This would cause the injected fluid to be diverted to the other pore throats. The increase in pressure as a result of decreased permeability would allow the fluid to overcome the force needed to mobilize the viscous oil. Illustration inspired by work from Spildo et al. (2009).

This mechanical displacement mechanism can be indirectly evaluated by assessing core flooding data. If the differential pressure (dP) across the core plug is increasing throughout the EOR flooding, that insinuates blockage and rerouting in the pore network. This proposed conceptual model is an expansion on the dP discussion by Spildo et al. (2009):

The dP across a core plug is a function of the components in Darcy's Law such as injection rate, phase viscosities and permeability in an unsteady-state core flooding test, where one fluid is injected at a time. Residual oil saturation, which affects the relative permeabilities, and particle retention will also influence the dP. When water flooding is initiated, dP will increase until the water (injected phase) breaks through at the outlet (Spildo et al., 2009). After water breakthrough, dP will decrease as oil continues to be produced and the relative permeability to

water increases (Spildo et al., 2009). The dP will stabilize, or plateau, after oil production ceases and residual oil saturation is reached (Spildo et al., 2009). When the injection rate is increased, the dP will also increase. If additional oil is mobilized during the injection rate bump, the dP will exhibit a similar trend, where it decreases to a stabile value after oil production ceases. Oil production during EOR flooding (assuming no polymer flooding = no injection phase viscosity increase) displays a similar trend, with the dP curve plateauing after residual oil saturation is reached. If no more oil is produced during the EOR flooding and subsequent chase water flooding, the dP curves should be stable Figure 2-17.
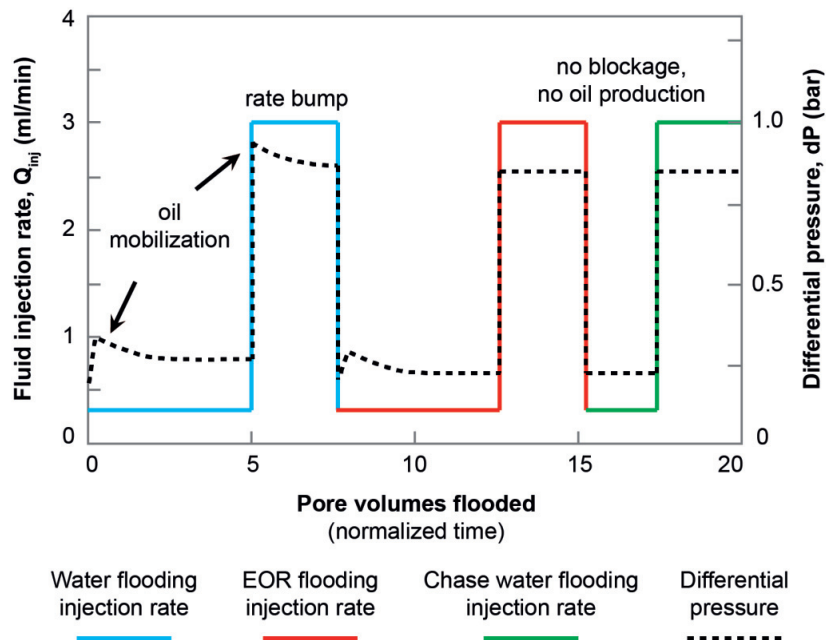
Figure 2-17. Differential pressure, dP, of an unsteady-state core flooding test with oil production during water flooding and the beginning of the EOR flooding at the low injection rate. No oil production occurs after EOR flooding at the low rate and all injected EOR additives propogate through the core plug (no retention = no dP increase).

If retention is occurring during the EOR flooding, the dP will increase as the permeability decreases. If the maximum dP value from the EOR flooding is greater than the maximum dP value from water flooding and is continually increasing, then incremental oil could be a result of more pressure added to the system as a whole, not just pressure redistribution in the core. Additionally, pore throat blockage forces the injection phase to take a more tortuous path, delaying breakthrough time (Rezaei and Firoozabadi, 2014).

A dP increase from particle retention will also be observed at the higher injection rate for the EOR flooding, although some of the pore throats could be reopened if the shear rate is great enough to overcome the particles' barriers. If particle retention is reversible, then the dP should decrease during the chase water flooding assuming that no oil production is taking place (Figure 2-18). This is because general fluctuations in dP can be explained by pore blockage and pore opening (Rezaei and Firoozabadi, 2014).
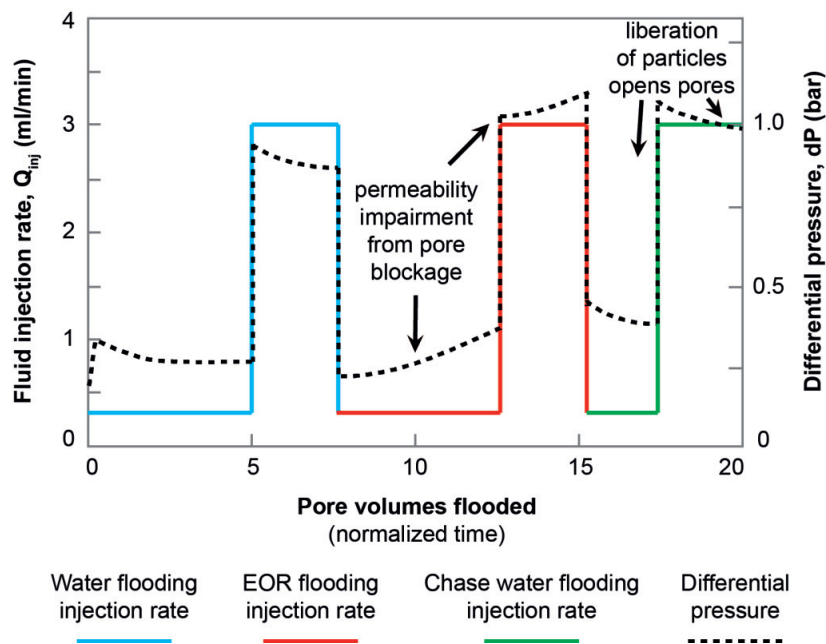
Figure 2-18. Differential pressure, dP, of an unsteady-state core flooding test with oil production during water flooding and extensive particle retention during EOR flooding. The chase water flooding is extracting retained particles if the dP is decreasing, assuming no oil production is taking place after EOR flooding.

A mass balance of the EOR additive from injection through a core can confirm whether retention is occurring without considering the oil phase. Computer tomography (CT) scans of the core can display saturation distribution and therefore identify which channels have flow diversion.

Studies that have microscopic displacement for nanoparticles are often employing nanoparticles in combination with polymers or using nanoparticles that have viscoelastic properties themselves. For example, nano polymer microspheres have produced positive results in a heterogeneous reservoir, where hydration and associated swelling from 70 nm to 10 μm after 20 days resulted in a water cut decrease and hence oil production increase (Tian et al., 2012). A number of experimental tests by Spildo et al. (2009) and Skauge et al. (2010) indicate that colloidal dispersion gels increase oil recovery due to microscopic diversion.

For silica nanoparticles used without viscoelastic materials, little research has been done on microscopic flow diversion. Also, there is a general problem with core flooding studies not reporting dP curves with the oil recovery curves. For example, out of all of the studies cited in the oil production section, only Hendraningrat et al. (2013b) and Skauge et al. (2010) provide dP curves. Youssif et al. (2017) showed that all their silica nanofluids resulted in permeability impairment in the sandstone cores, with a positive correlation between permeability impairment and nanoparticle concentration. They also determined that the 0.1 wt% nanofluid flooding delayed water breakthrough by almost one pore volume when compared with traditional water flooding, both at an injection rate of 0.5 ml/min. They concluded that this means a more favorable sweep efficiency is taking place with nanofluid flooding than water flooding. Skauge et al. (2010) concluded that log-jamming could be the only possible mechanical displacement mechanism for their tests due to the difference between the nanoparticle size and pore throat size. Because no oil was produced during their tests, they concluded that log-jamming alone is not sufficient for oil production. Additional tests on core flooding with various wettability by Hendraningrat and Torsæter (2014a) report dP increase throughout the entirety of nanofluid flooding for all tests. The nanoparticles visibly agglomerated at the core inlet, creating a "nano cake" that was likely the primary contributor to the dP increase. Therefore, a nanofluid stability analysis could give an indication of the dP curve prior to core flooding, because an unstable nanofluid will cause pore blockage.

3 Experimental materials and characterization

Five fluid types and two porous media types were used in this thesis and are related to the experimental methods in Table 3.1.

Table 3.1. Overview of materials.

Experimental method → Material ↓	Nanofluid stability	Interfacial tension	Contact angle	Core flooding Part 1	2	3	4	Micromodel flooding
Crude oil		X	X	X	X	X	X	X
n-Decane			X	X				
Synthetic formation water (3 wt% NaCl)				X	X	X	X	X
Synthetic sea water (SSW)		X	X	X	X	X	X	X
Nanofluids	X	X	X	X	X	X	X	X
Berea sandstone core plugs				X	X	X	X	
Soda glass micromodels								X

Five fluids types were used: two oils (a crude and n-decane), synthetic formation water, synthetic sea water (SSW) and nanofluids. The primary oleic phase was a light crude oil. Two core flooding tests and 19 contact angle experiments were conducted using n-decane, a model oil. The n-decane had a density of 0.73 g/cm^3 and a viscosity of 0.9 cP at 20°C. Most of the core flooding experiments has a synthetic formation water to establish initial water saturation (S_{wi}). The synthetic formation water was made with 3 wt% (3,000 ppm) NaCl dissolved in distilled water. Water flooding was conducted with a SSW resembling the composition of the North Sea. The SSW was also used as the base fluid for nanoparticle dispersions, or nanofluids.

The crude oil, SSW and nanofluid properties are described below. Density was measured with an Anton Paar density meter (DMA 4500M). Three consecutive measurements were taken for each value reported. Viscosity was measured with an Anton Paar modular compact rheometer (MCR 302) using a cone-in-cup configuration, and the viscosity was measured at a shear rate

of 50 sec^{-1}. Three tests were conducted for each value except for the SSW, where one measurement was taken for each value.

The two types of porous media used were Berea sandstone core plugs and soda glass micromodels.

3.1 Crude oil

The crude oil was taken from the Norwegian Continental Shelf. It was double-filtered at 5 μm. It had a density of 0.88 g/cm^3 (29.3 API°), classifying it as a light-medium oil. Its viscosity was 19 cP measured with the Anton Paar and 3.59 cP when measured with a capillary type viscometer at 20°C. The density and viscosity values for a range of temperatures are reported in **Table 3.2**.

Table 3.2. Density and viscosity measured for the crude oil.

Temperature (°C)	Density (g/cm^3)	Viscosity (cP)
20	0.876	19.1
40	0.862	7.1
60	0.848	4.7
80	not tested	3.5

A SARA analysis on a crude oil sample taken from the same reservoir yielded a composition of 61.2 wt% saturates, 32.4 wt% aromatics, 4.9 wt% resins and 1.5 wt% asphaltenes (Tichelkamp et al., 2014). The total acid number (TAN) and total base number (TBN) were 1.08 (no error available) and 1.16 ± 0.35 mg KOH/g, respectively (Tichelkamp et al., 2014). These values were from unfiltered samples.

3.2 **Synthetic sea water (SSW)**

Synthetic sea water resembling the composition of the North Sea was used for water flooding and as the base liquid for the nanofluids. The composition of the salts in one liter of sea water is presented in Table 3.3. The total dissolved solid (TDS) content was 35,000 ppm. The components were dissolved in distilled water.

Table 3.3. Composition of salt components in one liter of synthetic sea water (SSW).

Salt component	Chemical formula	Amount (g)
Sodium chloride	$NaCl$	28.500
Sodium sulfate	Na_2SO_4	4.066
Magnesium chloride hexahydrate	$MgCl_2 \times 6\ H_2O$	3.162
Calcium chloride dihydrate	$CaCl_2 \times 2\ H_2O$	1.625
Potassium chloride	KCl	0.721
Sodium hydrogren carbonate	$NaHCO_3$	0.220
Strontium chloride hexahydrate	$SrCl_2 \times 6\ H_2O$	0.024

The SSW had a density of 1.024 g/cm^3 and viscosity of 1.2 cP at 20°C. The density and viscosity values for a range of temperatures are reported in Table 3.4.

Table 3.4. Density and viscosity measured for the synthetic sea water.

Temperature (°C)	Density (g/cm^3)	Viscosity (cP)
20	1.024	1.2
40	1.016	0.8
60	1.002	0.6
80	not tested	0.5

3.3 **Nanofluids**

3.3.1 Nanoparticles

Eleven types of amorphous silica nanoparticles were tested. The three colloidal nanoparticles have a spherical structure. The eight nano-structured particles have a dendritic form and no mesoporous structure. Their surface area is a result of having many primary particles, not from pores within the primary particles themselves (Evonik Industries, 2015). Five of the nano-structured particles had a surface modification. The colloidal nanoparticles and three of the nano-structured particles were unmodified.

The unmodified nano-structured particles are the AEROSIL® product from Evonik Industries (received as AERODISP®, which is AEROSIL® particles in liquid solution). The particles are hydrophilic because they have freely accessible silanol groups (Si – OH) on the surface. They can be modified by reacting hydrophilic silanol groups with other organic compounds as shown in Figure 3-1 (Evonik Industries, 2015). These attachments are formed via covalent bonds, making for a very stable shell around the nano-structure.
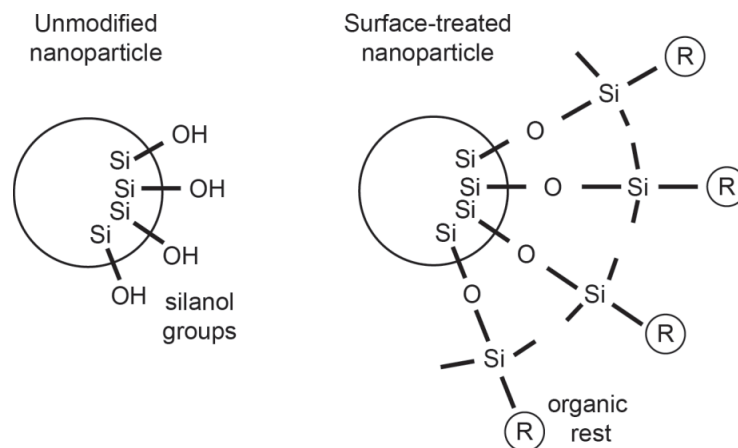
Figure 3-1. Illustration of how the AEROSIL® particle can undergo surface modification. Figure modified from Evonik (2015).

The particle size, particle size distribution, specific surface area and surface properties of the nano-structured particles are determined during pyrolysis. These variables are managed by the reactant concentration, the flame temperature and the length of time the gas resides in the combustion chamber (Evonik Industries, 2015). Silicas with large primary particles (and thereby low specific surface areas) are created at higher temperatures. Conversely, silicas with small primary particles (and thereby high specific surface areas) are created at lower flame temperatures. This is because when a hot flame is present, the particles have a longer zone of coalescence (during cooling), resulting in larger particles at the outlet stream (Evonik Industries, 2015). This concept can be explained by Evonik's (2015) droplet model. Nuclides of SiO_2 are created at the base of the flame, where the reaction begins. The nuclides collide and merge with each other in a random fashion. The SiO_2 droplet size continues to increase, while the number of droplets decreases, until the flame is no longer hot enough to keep the droplets in a liquid state (Evonik Industries, 2015). These droplets become the primary particles as they cool down to a solid state. The droplets continue colliding as they are partially solidified, resulting in the formation of the aggregate structure. This aggregate structure becomes solidified in the cooler temperature zones. As the aggregates continue colliding with each other in a solid state, they form agglomerates that are loosely held together by weak interactions such as van der Waals forces, hydrogen bonds and capillary forces (Evonik Industries, 2015).

The material properties for the 11 hydrophilic silica nanoparticles used in this thesis are presented in Table 3.5. The primary particle diameter and nano-aggregate diameter in DI water for the nano-structured particles were supplied by Evonik Industries and were measured by a Horiba Laser Scattering Particle Size Distribution Analyzer LA-950. The average particle diameter in SSW at 0.05 wt% is from nanofluid stability tests in this thesis as described in subsequent chapters. Evonik Industries supplied information about the surface area for the unmodified nanoparticles, which was measured using a surface analyzer and calculated with Brunauer-Emmett-Teller (BET) theory. The surface area was not tested for the surface modified nanoparticles.

Table 3.5. Nanoparticle material properties at ambient conditions.

	Nanoparticle	Surface modification	Average primary particle diameter (nm)	Average aggregate diameter in DI water (nm)	Average particle diameter in SSW (nm) [†]	Surface area (m^2/g)
Previously commercially available	Cnp_1	-	75	-	81	65
	Cnp_2	-	18	-	39	150
	Cnp_3	-	8	-	18	350
Commercially available as AERODISP®	Nsp_1a	-	16	106	144	130 ± 25
	Nsp_2a	-	10	81	96	200 ± 25
	Nsp_3a	-	7	86	133	300 ± 30
Produced exclusively for this thesis	Nsp_1b	Silanization	16[*]	128	-	-
	Nsp_2b	Silanization	10[*]	72	100	-
	Nsp_3b	Silanization	7[*]	112	109	-
	Nsp_3c	PEG[‡]	7[*]	111	104	-
	Nsp_3d	Epoxy	7[*]	-	16	-

[*] The same as its corresponding base particle prior to surface modification.
[†] Measured within 30 min of dispersion (t ≈ 0).
[‡] Modified by polyethylene terminated silane groups.
- Not measured / not applicable.

Six commercially available, unmodified nanoparticles (Cnp_1, 2 and 3 and Nsp_1a, 2a and 3a) were initially tested in Part 1 (screening of unmodified nanoparticles). From there, the most viable three candidates (Nsp_1a, 2a and 3a) were modified by a silanization process by Evonik Industries to meet specific reservoir criteria defined in this thesis. Those three modified nanoparticles (Nsp_1b, 2b and 3b) were tested in Part 2 (screening of silanized nanoparticles). The nanoparticle with the largest surface area was further modified by polyethylene terminated silane groups (hereafter referred to as PEG) on the nanoparticle surface (Nsp_3c) and by epoxy-terminated groups (hereafter referred to simply as epoxy) (Nsp_3d) to increase the stability at higher temperatures. Nsp_3c and 3d were tested in Part 3 (evaluation of surface-modified Nsp_3a) at ambient conditions and in Part 4 (testing with aged cores and elevated temperature) at 60°C. These eleven nanoparticles, their naming conventions and their respective core flooding evaluation parts are presented in Figure 3-2.

Part 1: Screening of unmodified nanoparticles
Ambient conditions (20°C)

**Colloidal nanoparticles
(Cnp)**

classified by surface area

small
(65 m²/g)

medium
(150 m²/g)

large
(350 m²/g)

Cnp_1

Cnp_2

Cnp_3

**Nano-structured particles
(Nsp)**

classified by surface area

small
(130 m²/g)

medium
(200 m²/g)

large
(300 m²/g)

Nsp_1a

Nsp_2a

Nsp_3a

Part 2: Screening of silanized nanoparticles
Ambient conditions (20°C)

modified
by silanization

modified
by silanization

modified
by silanization

Nsp_1b

Nsp_2b

Nsp_3b

Part 4: Testing with
aged cores and
elevated temperature
(60°C)

Part 3: Evaluation of surface-modified Nsp_3a
Ambient conditions (20°C)

modified
by PEG*

Nsp_3c

modified
by epoxy

Nsp_3d

*Modified by polyethylene terminated silane groups.

Figure 3-2. Overview of the nanoparticles evaluated in the thesis and their respective core flooding assemblage.

3.3.2 Nanofluid preparation and properties

All nanoparticles were received as suspended concentrate in aqueous solutions from Evonik Industries. The particles were suspended in distilled water at 20 wt%. Minor amounts (<5 wt%) of stabilizers such as sodium hydroxide, potassium hydroxide or methanol were present in the concentrated mixture to aid stabilization. When these concentrated mixtures were diluted to 0.05 wt%, the stabilizer concentration was subsequently diluted to < 0.0125 wt%.

For the unmodified nanoparticles, the concentrated solutions were first diluted to 2 wt% with distilled water because they instantly agglomerated when added directly to the SSW. The 2 wt% nanoparticle solution was further diluted to 0.05 wt% with SSW. The fluids were hand-shaken for a few seconds to ensure mixing. All experiments used nanofluids that were mixed within the previous 24 hours.

For the modified nanoparticles, the concentrated solution was added to a flask and directly diluted to 0.05 wt% with the SSW. This resulted in the final nanofluid. Batches were made in 1 liter quantities within 24 hours prior to the start of the experiment.

The surface areas for the unmodified nanoparticles are reported in Table 3.6. The density and viscosity were measured for nanoparticles dispersed in the SSW at 0.05 wt% at the range of temperatures at which the nanoparticles were tested (Table 3.6). Density ranged from 1.023 to 1.025 g/cm^3 and viscosity ranged from 1.1 to 1.2 cP at 20°C.

Table 3.6. Nanofluid properties for nanoparticles dispersed in SSW at 0.05 wt%.

	Nanoparticle	Density (g/cm^3)			Viscosity (cP)		
		20°C	40°C	60°C	20°C	40°C	60°C
Colloidal nanoparticles	Cnp_1	1.023	-	-	1.2	-	-
	Cnp_2	1.024	-	-	1.2	-	-
	Cnp_3	1.024	-	-	1.1	-	-
Nano-structured particles	Nsp_1a	1.024	-	-	1.2	-	-
	Nsp_2a	1.024	-	-	1.2	-	-
	Nsp_3a	1.024	-	-	1.2	-	-
Silanized	Nsp_1b	1.024	-	-	1.2	0.8	0.6
	Nsp_2b	1.025	-	-	1.2	0.8	0.6
	Nsp_3b	1.024	-	-	1.2	0.8	0.6
PEG modified	Nsp_3c	1.024	1.018	1.008	1.2	0.8	0.6
Epoxy modified	Nsp_3d	1.025	1.018	1.007	1.2	0.8	0.6

- Not measured / not applicable

3.4 **Core plug properties**

The Berea sandstone core plugs, hereafter referred to simply as "cores", were used for all core flooding experiments. Each core plug was only used once. This is because the possibility of irreversible nanoparticle adsorption to the rock during core flooding could affect the recovery factor for subsequent experiments. Additionally, reuse of core plugs with crude oil could result in variations in the wettability and therefore recovery factor, as it is difficult to remove all of the adsorption components from the crude oil (Anderson, 1986).

Berea sandstone is the most common sandstone used in core flooding research (Churcher et al., 1991). Berea sandstone core blocks were obtained from a quarry in Ohio, USA. The blocks were about 35 x 35 x 35 cm. Cylindrical core plugs were drilled from three different blocks which were numbered #8, #9 and #16 for internal use at NTNU. The core plugs used for the first six tests are from block #9. Most of the cores are from block #8 because block #9 was consumed, but the final few cores tested are from block #16 because block #8 was consumed. All core plugs had a standard diameter of 1.5 inches (3.8 cm) and were either 13 cm, 10 cm or 4.5 cm in length.

Berea sandstone is an early Mississipian age channel sandstone (Pepper et al., 1954). The blocks used in this study were taken from the Upper Berea unit, which is characterized by medium- to fine-sized grains held together by silica cement (Churcher et al., 1991). The sandstone has few laminations and is quite homogenous. Cylindrical core plugs with visible laminations were not used in the study.

The bulk mineral composition was measured using X-ray diffraction (XRD). Five samples from blocks 8 and 9 were analyzed (Table 3.7). The two blocks had a similar mineralogical composition. All samples were composed of more than 90 vol% quartz. This coincides with other XRD results, which obtain quartz values of at least 85 vol% (Churcher et al., 1991). Lai et al. (2015) used X-ray computed tomography (CT) to compare the bulk mineral composition to the mineral composition on the surface of the pores. In their four Berea samples, the bulk (volumetric) clay content was less than 5%, but the surface area coverage of clay was 5.5 to 8 times that (up to 37.5% clay). This confirms that the bulk composition of the core plug does not necessarily represent the surface mineralogy upon which the chemical EOR method is reacting.

Brunauer-Emmett-Teller (BET) surface area measurements for Berea sandstone are within the range of 0.6 to 1.4 m^2/g (Churcher et al., 1991; Lai et al., 2015; Sen et al., 1990).

Table 3.7. XRD analysis for Berea core plugs.

Block #		Sample #					Average
		1	**2**	**3**	**4**	**5**	
8	Quartz	92.73	92.74	93.84	92.25	92.78	92.87
	Microcline (Alkali feldspar)	5.98	6.08	5.05	6.43	5.95	5.90
	Diopside	1.30	1.18	1.11	1.32	1.27	1.24
9	Quartz	94.59	93.1	92.99	94.84	93.06	93.70
	Microcline (Alkali feldspar)	3.94	5.67	5.65	4.07	5.62	5.00
	Diopside	1.47	1.23	1.36	1.09	1.32	1.30

The mineral grains in Berea sandstone tend to be well-rounded and well-sorted (Churcher et al., 1991). Churcher et al. (1991) averaged 10 sets of thin section measurements each to determine grain size and pore body sizes for four Berea sandstone samples. Grain size ranged from 70 to 310 μm, with average grain size ranging from 99 to 214 μm. The pore body size ranged from 35 to 180 μm, with average pore body size ranging from 79 to 114 μm. The pore shape was round to oval, and the aspect ratio of pore bodies to pore throats ranged from 5 to 11. A thin section from Berea block 8 was analyzed specifically for this study (Figure 3-3). The larger grains were up to 372 μm in diameter (measurement 3), while the smaller grains are around 95 μm in diameter (measurement 4). The smallest pore throats range from 15 μm to 36 μm (measurements 6 and 1, respectively).
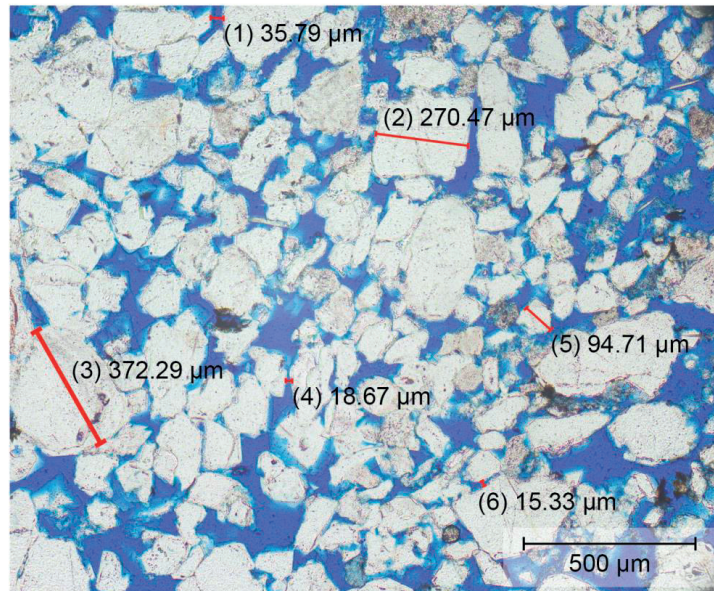
Figure 3-3. Thin section from Berea block 8.

Effective porosity was measured with a helium porosimeter (Core Laboratories, Inc., porosimeter model O.S.) or with the saturation method. Permeability was measured with a constant head permeameter using air as the through-fluid and a sleeve pressure of 20 bar. The Klinkenberg correction (Klinkenberg, 1941) was used to adjust the permeability measurements to reflect liquid permeability through the core. This is the permeability reported for each experiment.

Core data is summarized in Table 3.8. Cores 1 to 21 and 24 to 25 were unaged and therefore water-wet. Cores 22 to 23 and 26 to 35 were aged and therefore intermediate- to oil-wet. Core preparation is described in section 4.4.1**:** Core preparation (page 74). Average porosity was 17.6% and ranged from 13.8% to 20.8%. Average permeability was 357 mD and ranged from 224 mD to 632 mD. Porosity and permeability measurements are compared in Figure 3-4.

Table 3.8. Core data. All cores were quartz-rich Berea sandstone and were 1.5 inches (3.8 cm) in diameter.

Test #	Block #	Length (cm)	Porosity	Permeability (mD)	Pore Volume (ml)	OOIP (ml)	Swi
1	9	13.0	20.8	285	24.8	18.3	0.26
2	9	13.0	18.5	363	24.8	14.9	0.40
3	9	13.0	18.4	438	26.1	18.7	0.28
4	9	13.0	17.8	337	24.7	17.3	0.30
5	9	13.0	18.1	394	23.2	17.0	0.27
6	9	13.0	18.2	358	25.4	18.3	0.28
7	8	13.0	15.1*	327	22.8	17.3	0.24
8	8	13.0	16.3*	276	24.6	15.5	0.37
9	8	13.0	15.6*	394	23.5	12.8	0.46
10	8	13.0	15.5*	224	23.7	16.8	0.29
11	8	13.0	15.5*	363	23.5	16.8	0.29
12	8	13.0	16.3*	453	24.7	16.7	0.32
13	8	13.0	15.7*	332	23.7	16.6	0.33
14	8	10.0	16.9*	320	19.4	12.3	0.37
15	8	10.0	17.7*	396	20.1	12.8	0.37
16	8	4.5	17.8*	322	8.7	5.9	0.33
17	8	4.5	17.5*	300	9.0	5.8	0.36
18	8	4.5	17.2	264	8.5	5.6	0.34
19	8	4.5	17.3*	364	8.9	5.5	0.38
20	8	4.5	17.7*	304	9.0	5.3	0.41
21	8	4.5	17.3*	353	8.5	5.6	0.35
22	8	10.0	13.8	382	15.7	15.7	0
23	8	10.0	14.9	357	17.0	17.0	0
24	8	10.0	17.7*	339	20.2	10.6	0.47
25	8	10.0	17.2*	632	20.2	13.0	0.36
26	8	10.0	19.3	393	22.3	22.3	0
27	16	10.0	20.7	389	22.6	22.6	0
28	16	10.0	20.6	319	22.6	22.6	0
29	8	10.0	18.0	279	20.6	20.6	0
30	16	10.0	20.2	301	22.1	22.1	0
31	8	10.0	19.2	328	22.0	22.0	0
32	8	10.0	18.1	379	20.9	20.9	0
33	16	10.0	20.8	466	22.5	22.5	0
34	8	10.0	18.2	270	20.9	20.9	0
35	8	10.0	15.9	489	18.2	18.2	0

* These porosity measurements were conducted using the saturation method. The other porosity measurements were taken with a helium porosimeter.

	Single test
	Duplicate test
	Triplicate test
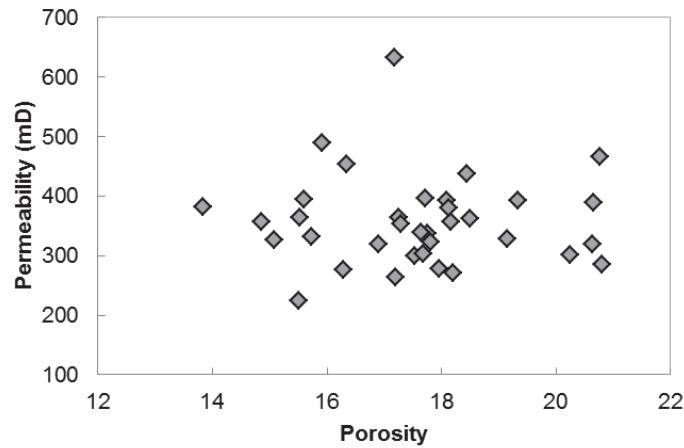
Figure 3-4. Permeability vs. porosity for the cores used in this thesis. There is no correlation between the porosity and permeability values.

3.5 **Micromodels**

Two regular-pattern soda-glass micromodels were used to visualize flow through porous media. One model was naturally water-wet, while the other model was treated with hexamethyldisilazane (HMDS) to render it oil-wet. To produce the oil-wet state, the micromodel was first cleaned and then saturated with HMDS and placed in an oven set to 90°C for 20 hours. HMDS was then removed by vacuum suction and the micromodel was rinsed first with hexane, then 2-propanol and finally distilled water. This oil-wetting process was conducted according to the procedure described in Sandengen et al. (2016), which was a modification of the procedure presented in Grate et al. (2013).

The dimensions of the models were 6.0 cm x 4.0 cm. The micromodels were assumed to have a pore volume of 0.06 cm^3 as described in Sandengen et al. (2016). Both models were labeled as having an aspect ratio of 5 (pore to pore throat ratio), but an analysis of the micromodel dimensions shows that the aspect ratio was closer to 4 or 4.5 as exhibited in Figure 3-5 (water-wet) and Figure 3-6 (oil-wet).

Table 3.9. Micromodel physical properties.

Micromodel properties	water-wet (tests #36 and 37)	oil-wet (test #38)
Length (cm)*	6.0	6.0
Width (cm)*	4.0	4.0
Porosity (%)	38.31	38.31
Pore volume (ml)*	0.06	0.06
Avg. pore throat diameter (µm)	128	104

* Assumed the same as values given in Sandengen et al. (2016) because the same models were used. Channel depth, permeability and avg. pore body volume were not measured.
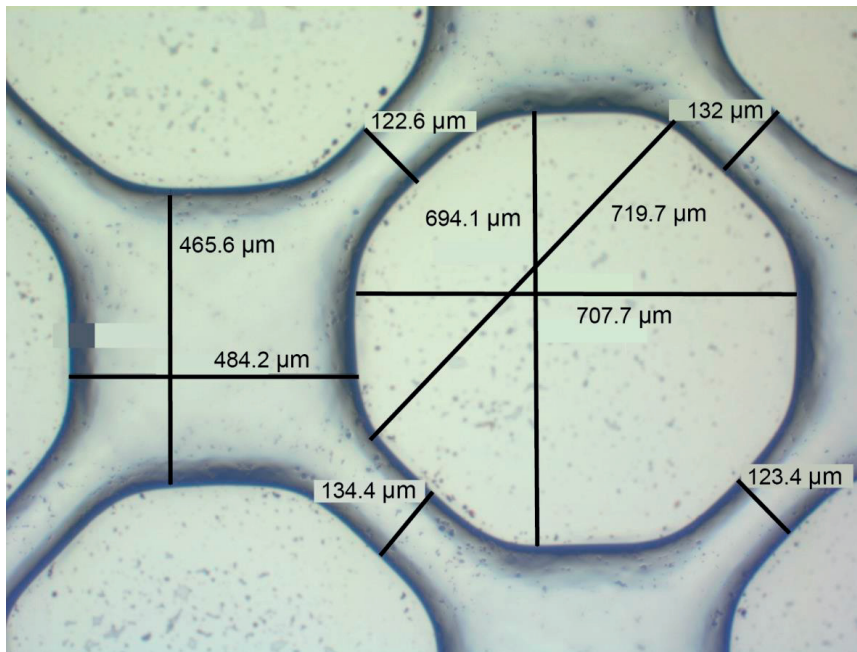
Figure 3-5. Micromodel dimensions for the water-wet model (AR 5 No. 4). Photo by Espen Kowalewski / Statoil AS.
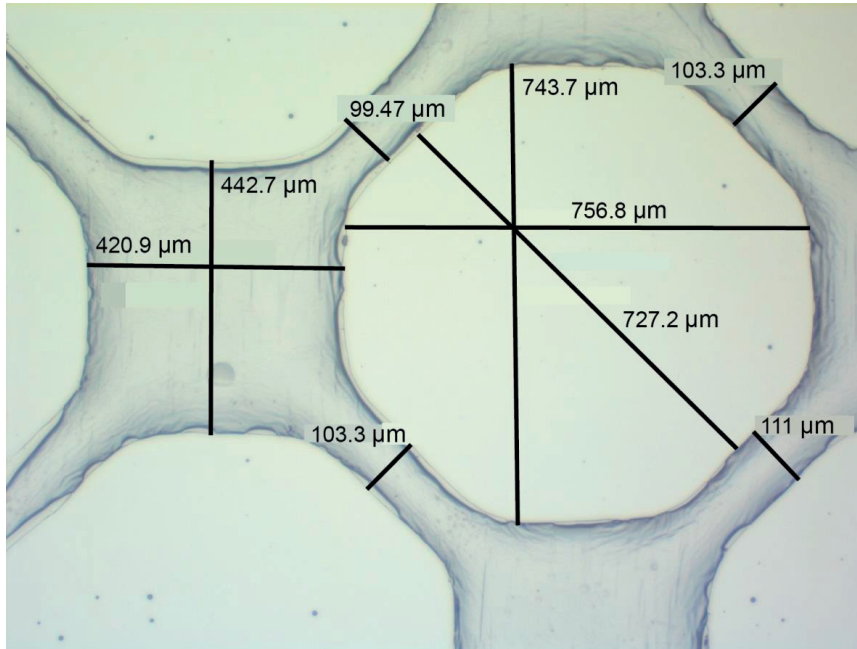
Figure 3-6. Micromodel dimensions for the oil-wet model (AR 5 No. 2). Photo by Espen Kowalewski / Statoil AS.

4 Experimental methods

This chapter presents a general overview of the experimental methods. Where applicable, detailed procedures are described before their respective results in Chapter 5. The experimental methods are related to the research questions they address in Table 4.1.

Table 4.1. Overview of experimental methods.

Section	Sub-section	Research question
Nanofluid stability (4.1)		RQ1
Interfacial tension (4.2)		RQ3
Contact angle (4.3)		RQ3
Core flooding (4.4)	1. Core preparation 2. Rig design 3. Flooding procedure 4. Effluent sampling	RQ2 + 3
Micromodels (4.5)	1. Experimental set-up 2. Image processing	RQ2 + 3

4.1 Nanofluid stability

The stability analysis was conducted by measuring and comparing the nanoparticles' particle size distribution (PSD) over time using dynamic light scattering (DLS) measured with a Malvern Zetasizer Nano series model ZEN 3600. As a laser shines through a nanofluid sample in a cuvette, the Brownian motion of the nanoparticles causes the light to be scattered at various intensities. An analysis of the light intensity fluctuations is a function of the Brownian motion velocity, which can be converted to particle size using the Stokes-Einstein relationship (Malvern Instruments, 2017). DLS measures particle mobility, which is converted to particle size by applying a cumulants analysis to the raw data. Frisken (2001) presents a good overview of the method of cumulants for dynamic light-scattering data analysis.

The cumulant mean hydrodynamic particle size (also known as the z-average) and the polydispersity index (PdI) describe the overall form of the size distribution. This is different than the peak size as calculated by the size distribution by intensity, which can be used to describe individual peaks in a distribution that is not unimodal. The z-average is the intensity-based overall mean size of the particles, and the calculation of the z-average is described in ISO

22412:2017. The z-average is referred to as D_{avg} throughout this thesis. The PdI reflects the monodispersity; smaller values (< 0.05) reflect a highly monodisperse sample, while values greater than 0.7 reflect a broad size distribution that is not applicable for dynamic light scattering techniques.

The following nanoparticle material properties were set based on communication with the nanoparticle supplier (Evonik Industries). The nanoparticle material properties were set as refractive index = 1.460 and absorption = 0. The dispersant viscosity was used as the nanofluid viscosity. The dispersant was always set to distilled water due to a lack of data for SSW at the start of the stability tests. Even though selecting distilled water properties for the instrument does not perfectly reflect the reality of the saltwater dispersant, the goal of the stability tests was to compare samples over time. Therefore, it was more important to maintain consistency for the input parameters by using distilled water settings. It did not seem to affect the tests based upon the data for stable nanoparticles measured in both distilled water and SSW.

The temperature was set to 20°C with an equilibration time of 120 seconds. Disposable cuvettes (DTS0012) were used. Three measurements were taken for each sample, and the average of these measurements is reported. The measurement duration was automatically determined by the instrument (typically 11 to 15 runs per measurement). The angle of detection was set to the non-invasive backscatter (NIBS) default of 173° backscatter. The measurement duration was not extended for large particles. The positioning method was allowed to seek for the optimum location, and automatic attenuation selection was allowed.

Measurements taken with the nanoparticles dispersed in distilled water at 0.05 wt% were considered to provide an optimal (stable) distribution. This was compared to the values obtained with the nanoparticles dispersed in the SSW at 0.05 wt%. The nanofluid was considered stable if it met two criteria: it maintained its unimodal distribution and D_{avg} did not increase by more than 50 nm from the original measurement in DI water at t = 0.

It was assumed that the unmodified nanoparticles would not be stable for very long based on visual observations in the lab. The first measurement was taken within 30 minutes after nanofluid mixing (t = 0). Additional measurements were taken 8 and 24 hours after mixing.

For the modified nanoparticles, after nanofluid mixing, samples were either left in ambient conditions (20°C) or placed in an oven set at 40°C or 60°C. Samples were taken from their respective holding places directly prior to the stability measurement. The temperature was set to 20°C, 40°C or 60°C with an equilibration time of 120 seconds. Each sample was measured three times, and the average of these measurements is reported.

The first measurement was taken within 30 minutes after nanofluid mixing (t = 0). Additional measurements were taken at 1, 4, 8, 12 and 16 weeks after mixing. Nsp_3c was also tested at concentrations of 0.1 wt% and 0.5 wt% in addition to 0.05 wt%.

4.2 Interfacial tension and capillary number

The pendent drop method was used to determine interfacial tension. The spinning drop method was also used to compare the interfacial tension of the unmodified nanoparticles to the pendant drop results. The interfacial tension values were used to calculate the capillary numbers for core flooding tests conducted at 20°C.

For the pendant drop analysis, a Krüss drop shape analyzer (DSA) 100 was used with a J-shape syringe needle having an inner diameter of 1.0047 mm. Crude oil droplets were dosed at a rate of 2.67 μl/s. Droplet size varied from 13.6 to 20.6 μl. The surrounding fluid (sea water or nanofluid) was between 20.0 and 22.7°C. The interfacial tension was calculated using the Young Laplace fitting method. Seven tests were conducted for each fluid system.

For the spinning drop method, a SVT20 spinning drop video tensiometer was used with a rotation of 4000 to 6000 rpm. Temperature was held constant at 22.8°C. The experiment was run for 45 minutes to 2 hours or until the interfacial tension was stable for at least 15 minutes. The stable interfacial tension at the end of the experiment is reported.

4.3 **Contact angle**

Contact angle measurements were performed using a KSV CAM 200 goniometer at ambient conditions (20°C) or at 60°C. The inverted sessile drop method (also known as the captive bubble technique) was used for all experiments. Because quartz is the dominant mineral for the Berea core plugs, a silica substrate was selected to best represent the wettability conditions for the unaged core flooding tests. A glass plate was therefore used as the substrate for the contact angle tests. Cleaning between tests was conducted by rinsing thoroughly with distilled water. A polished quartz crystal was available as the substrate for experiments conducted with Nsp_3c. It was cleaned by first being rinsed thoroughly with distilled water and then being placed in an ultrasonic bath for five minutes filled with distilled water. Neither the glass plate nor the quartz crystal could be modified to alter the initial wettability due to chemical lab restrictions, although the base values for the quartz crystal suggest that it had already been altered towards a more intermediate-wet state with a surface coating.

The contact angle was measured every 10 minutes for 8, 10 or 24 hours to see if there was an interaction between the nanofluid and the oil droplet. The first six measurements of the contact angle values (the first hour) were averaged to determine the starting contact angle. The last six contact angle measurements were averaged to determine the final contact angle.

4.4 **Core flooding**

The components of core flooding are the following: core plug preparation, rig design, flooding procedures and effluent analysis. The core flooding procedures are explained in more detail in Chapter 5.

4.4.1 Core preparation

Core plugs were drilled from their respective Berea sandstone blocks as described in Chapter 3. The Berea sandstone blocks were initially dry/ unsaturated. The core plugs were rinsed in a soxhlet apparatus with methanol for six to eight hours to be cleaned and flush out fine sand particles. The core plugs were then dried in an oven at 60°C for at least three days or until the

core weight was stable (± 0.05 g) for at least two days. The 60°C oven temperature was chosen to preserve the cores' clay framework as demonstrated in Byrne and Patey (2004), where illite clay fibers maintained their structure at that temperature. Porosity and permeability were measured.

For core plugs using initial water saturation (no aging), the following procedure was followed: After cleaning and drying, the core plugs were saturated with reservoir brine using a vacuum pump with a chamber pressure set at 100 mbar for two hours. The core plugs were kept in a covered glass beaker filled with reservoir brine until the oil flooding portion of the core flooding began. Beaker residence time ranged from three days to 2 months.

For core plugs that underwent aging (no initial water saturation), the following procedure was followed: After cleaning and drying, the cores were saturated with crude oil using a vacuum pump with chamber pressure less than 1 mbar. They were held in the chamber for at least two hours under vacuum pressure. After saturation, they were placed in individual, sealed metal containers called aging cells. The aging cells were filled with additional crude oil and placed in an oven at 60°C for the duration of the aging process. Core flooding was performed immediately after the aging process was completed. Cores flooded at 20°C were cooled in the aging cell at ambient conditions for a few hours before the test began. All cores in Part 4 were prepared using this method and were aged in the oven for four weeks. The other two cores that were aged were in Part 3, with aging conducted for 11.5 weeks (test #22) and 10.5 weeks (test #23).

Each saturated core was weighed before being placed in the core holder for the core flooding experiment. Effective porosity was calculated from the unsaturated and saturated core weights and density of the reservoir brine. The effective porosity value that resulted in a grain density closest to 2.6 g/cm^3 was used. This value was selected based on Berea sandstone grain density measurements from Churcher et al. (1991). The pore volume was calculated from the bulk volume multiplied by the selected effective porosity.

For Part 2 core flooding tests, the post- core flooding porosity and permeability was evaluated. Therefore, after core flooding, the core plugs were rinsed in the soxhlet with toluene for 1 to 2 days followed by one day with methanol. The core plugs were then dried in an oven at 60°C for at least two days or until the core weight was stable (± 0.05 g) for at least four hours. Post-

flooding porosity and permeability were determined using the helium porosimeter and the constant head permeameter. These results were compared to pre-core flooding values.

4.4.2 Rig design

The core flooding rigs were custom-built by the author and are shown in Figure 4-1 and Figure 4-2. The core plug was mounted in a Hassler type core holder with a Viton® sleeve. The core holder was mounted horizontally. Sleeve pressure was maintained between 16 and 22 bars using nitrogen gas and was constantly monitored with a Keller Leo3 pressure transmitter (0 – 30 bar; ± 0.1%). Polytetrafluoroethylene (PFTE) tubing with an inner diameter of 1/16 in. (≈ 1.59 mm) was used to convey all liquids. Swagelok® tube fittings and valves were used to direct fluid flow. The inlet tubing was saturated with the first injection fluid all the way to the inlet core face to ensure that no air was injected into the system. During fluid switches, the tubing was flushed to as close to the core inlet as possible to reduce the inlet dead volume.
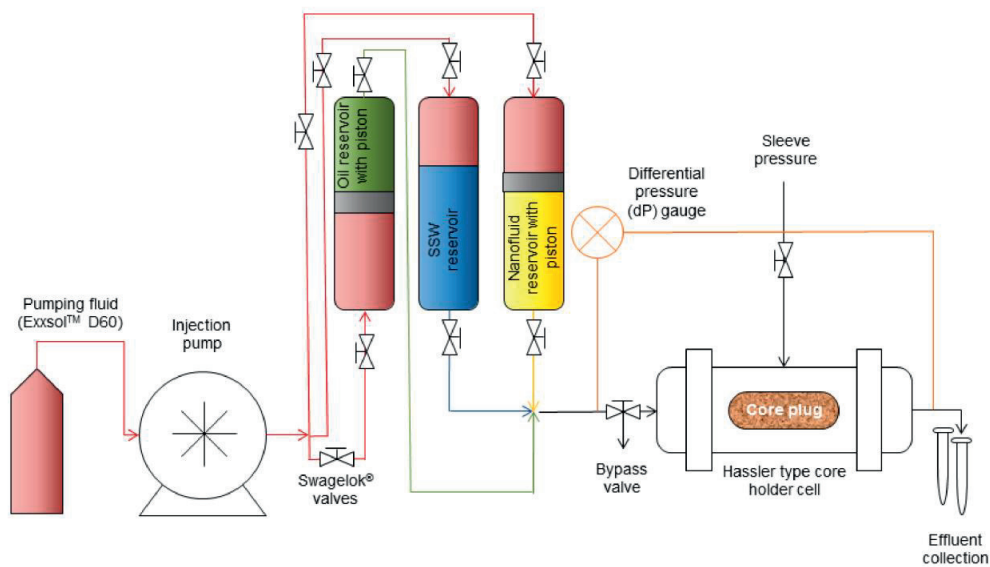
Figure 4-1. Experimental set-up for core flooding at ambient conditions designed and built by author.
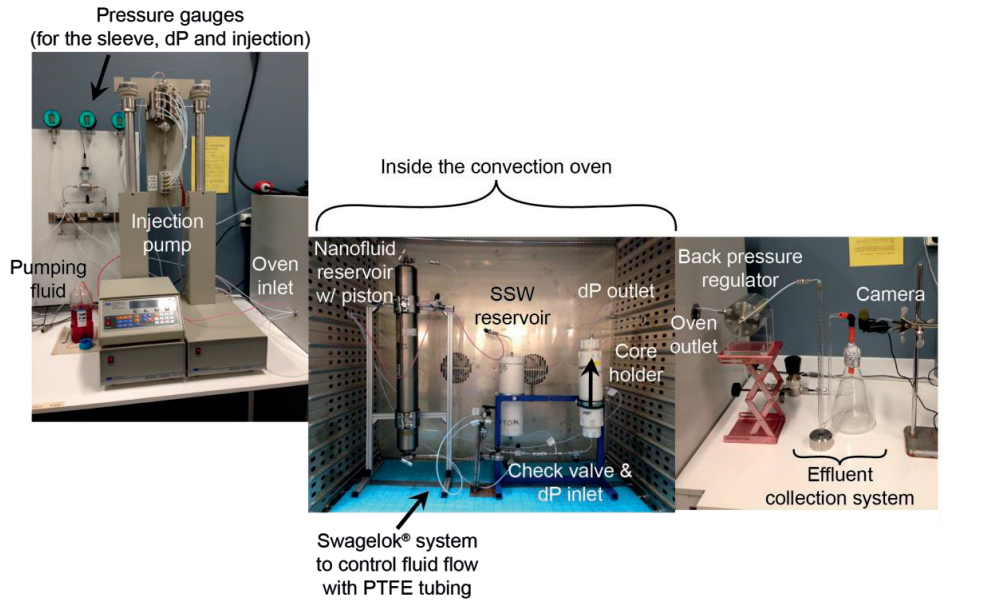
A) Core flooding rig for elevated temperatures
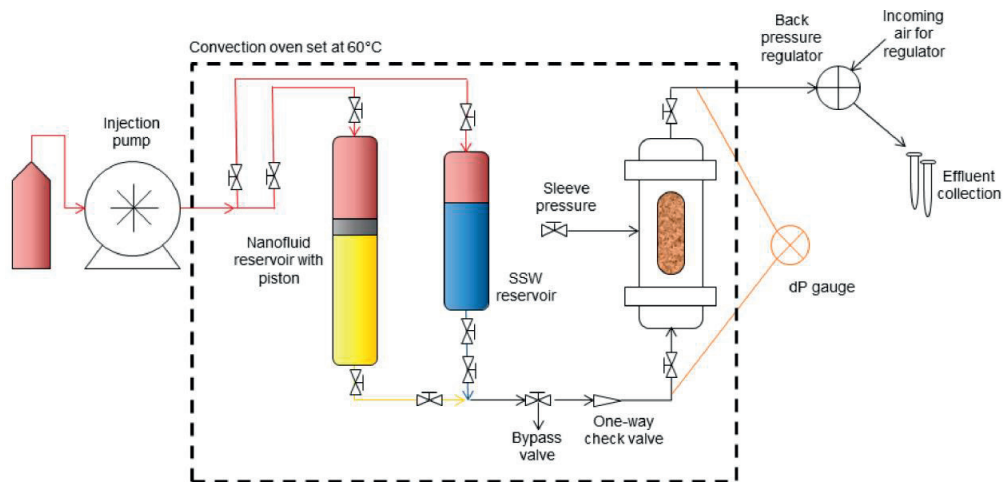
B) Schematic of core flooding process at elevated temperatures

Figure 4-2. Experimental setup for core flooding experiments at elevated temperatures designed and built by author. A) Core flooding rig in the laboratory and B) experimental design.

A Pharmacia Biotech Pump P-500 (0.017 – 8.317 ml/min; ± 1.5%) was used with Exxsol™ D60 as the pumping fluid. The pumping fluid was routed to a cylindrical chamber, where it displaced the liquid designated for core. A piston was placed in the chamber to separate the liquids if crude oil or nanofluids were being injected. A piston was not used for the water flooding chamber because saltwater is immiscible and nonreactive with Exxsol™ D60. A Keller PD 33X pressure transmitter (0 – 30 bar; ± 0.05%) was used for measuring the differential pressure across the core holder. The inlet sensor was connected close to the core holder inlet. The outlet sensor was kept open, reflecting the ambient conditions experienced at the core holder outlet. This setup made effluent collection easier. Back pressure was not used. Effluent was collected in test tubes with a 0.1 ml gradation (accuracy ± 0.05 ml).

For Part 2 core flooding tests, the only difference was that a more accurate Quizix QX 6000 pump (0.001 – 50 ml/min; ± 0.1%) was used with Exxsol™ D60 as the pumping fluid instead of the Pharmacia pump, as it was then available. Both pumps were used for Part 3 tests, along with a Teledyne ISCO 260D continuous flow dual pump (0.001 – 70 ml/min; ± 0.5%). A Teledyne ISCO 100DX continuous flow dual pump (0.00001 – 32 ml/min; ± 0.3%) was also used for some of the Part 4 tests when the Teledyne ISCO 260D pump was unavailable. Part 4 tests were conducted in an oven set at 60°C. The core holder was also oriented vertically, with flow from the bottom to the top. Back pressure was set at around 4.5 bar.

For Part 1 tests, all effluent was collected in test tubes with a 0.1 ml gradation (accuracy ± 0.05 ml). For Part 2 tests, effluent was collected in test tubes with a 0.1 ml gradation (accuracy ± 0.05 ml). At the end of a flooding series when the displaced fluid was not being produced, a larger tube with a 0.2 ml gradation (accuracy ± 0.1 ml) or 0.5 ml gradation (accuracy ± 0.25 ml) was used to collect the displacing fluid. For Parts 3 and 4, effluent was combined in a continuous sampler with gradation 0.1 ml (accuracy ± 0.05 ml).

A camera with automated capturing was installed to record the oil production for experiments running overnight. The pictures were then analyzed to determine the oil production over time. These values were compared to the final oil production volume read the following day.

Differential pressure was continuously recorded during the experiments (values captured every 15 or 30 seconds). The Control Center Series 30 program was used for pressure data acquisition. The Hassler core holder cells did not have the capability for intermediate pressure taps. Pressure

lines were filled with a liquid (Exxsol™ D60 or distilled water) to prevent air compressibility that would cause the injected fluid to flow into the pressure lines.

4.4.3 Flooding procedure

All core flooding tests were conducted using the unsteady state core flooding procedure, where one fluid is injected at a time. Nanofluid flooding was always conducted as tertiary flooding after water flooding with SSW. Detailed procedures were different for each of the core flooding parts and are therefore presented prior to the results for easier comparison.

4.4.4 Effluent sampling

4.4.4.1 Part 1: Screening of unmodified nanoparticles

Nanoparticle concentration analysis was conducted for the nano-structured particle tests (#4 to #6). Because at least 10 ml were needed for each sample, the effluent test tubes were emptied into 15 ml plastic vials. Three samples at the end of nanofluid flooding were taken for analysis. The concentration was measured by Evonik Industries using ICP-OES (inductively coupled plasma optical emission spectrometry). Silicon content was determined as elemental concentration and then calculated to oxide (SiO_2). Two measurements were taken for each reported value. The average with an estimated measurement uncertainty was used for the concentration calculations. Because the method measures silica content and does not differentiate between silica nanoparticles and silica fines produced from the core plug, an effluent sample at the end of water flooding was taken to establish background silica concentration. This value was subtracted from the measured influent nanoparticle concentration to establish the "true" nanoparticle concentration that should be found in the effluent if all nanoparticle are passing through the core plug. The dimensionless effluent nanoparticle concentration was calculated by dividing the measured effluent nanoparticle concentration by the "true" nanoparticle concentration and multiplying by 100. A value of 100 would mean that all of the nanoparticles are passing through the core plug. As the value approaches 0,

nanoparticles are being retained inside the core plug. This method does not differentiate between retention and adsorption of the nanoparticles.

Silica content in the influent and effluent crude oil was also determined by Evonik Industries using ICP-OES by first rinsing the tubes with hexane to extract the small sample amount. Next, the sample mass was determined with difference-weighting. The samples were then baked at 450°C, the residues were melted in NaOH and the melt was dissolved in water for the test. Two measurements were conducted for the influent crude oil and effluent crude oil produced from water flooding. Only one measurement was conducted for the crude oil produced from nanofluid flooding because the volume was too small to allow for duplicate measurements. The effluent crude oil samples were compared to the influent crude oil samples.

4.4.4.2 Part 2: Screening of silanized nanoparticles

Effluent pH and nanoparticle concentration were measured for all experiments. The pH measurements were conducted with a pH meter (VWR pHenomenal® 1000L) at the very end of water flooding (WF-Q_{high}), the very end of nanofluid flooding (NF-Q_{high}), and at the beginning of both chase water flooding stages (Flush-Q_{low} and Flush-Q_{high}). Samples for nanoparticle concentration analysis were collected between 0.6 and 1.4 PV after NF-Q_{high} began for the nanofluid flooding value. The chase water flooding samples were taken every ½ PV starting after ½ PV of Flush-Q_{low} and after ½ PV Flush-Q_{high}. Refer to Figure 4-3 for an illustration of effluent sample collection times. The nanofluid flooding influent was also measured. Effluent samples were collected directly into 15 ml plastic vials that were sent to Evonik Industries for analysis using ICP-OES. Because of limited resources, not all samples were analyzed. The following is an overview of analyzed samples:

Exp. #7: nanofluid influent and two measurements during NF-Q_{high} (NF$_{1a}$ and NF$_{1b}$)

Exp. #8: nanofluid influent, NF$_1$ and Flush$_1$

Exp. #10: nanofluid influent, end of WF-Q_{high}, NF$_1$ and Flush$_1$, Flush$_2$, Flush$_3$ and Flush$_4$

Exp. #11: nanofluid influent, NF$_1$ and Flush$_1$
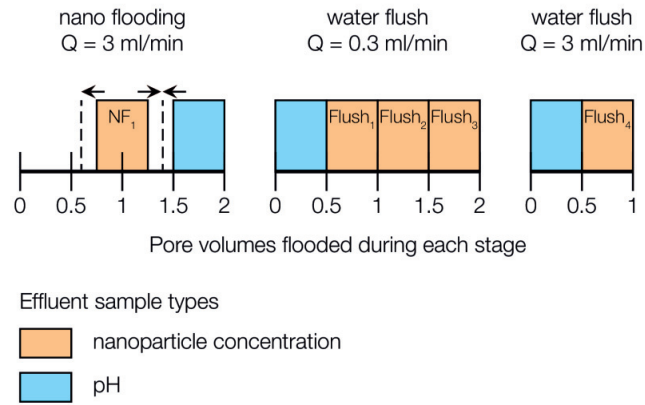
Figure 4-3. Illustration of effluent sample collection points for the Part 2 core flooding tests. There was some variance as to when the nanofluid flooding samples were collected because sampling was based on time and not pore volumes flooded. Water flush refers to chase water flooding.

4.5 **Micromodels**

4.5.1 Experimental set-up

The micromodel was secured horizontally on an Olympus SZX16 microscope with a Märzhäuser Scan 130x85-4mm motorized stage. Images were taken with an Olympus UC 90 camera attached to a SDF PLAPO 1XPF objective lens. Image post-processing was conducted in Adobe Illustrator. A KD Scientific Legato 100 syringe pump was connected to the micromodel via polytetrafluoroethylene (PTFE) tubing having an inner diameter of 1/16 in. ($\approx$ 1.59 mm). Glass syringes with 1 ml capacity were used for fluid injection. A Druck PTX610 pressure gauge recording at 0.1 bar intervals was placed between the syringe pump and the micromodel inlet. Back pressure was not applied. The experimental set-up is shown in Figure 4-4.
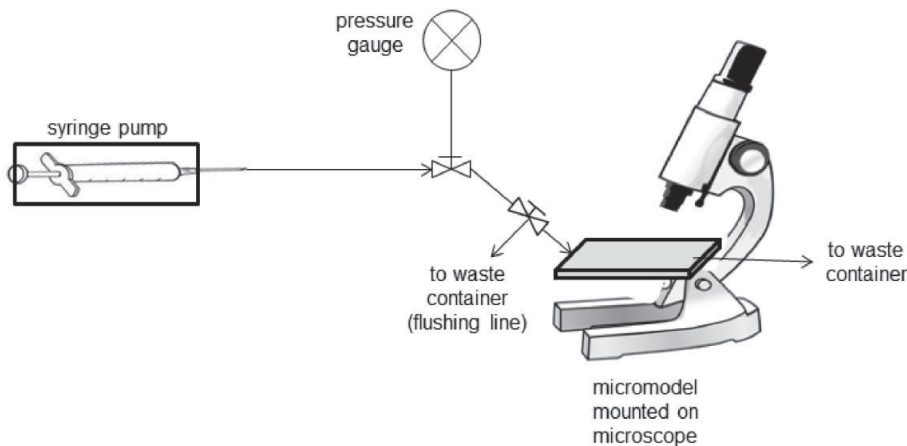
Figure 4-4. Experimental set-up for the micromodel tests.

Three tests were conducted. The first two tests used a water-wet micromodel. The second test was identical to the first, but blue dye was added to the nanofluid phase to better visualize the flow path of the nanofluid. The third test used an oil-wet micromodel. The flooding procedure was similar for all tests in that the micromodel was first saturated with 3% NaCl followed by injection of crude oil. Water flooding with SSW was then conducted followed by nanofluid flooding with 0.05 wt% Nsp_3c in SSW. Additional flooding details are provided in Chapter 5.

4.5.2 Micromodel flooding procedure

An overview of the micromodel flooding procedure for each test is given in Table 4.2 Details are given before the results in Chapter 5.

Table 4.2. Overview of micromodel flooding procedures.

Test #	36	37	38
Type of micromodel	Water-wet	Water-wet	Oil-wet (HMDS treatment)
Cleaning procedure	None prior to use; assumed clean	167 PV toluene 167 PV methanol 167 PV DI water	84 PV toluene 84 PV methanol 84 PV DI water
100% Sw procedure	42 PV isopropanol to wet the model then 167 PV 3wt% NaCl	67 PV isopropanol then 167 PV 3wt% NaCl	67 PV isopropanol then 84 PV 3wt% NaCl
Oil flooding	3 PV	3 PV	3 PV
Water flooding	6.5 PV	8.5 PV	7.5 PV
Nanofluid flooding	3 PV + 1 PV	4 PV + 6 PV	4.5 PV

4.5.3 Image processing

All photos are presented with flow from left to right. The pictures were processed in Adobe Photoshop CS6. Pre- and post-processing photos for the determination of porosity and S_{wi} for test #36 are shown in Figure 4-5 and Figure 4-6, respectively. The procedure to prepare each the photos for tests #36 and #37 was as follows:

1. Crop the photo down to the area of interest. This is defined as the micromodel pore area between the channel dead volume zones.
2. Apply Image → Auto Tone, Image → Auto Contrast and Image → Auto Color
3. Apply Image → Adjustments → Black and White; accept automatic settings
4. Apply Image → Adjustments → Brightness and Contrast; keep Brightness as default (0 value) but increase Contrast to maximum (100 value). Do this for a total of 4 times for maximum contrast.
5. Apply Image → Mode → Grayscale
6. Apply Image → Mode → Bitmap; output resolution = input resolution; use 50% Threshold method
7. Apply Image → Mode → Grayscale to convert back to a readable format for the following steps

To analyze the photo, the histogram tool was opened. All pixels were selected and counted. Because of the error introduced by cropping, the total pixel amount varied by 1.3%. To select all areas not occupied by the oil phase, the Magic Wand tool was used to select a white area. The command Select → Similar was applied to highlight all white pixels. The histogram tool was then used to count the number of white pixels. The number of white pixels representing the glass islands in the micromodel was subtracted from the newly calculated white pixel count. This produced a pixel count that represented all non-oil phases in the pore space. Microsoft Excel was then used to calculate the saturation of oil occupying the pore space.
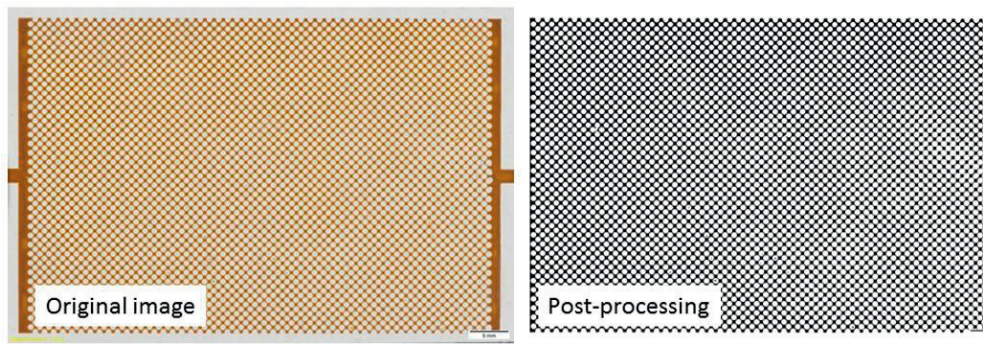
Figure 4-5. Pre- and post-processing for the determination of porosity for tests #36 and #37.
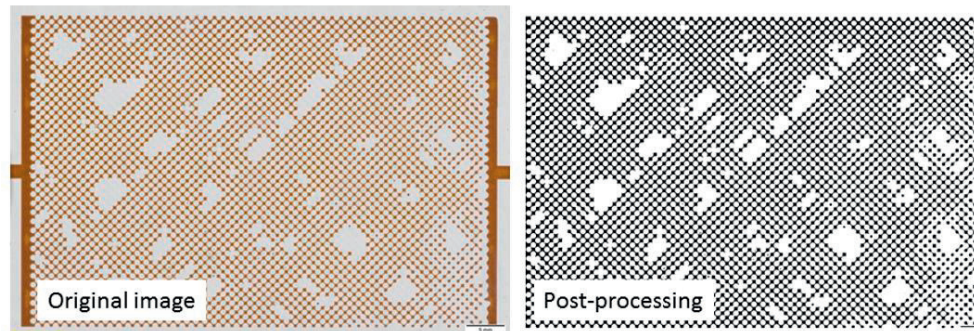
Figure 4-6. Pre- and post-processing for the determination of Swi for test #36.

The image coloring was different for test #38. There were also more smudges on many of the pictures that counted as oil pixels when using the standard post-processing procedure. Therefore, step 3 was adjusted manually as shown in Figure 4-7, and step 4 was not conducted.
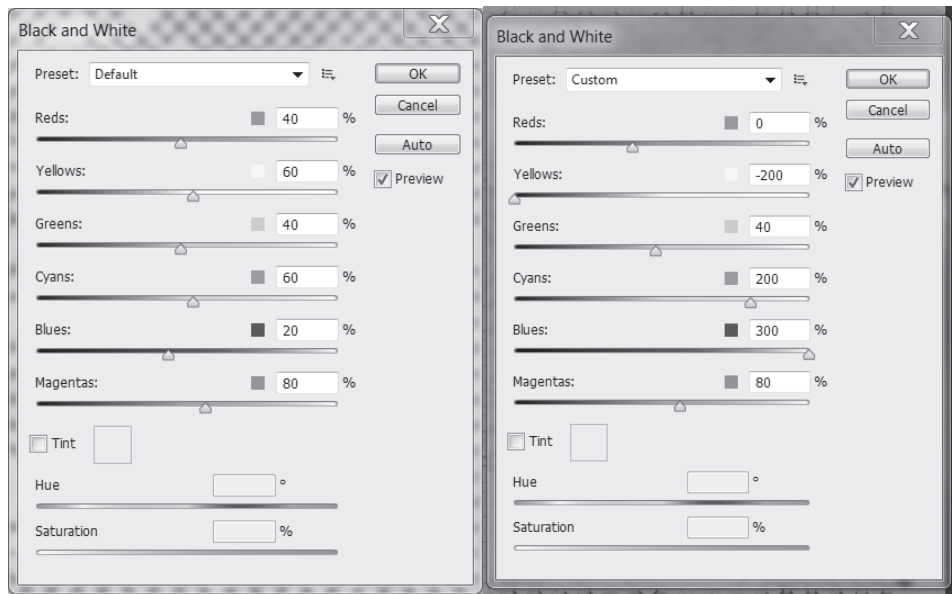
A) Automatic settings for tests #36 and #37.   B) Adjusted settings for test #38.

Figure 4-7. Black and white settings used for post-processing of micromodel images.

5 Results

The results are presented in the same order as Chapter 4. Each sub-section includes an objective statement, experimental results and a summary. The nanoparticles are evaluated in the following order for all experiments: Unmodified nanoparticles (colloidal and nano-structured) are evaluated first (Cnp_1, 2 and 3 and Nsp_1a, 2a and 3a). This is followed by the silanized nanoparticles (Nsp_1b, 2b and 3b). Finally, the PEG and epoxy modified nanoparticles are presented (Nsp_3c and 3d, respectively). An overview of the results and associated data in the appendices is shown in Table 5.1.

Table 5.1. Overiview of experimental results.

Section	Sub-section	Additional data in appendix	Research question
Nanofluid stability (5.1)		B	**RQ1:** Are the nanoparticles stable in synthetic sea water?
Interfacial tension (5.2)			**RQ3:** What are the EOR mechanisms contributing to nanoparticle-induced oil recovery?
Contact angle (5.3)			**RQ3**
Core flooding (5.4)	Water flooding	C	**RQ2:** Do the nanoparticles increase the oil recovery?
	Part 1: Screening of unmodified nanoparticles	D	**RQ2 + RQ3**
	Part 2: Screening of silanized nanoparticles	E	**RQ2 + RQ3**
	Part 3: Evaluation of surface-modified Nsp_3a	F	**RQ2 + RQ3**
	Part 4: Testing with aged cores and elevated temperature	G	**RQ2 + RQ3**
Micromodels (5.5)		H	**RQ2 + RQ3**

5.1 **Nanofluid stability**

5.1.1 Objectives

The nanoparticles' stability in SSW was evaluated using particle size distribution (PSD) measurements to determine if agglomeration occurred over time. The unmodified nanoparticles (Cnp_1, 2 and 3 and Nsp_1a, 2a and 3a) were evaluated over only 24 hours at 20°C because they were already agglomerating by the end of the measuring period. The 8-hour measurement point was selected because that would describe the PSD at the end of the core flooding experiment.

The 130 and 300 m^2/g nano-structured particles (Nsp_1a and Nsp_3a) were the only nanoparticles tested prior to these experiments in Part 1. Agglomeration had been visually observed when dispersed in the 3 wt% NaCl solution, especially when the nanoparticle concentration was increased to 1 wt% (Hendraningrat et al., 2013c). It was hypothesized that agglomeration would occur due to the introduction of multivalent cations to the solution from the SSW, but that agglomeration would be limited when used with the 0.05 wt% nanoparticle concentration.

All the modified nanoparticles (Nsp_1b, 2b, 3b, 3c and 3d) were measured over a four-month (16 week) period. These modified nanoparticles were tested at 20°C, 40°C and 60°C. Within 16 weeks, agglomeration had occurred for all nanofluids in the 60°C tests except for one nanofluid, which is why measurements were not taken after 16 weeks.

Each nanoparticle's average diameter (D_{avg}) is plotted over time. Because many of the measurements exhibit bimodal distributions and/or large values for the polydispersity index (PdI), the D_{avg} fails to adequately describe the PSD. Therefore, PSD by intensity curves are published in Appendix B.

5.1.2 Results

Both Cnp_1 and Cnp_3 agglomerate immediately after being dispersed in SSW. The colloidal nanoparticle with the smallest surface area (Cnp_1) exhibited the greatest agglomeration of all the colloidal nanoparticles (Figure 5-1a).
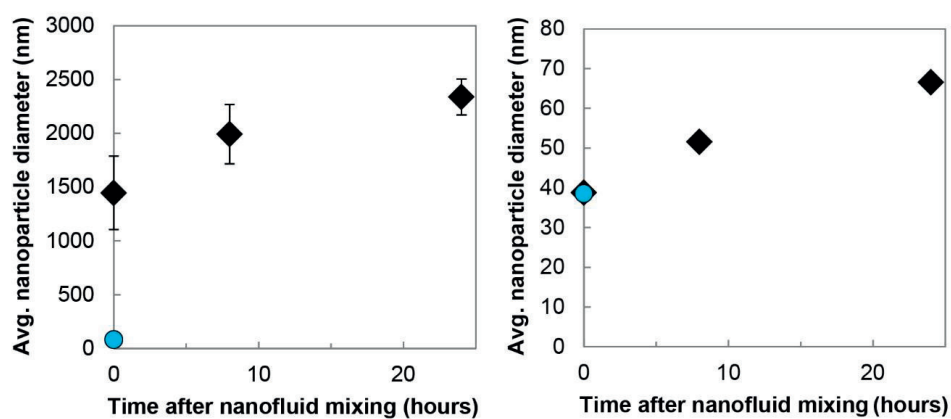
A) Cnp_1 nanoparticles (65 m^2/g) at 20°C

B) Cnp_2 nanoparticles (150 m^2/g) at 20°C
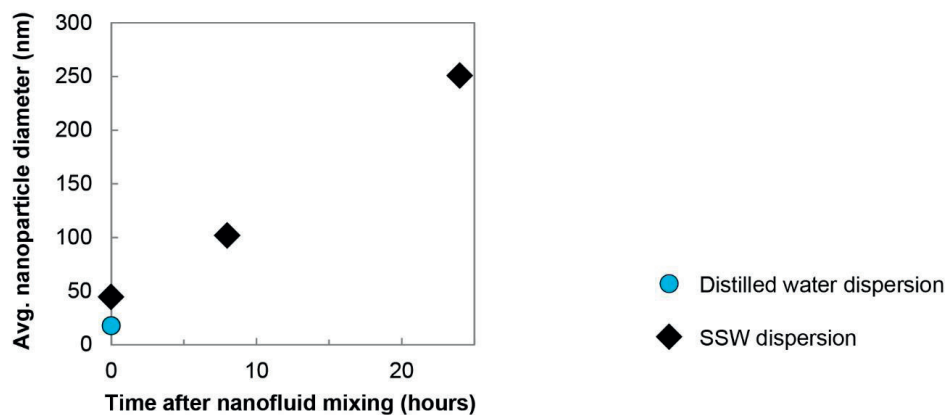
C) Cnp_3 nanoparticles (350 m^2/g) at 20°C

Figure 5-1. Average particle diameter for the colloidal nanoparticles A) Cnp_1, B) Cnp_2 and C) Cnp_3.

Immediately after mixing, the Cnp_1 D_{avg} was 1.4 μm. The nanoparticles aggregated so much within eight hours that they settled out of solution and formed a coating on the bottom of the cuvette. The samples for eight and 24 hours were briefly hand shaken to encourage re-dispersion of the sample prior to measuring. The D_{avg} after 24 hours was greater than 2.3 μm.

Cnp_2 had the least agglomeration of the colloidal particles (Figure 5-1b). There was essentially no agglomeration at t = 0 in the SSW solution. However, the D_{avg} had nearly doubled by the end of 24 hours. The D_{avg} of Cnp_3 had more than doubled immediately after dispersion into SSW (Figure 5-1c).

The unmodified nano-structured particles (Nsp_1a, 1b and 1c) all agglomerated within 24 hours, but not at the same magnitude as the colloidal nanoparticles (Figure 5-2). Measurements were not taken after 8 hours because a visual analysis had shown that little to no agglomeration was occurring throughout the duration of the core flooding test.
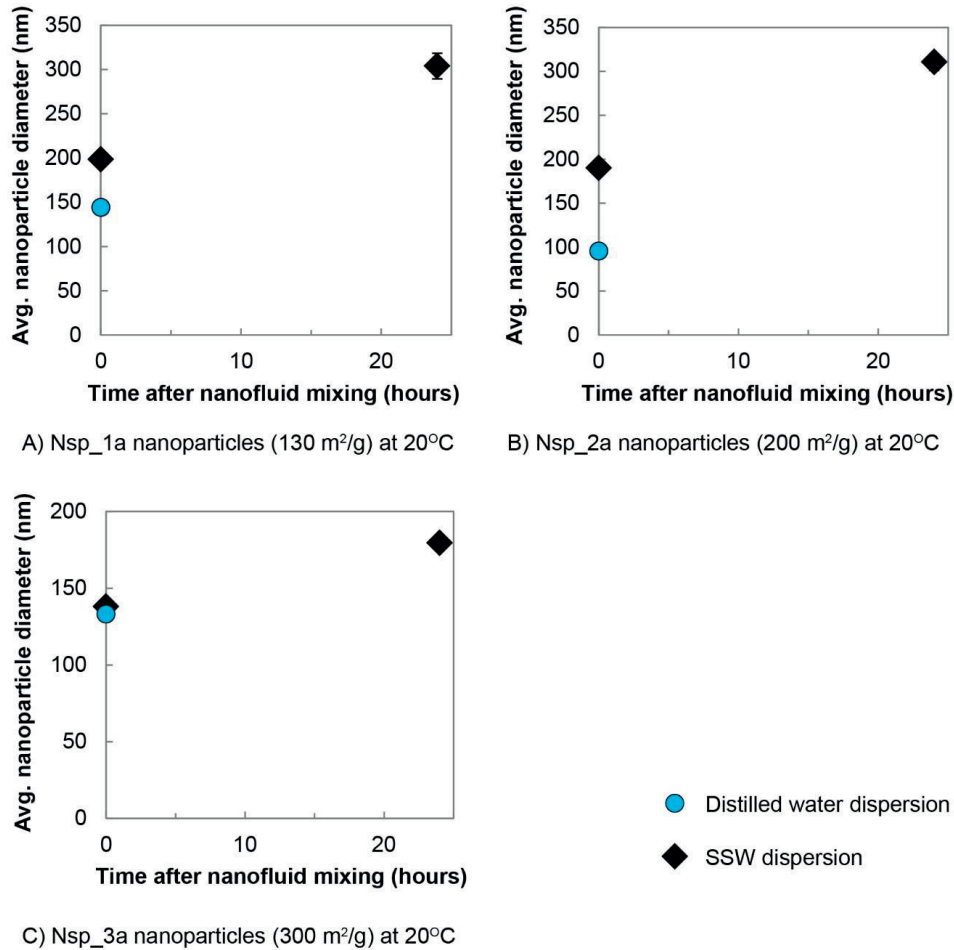
Figure 5-2. Average particle diameter for the nano-structured particles measured in distilled water immediately after nanofluid mixing and in SSW immediately after nanofluid mixing and after 24 hours.

Nsp_1a and Nsp_2a agglomerated immediately upon dispersion in SSW (Figure 5-2). Because of the bimodal distribution of Nsp_1a and Nsp_2a at 24 hours (Figure B.2 in Appendix B), the D_{avg} gives a skewed picture of the actual particle size diameter. For Nsp_1a, about 50% (by intensity) of the nanoparticles managed to stay within 196 ± 101 nm, while the remaining 50% (84% by volume) agglomerated into the micrometer scale within 24 hours (second peak at 2.0 ± 1.1 μm). Nsp_2a also had agglomeration into the micrometer scale within 24 hours, with a

peak at 1.2 ± 0.8 μm (representing 56% of the particles by intensity or 78% by volume). Nsp_3a displayed the least amount of agglomeration, with a D_{avg} increase of 3.6% immediately after SSW dispersion when compared with the distilled water dispersion. Agglomeration occurred within 24 hours, with a 34.8% increase in the D_{avg} as compared to the distilled water dispersion.

All the silanized nanoparticles (Nsp_1b, 2b and 3b) were stable in SSW at 20°C for the entire 16 week measuring period (Figure 5-3). There was no significant difference between the D_{avg} measured in distilled water and SSW directly after nanofluid mixing (t = 0). Nsp_1b was stable at 40°C through week 12. Nsp_3b was stable throughout all 16 weeks at 40°C. Nsp_2b became unstable sometime between weeks 4 and 8. None were stable at 60°C after t = 0.

A) Nsp_1b nanoparticle at 20°, 40° and 60°C.

B) Nsp_2b nanoparticle at 20°, 40° and 60°C.

C) Nsp_3b nanoparticle at 20°, 40° and 60°C.

● Distilled water dispersion at 20°C   ■ SSW dispersion at 40°C

◆ SSW dispersion at 20°C   ▲ SSW dispersion at 60°C
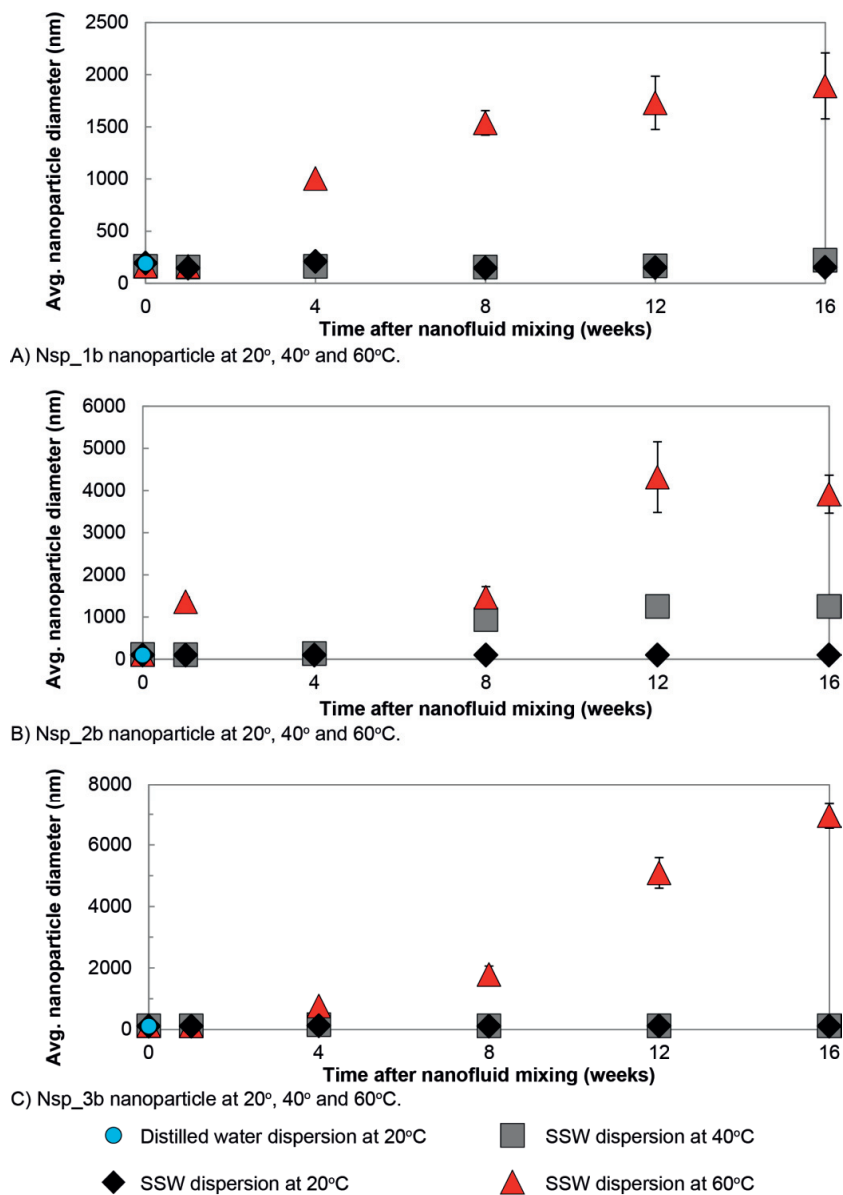
Figure 5-3. Average particle diameter for nanoparticles A) Nsp_1b, B) Nsp_2b and C) Nsp_3b dispersed in SSW over a 16 week period at 20°, 40° and 60°C. The 60°C test for Nsp_2b at 4 weeks was too polydisperse to produce an accurate value.

The PEG modified nanoparticle (Nsp_3c) was stable for 16 weeks at 0.05 wt%, 0.10 wt% and 0.50 wt% at 20°C and 40°C (Figure 5-4). The 0.05 wt% and 0.10 wt% concentrations became unstable between weeks 4 and 8 at 60°C. The 0.50 wt% concentration was the only nanofluid stable for the duration of the 16-week test.
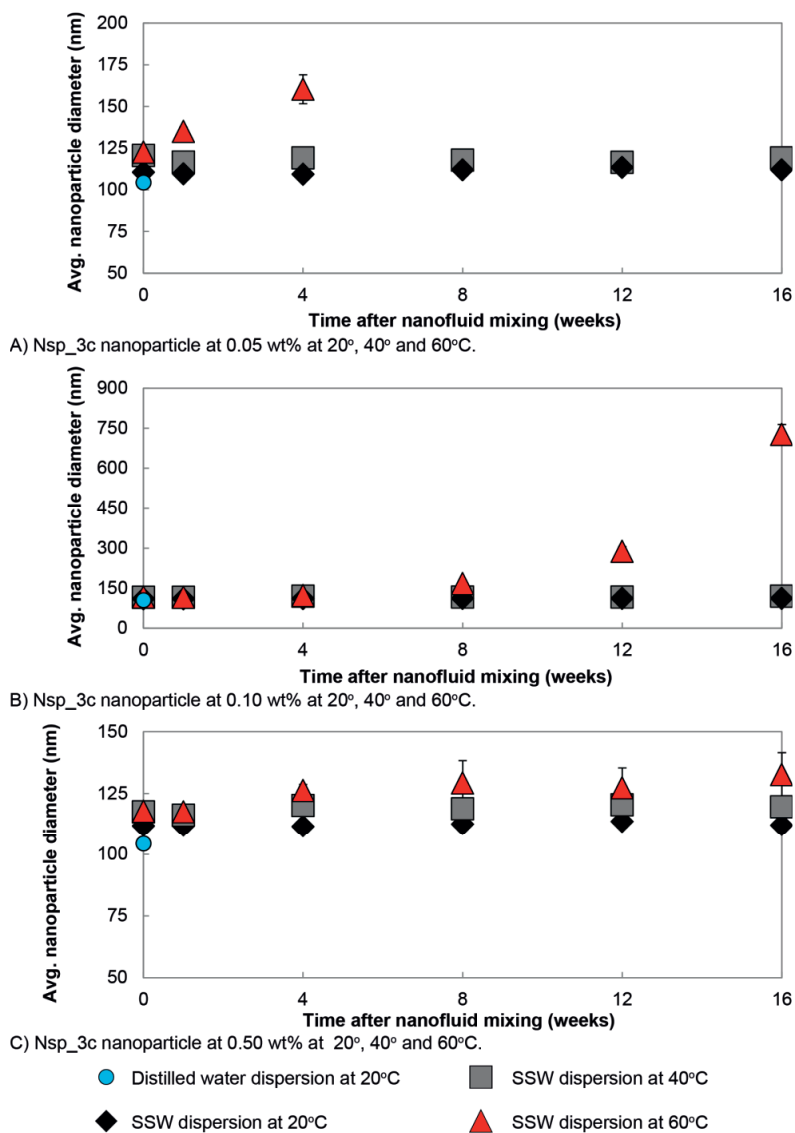
Figure 5-4. Average particle diameter dispersed in SSW over a 16 week period A) Nsp_3c at 0.05 wt%. The values from weeks 8 to 16 at 60°C were too polydisperse to give accurate D_{avg} values; B) Nsp_3c at 0.10 wt% and C) Nsp_3c at 0.50 wt%.

The epoxy modified nanoparticle (Nsp_3d) began to produce a small fraction of agglomerates sometime between 1 and 4 weeks at 20°C (Figure B.9 in Appendix B). The D_{avg} reflects this and increases after 1 week (Figure 5-5). The tests at 40°C had many errors in the measurements and are not reported. The tests at 60°C show agglomeration beginning between weeks 1 and 4, with substantial agglomeration occurring between weeks 4 and 8.
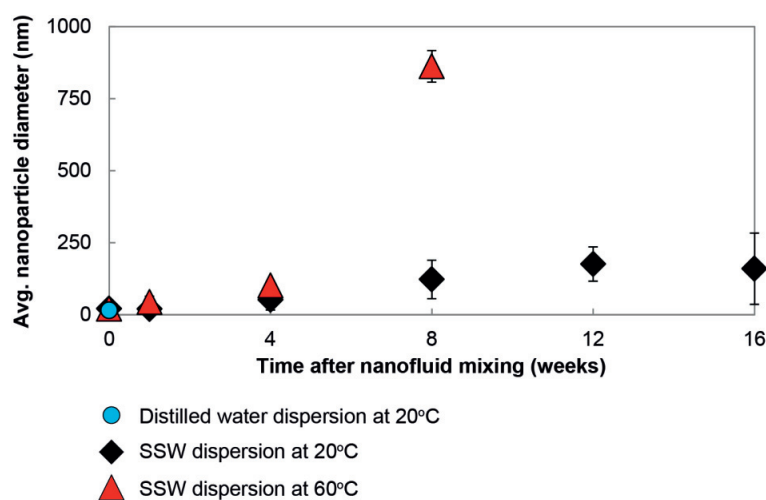
Figure 5-5. Average particle diameter for Nsp_3d at 0.05 wt% for 20°C, 40°C and 60°C.

5.1.3 Summary

All unmodified particles (Cnp_1, 2 and 3 and Nsp_1a, 2a and 3a) agglomerate within 24 hours after nanofluid mixing. The agglomeration was generally greater for the colloidal nanoparticles than the nano-structured particles. It was assumed that the unmodified particles would not be stable at 60°C. Therefore, the nano-structured particles, which demonstrated the least amount of agglomeration on average, were modified by silanization to increase their stability.

All the silanized nanoparticles (Nsp_1b, 2b and 3b) were stable in SSW at 20°C for the entire 16 week measuring period, but none were stable at 60°C throughout the 16 weeks. Measurements at 40°C were stable throughout the 16 week period for Nsp_3b, but not for Nsp_1b or Nsp_2b. This led to further surface modification for the nano-structured particle with the largest surface area (Nsp_3b) to improve the dispersion stability.

95

The epoxy modified nanoparticles (Nsp_3d) did not perform as well as Nsp_3b. The PEG modified nanoparticles (Nsp_3c) were stable at 20°C and 40°C at a concentration of 0.05 wt% and 0.10 wt%, but not at 60°C. Nsp_3c at 0.50 wt% was the only nanofluid that was stable at 60°C. An interpretation of the stability along with a summary table is provided in the discussion chapter.

5.2 Interfacial tension and capillary number

5.2.1 Objectives

The interfacial tension between crude oil and each nanofluid with a concentration of 0.05 wt% was evaluated. If the addition of nanoparticles to the SSW causes a reduction in interfacial tension down to 10^{-3} mN/m, then interfacial tension reduction could be a significant mechanism for oil recovery.

The nanoparticles could be centrifuged away from the oil droplet in the center of the glass tube during the spinning drop measurements, causing inaccurate readings. Therefore, the unmodified nanoparticles (Cnp_1, 2 and 3 and Nsp_1a, 2a and 3a) were evaluated using both a spinning drop tensiometer and pendant drop tensiometer to compare results. The modified nanoparticles (Nsp_1b, 2b, 3b, 3c and 3d) were evaluated using the pendant drop tensiometer only. All tests were conducted at 22°C. Increasing the temperature causes a decrease in interfacial tension, but not on orders of magnitude for saltwater or silica nanoparticle dispersions as demonstrated in Hendraningrat and Torsæter (2014a).

The interfacial tension was also used to calculate the capillary number per Eq. 2.5. Because interfacial tension was not measured at 60°C, the capillary number could only be calculated for core flooding tests conducted at 20°C. The goal of calculating the capillary numbers for water flooding and nanofluid flooding was to confirm that the ratio of viscous to local capillary forces was within the appropriate magnitude for water flooding in water-wet sandstones.

5.2.2 Results

For the unmodified particles, the interfacial tension slightly decreased when nanoparticles were added to the solution, but the decrease was 4.5 mN/m or less for all nanofluid systems (Table 5.2). This was confirmed with both the spinning drop and pendant drop methods. Only one measurement was conducted for each spinning drop interfacial tension value. Seven measurements were conducted for each pendant drop interfacial tension value.

Table 5.2. Summary of interfacial tension experiments for unmodified nanoparticles. The tests are conducted at 22°C using crude oil. The interfacial tension value from the spinning drop method is from one measurement and the standard deviation is therefore not reported. The interfacial tension value from the pendant drop method is an average of seven measurements. It is reported with its standard deviation. The average drop size for the pendant drop method is also reported with its standard deviation.

| Nanoparticle | Interfacial tension (mN/m) | | Average |
at 0.05 wt%	Spinning drop	Pendant drop	droplet size (μl)
None	16.4	11.5 ± 0.1	19.5 ± 0.5
Cnp_1	12.2	8.7 ± 0.4	14.0 ± 0.5
Cnp_2	15.4	10.8 ± 0.3	18.0 ± 0.6
Cnp_3	13.0	9.6 ± 0.6	16.1 ± 0.8
Nsp_1a	12.6	10.9 ± 0.3	17.8 ± 0.5
Nsp_2a	12.0	11.1 ± 0.4	18.6 ± 0.7
Nsp_3a	14.9	10.8 ± 0.7	17.9 ± 0.7

The modified nanoparticles also did not significantly change the interfacial tension (Table 5.3).

Table 5.3. Summary of interfacial tension experiments for the modified nanoparticles. The tests are conducted at 22°C using crude oil. The interfacial tension value from the pendant drop method is an average of seven measurements. It is reported with its standard deviation. The average drop size for the pendant drop method is also reported with its standard deviation.

Nanoparticle at 0.05 wt%	Interfacial tension (mN/m)	Average droplet size (μl)
None	11.5 ± 0.1	19.5 ± 0.5
Nsp_1b	10.6 ± 0.6	17.4 ± 0.8
Nsp_2b	10.7 ± 0.8	18.0 ± 1.0
Nsp_3b	11.9 ± 0.2	18.2 ± 0.4
Nsp_3c	10.9 ± 0.4	18.4 ± 0.4
Nsp_3d	11.6 ± 0.6	19.8 ± 0.8

97

The capillary numbers for water flooding were 10^{-6} for low injection rates (0.3 or 0.4 ml/min) and 10^{-5} for the high injection rate (3.0 ml/min). The capillary numbers for nanofluid flooding produced values in the same order of magnitude as the water flooding. The specific capillary numbers for each core flooding test are presented in Appendices D to F.

5.2.3 Summary

The SSW without added nanoparticles has an interfacial tension of 11.5 mN/m at 22°C with the crude oil per the pendant drop method. The addition of nanoparticles does not significantly alter the interfacial tension, with the largest difference being a reduction of 2.8 mN/m for the Cnp_1 / crude oil system when comparing the pendant drop method. The spinning drop method resulted in larger interfacial tension values than the pendant drop method, but all values were still within 5 mN/m. The effect of concentration on the interfacial tension was not analyzed but should be the next step in the evaluation. The capillary numbers for the core flooding tests were within the expected range of 10^{-6} and 10^{-5}.

5.3 **Contact angle**

5.3.1 Objectives

Contact angles were evaluated to determine if the addition of nanoparticles altered the substrate's wettability. The contact angle was measured over time to see how the contact angle was affected by the static system. If the contact angle decreases when nanoparticles are added, then those nanoparticles are increasing the water-wetness and causing the substrate to release the crude oil. Because 12 of the core flooding tests assess the oil recovery from core plugs with an intermediate-wet initial wettability, the contact angle tests can provide insight as to whether the nanoparticles are rendering the system more water-wet, thereby releasing additional oil for production. However, only initially water-wet substrates were available for contact angle experiments.

5.3.2 Results

For the unmodified nanoparticles (Cnp_1, 2 and 3 and Nsp_1a, 2a and 3a), all contact angles were in the water-wet regime as was expected for the glass plate substrate (Table 5.4). The contact angle increased over time for both SSW measurements. The colloidal nanoparticles displayed different trends. Cnp_1 had an initial contact angle that was larger than the base system, and the contact angle did not change over time. Cnp_2 had an initial contact angle equivalent to the base system, with a slight decrease over time for both measurements. Cnp_3 had a very small contact angle that was stable over time.

All the nano-structured particles had initial contact angles smaller than the SSW measurements. Nsp_2a had the largest contact angle decrease of all the nanoparticle systems. Nsp_1a and Nsp_3a had slight decreases in contact angle.

Table 5.4. Summary of contact angle experiments for the unmodified nanoparticles. Measurements were conducted every 10 minutes. The contact angle at the start of the experiment is an average of the six measurements taken within the first hour, while the end value is an average of the six measurements taken between the seventh and eighth hour. Error for the instrument is $\pm 3°$. The substrate was a glass plate. An inverted sessile drop method was used, with crude oil as the droplet. Temperature was 20°C. The concentration of the nanoparticles is 0.05 wt% in SSW.

Nanoparticle	Contact angle	
	Average of 1st hour	Average of 7th hour
None	42°	59°
None	48°	64°
Cnp_1	63°	60°
Cnp_2	42°	38°
Cnp_2	39°	30°
Cnp_3	12°	14°*
Nsp_1a	22°	18°
Nsp_2a	31°	19°
Nsp_3a	32°	26°

* This value was taken between 5.5 and 6.5 hours because the droplet disappeared.

The average contact angles for the silanized nanoparticles (Nsp_1b, 2b and 3b) are presented in Table 5.5. All the contact angle measurements conducted with n-decane were in the oil-wet regime, while all the measurements with crude oil were in the water-wet regime. The contact angle decreased over time for the experiments with n-decane and increased over time for the

experiments with crude oil. There is no apparent difference in the wettability when nanoparticles are added to the n-decane system. There appears to be a slight reduction in contact angle when Nsp_1b and Nsp_2b are added to the crude oil system. Nsp_3b does not appear to influence wettability.

Table 5.5. Average contact angle values for silanized nanoparticles. Measurements were conducted every 10 minutes. The contact angle at the start of the experiment is an average of the six measurements taken within the first hour, while the end value is an average of the six measurements taken between the eighth and ninth hour. The standard deviation of the results is reported where more than one experiment was conducted. The substrate was glass. An inverted sessile drop method was used, with the specified oleic phase as the droplet. Temperature was 20°C. The concentration of the nanoparticles is 0.05 wt% in SSW.

Oleic phase	Nanoparticle	Contact angle		Number of tests
		Average of 1st hour	Average of 9th hour	
n-Decane	None	132° (±7)	120° (±8)	4
	Nsp_1b	134° (±18)	128° (±23)	5
	Nsp_2b	142° (±16)	139° (±18)	3
	Nsp_3b	135° (±15)	129° (±19)	7
Crude oil	None	46° (±9)	54° (±2)	2
	Nsp_1b	28°	45°	1
	Nsp_2b	37°	40°	1
	Nsp_3b	44° (±1)	49° (±3)	2

The average contact angles for the Nsp_3c at 0.05 wt% and 0.15 wt% are presented in Table 5.6. All experiments were conducted on a quartz plate with crude oil. The test duration was 24 hours, so the final hour average is from hour 23 (the final hour). Data were taken every 10 minutes, except for SSW tests (base system) at 20°C, where data were taken every 5 minutes instead of 10. Therefore, the first and last hour averages for those experiments are averages of 12 data points instead of 6.

Table 5.6. Average contact angle values for Nsp_3c. Measurements were conducted every 10 minutes. The contact angle at the start of the experiment is an average of the six measurements taken within the first hour, while the end value is an average of the six measurements taken between the 23rd and 24th hours.The standard deviation of the results is reported where more than one experiment was conducted. The substrate was a polished quartz plate. An inverted sessile drop method was used, with crude oil as the droplet. Temperature is specified below.

Nanoparticle	Conc. (wt%)	Temp. (°C)	Contact angle		Number of tests
			Average of 1st hour	Average of 23rd hour	
None	---	20	35°±6	41°±6	5
None	---	60	70°	93°	1
Nsp_3c	0.05	20	68°±13	65°±17	3
Nsp_3c	0.15	20	90°±30	91°±28	2
Nsp_3c	0.05	60	70°±11	67°±13	2
Nsp_3c	0.15	60	70°±20	62°±31	2

5.3.3 Summary

When multiple contact angle measurements were repeated for a given system, the variation between contact angle values was often around ±20°. This is exhibited in the large standard deviations presented for most values. The following summary is based upon the contact angle values reported and does not take into consideration the large variance.

SSW contact angles with crude oil at ambient conditions increase over time, but remain within the water-wet regime. When unmodified nanoparticles (Cnp_1, 2 or 3 or Nsp_1a, 2a or 3a) are added to the SSW, the contact angle does not increase over time. All initial contact angle values for the unmodified nanoparticles are lower than the SSW contact angles except for Cnp_1.

Silanized nanoparticle (Nsp_1b, 2b and 3b) contact angle measurements with n-decane show that there is no significant effect when nanoparticles are added to the system. All n-decane contact angle values are in the oil-wet regime. Conversely, silanized nanoparticles decrease the contact angle when crude oil is the oleic phase, and all those values are within the water-wet regime. The contact angle increases over time for the crude oil systems.

Tests conducted with Nsp_3c show that at ambient conditions, Nsp_3c causes the system to change from water-wet to intermediate-wet. This effect becomes more pronounced when the

nanoparticle concentration is increased from 0.05 wt% to 0.15 wt%. The contact angle does not change significantly within the 24-hour measuring period.

The SSW contact angle measured at 60°C increases by 23° within the 24-hour measuring period. The contact angles for Nsp_3c at both 0.05 wt% and 0.15 wt% at 60°C have the same initial contact angle as the SSW, but the contact angle does not increase as dramatically.

5.4 Core flooding

The core flooding tests are grouped into four parts based upon their research objectives. Each core flooding part is sub-divided into research objectives, detailed flooding procedure, results and finally a summary. An analysis of the variations in the water flooding conducted prior to nanofluid flooding for each test is presented in a separate section. All recovery factors are expressed as a percentage of original oil in place (% OOIP) in the core plug prior to initiation of water flooding.

The overview for the core flooding tests is presented in Table 5.7 An overview of the water flooding and nanofluid flooding schemes is presented in Table 5.8. An overview of the nanofluids and oil type used for each core flooding test is presented in Table 5.9. In the oil recovery graphs in Part 1, data collection points are shown on the graphs to depict where data was recorded over time. The oil recovery graphs in Parts 2 through 4 do not show these sampling points because of the scale of the graphs (there are so many points that they are indistinguishable). This is because the flooding sequence is much longer for tests conducted in Parts 2 through 4. In general, the oil recovery was recorded every one-fourth pore volume.

Table 5.7. Overview of core flooding tests.

Part	Test number	Core length (cm)	Temperature (°C)	Core holder orientation
1: Screening of unmodified nanoparticles	1 – 6	13.0	20	Horizontal
2: Screening of silanized nanoparticles	7 – 13	13.0	20	Horizontal
3: Evaluation of surface-modified Nsp_3a	14 – 23	4.5 and 10.0	20	Horizontal
4: Testing with aged cores and elevated temperature	24 - 35	10.0	60	Vertical[†]

[†] Two cores were oriented horizontally: Test #24 and #25.
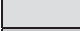
Table 5.8. Overview of water flooding and nanofluid flooding schemes.

Part	Water flooding scheme	Nanofluid flooding scheme
1	0.4 ml/min until no oil produced (1.25 to 3 PV)	0.4 ml/min until no oil produced (1.5 to 3 PV)
2	1. 0.3 ml/min for 5 PV 2. 3 ml/min until no oil produced (2 to 5 PV)	1. 0.3 ml/min for 10 PV 2. 3 ml/min for 2 PV
3	1. 0.3 ml/min for 2 PV 2. 3 ml/min for 3 PV 3. 0.3 ml/min for 0.25 PV	1. 0.3 ml/min for 10 PV *or* 0.3 ml/min for 5 PV *or* 0.3 ml/min for 5 PV – shut-in for 14-15 hours – 0.3 ml/min for 5 PV 2. 3 ml/min for 3 PV
4*	1. 0.3 ml/min for 3 PV 2. 3 ml/min for 7 PV 3. relative permeability test	1. 0.3 ml/min for 10 PV 2. 3 ml/min for 3 PV 3. relative permeability test

[*] Test #24 and #25 were flooded according to the procedure in Part 3 for water flooding, with 5 PV at 0.3 ml/min followed by 3 PV at 3 ml/min for nanofluid flooding.

Table 5.9. Core flooding test overview.

Part	Test #	Nanofluid Type	Nanofluid Surface modification	Nanofluid Conc. (wt%)	Oleic phase	Temp. (°C)	Aging
1	1	Cnp_1	-	0.05	Crude oil	20	No
	2	Cnp_2	-	0.05	Crude oil	20	No
	3	Cnp_3	-	0.05	Crude oil	20	No
	4	Nsp_1a	-	0.05	Crude oil	20	No
	5	Nsp_2a	-	0.05	Crude oil	20	No
	6	Nsp_3a	-	0.05	Crude oil	20	No
2	7	Nsp_1b	Silanization	0.05	Crude oil	20	No
	8						
	9	Nsp_1b	Silanization	0.05	n-Decane	20	No
	10	Nsp_2b	Silanization	0.05	Crude oil	20	No
	11						
	12	Nsp_2b	Silanization	0.05	n-Decane	20	No
	13	Nsp_3b	Silanization	0.05	Crude oil	20	No
3	14	Nsp_3c	PEG	0.05	Crude oil	20	No
	15						
	16	Nsp_3c	PEG	0.05	Crude oil	20	No
	17	Nsp_3c	PEG	0.025	Crude oil	20	No
	18	Nsp_3c	PEG	0.01	Crude oil	20	No
	19	Nsp_3c	PEG	0.05	Crude oil	20	No
	20	Nsp_3c	PEG	0.10	Crude oil	20	No
	21	Nsp_3d	Epoxy	0.05	Crude oil	20	No
	22	Nsp_3c	PEG	0.05	Crude oil	20	11.5 weeks at 60°C
	23	Nsp_3c	PEG	0.05	Crude oil	20	10.5 weeks at 60°C
4	24	Nsp_3c	PEG	0.05	Crude oil	60	No
	25	Nsp_3d	Epoxy	0.05	Crude oil	60	No
	26	Nsp_3a	-	0.05	Crude oil	60	4 weeks at 60°C
	27						
	28	Nsp_3c	PEG	0.01	Crude oil	60	4 weeks at 60°C
	29	Nsp_3c	PEG	0.05	Crude oil	60	4 weeks at 60°C
	30						
	31	Nsp_3c	PEG	0.15	Crude oil	60	4 weeks at 60°C
	32						
	33						
	34	Nsp_3d	Epoxy	0.05	Crude oil	60	4 weeks at 60°C
	35						

- Single test
- Duplicate test
- Triplicate test
- Not modified / not applicable

5.4.1 <u>Water flooding</u>

5.4.1.1 Water flooding objective

Water flooding was conducted prior to nanoparticle flooding for all tests. The variations amongst the core flooding experiments can be investigated by comparing the initial water saturation, recovery factor from water flooding and residual oil saturation after water flooding with SSW for each core. Variation in core flooding can be due to experimental error and/or differences in the core plug material. The nature of the water flooding can also give an indication of the core's initial wettability.

5.4.1.2 Water flooding procedure

The detailed procedures for water flooding are presented in sections 5.5.2 through 5.5.5, but the water flooding procedures are summarized in Table 5.10. Cores for tests #22, 23 and 26 to 35 have no initial water saturation.

Table 5.10. Summary of water flooding procedures.

Part	Test #	Water flooding procedure
1: Screening of unmodified nanoparticles	1 to 6	0.4 ml/min for 1.25 to 3 PV
2: Screening of silanized nanoparticles	7 to 13	0.3 ml/min for 5 PV 3.0 ml/min for 2 to 5 PV
3: Evaluation of surface-modified Nsp_3a	14 to 25	0.3 ml/min for 2 PV 3.0 ml/min for 3 PV 0.3 ml/min for 0.25 PV
4: Testing with aged cores and elevated temperature	26 to 35	0.3 ml/min for 3 PV 3.0 ml/min for 7 PV Relative permeability test[*]

5.4.1.3 Water flooding results

The initial water saturation, residual oil saturation, recovery factor and relative permeability to water end-points (where available) are presented in their respective core flooding groupings based upon the differences in initial core conditions and flooding procedures (Parts 1 through 4). The Part 2 tests conducted with n-decane (tests #9 and #12) are considered separately.

The average initial water saturation was 0.33 (± 0.06) and varied from 0.24 to 0.47 (Table 5.11 and Figure 5-6). The initial water saturations for tests #14 to #21 (Part 3) and #24 and #25 (Part 4) were the highest on average. Tests #22 and #23 (Part 3) and #26 to #35 (Part 4) core plugs had no initial water saturation and are therefore not considered here. The initial saturations for tests #9 and #12 conducted with n-decane were 0.46 and 0.32, respectively.

Table 5.11. Variation of initial water saturation values.

Initial water saturation	Core flooding tests			
	Part 1 (#1 to 6)	Part 2 (#7, 8, 10, 11 and 13)	Part 3 (#14 to 21, 24 and 25)	All
Maximum	0.40	0.37	0.47	0.47
Average	0.30	0.30	0.37	0.33
Minimum	0.26	0.24	0.33	0.24
Standard Deviation	0.05	0.05	0.04	0.06
# of core flooding tests (n)	6	5	10	21
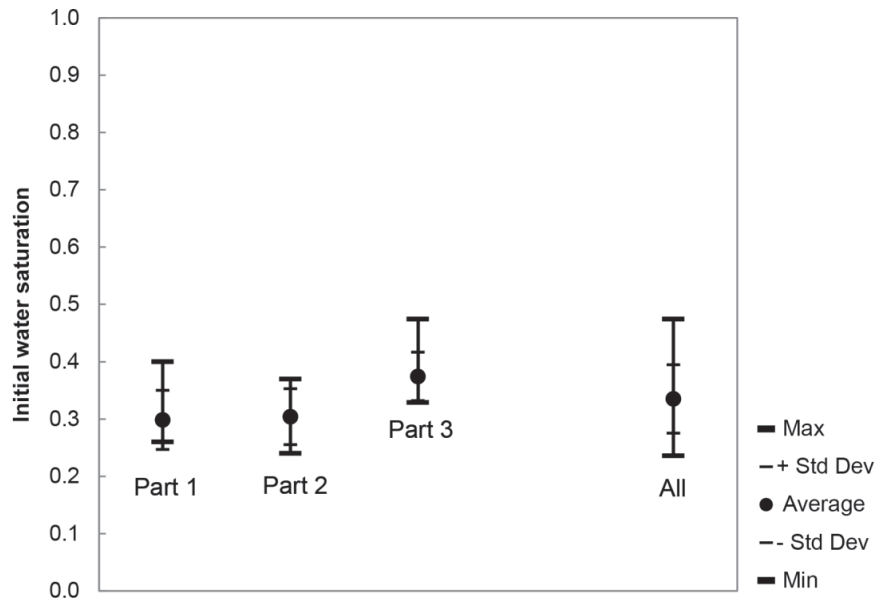
Figure 5-6. The maximum, minimum and average (± standard deviation) of the initial water saturation. Data are a visual representation of values presented in Table 5.11.

The average recovery factor at the end of water flooding was 61.8% OOIP (± 9.3) and varied from 47.3% to 82.3% OOIP (Table 5.12 and Figure 5-7). This final recovery is the amount of oil recovered after both the low rate and the high rate water flooding has been conducted for Parts 2 through 4. Only low rate water flooding was conducted for Part 1. The water flooding recovery from Part 3 shows the greatest degree of variation, with a standard deviation of 12.0% OOIP compared to 5.1%, 7.7% and 7.3% OOIP for Parts 1, 2 and 4, respectively. The water flooding recovery factors from the n-decane tests were 58.6% and 52.2% OOIP.

Table 5.12. Variation of ultimate recovery factors from water flooding.

Water flooding recovery factor	Part 1 (#1 to 6)	Part 2 (#7, 8, 10, 11 and 13)	Part 3 (#14 to 21, 24 and 25)	Part 4 (#22 and 23, 26 to 35)	All
Maximum	62.3	78.2	82.3	69.6	82.3
Average	57.2	65.7	66.5	58.5	61.8
Minimum	50.0	57.9	47.3	47.8	47.3
Standard Deviation	5.1	7.7	12.0	7.3	9.3
# of core flooding tests (n)	6	5	10	12	33
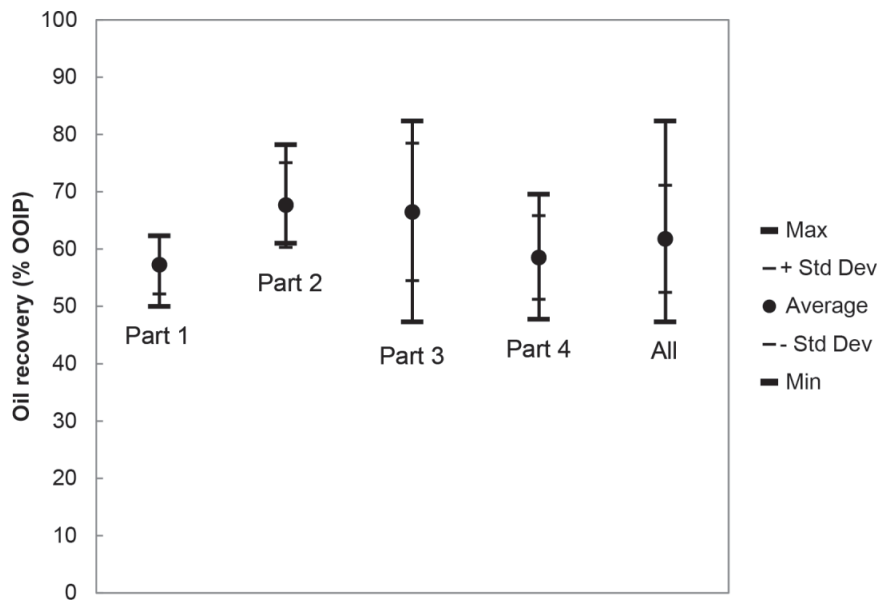
Figure 5-7. The maximum, minimum and average (± standard deviation) of the ultimate recovery factor from water flooding expressed as a percentage of the original oil in place. Data are a visual representation of values presented in Table 5.12.

The nature of the oil production during water flooding can give an indication of the core plug's wettability (Alagic et al., 2011). Typically, little to no oil production occurs after water breakthrough for a water-wet system, while an oil-wet system exhibits an earlier water breakthrough but additional production after water breakthrough (Alagic et al., 2011). The oil recovery curves for Parts 1 through 3 (Figures C.1 through C.3 in Appendix C) exhibit little oil

production after breakthrough compared to the oil recovery curves for Part 4 (Figure C.4), which have relatively continual production over time. Recovery curves for Part 2 show a clear increase in oil production after five pore volumes of flooding, when the injection rate was increased to 3 ml/min. This same procedure was applied to water flooding during Parts 3 and 4 (although not at the 5 PV mark), but there is little apparent increase in oil production due to the rate increase. Tests #22 and #23, which were aged the longest, have the highest ultimate recovery factors of the aged cores (Figure C.3). The tests with n-decane as the oil stage (#9 and #12) had no oil production after water breakthrough (Figure C.5). Some additional oil was produced at the end of water flooding after the injection rate was increased 10-fold.

The end-point relative permeability to water (k_{rw}) at residual oil saturation ranged was calculated with absolute permeability determined from air measurements as the reference permeability. The average k_{rw} for the aged cores was higher and exhibited more variability than the unaged cores (Table 5.13 and Figure 5-8). Data was not collected to compute relative permeability for tests #1 through #13, #15, #16, #24 and #25.

Table 5.13. Variation of relative permeability to water calculated at residual oil saturation (from water flooding) with absolute permeability as the reference permeability. The data from unaged cores with initial water saturation are from tests #14 and #17 through #21. The data from cores aged for four weeks at 60°C with no initial water saturation are from tests #26 through #35.

k_{rw} end-point from water flooding	Unaged cores with S_{wi}	Aged cores with no S_{wi}
Maximum	0.10	0.57
Average	0.08	0.34
Minimum	0.08	0.20
Standard Deviation	0.01	0.11
# of core flooding tests (n)	6	12
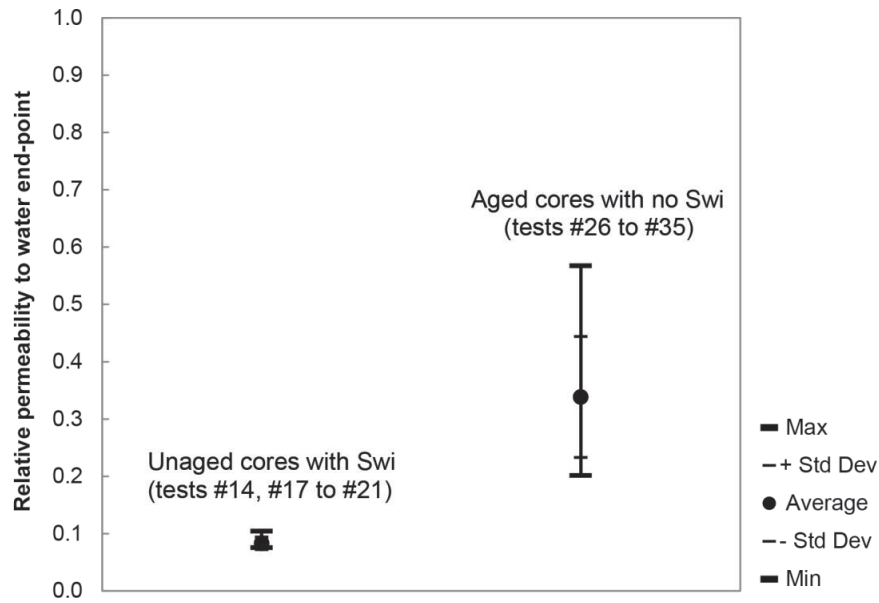
Figure 5-8. Relative permeability to water calculated at residual oil saturation (from water flooding) with absolute permeability as the reference permeability. Data are a visualization of values presented in Table 5.13.

The oil recovery from each water flooding test is compared with its respective porosity (Figure 5-9), permeability (Figure 5-10) and initial water saturation (Figure 5-11) to determine the effects of these core plug properties on the results.
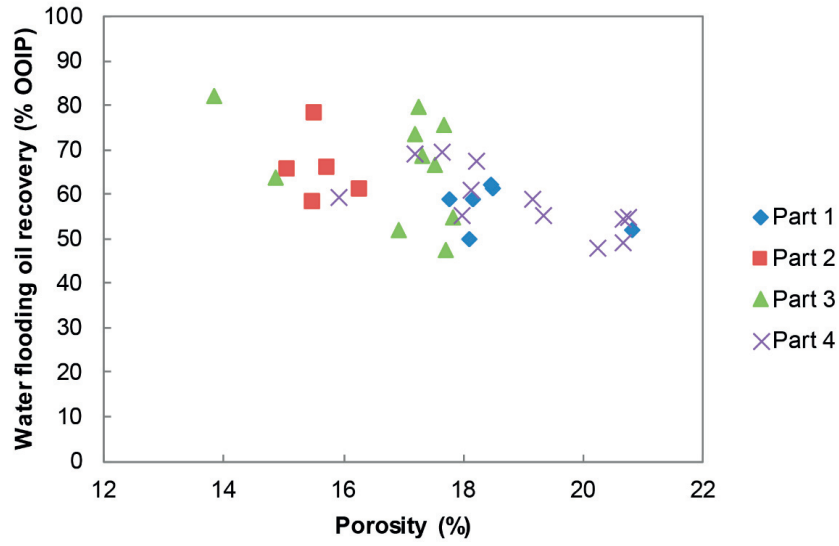
Figure 5-9. Water flooding oil recovery vs. core plug porosity.
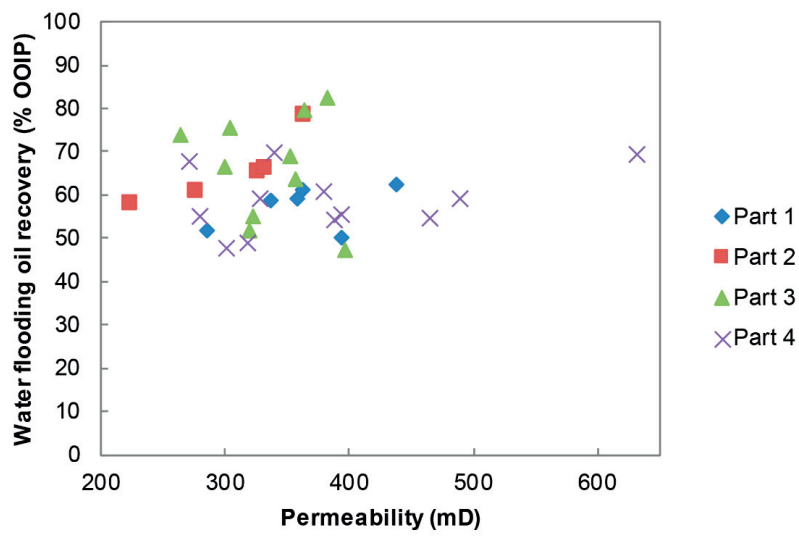
Figure 5-10. Water flooding oil recovery vs. core plug permeabilty.
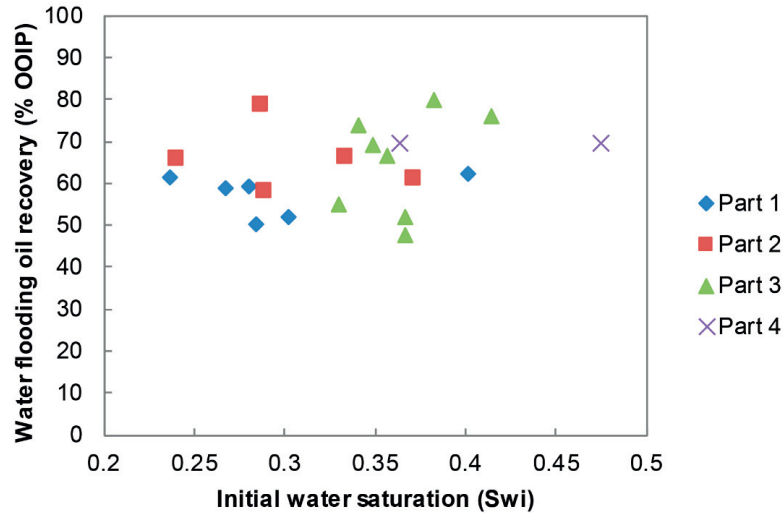
Figure 5-11. Water flooding oil recovery vs. initial water saturation. Tests without initial water saturation are not shown.

The capillary number ranged from 2.58×10^{-6} to 3.45×10^{-6} for low-injection rate water flooding. The capillary number ranged from 2.58×10^{-5} to 3.32×10^{-5} for high-injection rate water flooding.

5.4.1.4 Water flooding summary

The average initial water saturation was 0.33 and it varied from 0.24 to 0.47. Part 3 core flooding tests showed the greatest variability in water flooding recovery factors. The average recovery factor from water flooding was 61.8% OOIP and it varied from 47.3% to 82.3% OOIP. For the four core flooding tests in Part 2 that were conducted with crude oil and produced significant oil when the nanofluid flooding rate was increased, the amount of oil produced after the water flooding rate was also large (greater than 23.0% OOIP). Part 3 core flooding tests showed the most variability in water flooding recovery factors. The relative permeability to water calculated at the residual oil saturation after water flooding for tests in Part 3 and Part 4 confirm that tests with initial water saturation and no aging have relative permeability around 0.10, which is in the water-wet regime. Conversely, the tests with no initial water saturation

and that were aged produce larger relative permeability values ranging from 0.20 to 0.57. There is a subtle negative correlation between oil recovery from water flooding and core plug porosity. There is no apparent correlation between water flooding oil recovery and core plug permeability or initial water saturation. The capillary numbers for the low-injection rate are within the range for reservoir flooding (10^{-6}).

5.4.2 Part 1: Screening of unmodified nanoparticles

5.4.2.1 Core flooding Part 1 objectives

The objectives of Part 1 were to compare two nanoparticle morphologies and to determine the relationship between nanoparticle surface area and recovery factor by core flooding. By comparing two morphologies, additional EOR agents could be assessed while providing a check for the surface area / recovery factor relationships. Colloidal nanoparticles and nano-structured particles were the two types of morphologies tested. Colloidal nanoparticles are spherical, while nano-structured particles have a dendritic form. There was no hypothesis as to which morphology would produce the most oil during core flooding.

Six commercially available nanoparticles, each with a different surface area, were investigated. The colloidal nanoparticles were available with surface areas of 65, 150 and 350 m^2/g (hereafter referred to as Cnp_1, Cnp_2 and Cnp_3, respectively). The nano-structured particles were available at 130, 200 and 300 m^2/g (hereafter referred to as Nsp_1a, Nsp_2a and Nsp_3a, respectively). It was hypothesized that the largest surface areas would result in the highest recovery factors for their respective morphologies. This is because a larger surface area means there is a higher propensity for reactivity given the same particle concentration. All experiments were conducted with the nanoparticles dispersed in synthetic sea water (SSW) at a concentration of 0.05 wt%.

The 130 and 300 m^2/g nano-structured particles (Nsp_1a and Nsp_3a) were the only nanoparticles tested prior to these experiments in Part 1 and produced varying oil recovery factors (refer to Table A.1 in Appendix A for an overview).

One core flooding experiment was conducted for each nanofluid. This assumes that having one result from each nanofluid is sufficient to determine the relationships amongst morphology, surface area and recovery factor. This is due to the time-consuming nature of core flooding tests. Effluent silica concentration was determined for the nano-structured particle core flooding tests.

5.4.2.2 Core flooding Part 1 detailed procedure

The primary drainage process was conducted by injecting crude oil at 0.4 ml/min into the core plug until no more 3% NaCl brine was produced for at least 0.2 PV. Drainage was therefore typically conducted for 2 PV. This procedure established the initial water saturation and the original oil in place.

Water flooding was then conducted with SSW to simulate imbibition conditions in the North Sea. SSW was injected at 0.4 ml/min until no oil was produced for at least 0.35 PV. The water flooding determined the residual oil saturation and recovery factor from water flooding.

Tertiary nanofluid flooding was then conducted at an injection rate of 0.4 ml/min until no oil was produced for at least 0.25 PV. This step determined the residual oil saturation and recovery factor from nanofluid flooding. Test #2 had ceased to produce oil during water flooding for only 0.16 PV when the switch to nanofluid flooding was made. This test was made before the 0.35 PV criteria was established. It also had continuous oil production during nanofluid flooding, and the test had to be stopped at the end of the day.

5.4.2.3 Core flooding Part 1 results

The nano-structured particles produced larger recovery factors on average than the colloidal particles (Table 5.14). The residual oil saturation ranged from 0.21 to 0.31 after nanofluid flooding (Table 5.15). The main oil bank from nanofluid flooding was produced within the first 0.6 PV for all tests (Table 5.16). The nanofluid flooding recovery factor after one pore volume ranged from 2.03 to 7.06%. A summary of each core flooding test is presented in Appendix D.

Table 5.14. Part 1 core flooding recovery factors. The nanoparticles were dipsersed in SSW at 0.05 wt%.

Test #	Nanoparticle	Recovery factor (% OOIP)		
		Water flood	**Nano flood**	**Total**
1	Cnp_1	51.9	3.5	55.4
2	Cnp_2	61.4	6.6	68.0
3	Cnp_3	62.3	2.4	64.7
4	Nsp_1a	58.8	11.8	70.6
5	Nsp_2a	50.0	8.3	58.3
6	Nsp_3a	59.0	5.7	64.7

Table 5.15. Part 1 intial water saturation and residual oil saturations.

Test #	Nanoparticle	Swi	Sor	
			Water flood	**Nano flood**
1	Cnp_1	0.30	0.34	0.31
2	Cnp_2	0.26	0.29	0.24
3	Cnp_3	0.40	0.23	0.21
4	Nsp_1a	0.27	0.30	0.22
5	Nsp_2a	0.28	0.36	0.30
6	Nsp_3a	0.28	0.29	0.25

Table 5.16. Summary of Part 1 core flooding parameters to determine EOR viability.

Test #	Nanoparticle	Occurrence of initial oil bank (after _ PV of nanofluid flooding)	Recovery factor (% OOIP) after 1 PV of nanofluid flooding	Total recovery factor (% OOIP) from nanofluid flooding
1	Cnp_1	0.2	2.0	3.5
2	Cnp_2	0.6	4.1	6.6
3	Cnp_3	0.6	2.4	2.4
4	Nsp_1a	0.4	7.1	11.8
5	Nsp_2a	0.5	4.0	8.3
6	Nsp_3a	0.3	3.0	5.7

The differential pressure across the core plug increased throughout the duration of the nanofluid flooding for all tests (Figures D.2 through D.7 in Appendix D). This increase varied from 0.06 bar (test #3) to 0.40 bar (test #6). The maximum differential pressure during nanofluid flooding was also greater than the maximum differential pressure during water flooding for all tests. This difference varied from 0.05 bar (test #1) to 0.29 bar (test #4).

Nanoparticle concentration samples were taken from the nanofluid effluent for tests #4 through #6 (tested with the nano-structured particles). Over 98% of the nanoparticles were retained in the core during Nsp_1a and Nsp_2a nanofluid flooding. Nanofluid flooding with Nsp_3a resulted in 95% of the injected nanoparticles being retained (Figure 5-12).
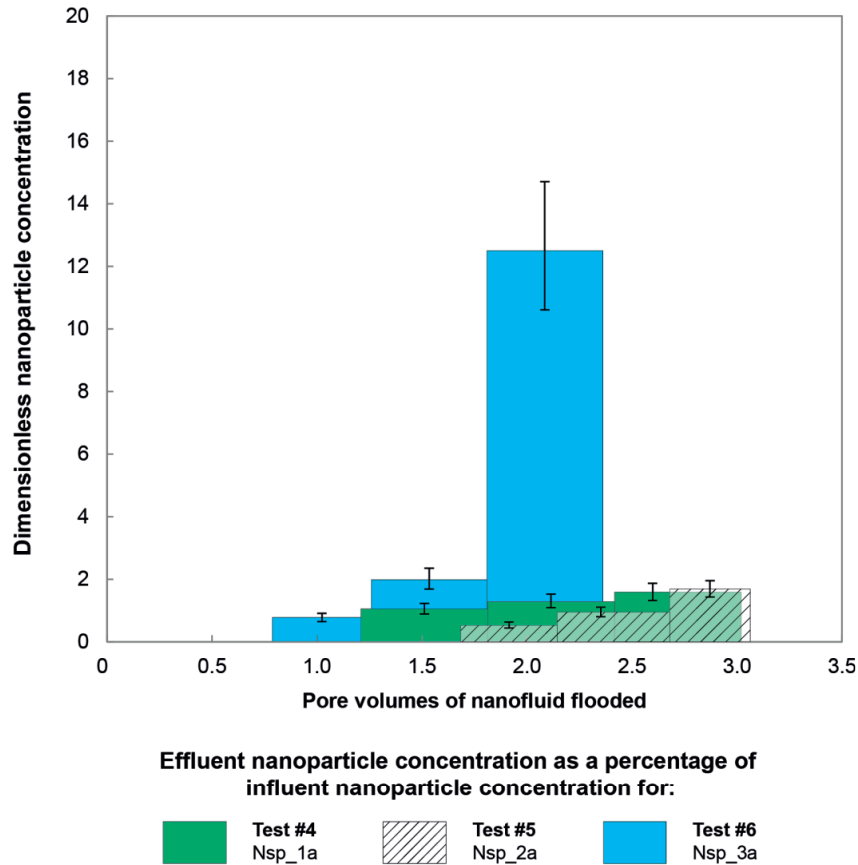
Figure 5-12. Nanoparticle retention from the nanofluid flooding effluent during tests #4, 5 and 6.

The concentration of silica in crude oil was also determined for core flooding tests #4 through #6. The influent crude oil had two measured values for silica content: 6 and 14 μg/g. The silica concentration in the effluent crude oil produced from water flooding varied from 12 (± 2) μg/g to 15 (± 3) μg/g for all tests (Table 5.17). The silica content in the crude oil increased by two- to fourfold throughout nanofluid flooding.

Table 5.17. Concentration of silica in crude oil influent and effluent for core flooding tests #4 through #6.

Test # / Nanoparticle	Crude oil phase	Silica content (µg/g)
	Influent	14[*]
	Influent	6[*]
#4 / Nsp_1a	Water flooding effluent	12 ± 2
	Nanofluid flooding effluent	25[*]
#5 / Nsp_2a	Water flooding effluent	14 ± 4
	Nanofluid flooding effluent	80[*]
#6 / Nsp_3a	Water flooding effluent	15 ± 3
	Nanofluid flooding effluent	61[*]

* Only one measurement conducted.

5.4.2.4 Core flooding Part 1 summary

Oil was produced during nanofluid flooding for all tests. Nanofluid flooding oil recovery varied from 2.4% to 11.8%. The nano-structured particles Nsp_1a and Nsp_2a produced the highest oil recoveries (11.8% and 8.6%, respectively). The occurrence of the first oil bank was between 0.2 and 0.6 PV for all tests. Only one test (#4/ Nsp_1a) had an oil recovery greater than 5% within the first pore volume.

The differential pressure during nanofluid flooding was greater than the differential pressure during water flooding. Effluent analysis from the nano-structured particle tests (#4 through #6) confirms that over 95% of the nanoparticles are retained in the core plug. Nanoparticle absorption to the crude oil is minimal. It was concluded that the nano-structured particles should be surface modified to prevent agglomeration and therefore improve propagation through the core plug.

5.4.3 Part 2: Screening of silanized nanoparticles

5.4.3.1 Core flooding Part 2 objectives

Part 1 concluded that the nanoparticles must be modified to prevent agglomeration in SSW. The nano-structured particles performed better for enhanced oil recovery (EOR) than the colloidal nanoparticles. Additionally, Evonik Industries (the nanoparticle supplier) concluded that the nano-structured particles were easier to modify from a chemical standpoint. Therefore, they produced surface modifications for the three nano-structured particles tested in Part 1. They are named Nsp_1b, Nsp_2b and Nsp_3b.

The injection rate in Part 2 was decreased to 0.3 ml/min (as compared to Part 1's 0.4 ml/min) to better mimic the flow velocity in the reservoir. For all core flooding tests in Part 1, the differential pressure increased throughout the nanofluid flooding to reach pressure values higher than that achieved during the water flooding. Therefore, the core flooding procedure was modified to guarantee that the maximum differential pressure during the nanofluid flooding stage would not exceed the maximum differential pressure from the water flooding stage, thereby ensuring that any nanofluid oil production was a result of chemical, not mechanical, processes. The injection rate was therefore increased 10-fold (from 0.3 ml/min to 3.0 ml/min) at the end of water flooding. The length of water flooding and nanofluid flooding was extended to confirm residual oil saturation values. A nanofluid flooding injection rate increase was added to overcome capillary end effects after nanofluid flooding. A chase water flood with SSW was conducted after the nanofluid flooding to investigate the reversibility of the nanoparticle retention. Post- core flooding absolute permeability measurements were conducted after cleaning the cores to determine if permeability impairment was occurring as a result of nanoparticle agglomeration and/or adsorption.

The core flooding tests with the nanoparticles with the smallest and medium surface area (Nsp_1b and Nsp_2b) were duplicated to confirm results. The nanoparticle with the largest surface area (Nsp_3b) should have been duplicated, but it was decided to further modify it and therefore duplication was deprioritized. Core flooding repeatability can have large scatter, especially when unique cores are used for each experiment.

N-decane was used as the oil phase for two core flooding tests to compare with crude oil. By eliminating complex crude oil components, such as asphaltenes and resins that have been shown to react with Nsp_2a (Hannisdal et al., 2006), the potency of chemical mechanisms leading to enhanced oil recovery should be dampened. It was hypothesized that the nanofluid flooding recovery factor would be lower in the n-decane experiments than the crude oil experiments. Nanoparticles Nsp_1b and Nsp_2b were tested using n-decane.

5.4.3.2 Core flooding Part 2 detailed procedure

The primary drainage process was conducted by injecting crude oil or n-decane at 0.3 ml/min for 2 PV. The injection rate was then increased to 3 ml/min and oil was injected until no 3 wt% NaCl reservoir brine was produced for at least 0.3 PV. This second injection step lasted between 5 and 10 PV. This procedure established the initial water saturation and the original oil in place.

Water flooding was then conducted with SSW to simulate conditions in the North Sea. The sea water was injected at 0.3 ml/min for 5 PV. This stage is hereafter referred to as WF-Q_{low} (water flooding low injection rate). Then the injection rate was increased to 3 ml/min to increase the differential pressure and to be certain that any oil produced during the subsequent nanofluid flooding stage is a result of an interaction between the nanofluid and the oil phase (and perhaps the sandstone) and not just from a pressure increase or time increase. The 3 ml/min water flooding stage was performed for 2 to 5 PV. This stage is hereafter referred to as WF-Q_{high}. Recovery factors and oil saturations were calculated at the end of both water flooding stages.

Nanofluid flooding was performed by injecting a nanofluid into the core at 0.3 ml/min for 10 PV. After the initial nanofluid flooding stage, the injection rate was increased to 3 ml/min for 2 PV to see if any oil would dislodge from the system. Recovery factors and oil saturations were calculated at the end of both nanofluid flooding stages (NF-Q_{low} and NF-Q_{high}, respectively).

The SSW was injected into the core after the nanofluid flooding to flush out nanoparticles retained in the core plug. The chase water flooding was conducted at 0.3 ml/min for 2 PV followed by 3 ml/min for 2 PV. These stages are hereafter referred to as Chase-Q_{low} and Chase-Q_{high}, respectively.

5.4.3.3 Core flooding Part 2 results

Recovery factors for the four flooding stages (water flooding and nanofluid flooding) are presented in Table 5.18. Total water flooding recovery varied from 52% to 78%. Residual oil saturation after nanofluid flooding ranged from 0.11 to 0.32 (Table 5.19). No oil recovery occurred during the chase water flooding. Details for each core flooding test are presented in Appendix E.

Overall nanofluid flooding recovery was lowest for the tests conducted with n-decane. None of the experiments had recovery factors greater than 1.2% throughout the entire nanofluid flooding stage conducted at Q_{inj} = 0.3 ml/min. The first oil bank from nanofluid flooding occurred between 2.5 and 8.5 PV (Table 5.20).

In four of the five tests with crude oil, significant oil production occurred during the nanofluid flooding at Q_{inj} = 3.0 ml/min. The duplicate experiments for Nsp_1b and Nsp_2b gave inconsistent total nanofluid flooding recovery results. For the tests with Nsp_1b and crude oil, the recovery factor during NF-Q_{low} was 0.1% and 1.1% for the two tests, while the recovery factor during NF-Q_{high} was 6.0% and 0%. For the tests with Nsp_2b and crude oil, the recovery factor during NF-Q_{low} was 0.9% and 1.2%, which is similar. But the recovery factor during NF-Q_{high} was 13.8% and 5.6% for the two tests.

Table 5.18. Summary of recovery factors (as % OOIP) for each of the flooding stages (water flooding at 0.3 and 3.0 ml/min and nanofluid flooding at 0.3 and 3.0 ml/min). All nanoparticles were dispersed in SSW at 0.05 wt%.

Test #	Nanoparticle	Oil phase	Recovery factor (% OOIP)				
			WF-Q_{low}	WF-Q_{high}	NF-Q_{low}	NF-Q_{high}	Total
7	Nsp_1b	Crude	41.3	24.1	0.1	6.0	71.5
8	Nsp_1b	Crude	52.0	9.0	1.1	0.0	62.1
9	Nsp_1b	n-Decane	55.4	3.1	0.4	0.0	58.9
10	Nsp_2b	Crude	34.9	23.0	0.9	13.8	72.6
11	Nsp_2b	Crude	49.9	28.3	1.2	5.6	85.0
12	Nsp_2b	n-Decane	51.0	1.2	0.0	0.9	53.1
13	Nsp_3b	Crude	40.0	26.0	1.1	7.2	74.3

Table 5.19. Part 2 initial water saturation and residual oil saturations.

Test #	Nanoparticle	Oil phase	Swi	Sor	
				Water flood	Nano flood
7	Nsp_1b	Crude	0.24	0.26	0.22
8	Nsp_1b	Crude	0.37	0.25	0.24
9	Nsp_1b	n-Decane	0.46	0.24	0.22
10	Nsp_2b	Crude	0.29	0.30	0.19
11	Nsp_2b	Crude	0.29	0.16	0.11
12	Nsp_2b	n-Decane	0.32	0.32	0.32
13	Nsp_3b	Crude	0.33	0.23	0.17

Table 5.20. Summary of Part 2 core flooding parameters to determine EOR viability.

Test #	Nanoparticle	Occurrence of initial oil bank (after _ PV of nanofluid flooding)	Recovery factor (% OOIP) after 1 PV of nanofluid flooding	Total recovery factor (% OOIP) from nanofluid flooding
7	Nsp_1b	3*	0	6.1
8	Nsp_1b	5.2	0	1.1
9	Nsp_1b	8.5*	0	0.4
10	Nsp_2b	7.9	0	14.7
11	Nsp_2b	2.6	0	6.8
12	Nsp_2b	10.3†	0	0.9
13	Nsp_3b	1.0*	0.03	8.3

*Only a trace amount of oil (<0.1% OOIP) was produced at the initial oil bank.
†The initial oil bank occurred after the nanofluid flooding injection rate was increased to 3 ml/min.

The differential pressure across the core plug increased throughout the 10 PV duration of the nanofluid flooding by 0.1 bar or less for all tests (Figures E.2 through E.8 in Appendix E). Test #9 had an increase of slightly higher than 0.1 bar (Nsp_1b with n-decane). The maximum differential pressure during NF-Q_{high} was less than the maximum differential pressure during WF-Q_{high} for all experiments except #12 (Nsp_2b with n-decane). However, the plateau differential pressure values were greater during nanofluid flooding than water flooding for all experiments that achieved incremental oil production during the NF-Q_{high} stage (all tests except #8 and #9). The average differential pressure during NF-Q_{low} was less than the differential

pressure during WF-Q_{high}. The maximum NF-Q_{low} differential pressure was also less than the differential pressure for WF-Q_{low} for all tests except #12 (Nsp_2b with n-decane).

Post- core flooding absolute permeability measurements revealed that permeability decreased for all cores (Table 5.21).

Table 5.21. Core plug aboslute permeability measured pre- and post- core flooding in dried cores using a gas permeameter and the Klinkenberg correction. The percent difference is shown. A negative value indicates permeability impairment (a decrease in permeability post- core flooding).

Core / test #	Absolute permeability (mD)		
	Before	After	% difference
7	327	257	-21 %
8	276	238	-14 %
9	394	373	-6 %
10	224	195	-13 %
11	363	274	-25 %
12	453	361	-20 %
13	332	215	-35 %

Effluent pH measurements taken at the end of water flooding, the end of nanofluid flooding, and at the beginning of each chase water flooding stage were all within the range of 7.17 to 7.85. The effluent from the water flooding occasionally appeared as weak oil-in-water emulsions. The effluent from the nanofluid flooding, especially when the injection rate was increased, was produced as oil-in-water emulsions that separated within 3 hours. An example of the nanofluid flooding effluent from test #13 is shown in Figure 5-13. The experiments with n-decane did not exhibit this behavior.
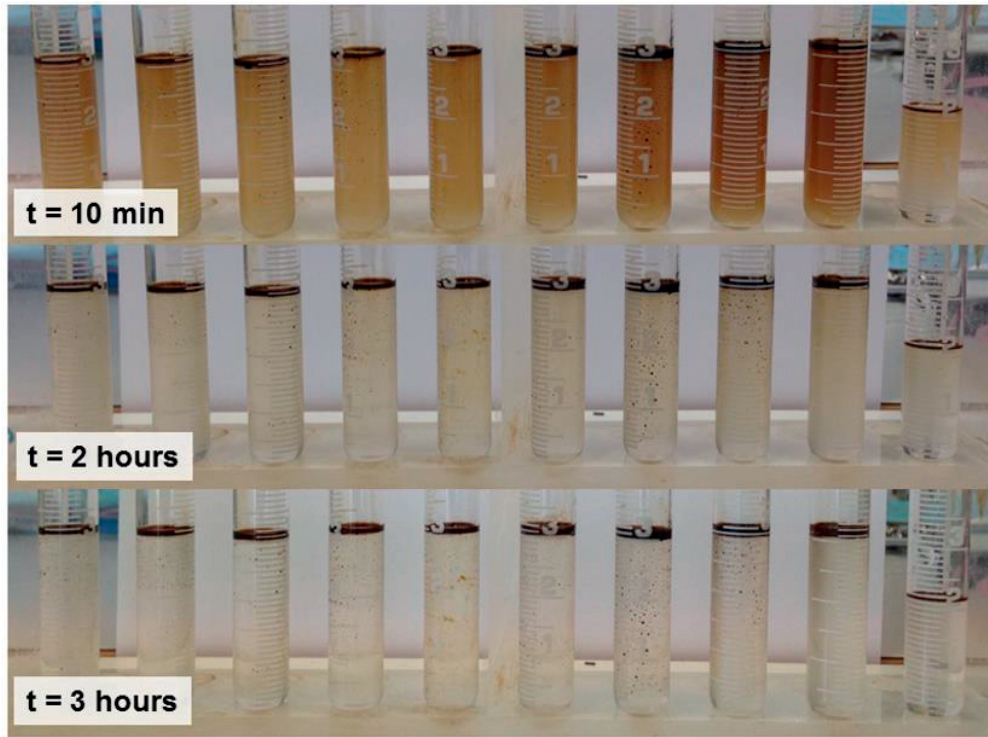
Figure 5-13. Core flooding effluent from test #13 taken during NF-Q$_{high}$. The samples were filled from left to right, and the time displayed corresponds to the time after the final sample vial was collected.

The nanoparticle concentration analysis included nanoparticle influent data for tests #7, 8, 10 and 11 (Figure 5-14). The values reported are a percentage of the influent nanoparticle concentration. A value of 100% means that all the nanoparticles are propagating through the core plug, while a value of 0% means that all of the nanoparticles are being retained.
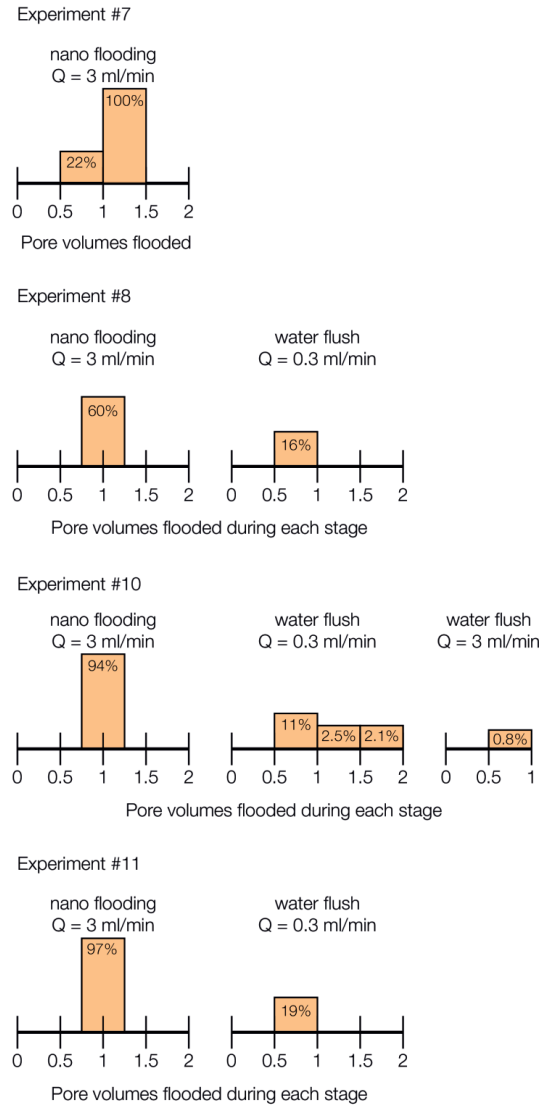
Figure 5-14. Nanoparticle effluent concentration expressed as a percentage of influent nanoparticle concentration that should be in the effluent for each testing point for tests #7, 8, 10 and 11. Error is ± 10%.

5.4.3.4 Core flooding Part 2 summary

Little to no oil was produced during the first 10 PV of nanofluid flooding at the 0.3 ml/min injection rate for tests #7 to #13. When the nanofluid flooding injection rate was increased to 3 ml/min, more than 5% OOIP was produced for four of the tests (#7, 10, 11 and 13). The tests conducted with n-decane produced less than 1% OOIP during the entire nanofluid flooding stage. Only test #13 with Nsp_3b and crude oil had oil recovery after the first PV of nanofluid flooding. There was a large variation in the recovery factors for water flooding and nanofluid flooding for the duplicate tests (#7 vs. #8 and #10 vs. #11).

The differential pressure during nanofluid flooding at 0.3 ml/min was less than the differential pressure during water flooding at 0.3 ml/min for all tests conducted with crude oil. The opposite was true for the two tests conducted with n-decane. The maximum differential pressure during water flooding at 3.0 ml/min was greater than the maximum differential pressure during nanofluid flooding at 3.0 ml/min for all tests conducted with crude oil. Once again, the opposite was true for the two tests conducted with n-decane.

Comparison of absolute permeability values measured in dry cores before and after core flooding show a permeability decrease for all cores.

Effluent pH measurements gave neutral values (between 7.2 and 7.9). The nano fluid effluent from the crude oil measurements often occurred as an oil in water emulsion. The tests with n-decane did not exhibit this phenomenon. Effluent nanofluid flooding samples for tests #7, 8, 10 and 11 suggest that most nanoparticles are propagating through the core plug. Effluent chase water flooding samples show that nanoparticles retained during nanofluid flooding can be produced when the SSW is injected.

5.4.4 Part 3: Evaluation of surface-modified Nsp_3a

5.4.4.1 Core flooding Part 3 objectives

Because the modified nanoparticles in Part 2 were unstable at 60°C, the lower threshold for practical use in a reservoir, the nanoparticle with the highest surface area was selected for further surface modification. Two different types of surface modification were applied, resulting in nanoparticles Nsp_3c and Nsp_3d. Nsp_3c was evaluated via core flooding, where the core length, initial wettability and nanofluid injection procedure were varied. It was also tested at a variety of concentrations to determine the correlation between concentration and oil production. The concentrations tested in addition to the standard 0.05 wt% were 0.01 wt%, 0.025 wt% and 0.10 wt%. Nsp_3d was tested per the standard core flooding procedure applied to Part 2.

The cores that were treated to be intermediate-wet instead of water-wet should result in more oil production according to Amott cell tests conducted by Li and Torsæter (2015). Additionally, shortening the nanofluid flooding injection time from 10 PV to 5 PV during the low rate (0.3 ml/min) should not impact the overall recovery, because if oil recovery is occurring during the low injection rate it should come within the first 5 PV. This can be compared to other tests conducted with 10 PV. The nanofluid was statically "shut-in" the core overnight after 5 PV of nanofluid flooding for two tests. This was to see if allowing the nanoparticles to react with the porous media would produce more oil after flooding was re-initiated post-shut-in. An additional 5 PV were nano flooded after the shut-in to mobilize oil that had been released by the nanoparticles during static shut-in.

5.4.4.2 Core flooding Part 3 detailed procedure

The primary drainage process was conducted by injecting crude oil at 0.3 ml/min for at least 0.5 PV. The injection rate was then increased to 3 ml/min and oil was injected until no reservoir brine was produced for at least 0.5 PV. This second injection step lasted between 3 and 5 PV. This procedure established the initial water saturation and the original oil in place. Tests #22 and #23, which were aged and did not have initial water saturation, were prepared according to

the procedure for oil saturation described in Section 4.4.1: Core preparation (page 74) and did not have any oil injection.

Water flooding was then conducted with SSW to simulate conditions in the North Sea. The sea water was injected at 0.3 ml/min for 2 PV[1] (WF-Q_{low}). Then the injection rate was increased to 3 ml/min. The 3 ml/min water flooding stage was performed for 3 PV[2] (WF-Q_{high}). Recovery factors and oil saturations were calculated at the end of both water flooding stages. The water flooding injection rate was then decreased to 0.3 ml/min for 0.25 PV[3] to re-equilibrate the rate of flow through the core. This stage is graphed as part of WF-Q_{high} on the figures.

Nanofluid flooding was performed by injecting a nanofluid into the core continuously at 0.3 ml/min for 10 PV, with five exceptions. Tests #19 through #21 were flooded for 5 PV at this stage, because the focus was on how much oil would come out within the first few pore volumes. Tests #16 and #23 were stopped after 5 PV of nanofluid flooding. The nanofluid was "shut-in" the core overnight (14 to 15 hours). After that, the low rate nanofluid flooding was started again and conducted for 5 PV. This was to see how much oil would be produced after the nanoparticles were allowed to react with the system.

After the initial nanofluid flooding stage, the injection rate was increased to 3 ml/min for 3 PV[4] to see if any oil would dislodge from the system. Recovery factors and oil saturations were calculated at the end of both nanofluid flooding stages (NF-Q_{low} and NF-Q_{high}, respectively).

---

[1] Test #14 was flooded for 1.2 PV and Test #22 was flooded for 1.75 PV for this stage.
[2] Test #14 was flooded for 2.86 PV during this stage.
[3] Tests #14 and #15 did not have this rate decrease stage. Test #22 ran this stage for 0.5 PV and Test #23 ran this stage for 0.8 PV to ensure no more oil was being produced.
[4] Test #14 had this stage for 2.5 PV.

5.4.4.3 Core flooding Part 3 results

The summary of the core flooding results is shown in Table 5.22. The fluid saturations and EOR viability from each test are shown in Table 5.23 and 5.24, respectively. Details for each core flooding test are presented in Appendix F.

Table 5.22. Summary of recovery factors (as % OOIP) for each of the flooding stages (water flooding at 0.3 and 3.0 ml/min and nanofluid flooding at 0.3 and 3.0 ml/min).

Test #	Nanoparticle / Concentration	Recovery Factor (RF) as % of OOIP						Total
		Water flooding			Nanofluid flooding			
		0.3 ml/min	3.0 ml/min	Total	0.3 ml/min	3.0 ml/min	Total	
14	Nsp_3c 0.05 wt%	43.6	8.2	51.8	1.2	1.2	2.4	54.2
15	Nsp_3c 0.05 wt%	39.5	7.8	47.3	1.9	0.9	2.8	50.1
16	Nsp_3c 0.05 wt%	53.8	1.0	54.8	0	0.1	0.1	54.9
17	Nsp_3c 0.025 wt%	59.6	7.0	66.6	0.0	1.8	1.8	68.4
18	Nsp_3c 0.01 wt%	63.7	10.0	73.7	0.0	0.8	0.8	74.5
19	Nsp_3c 0.05 wt%	73.3	6.4	79.7	0.0	2.1	2.1	81.8
20	Nsp_3c 0.10 wt%	68.1	7.6	75.7	0.0	1.0	1.0	76.7
21	Nsp_3d 0.05 wt%	62.6	6.3	68.9	0.0	2.7	2.7	71.6
22	Nsp_3c 0.05 wt%	53.2	16.4	69.6	5.4	5.4	10.8	80.4
23	Nsp_3c 0.05 wt%	52.9	16.3	69.2	4.7[*]	4.1	8.8	78.0

[*] This represents the recovery from the first 5 PV of nanofluid flooding (2.0% produced) and from the second 5 PV of nanofluid flooding conducted after ca. 15 hours of immobile nanofluid shut-in time (2.7% produced).

Table 5.23. Part 3 initial water saturation and residual oil saturations.

Test #	Nanoparticle	Swi	Sor	
			Water flood	Nano flood
14	Nsp_3c at 0.05 wt%	0.37	0.31	0.29
15	Nsp_3c at 0.05 wt%	0.37	0.33	0.32
16	Nsp_3c at 0.05 wt%	0.33	0.30	0.30
17	Nsp_3c at 0.025 wt%	0.36	0.22	0.20
18	Nsp_3c at 0.01 wt%	0.34	0.17	0.17
19	Nsp_3c at 0.05 wt%	0.38	0.13	0.11
20	Nsp_3c at 0.10 wt%	0.41	0.14	0.14
21	Nsp_3d at 0.05 wt%	0.35	0.20	0.18
22	Nsp_3c at 0.05 wt%	0	0.30	0.20
23	Nsp_3c at 0.05 wt%	0	0.31	0.22

Table 5.24. Summary of Part 3 core flooding parameters to determine EOR viability.

Test #	Nanoparticle / Concentration	Occurrence of initial oil bank (after _ PV of nanofluid flooding)	Recovery factor (% OOIP) after 1 PV of nanofluid flooding	Total recovery factor (% OOIP) from nanofluid flooding
14	Nsp_3c 0.05 wt%	3.9*	0	2.4
15	Nsp_3c 0.05 wt%	2.3	0	2.8
16	Nsp_3c 0.05 wt%	12.4*†	0	0.1
17	Nsp_3c 0.025 wt%	10.2†	0	1.8
18	Nsp_3c 0.01 wt%	11*†	0	0.8
19	Nsp_3c 0.05 wt%	8†	0	2.1
20	Nsp_3c 0.10 wt%	7*†	0	1.0
21	Nsp_3d 0.05 wt%	0.7	0.9	2.7
22	Nsp_3c 0.05 wt%	3.8	0	10.8
23	Nsp_3c 0.05 wt%	2.5	0	8.8

*Only a trace amount of oil (<0.1% OOIP) was produced at the initial oil bank.
†The initial oil bank occurred after the nanofluid flooding injection rate was increased to 3 ml/min.

5.4.4.4 Core flooding Part 3 summary

For all of the tests with initially water-wet conditions and Swi (#14 to #21), little to no oil was produced during nanofluid flooding at the 0.3 ml/min injection rate. When the nanofluid flooding injection rate was increased to 3 ml/min, up to 2.7% OOIP oil was produced. The total nanofluid flooding recovery factor was 2.8% OOIP or less for all these tests. For the two oil-wet cores with no Swi (tests #22 and #23), up to 5.4% OOIP was produced during nanofluid flooding at 0.3 ml/min. An additional 5.4% or 4.1% OOIP was produced after the injection rate was increased to 3.0 ml/min, resulting in total nanofluid flooding recovery factors of 10.8% and 8.8% OOIP, respectively. However, of all the tests in Part 3, only #21 with Nsp_3d at 0.05 wt% had oil production within the first PV of nanofluid flooding (0.9% OOIP).

The differential pressure during nanofluid flooding at 0.3 ml/min was less than the differential pressure during water flooding at 0.3 ml/min for all tests except #15 (Nsp_3c at 0.05 wt%).

5.4.5 Part 4: Testing with aged cores and elevated temperature

5.4.5.1 Core flooding Part 4 objectives

The goal was to test the final modified nanoparticles (Nsp_3c and Nsp_3d) via core flooding at 60°C and compare them to their unmodified, base nanoparticle (Nsp_3a). Because a result of Part 3 was that cores that were more intermediate-wet produced more oil, the cores in Part 4 were aged to be intermediate-wet. Triplicates were planned for all the experiments, but because of instrument issues in the lab, some experiments were duplicated instead of triplicated. Nsp_3a was tested at 0.05 wt%, Nsp_3c was tested at 0.01 wt%, 0.05 wt% and 0.15 wt%, and Nsp_3d was tested at 0.05 wt%. Particle size distribution measurements were taken from the effluent throughout the nanofluid flooding stage to see how the nature of particle transport could be changing over time. An instrument to evaluate nanoparticle concentration in-house was not available at the time of testing, but this would be valuable for future work.

It was hypothesized that the unmodified nanoparticle (Nsp_3a) would exhibit significant agglomeration during the core flooding at 60°C, while the modified nanoparticles should not. If oil recovery is truly a result of nanofluid flooding, here should be a positive correlation

between nanoparticle concentration and oil recovery for Nsp_3c tests. As temperature tends to speed up the rate of chemical reactions, increasing the core flooding temperature could lead to additional oil recovery if an EOR mechanism is chemical interaction between the nanofluid and the reservoir system.

Micromodel experiments were conducted to better visualize the nanofluid flow and EOR mechanisms. Two tests were conducted in strongly water-wet micromodels, and one test was conducted in a strongly oil-wet micromodel. All tests were conducted with Nsp_3c at 0.05 wt%. It was hypothesized that the water-wet tests would show limited to no recovery, but the oil-wet test should show oil production from wettability alteration and/or in-situ emulsion generation.

5.4.5.2 Core flooding Part 4 detailed procedure

All cores except those used in tests #24 and #25 were aged and did not have initial water saturation, so drainage was conducted according to the procedure for oil saturation described in Section 4.4.1: Core preparation (page 74). Cores for tests #24 and #25 underwent drainage flooding per the procedure described in Part 3.

Test #24 and #25 had a different flooding procedure that those in tests #26 through #35. Water flooding was conducted with SSW at 0.3 ml/min for 2 PV followed by injection at 3 ml/min for 3 PV. Then the rate was decreased to 0.3 ml/min for 0.25 PV for re-equilibrate the system. This rate reduction step is graphed as part of the 3 ml/min stage. Nanofluid flooding was conducted at 0.3 ml/min for 5 PV followed by 3 ml/min for 3 PV.

For tests #26 through #35, which had no initial water saturation, water flooding was conducted with SSW at 0.3 ml/min for 3 PV followed by 3 ml/min for 7 PV. Recovery factors and oil saturations were calculated at the end of both water flooding stages. To estimate the relative permeability of water after water flooding, SSW was then injected at 2.5 ml/min for 10 min., 2.0 ml/min for 10 min., 1.5 ml/min for 10 min., 1.0 ml/min for 10 min and finally 0.5 ml/min. The differential pressure associated with each of these injection rates was recorded.

Nanofluid flooding was then performed by injecting a nanofluid into the core continuously at 0.3 ml/min for 10 PV followed by 3 ml/min for 3 PV. After the final stage, the relative

permeability of the nanofluid was estimated by following the same procedure conducted at the end of water flooding (decreasing the rates in a step-wise fashion and recording the resulting differential pressure). This was then compared to the value achieved at the end of water flooding.

The relative permeability values were then determined for water flooding and nanofluid flooding by first plotting the flow rate in ml/s versus the differential pressure in atm. A line was fit to the data with an intercept forced through (0,0). The slope of this line was then put in to Darcy's equation as Q / ΔP, and the equation was solved for permeability, k. This was the effective permeability of water (k_{ew}), and it was placed in Eq. 2.3 along with the absolute permeability for the core to determine the relative permeability for water (k_{rw}). A reduction in the value meant that the nanofluid could flow more easily through the core than the SSW.

Effluent samples were collected for tests #26 through #35 to test for the particle size distribution with the Malvern Zetasizer. Sample NF-1 was the nanofluid influent particle size distribution. Effluent sample NF-2 was taken at the end of the nanofluid flooding at the low injection rate (0.3 ml/min). It was collected during from the effluent emerging during 9.5 to 10 PV of nanofluid flooding. NF-3 was taken at the end of the high injection rate (3 ml/min) during the last half pore volume (from 2.5 to 3 PV flooding). Sample NF-4 was taken during the relative permeability flooding and was collected during the 10 minutes when the injection rate was 1.0 ml/min. NF-5 was taken immediately after, when the injection rate was 0.5 ml/min for 10 min. NF-6 was taken directly from the nanofluid reservoir outlet after core flooding to see what the particle size distribution looks like before entering the core plug.

5.4.5.3 Core flooding Part 4 results

5.4.5.3.1 Core flooding

The summary of the core flooding results is shown in Table 5.25. Cores for tests #24 and #25 were not aged. Cores for tests #26 to #35 were aged for four weeks with no initial water saturation. The fluid saturations and EOR viability from each test are shown in Table 5.26 and Table 5.27, respectively. Details of the core flooding tests are presented in Appendix G.

Table 5.25. Summary of recovery factors (as % OOIP) for each of the flooding stages at 60°C.

Test #	Nanoparticle		Recovery Factor (RF) as % of OOIP						
			Water flooding			Nanofluid flooding			
	Type	Conc. (wt%)	0.3 ml/min	3.0 ml/min	Total	0.3 ml/min	3.0 ml/min	Total	Total
24	Nsp_3c	0.05	79.0	3.3	82.3	0.6	0.0	0.6	82.9
25	Nsp_3d	0.05	61.4	2.3	63.7	0.4	0.0	0.4	64.1
26	Nsp_3a	0.05	44.3	11.1	55.4	3.1	0.0	3.1	58.5
27	Nsp_3a	0.05	51.3	3.0	54.3	1.3	0.2	1.5	55.8
28	Nsp_3c	0.01	41.9	7.1	49.0	1.8	0.1	1.9	50.9
29	Nsp_3c	0.05	42.5	12.6	55.1	2.1	0.0	2.1	57.2
30	Nsp_3c	0.05	46.8	0.9	47.7	0.0	0.1	0.1	47.8
31	Nsp_3c	0.15	47.9	11.1	59.0	1.7	0.0	1.7	60.7
32	Nsp_3c	0.15	49.1	11.9	61.0	4.0	0.0	4.0	65.0
33	Nsp_3c	0.15	52.6	2.2	54.8	0.0	0.0	0.0	54.8
34	Nsp_3d	0.05	60.0	7.6	67.6	2.7	0.0	2.7	70.4
35	Nsp_3d	0.05	49.8	9.4	59.2	0.1	0.0	0.1	59.3

Table 5.26. Part 4 initial water saturation and residual oil saturations.

Test #	Nanoparticle type	Nanoparticle concentration	S_{wi}	S_{or}	
				Water flood	Nano flood
24	Nsp_3c	0.05 wt%	0.47	0.09	0.09
25	Nsp_3d	0.05 wt%	0.36	0.23	0.23
26	Nsp_3a	0.05 wt%	0	0.48	0.41
27	Nsp_3a	0.05 wt%	0	0.48	0.44
28	Nsp_3c	0.01 wt%	0	0.51	0.49
29	Nsp_3c	0.05 wt%	0	0.45	0.43
30	Nsp_3c	0.05 wt%	0	0.52	0.52
31	Nsp_3c	0.15 wt%	0	0.41	0.39
32	Nsp_3c	0.15 wt%	0	0.39	0.35
33	Nsp_3c	0.15 wt%	0	0.45	0.45
34	Nsp_3d	0.05 wt%	0	0.32	0.30
35	Nsp_3d	0.05 wt%	0	0.41	0.41

Table 5.27. Summary of Part 4 core flooding parameters to determine EOR viability.

Test #	Nanoparticle / Concentration	Occurrence of initial oil bank (after _ PV of nanofluid flooding)	Recovery factor (% OOIP) after 1 PV of nanofluid flooding	Total recovery factor (% OOIP) from nanofluid flooding
24	Nsp_3c 0.05 wt%	2.7*	0	0.6
25	Nsp_3d 0.05 wt%	0.25*	0.4	0.4
26	Nsp_3a 0.05 wt%	3.7	0	3.1
27	Nsp_3a 0.05 wt%	0.7*	0.02	1.5
28	Nsp_3c 0.01 wt%	2*	0	1.9
29	Nsp_3c 0.05 wt%	5.3	0	2.1
30	Nsp_3c 0.05 wt%	10*†	0	0.1
31	Nsp_3c 0.15 wt%	5.5	0	1.7
32	Nsp_3c 0.15 wt%	2.5*	0	4.0
33	Nsp_3c 0.15 wt%	‡	0	0.0
34	Nsp_3d 0.05 wt%	5.2	0	2.7
35	Nsp_3d 0.05 wt%	5.2*	0	0.1

* Only a trace amount of oil (<0.1% OOIP) was produced at the initial oil bank.
† The initial oil bank occurred after the nanofluid flooding injection rate was increased to 3 ml/min.
‡ No oil produced during nanofluid flooding.

The relative permeability to water values calculated at the end of water flooding and nanofluid flooding are presented in Table 5.28. The absolute permeability is the permeability of the core presented in Table 3.8.

Table 5.28. Summary of relative permeability to water values, k_{rw}, for tests #26 through #35 measured at residual oil saturation at the end of water flooding and the end of nanofluid flooding. The reference permeability is the absolute permeability for the core plug.

Test #	Water flooding		Nanofluid flooding	
	k_{rw}	S_{or}	k_{rw}	S_{or}
26	0.38	0.48	0.13	0.41
27	0.25	0.48	0.06	0.44
28	0.28	0.51	0.23	0.49
29	0.38	0.45	0.26	0.43
30	0.45	0.52	0.35	0.52
31	0.57	0.41	0.43	0.39
32	0.38	0.39	0.38	0.35
33	0.22	0.45	0.22	0.45
34	0.39	0.32	0.31	0.30
35	0.29	0.41	0.29	0.41

5.4.5.3.2 Effluent analysis

The particle size distributions taken from influent and effluent data are presented for tests #26 through #35 in Appendix G. Test #27 effluent nanoparticles had agglomerated so much that it was not possible to measure with the Malvern Zetasizer.

5.4.5.4 Core flooding Part 4 summary

Oil production during the first 10 PV of nanofluid flooding at the 0.3 ml/min injection rate varied from no oil to 4.0% OOIP. Only three tests (#27, 28 and 30) had oil production when the nanofluid flooding injection rate was increased to 3.0 ml/min. That oil production was 0.1% or 0.2% OOIP. Nanofluid flooding recovery factors varied from 0% to 4.0% OOIP. Only two tests had oil production within the first PV of nanofluid flooding – tests #25 and #27. The occurrence of the initial oil bank was after 5 PV of nanofluid flooding for five of the tests. There was a large variation in the recovery factors for water flooding and nanofluid flooding for the duplicate tests. There was no correlation between nanoparticle concentration and oil recovery.

The differential pressure during nanofluid flooding at 0.3 ml/min was equal to or less than the differential pressure during water flooding at 0.3 ml/min for all tests except the two conducted with the unmodified particle (Nsp_3a / tests #26 and #27). The differential pressure during nanofluid flooding at 3.0 ml/min for the Nsp_1a tests was 0.3 and 0.6 bars greater (tests #26 and #27) than the differential pressure for the water flooding at 3.0 ml/min.

Tests #26 and #27 had visible agglomeration in the nanofluid container in the oven. The effluent samples confirm that the particle size distribution for these two tests with the unmodified nanoparticle Nsp_3a have a high degree of agglomeration. The tests conducted with the modified nanoparticles Nsp_3c and Nsp_3d show that little to no agglomeration occurs throughout the nanofluid flooding. In tests #31 and #32 with Nsp_3c at 0.15 wt%, agglomeration began to occur at the end of nanofluid flooding.

5.5 Micromodel flooding

5.5.1 Objectives

Micromodel tests were conducted with crude oil to better visualize the EOR mechanisms and compare the nanofluid flooding in a water-wet system to an oil-wet system. After the in-situ emulsion generation produced during Part 2 core flooding, it was hypothesized that emulsion generation could be seen in the micromodel tests. Nsp_3c dispersed in SSW at 0.05 wt% was selected as the nanofluid because 1) it was the most stable, and therefore most promising, modified nanoparticle and 2) it produced a significant oil recovery in oil-wet tests (#22 and #23) but not in water-wet tests. It was therefore hypothesized that Nsp_3c would have little to no affect in the water-wet micromodel, but oil production from either in-situ emulsion generation or wettability alteration would take place in the oil-wet micromodel. As with the core flooding tests, the nanofluid flooding was conducted after water flooding with SSW. Two tests were conducted with a water-wet micromodel (tests #36 and #37, continuing the nomenclature from the core flooding). The third test (#38) used a micromodel altered to an oil-wet state with HMDS.

5.5.2 Detailed procedure

Detailed flooding procedures are shown in Table 5.29.

Table 5.29. Detailed flooding procedures for micromodel tests.

Test #36 (water-wet)					
Oil flooding		**Water flooding**		**Nanofluid flooding**	
PV flooded	Q_{inj} (ml/min)	PV flooded	Q_{inj} (ml/min)	PV flooded	Q_{inj} (ml/min)
1	0.0025	2	0.0025	1	0.0025
1	0.005	4.5	0.005	2	0.00375
1	0.010				
				16:22 hours	Stopped
				1	0.00375
Test #37 (water-wet)					
Oil flooding		**Water flooding**		**Nanofluid flooding**	
PV flooded	Q_{inj} (ml/min)	PV flooded	Q_{inj} (ml/min)	PV flooded	Q_{inj} (ml/min)
1	0.0025	2	0.0025	1	0.0025
1	0.005	2.5	0.005	2	0.00375
1	0.010	4	0.010	1	0.005
				16:32 hours	Stopped
				1	0.005
				1	0.010
				1	0.020
				1	0.050
				2	0.200
Test #38 (oil-wet)					
Oil flooding		**Water flooding**		**Nanofluid flooding**	
PV flooded	Q_{inj} (ml/min)	PV flooded	Q_{inj} (ml/min)	PV flooded	Q_{inj} (ml/min)
1	0.0025	2	0.0025	1	0.0025
1	0.005	5.5	0.005	2	0.00375
1	0.010			1	0.005
				0.5	0.010

5.5.3 <u>Results</u>

A summary of saturations and recovery factors for the three experiments is presented in Table 5.30. Images from the micromodel test are presented in Appendix H.

Table 5.30. Overview of saturation values and recovery factors from the three experiments. Error is introduced during image post-processing. The values presented below could vary by as much as 5%. However, when comparing values within any given experiment, the degree of change should be constant.

Test #	36	37	38
Swi	17.4 %	16.0 %	38.7 %
So after 1 PV WF	62.8 %	68.0 %	34.1 %
Sor$_1$ (end of WF)	55.9 %	59.7 %	28.3 %
So after 1 PV NF	55.9 %	59.7 %	28.0 %
Sor$_2$ (end of NF)	55.9 %	59.7 %	27.6 %
RF$_1$ (end of WF)	32.4 %	28.9 %	53.8 %
Final RF$_2$ (end of NF)	32.4 %	28.9 %	54.9 %

Swi = Initial water saturation; So = Oil saturation; PV = Pore volume; WF = Water flooding; NF = Nanofluid flooding; RF = Recovery factor (as a percent of original oil in place, OOIP)

5.5.3.1 Water-wet micromodel test

During oil flooding, oil breakthrough occurred at 0.73 PV. Initial water saturation (Swi) was established at 17.4% (Figure H.1). During water flooding, breakthrough occurred at 0.43 PV. Oil saturation was 62.8% after 1 PV of water flooding (Figure H.2). Residual oil saturation (Sor$_1$) was 55.8% at the end of water flooding (total of 6.5 PV at various flow rates; Figure H.3). The recovery factor from water flooding was 32.4% of the original oil in place. No oil was produced during the nanofluid flooding. The saturation distribution is almost identical both after 1 PV (Figure H.4) and at the end of the nanofluid flooding (after 4 PV total at various rates and after being allowed to statically react for over 16 hours; Figure H.5). Final residual oil saturation (Sor$_2$) was 55.8%. The recovery factor at the end of water flooding and nanofluid flooding was 32.4%. The differential pressure was 1.2 bar throughout oil flooding and 1.1 bar throughout water flooding and nanofluid flooding.

5.5.3.2 Water-wet micromodel test with dye added to the nanofluid

During oil flooding, oil breakthrough occurred at 0.94 PV. Initial water saturation (Swi) was established at 16.0% (Figure H.6). During water flooding, breakthrough occurred at 0.14 PV. Oil saturation was 68.0% after 1 PV of water flooding (Figure H.7). Residual oil saturation (Sor_1) was 59.7% at the end of water flooding (total of 8.5 PV at various flow rates; Figure H.8). Little to no oil was produced during the nanofluid flooding. The saturation distribution is almost identical both after 1 PV (Figure H.9) and at the end of the nanofluid flooding (after 10 PV total at various rates and after being allowed to statically react for over 16 hours). Final residual oil saturation (Sor_2) was 59.7% (Figure H.10). The recovery factor at the end of water flooding and nanofluid flooding was 28.9%. The differential pressure was 1.1 bar throughout the entire test except for during water flooding when the injection rate was 0.010 ml/min, which is when the pressure increased to 1.2 bars.

5.5.3.3 Oil-wet micromodel test

During oil flooding, oil breakthrough occurred between 0.7 and 0.8 PV. Initial water saturation (Swi) was established at 38.7% (Figure H.11). Breakthrough during water flooding was not recorded. Oil saturation was 34.1% after 1 PV of water flooding (Figure H.12). Residual oil saturation (Sor_1) was 28.3% at the end of water flooding (total of 7.5 PV at various flow rates; Figure H.13). There was limited mobilization of oil during the nanofluid flooding. The oil droplets at the outlet trough visibly increase throughout the nanofluid flooding, and many single pore throats have had oil production. This is visible even after 1 PV of nanofluid flooding (Figure H.14). The final picture after nanofluid flooding (at Sor_2) shows limited oil production (Figure H.15). It is difficult to separate this oil production from what would have occurred naturally with more water flooding at corresponding flow rates. Final residual oil saturation (Sor_2) was 27.6% after 4.5 PV of nanofluid flooding at various rates. The recovery factor at the end of water flooding was 53.8%. The final recovery factor after nanofluid flooding was and nanofluid flooding was 54.9%. The differential pressure was 1.2 bar throughout oil flooding at 0.0025 ml/min, and then increased to 1.3 bar when the injection rate was increased to 0.005 ml/min. The differential pressure increased to 1.5 bar when the oil injection rate was increased

to 0.010 ml/min. The differential pressure was 1.2 bar throughout both water flooding and nanofluid flooding.

5.5.4 Summary

There was no oil production from nanofluid flooding during the water-wet micromodel experiments. The oil-wet micromodel experiment exhibited limited oil production during the first pore volume of nanofluid flooding, with a bit more production occurring during the next 3.5 pore volumes of nanofluid flooding. The oil saturation did not change more than 1 to 2% during the nanofluid flooding.

6 Discussion

The discussion sections and their relation to the experimental results and research questions are shown in Table 6.1.

Table 6.1. Discussion overview.

Section	Sub-section	Experimental method	Research question
Nanofluid Stability (6.1)		Particle size distribution	**RQ1:** Are the nanoparticles stable in synthetic sea water?
Oil Production (6.2)	Reproducibility and variation	Water flooding	**RQ2:** Do the nanoparticles increase the oil recovery?
	Results	All core flooding and micromodels	**RQ2**
	Experimental artifacts	All core flooding	**RQ2**
EOR Mechanisms (6.3)	Fluid-fluid interactions	IFT and core flooding effluent	**RQ3:** What are the EOR mechanisms contributing to nanoparticle-induced oil recovery?
	Fluid-rock interactions	Contact angle and relative permeability	**RQ3**
	Mechanical displacement	Differential pressure (core flooding)	**RQ3**
	Nanoparticle transport	Core flooding effluent	**N/A**

6.1 Nanofluid stability

The unmodified nanoparticles (Cnp_1, 2 and 3 and Nsp_1a, 2a and 3a) agglomerate in SSW and are therefore not suitable for field application using sea water injection. The particle size distribution tests showed that agglomeration occurs within the first 24 hours of nanofluid mixing. This is likely a result of the compression of each nanoparticle's electrical double layer due to the addition of multivalent cations to the solution as described in Chapter 2.

The first round of modified nanoparticles (Nsp_1b, 2b and 3b) were silanized by Evonik Industries to improve stability. These nanoparticles were stable in dispersion throughout the 16-week testing period at 20°C. None of them were stable at 60°C. Agglomeration was therefore

not an issue for the core flooding tests. This is confirmed by the lower differential pressure profiles and by the increased propagation of the nanoparticles through the core plugs. Further modifications must be conducted to achieve stability at 60°C, which is suggested to be the lowest threshold for field application in the North Sea.

Depletion stabilization in the presence of polyethylene glycol (PEG) has been shown to stabilize many types of nanoparticles, including silica (Zhang et al., 2012). The nanoparticle surface modification with PEG (Nsp_3c) was stable throughout 20°C and 40°C. However, only the concentration at 0.50 wt% was stable for 16 weeks at 60°C.

Nsp_3d, modified by epoxy, has a smaller particle size than Nsp_1b but this could be because the surface modification prevents initial aggregation. It was not stable at 60°C.

An interpretation of the nanofluid stability studies is given in Figure 6-1.

Figure 6-1. Nanofluid stability in SSW.

Nanoparticle / nanofluid					Temperature		
Type	**Name**	**Modification**	**Surface area (m²/g)**	**Concentration (wt %)**	**20°C**	**40°C**	**60°C**
Colloidal	Cnp_1	None	65	0.05		-	-
	Cnp_2	None	150	0.05	*	-	-
	Cnp_3	None	350	0.05		-	-
Nano-structured	Nsp_1a	None	130	0.05		-	-
	Nsp_2a	None	200	0.05		-	-
	Nsp_3a	None	300	0.05	*	-	-
	Nsp_1b	Silanization	-	0.05		12	
	Nsp_2b		-	0.05		4	
	Nsp_3b		-	0.05			1
	Nsp_3c	PEG	-	0.05			4
	Nsp_3c		-	0.10			4
	Nsp_3c		-	0.50			
	Nsp_3d	Epoxy	-	0.05	†	-	1

🟥	Not stable for 24 hours (unmodified) or 1 week (modified)
4	Number in the box means the nanofluid was stable for at least that many weeks
🟩	Still stable after 16 weeks
-	Not tested / not applicable

* The D_{avg} values at the end of 24 hours are similar to those measured at t = 0 in DI water, but the PSD curves in Appendix B suggest that agglomeration is occurring and measurements taken after a few weeks would should agglomeration. Agglomeration within one week was observed visually with samples in the lab but was not tested.

†A small percent of the particles begins to agglomerate between 1 and 4 weeks, but most of the particles appear to remain stable.

6.2 **Oil production**

6.2.1 Reproducibility and variation

The analysis of water flooding shows the variation already present in the core flooding tests. This makes reproducibility and repetition difficult, especially when using unique cores for each test due to the uncertainty of nanoparticle retention in already flooded core plugs.

Water flooding with a low rate followed by a high rate, as conducted for Parts 2 through 4, should provide reliable end-point saturations and water relative permeability, respectively (McPhee and Arthur, 1994). A low flow rate allows continual water imbibition into oil-saturated pores because capillary forces continue to dominate even after water breakthrough (McPhee and Arthur, 1994). Increasing the flow rate then helps negate capillary end effects. According to McPhee and Arthur (1994), a low flow rate should produce lower residual oil saturation values than a high flow rate. This is because oil becomes discontinuous earlier in the flooding process at a high flow rate, while a low rate has capillary stability at the fluid front. This prevents viscous fingering even if the mobility ratio is high.

The residual oil saturation depends upon the initial water saturation, especially in water-wet cores (McPhee and Arthur, 1994). In general, a larger S_{wi} occurs when the core is more water-wet. This leads to lower oil recovery from water flooding, as Morrow (1990) shows that oil recovery from water flooding is greatest at a wettability index (WI) of 0 (intermediate-wet) and decreases as the wettability becomes strongly oil-wet (WI $\rightarrow$ -1) or water-wet (WI $\rightarrow$ +1). However, if larger S_{wi} values are caused by lower permeability due to capillary effects, then the resulting oil recovery could have a different trend. There is no correlation between total oil recovery from water flooding and initial water saturation for the tests in this thesis (Figure 5-11). The tests conducted with n-decane and without initial water saturation are not included in this comparison.

The variation in initial water saturation by the oil flooding process has been found to vary by five saturation units according to McPhee and Arthur (1994). The initial water saturation values obtained in this thesis range from 24% to 47%, which is a larger variation. Additionally, many of the tests exhibit a higher initial water saturation than what is typically expected for Berea sandstone core plugs. For comparison, Berea sandstone core plugs flooded with crude oil at 1.5

143

ml/min for 5 to 8 PV have S_{wi} values ranging from 19.6 to 26.7% (Tang and Morrow, 1997). It is possible that the sandstone blocks which were used to produce the core plugs used in this study have more heterogeneity than typical Berea sandstone blocks.

Cores #22, 23 and 26 to 35 were aged without initial water saturation. Cores #22 and #23 were aged for 11.5 and 10.5 weeks compared to the four weeks for the other tests. They exhibited a larger oil recovery factor than all the four week aged cores with one exception. This concurs with Tang and Morrow (1997), where they concluded that oil recovery by water flooding increases with an increase in aging time.

Wettability affects many important core flooding factors including capillary pressure, relative permeability, water flood behavior and tertiary recovery (Anderson, 1986). The nature of the oil production during water flooding can give an indication of the core plug's wettability (Alagic et al., 2011). Typically, no oil production occurs after water breakthrough for a strongly water-wet system, while an oil-wet system exhibits an earlier water breakthrough but additional production after water breakthrough (Alagic et al., 2011). The water flooding tests in this thesis exhibit this behavior.

Cores typically exhibit more water-wet behavior when flooded at increased temperature because of the increased solubility of the polar compounds (Anderson, 1986; Buckley et al., 1998). This concurs with the results presented in this thesis. Additionally, IFT and contact angle typically decrease as temperature increases, rendering the system even more water-wet (Anderson, 1986).

There is a strong correlation between total oil recovery from water flooding and residual oil saturation after water flooding as is expected (Figure 6-2). The water-wet cores from Parts 1 through 3 exhibit a similar correlation between oil recovery and residual oil saturation. The tests from Part 4 (conducted at 60°C) have the largest residual oil saturation compared to oil recovery. The tests from Part 3 and 4 without initial water saturation are not plotted, as the residual oil saturation is directly correlated with oil recovery in the absence of initial water saturation.
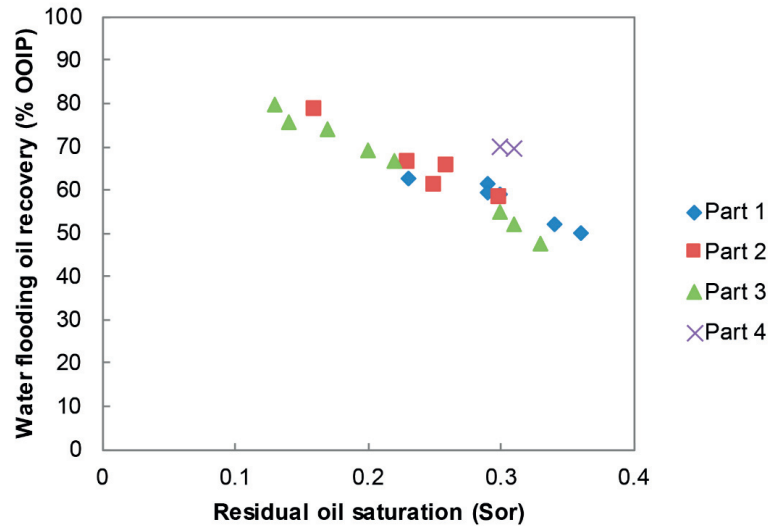
Figure 6-2. Total oil recovery from water flooding vs. residual oil saturation at the end of water flooding. Only tests with initial water saturation are shown.

The capillary numbers calculated for the core flooding tests concur with the expected values for water flooding in sandstone (10^{-6} to 10^{-5}) as presented in Lake (1989). The core flooding tests have a capillary-dominated flow regime.

6.2.2 Discussion of nanoparticle flooding

There is no clear correlation between oil recovery obtained from nanofluid flooding and core plug porosity, permeability or initial water saturation. Comparing the total oil recovery (water flooding + nanofluid flooding recovery factors) with porosity shows a subtle negative correlation. This mirrors the correlation shown between water flooding oil recovery and porosity in Figure 5-9. The total oil recovery does not have a clear correlation with core plug permeability or initial water saturation.
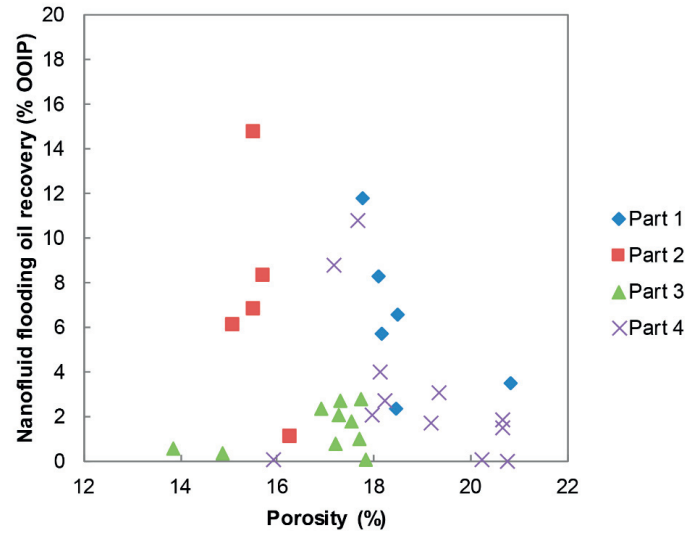
Figure 6-3. Nanofluid flooding oil recovery vs. core plug porosity.
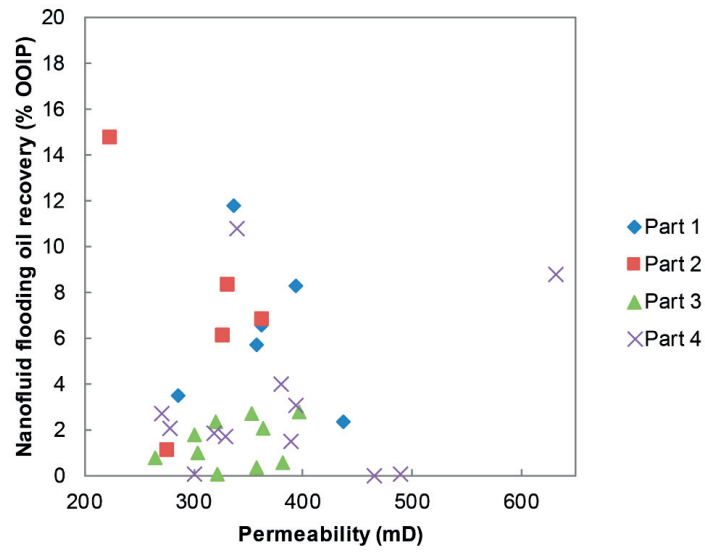
Figure 6-4. Nanofluid flooding oil recovery vs. core plug permeability.
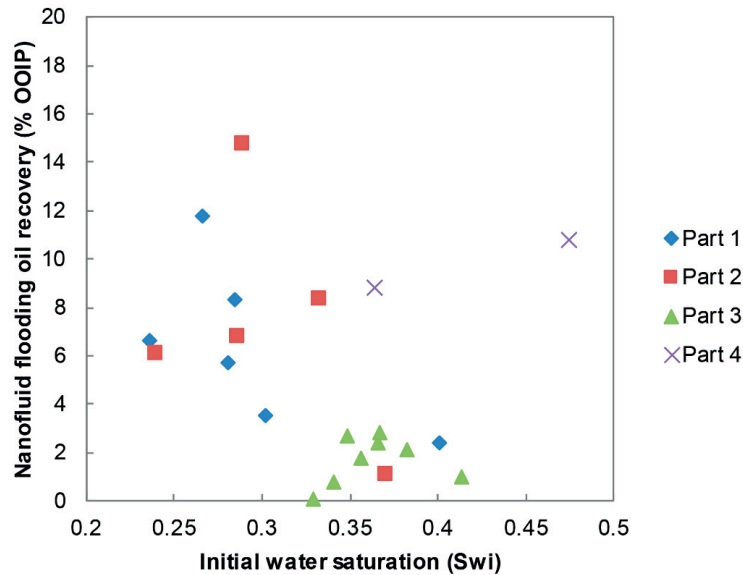
Figure 6-5. Nanofluid flooding oil recovery vs. initial water saturation. Only tests with initial water saturation are shown.

Part 1: Screening of unmodified nanoparticles. For core flooding conducted in Part 1, all nanoparticle floods produced additional oil recovery, but Nsp_1a is the most successful EOR candidate based upon the core flooding data. All the nano-structured particles and Cnp_2 produced a nanofluid flooding recovery factor greater than 5% OOIP. However, only Nsp_1a produced more than 5% OOIP within the first pore volume of nanofluid flooding. Its initial oil bank appeared quite early (after 0.4 PV of nanofluid flooding). The Nsp_3a nanoparticle was tested by (Hendraningrat et al., 2013c) at 0.05 wt% in 3 wt% NaCl, and the recovery factors for two tests were 5.3% and 4.7%. The Nsp_3a nanoparticle produced 5.7 % OOIP recovery in this thesis when dispersed at 0.05 wt% in SSW.

The nano-structured particles appear to be better candidates for increasing the tertiary recovery factor. This is because the average nanofluid flooding recovery factor for the nano-structured particles was greater than that obtained for the colloidal nanoparticles. The average recovery factor after 1 PV of nanofluid flooding was also greater for the nano-structured particles. Water flooding and nanofluid flooding were not conducted for the same length of time for all tests.

147

This could affect how much oil is available for production post- water flooding. Additionally, permeability and porosity varied for each core plug, which may affect the geometry whereby nanoparticles and oil can flow through the core plug even though there is no clear correlation between these core properties and oil recovery.

There is no positive trend between surface area and the nanofluid flooding recovery factor. In fact, there is a negative trend between surface area and nanofluid flooding recovery factor for the nano-structured particles. This could be explained by agglomeration plugging pore channels and displacing more oil, but the D_{avg} for the agglomerated nanoparticles is smaller than the average pore channel size. Also, the difference in the D_{avg} between Nsp_1a and Nsp_2a is not large enough to completely explain the difference. It is concluded that there are other factors affecting the recovery factor than the chemical reactivity of the nanoparticle surface. This does not mean that the surface area does not influence the recovery factor, but it does mean that it is not the primary contributor.

Part 2: Screening of silanized nanoparticles. For core flooding tests conducted in Part 2, all tests resulted in an increase in oil recovery during the low injection rate stage. The oil was typically produced after a few pore volumes of nanoparticle flooding, indicating that it takes time for the nanoparticles to interact with the system before they can produce more oil. Although all tests resulted in incremental oil production during nanofluid flooding, none met the criteria as a positive candidate for EOR (initial oil bank produced within the first 0.6 PV of nanofluid flooding and a recovery factor of $\geq$5% OOIP within the first PV of nanofluid flooding). The recovery factors during nanofluid flooding for all of the nanofluid – crude oil systems are not significantly different, so it is not clear which nanoparticle system performs best.

The repeatability of the core flooding is poor. A new core was used for each experiment because the reaction between the nanoparticles and the rock is unknown. The two tests for Nsp_1b had total nanofluid flooding recovery factors of 6.09% and 1.13%. The two tests for the Nsp_2b had total nanofluid flooding recovery factors of 14.68% and 6.76%. The cause for this variation is unknown.

The nanofluid flooding recovery factors for the crude oil experiments were less than 1.5% for the low injection rate, which was conducted over 10 pore volumes of injection. When the injection rate was increased tenfold to release oil trapped at the core outlet, an additional 13% of OOIP was produced. This oil was produced as an oil-in-water emulsion that separated within 3 hours. The oil produced during the high rate water flooding was also an oil-in-water emulsion, but it was not as apparent as the nanofluid flooding emulsion.

The modified particles with the largest surface area (Nsp_1b) had the poorest performance. Recovery factors of 0.06% and 1.13% were achieved for the low injection rate during 10 pore volumes of nanofluid flooding. This is much lower than the 11.8% recovery factor achieved from the unmodified particle (Nsp_1a) in Part 1, which was produced within three pore volumes. When the nanofluid injection rate was increased, recovery factors of 6.03% and 0% were obtained for the two tests, respectively. The total recovery factor from nanofluid flooding was therefore 6.09% for test #7 and 1.13% for test #8.

The modified particle with the medium surface area (Nsp_2b) obtained recovery factors of 1.19% and 0.89% for the low injection rate during nanofluid flooding. The nanofluid flooding recovery factor from Part 1 was 8.6% and was achieved within 3.1 pore volumes. When the nanofluid injection rate was increased, recovery factors of 5.57% and 13.79% were achieved.

The nature and magnitude of the oil production is different for the crude oil and n-decane tests. The crude oil was produced in oil in water (o/w) emulsions. The n-decane interacted with the nanoparticles as water in oil (w/o) emulsions. The core flooding experiments with crude oil had larger recovery factors for both the water flooding and nanofluid flooding stages than the experiments with n-decane. The total nanofluid flooding recovery factors from the tests with n-decane were less than 1% OOIP. The primary reason is probably due to the lack of components in the n-decane that could interact with the nanofluids. The asphaltenes and resins in the crude oil have shown attraction to similar silica nanoparticles (Hannisdal et al., 2006). There is likely an interaction between the nanoparticles and the resins and/or asphaltenes in the crude oil that allows additional oil recovery to take place. Additionally, the n-decane could produce a more water-wet behavior than the crude oil, resulting in a lower oil recovery from both the water flooding and hence the nanofluid flooding.

A comparison of the nanofluid flooding recovery factor to the nanoparticle surface area does not yield a clear linear correlation (Figure 6-8). The replicability of the experiments is poor, as the duplicates for Nsp_1b and Nsp_2b yield large variations in total nanofluid flooding recovery factor.
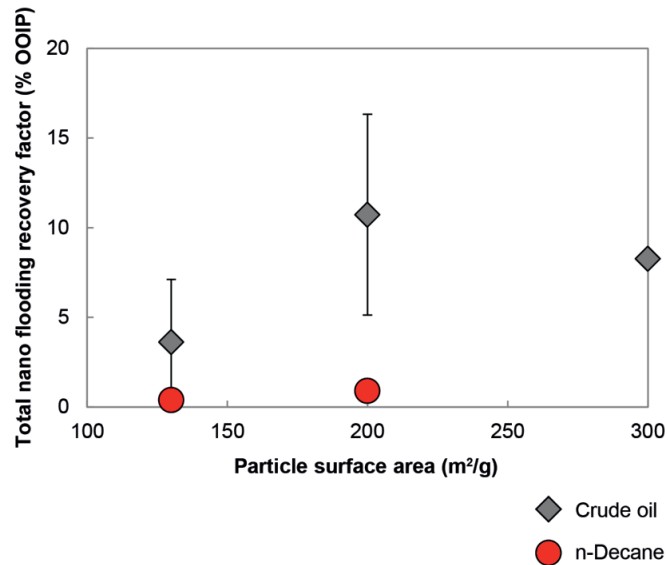
Figure 6-6. Particle surface area versus nanofluid flooding recovery factor. The average total nanofluid flooding recovery factor and associated standard deviation (n=2) is reported for the nanoparticles with surface areas of 130 and 200 m^2/g (Nsp_1b and Nsp_2b). Only one experiment was conducted for the nanoparticle with a surface area of 300 m^2/g (Nsp_3b) and the tests with n-decane. Therefore, no standard deviation is available for these tests.

The crude oil left an oil film that was difficult to completely remove even with two days using toluene soxhlet extraction. The crude oil film could be influencing the permeability impairment. However, the core plugs saturated with n-decane instead of crude oil, and therefore were more similar to initial conditions, also showed a significant permeability decrease (6% and 20% permeability impairment). There is no linear correlation between permeability impairment and total nanofluid flooding recovery factor (Figure 6-7). The difference in pre- and post- porosity values was within the measurement error.
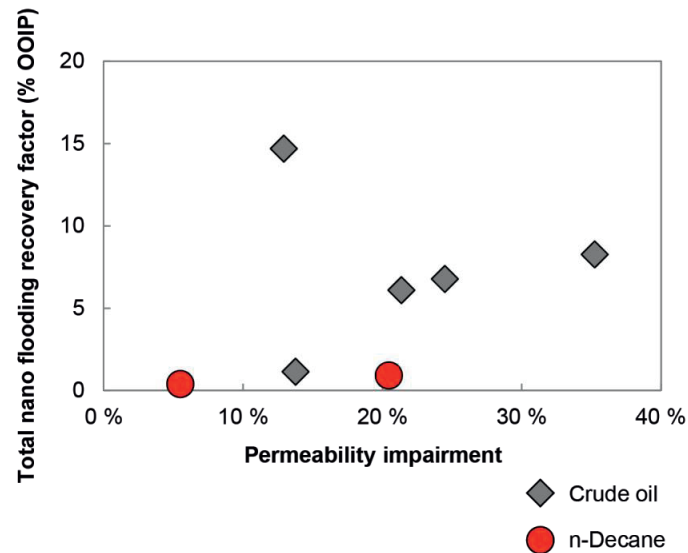
Figure 6-7. Comparison of core plug permeability impairment to the total nanofluid flooding recovery factor.The permeability measurements were taken prior to core plug saturation and also after the core was cleaned post- core flooding (unsaturated state).

Part 3: Evaluation of surface-modified Nsp_3a. For the core flooding tests in Part 3, less than 2% oil was produced during the low injection rate nanofluid flooding for all tests except #22 and #23. In fact, Tests #16 through #21 had no oil production during low rate nanofluid flooding, but up to 2.7% was produced when the injection rate was increased. This shows that Nsp_3c and Nsp_3d are unfavorable candidates for EOR. The two tests that had recovery rates of around 5% from low-rate nanofluid flooding both were aged for over 10 weeks and had no initial water saturation. The oil not produced immediately. Instead, oil production began after 3.75 PV (#22) and 2.75 PV (#23) and continued sporadically throughout the duration of the nanofluid flooding. This could be a result of continued flooding and release of oil from the core, and perhaps continued water flooding could have produced the same oil volumes.

Because little to no oil was produced, it was not possible to compare the recovery factor to the nanoparticle concentration. In summary, the nanoparticles did not work as intended.

Also, shut-in tests did not result in increased oil production after nanofluid flooding was re-started. This supports the theory that Nsp_3c is not reacting with the system and therefore explains why no oil is produced.

No oil was produced during the micromodel experiments with Nsp_3c at 0.05 wt%. This supports the hypothesis that Nsp_3c is not a candidate for EOR.

Part 4: Testing with aged cores and elevated temperature. Core flooding tests conducted during Part 4 did not have significant oil production. Replicate core flooding tests produced varied results as did the replicates in Part 2. The only somewhat positive test was Nsp_3c at 0.15 wt% (#32) with 4% OOIP incremental oil, but repeats of this test were less positive (1.7% for #31 and 0% for #33). As with Part 3, the lack of oil produced means that it is not possible to compare recovery factor to nanoparticle concentration.

6.2.3 Experimental artifacts

6.2.3.1 Fluid volume measurements

An important factor the core flooding experiments is that very little oil is produced during the nanofluid flooding. Even if a recovery factor of 5% OOIP is achieved in a 10 cm long core with a porosity of 20% and Swi of 0.25, the volume produced is quite small and close to the error margin of the graduated sampling tubes. In the aforementioned example, OOIP would be about 22.8 ml, and the 5% OOIP would be 1.15 ml. This volume significant if it is produced all at once in one graduated sampling tube, but this volume can be distributed over many sampling tubes if oil production occurs over a few pore volumes and that is when errors can begin to compound. In many cases, only 1% (or less) of OOIP is produced over one or two pore volumes, amounting to 0.23 ml or less of oil produced during nanofluid flooding. Therefore, it is difficult to statistically differentiate between core flooding tests producing oil recoveries of 1% and 3%, which are the recovery factors from many of the tests in Parts 3 and 4. It can be concluded that the error associated with the oil recovery volume increases with decreasing core length and associated OOIP volume.

6.2.3.2 Capillary end effects

The capillary end effect is when the discontinuity of capillarity occurs in the wetting phase at the core plug outlet. It is most pronounced in cases of oil displacing water in water-wet cores (Huang and Honarpour, 1998).

The capillary end effect could be affecting the core flooding results. However, it is difficult to estimate the magnitude of the capillary end effect because capillary pressure versus water saturation curves were not experimentally obtained for the core plugs. It could be that continuity of the oil phase in the water-wet cores is broken, and therefore oil collects behind the outlet water film and is only produced when the injection rate is increased enough to overcome the capillary pressure.

The magnitude of capillary end effect's impact on the core flooding data can be decreased by using a longer core or by increasing the injection rate (Lake, 1989). The reader is directed to the derivations by Huang and Honarpour (1998) for further reference.

6.3 EOR mechanisms

The proposed EOR mechanisms for the silica nanoparticles are summarized in Table 6.2. The table is based solely upon experimental data presented in this thesis.

Table 6.2. Potential EOR mechanisms.

Core flooding	Nanoparticles tested	Potential EOR mechanisms
Part 1: Screening of unmodified nanoparticles	Cnp_1 Cnp_2 Cnp_3 Nsp_1a Nsp_2a Nsp_3a	Mechanical displacement and, to a lesser extent, wettability alteration towards a strongly water-wet state
Part 2: Screening of silanized nanoparticles	Nsp_1b Nsp_2b Nsp_3b	In-situ o/w emulsification
Part 3: Evaluation of surface-modified Nsp_3a	Nsp_3c Nsp_3d	No significant recovery (< 3% OOIP) except for tests #22 and #23, which could be influenced by wettability alteration *or* simply continued injection of an aqueous phase.
Part 4: Testing with aged cores and elevated temperature	Nsp_3a Nsp_3c Nsp_3d	No significant recovery (< 4% OOIP)

Part 1: Screening of unmodified nanoparticles. The nanofluid flooding recovery factors obtained from the core flooding tests are likely a result of the physical microscopic diversion mechanism and, to a lesser extent, wettability alteration. The mechanism of interfacial tension reduction is not a contributing EOR mechanism for nanofluid flooding.

Part 2: Screening of silanized nanoparticles. The additional oil recovery during nanofluid flooding is not a result of microscopic diversion by increased differential pressure. In-situ oil-in-water emulsion generation could be the primary EOR mechanism resulting in oil recovery during nanofluid flooding at high injection rates. The nanofluid flooding recovery factor is not strongly influenced by pH alteration, wettability alteration or interfacial tension reduction.

Part 3: Evaluation of surface-modified Nsp_3a. Negligible oil production was observed for all tests except the two with no initial water saturation and altered initial wettability states (tests #22 and #23). Contact angle experiments with Nsp_3c do not reveal that wettability alteration is a primary mechanism. As the differential pressure remains low, mechanical displacement is likely not a mechanism. It is possible that the incremental oil recovery in tests #22 and #23 is due to wettability alteration. However, it is more likely that the incremental oil is slowly released from the rock surface simply because more flooding is taking place. It is possible that continuing water flooding would have produced comparable amounts of oil. This has been observed in other studies with oil-wet cores, where slow oil production occurs for a long time.

Part 4: Testing with aged cores and elevated temperature. Negligible oil production was observed for all tests. This indicates that there is not significant chemical reactivity taking place with Nsp_3c and Nsp_3d, as the increase in temperature does not result in more favorable recovery factors. The two tests with Nsp_3a showed significant pore blockage exhibited by the differential pressure increase. This confirms the results from Part 1.

The micromodels exhibited no to negligible oil production during the nanofluid flooding stage. Therefore, EOR mechanisms could not be observed. The tests do confirm that Nsp_3c is not a candidate for EOR.

6.3.1 Fluid – fluid interactions

For all nanoparticles, the magnitude of interfacial tension (IFT) reduction is too small for it to be a contributing EOR mechanism (Table 5.2 and Table 5.3). The nanoparticle interfacial tension did not decrease by orders of magnitude, which is necessary to produce immobile oil by this mechanism (Hamon, 2015). Even if there was a significant reduction of IFT with the unmodified particles, the modified particle would likely not display the same trend. This is because steric stabilization covers the original particle surface, preventing the reaction of the original particle with the system (Zhang et al., 2012).

Emulsions were present in the core flooding effluent for Part 2 core flooding tests (Figure 5-13). Therefore, the primary EOR mechanism for the silanized nanoparticles tested in Part 2 (Nsp_1b, Nsp_2b and Nsp_3b) is likely the alteration of the mobility ratio by the creation of in-situ oil in water emulsions. This is evidenced by the nanofluid flooding effluent and the increase in differential pressure for the high rate nanofluid flooding over the high rate water flooding.

The pH values for all flooding stages remained relatively constant and similar to the influent pH, staying between 7.2 and 7.9.

6.3.2 <u>Fluid – rock interactions</u>

For the unmodified nanoparticles, wettability alteration could be a contributing mechanism because wettability alteration towards a more water-wet system takes place for all nanoparticles except Cnp_1 (Table 5.4). Cnp_3 shows the largest difference from the base system followed by the three nano-structured particles. However, the nanofluid flooding recovery factor is not positively correlated to the decrease in contact angle. A glass surface is not a comprehensive representation of the core plug's mineralogy. Amott cell wettability tests, which use the entire core plug to determine changed in wettability, should be conducted to better assess the effect of nanoparticles on wettability alteration.

For the first round of modified nanoparticle contact angle tests with crude oil and n-decane, no large differences were observed. The contact angle increased throughout the 12-hour time period for all tests except one (Table 5.5). If this had only happened for the nanofluid experiments, it would support the theory that the nanoparticles are interacting with the oil and helping to mobilize oil globules. Therefore, it is not likely that oil production from Nsp_1b, Nsp_2b and Nsp_3b is due to wettability alteration.

For Nsp_3c, the tests at 20°C show that the nanoparticle is actually rendering the quartz plate towards more intermediate-wet when compared to the base system Table 5.6). There was no observable difference for the contact angle at 60°C. There was also no observable effect of nanoparticle concentration on the contact angle. Therefore, Nsp_3c is not using the mechanism of wettability alteration. This may be the reason why so little oil is produced during core flooding.

156

Conversely, the relative permeability calculations for tests #26 through #25 reveal that an alteration towards water-wet is occurring for all but three tests (#32, 33 and 35) (Table 5.28). Tests #26, 29-30, 32 and 34 had relative permeability values in the intermediate-wet regime at the end of water flooding (between 0.3 and 0.5) (Craig, 1971). Test #31 had an oil-wet value (0.57) at the end of water flooding. Tests #27-28, 33 and 35 had water-wet values ranging from 0.22 to 0.29 (Craig, 1971). There was no correlation between wettability observed at the end of water flooding and magnitude of relative permeability reduction. There was also no correlation between the reduction and the total nanofluid flooding recovery factor.

When this data is compared to the micromodel results, where no oil was produced during the oil-wet scenario, it appears that the modified particle Nsp_3c does not perform as well as its earlier counterparts.

6.3.3 Mechanical displacement

For the core flooding tests conducted in Part 1 with a constant injection rate of 0.4 ml/min throughout both water flooding and nanofluid flooding, a comparison of the nanofluid flooding recovery factor to the nanoparticle surface area for the unmodified particles reveals that there is no trend for the colloidal nanoparticles but a trendline for the nano-structured particles (Figure 6-8a). The differential pressure increase throughout the Part 1 nanofluid flooding is plotted against the nanofluid flooding recovery factor (Figure 6-8b). The colloidal nanoparticles show a positive, somewhat linear correlation between nanofluid flooding recovery factor and the increase in differential pressure throughout nanofluid flooding. The nano-structured particles do not display a linear relationship between the two parameters. There is a trendline between the nanofluid flooding recovery factor and the difference in the maximum differential pressure between the nanofluid flooding and water flooding stages (Figure 6-8c).

The agglomeration was confirmed with the core flooding tests, where the differential pressure increased throughout the nanofluid flooding. Additional effluent analyses confirmed that most of the nanoparticles are retained in the core.
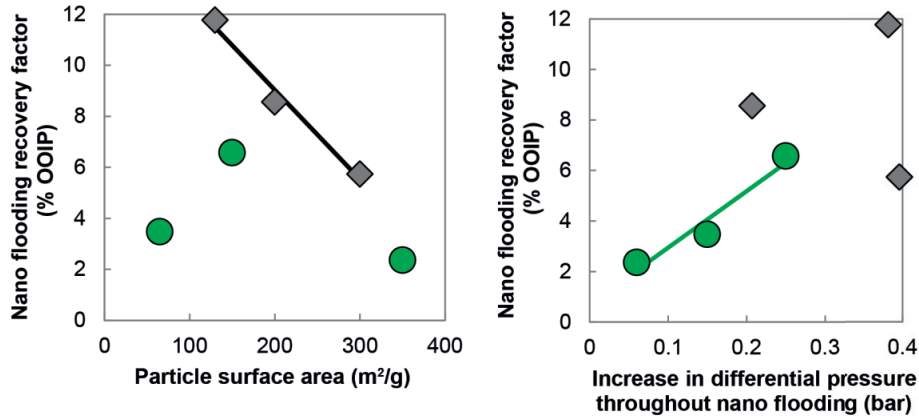
Figure 6-8. Nanofluid flooding recovery factor versus A) particle surface area; B) nanofluid flooding differential pressure increase; and C) the difference in maximum differential pressure between the nanofluid flooding and water flooding stages.

The microscopic diversion resulting from nanoparticle agglomeration and/or retention and resulting re-distribution of inter-pore pressure is likely the primary EOR mechanism. This can be concluded from the increase of differential pressure throughout nanofluid flooding and the correlation of differential pressure increase with initial oil bank occurrence.

The differential pressure increased throughout nanofluid flooding for all experiments. According to Darcy's Law, effective permeability must be decreasing if the differential pressure is increasing as long as all other variables (fluid viscosity, injection rate and core plug length and cross-sectional area) are constant. The permeability reduction can be explained by either nanoparticle adsorption to the rock grains or nanoparticle agglomeration. The magnitude of the increase in differential pressure does not correspond to the amount of nanoparticle agglomeration for either the colloidal or nano-structured particles. In fact, for the colloidal nanoparticles, Cnp_2 has the greatest differential pressure increase although it has the smallest agglomerate diameter. There is a positive correlation between the nanofluid flooding recovery factor and the differential pressure increase for the colloidal nanoparticle but not for the nano-structured particles. Therefore, it does not appear that nanoparticle agglomeration fully explains the permeability impairment and subsequent differential pressure increase. The negatively-charged nanoparticles could be adsorbing to the positively-charged clay components in the core plug. This could be confirmed directly with scanning electron microscopy (SEM) and indirectly by observing the fluid distribution in computed tomography (CT) scans.

There is a correlation between the differential pressure increase during nanofluid flooding and the occurrence of the initial oil bank for all tests. Two-phase flow tends to increase differential pressure according to the relative permeabilies. The differential pressure begins to increase immediately after initiation of nanofluid flooding for all tests. The initial oil bank occurs when the differential pressure temporarily plateaus. This indicates that the oil bank is a physical response to the pressure, and the release of the oil from the system causes temporary relief for the inter-pore pressure.

The maximum differential pressure during nanofluid flooding was greater than the maximum differential pressure during water flooding for all experiments. Therefore, oil produced during the nanofluid flooding could be a result of more pressure applied to the system, overcoming the capillary end effect and increasing the overall desaturation. Future studies should include an injection rate bump at the end of the water flooding to ensure that any oil produced during the nanofluid flooding is not a result of the capillary end effect. With the current method, increasing the injection rate for a continued water flood could produce comparable tertiary recovery factors to the tested systems where nanoparticles were added to SSW at the initial injection rate.

For the core flooding tests conducted during Part 2, the differences in differential pressure were compared to the total nanofluid flooding recovery factor to determine if pressure is affecting the oil production. The following three scenarios were investigated and plotted against the total nanofluid flooding recovery factor:

- (dP_{avg} for WF-Q_{low}) - (dP_{avg} for NF-Q_{low}) = the difference in average differential pressure between water flooding and nanofluid flooding at Q = 0.3 ml/min (**Figure 6-9a**).
- (dP_{avg} for NF-Q_{high}) - (dP_{avg} for WF-Q_{high}) = the difference in average differential pressure between nanofluid flooding and water flooding at Q = 3.0 ml/min (**Figure 6-9b**).
- (dP_{max} for WF-Q_{high}) - (dP_{max} for NF-Q_{high}) = the difference in maximum differential pressure between water flooding and nanofluid flooding at Q = 3.0 ml/min (**Figure 6-9c**).

There is no linear correlation between the difference in differential pressure and the total nanofluid flooding recovery factor.
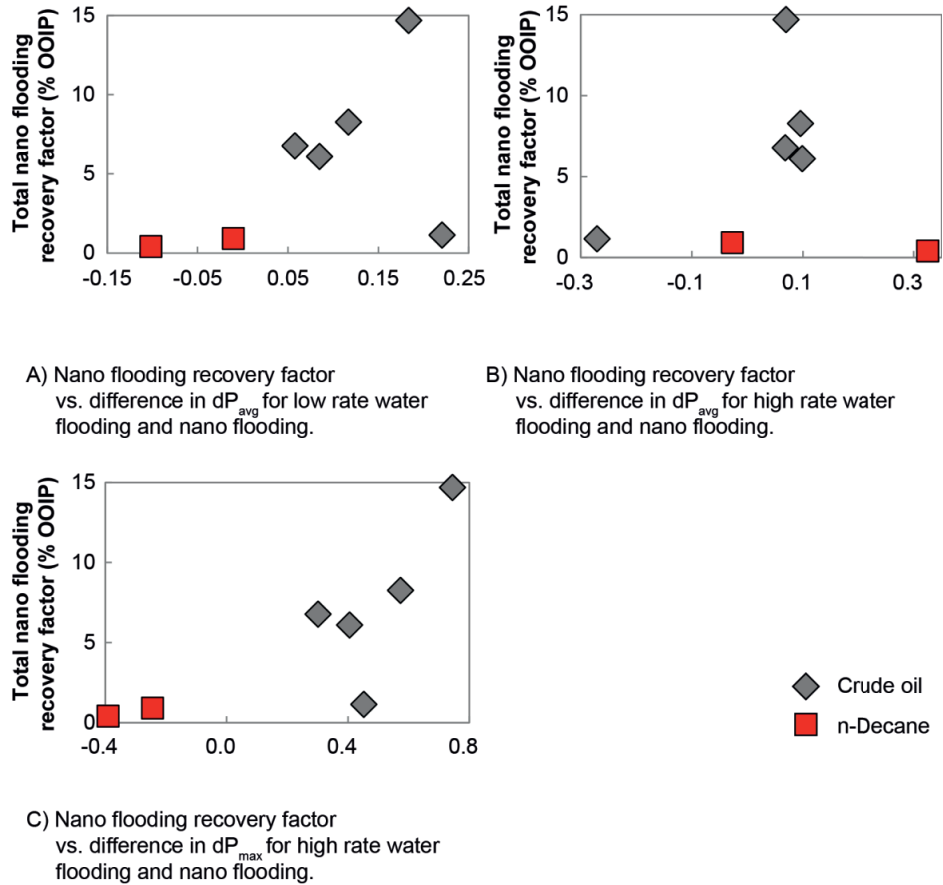
Figure 6-9. A) Nanofluid flooding recovery factor versus the difference in average differential pressure between water flooding and nanofluid flooding at Q = 0.3 ml/min; B) Nanofluid flooding recovery factor versus the difference in average differential pressure between nanofluid flooding and water flooding at Q = 3.0 ml/min; C) Nanofluid flooding recovery factor versus the difference in maximum differential pressure between water flooding and nanofluid flooding at Q = 3.0 ml/min.

The differential pressure increased throughout the NF-Q_{low} stage, but the increase was comparatively less than that observed in tests #4 through #6 in Part 1 with the unmodified nanoparticles. The nanofluid flooding effluent was produced as an oil-in-water emulsion, but it quickly separated and two distinct phases were visible after three hours.

Perhaps the small pressure increase is a result of oil globules mobilizing due to nanoparticle interaction at the interface, causing a pressure build-up where the globules are sitting in pore chambers attempting to squeeze through narrower pore throats on their way to the core outlet. This could explain why a significant increase in oil production occurred in all crude oil tests (with one exception) when the nanofluid injection rate was increased to 3 ml/min. This oil was typically produced towards the beginning of the increased rate stage, so the pressure wave from the increased injection rate could have provided the energy necessary to mobilize and produce oil droplets that were previously dislodged from the sandstone by nanoparticle interaction.

The chase water flooding conducted after the nanofluid flooding always had a lower differential pressure than during the nanofluid flooding stage. This indicates that the chase water flooding is effective at cleansing the system of nanoparticles. Effluent nanoparticle concentration was taken at four points throughout the chase water flooding, and the concentration decreased over time. The differential pressure during chase water flooding was also lower than the differential pressure during water flooding. Perhaps this is because it is slightly easier for the SSW to flow through the core after the nanofluid flooding extracted more oil out of the system that was blocking flow pathways. Also, the agglomerates could be disintegrating in the SSW.

In the core flooding tests with n-decane as the oil phase, the maximum differential pressure during nanofluid flooding was larger than the maximum differential pressure during water flooding. It is interesting to note that this still resulted in a lower oil recovery during the nanofluid flooding stage than with the crude oil systems where the maximum differential pressure during the nanofluid flooding was always lower than the maximum differential pressure during water flooding.

6.3.4 Nanoparticle transport

Part 1: Screening of unmodified nanoparticles. Effluent analysis from core flooding tests #4 through #6 shows that more than 95% of the nano-structured particles are retained in the core plug (Figure 5-12). Crude oil effluent shows a low concentration of nanoparticles Table 5.17). Therefore, the nanoparticle retention is likely a result of adsorption unto the rock grains and/or agglomeration and subsequent entrapment in the pore network. The methods used for this study

162

do not allow separation of these two processes. The average diameter of the agglomerated nanoparticles is smaller than the average diameter of the pore throats, but nanoparticle entrapment could still occur in the smaller pore throats. A complete mass balance was not conducted for the core plugs due to limited resources; that would have provided better data to compare nanoparticle breakthrough to initial oil bank production. Nevertheless, a lack of nanoparticle propagation through the reservoir is both uneconomic and potentially liable for permeability impairment. The nanoparticles should be modified to provide long-term stability in SSW.

Part 2: Screening of silanized nanoparticles. Limited effluent data was available for the Part 2 core flooding tests (Figure 5-14). Test #7 (Nsp_1b) is the only one with two samples taken during nanofluid flooding. The results show that nanoparticles are being retained within the core plug but the retention is less than that observed for the unmodified nanoparticles and retention decreases with time. Test #8, also with Nsp_1b, shows that nanoparticles are produced during the chase water flood. The nanoparticle production during the chase water flood indicates that nanoparticle retention is reversible. Because concentration values were not continuously taken throughout the entire core flood, it is impossible to do a mass balance to determine how much is being retained. Test #10 (Nsp_2b) shows that the concentration of nanoparticles decreases throughout the water flush. Test #11, also with Nsp_2b, once again shows that nanoparticle retention is reversible during the water flush. The two n-decane tests exhibit a decrease in differential pressure during the chase water flooding at 3.0 ml/min (Figures E.4 and E.7). This could be an indication of nanoparticle mobilization.

No clear relationship was found between the total oil recovery and nanoparticle retention. It is also unclear which particle has the greatest retention in the system. The permeability reduction does not correlate with the particle retention (Table 5.21). However, the permeability reduction is a function of both the particle retention and the effectiveness of the chase water flooding, so it appears that the concentration does not correlate with the permeability reduction.

There is still retention occurring, but in most cases it is smaller than the retention observed with the unmodified particles. This is primarily due to the salt stability modification. Some of the apparent retention could be because the particles are being diluted and/or "lost" in the

previously injected SSW and reservoir brine (3 wt% NaCl) that is sitting in the core. This water occupies over 50% of the pore space at the beginning of the nanofluid flooding process, so it is difficult to get an accurate picture of exactly how many nanoparticles are making their way through the core. It appears that at least some of the nanoparticle retention in the system is reversible based upon the presence of nanoparticles in the chase water flooding stage.

7 Conclusion and recommendations for future work

7.1 Conclusion

Hydrophilic silica nanoparticles could be promising water flooding additives due to their large surface area and small size. Nanoparticle-EOR could therefore be used to increase oil production from existing reservoirs. As demonstrated in Section 2.3, the large variation in material parameters and testing procedures found in literature makes it difficult to compare experimental studies that investigate nanoparticle-EOR.

In this thesis, experimental methods were used to evaluate nanofluid stability, determine oil production from core flooding and investigate the EOR mechanisms. The original goal was to improve the understanding of the EOR mechanisms for the unmodified nanoparticles that had already shown positive oil recovery results. The key difference was that the unmodified nanoparticles were dispersed in SSW for this thesis instead of 3 wt% NaCl to better simulate oilfield conditions. However, because the unmodified nanoparticles were not stable in SSW, the research goal changed to assess the stability and oil production of surface modified nanoparticles. The development and subsequent testing of new nanoparticles left little time for experiments specifically designed to better understand the EOR mechanisms. Therefore, there is still a need for studies specifically investigating silica nanoparticle EOR mechanisms and their relation to reservoir parameters such as oil composition, increased pressure and geochemical interactions with various minerals.

The conclusions for each of the primary research questions are summarized in Table 7.1 along with primary assumptions and limitations.

Table 7.1. Conclusion summary.

Research question	Conclusions	Primary assumptions (and limitations)
RQ1: Are the nanoparticles stable in synthetic sea water?	• None of the unmodified nanoparticles are stable in SSW. • Only Nsp_2c at 0.50 wt% is stable for 16 weeks at 60°C (see table 6.1)	• The PSD method is an appropriate method to assess nanofluid stability. • The 0.05 wt% concentration is the best for stability (Nsp_3c tested at two other concentrations, but not the other particles). • The unmodified particles will continue to agglomerate after one day and are unstable.
RQ2: Do the nanoparticles increase the oil recovery?	• There is a large variation for water flooding oil recovery. • The unmodified nanoparticles are the most promising EOR candidates, followed by the silanized nanoparticles. • Tests with crude oil give larger oil recoveries than tests with n-decane. • No obvious correlation exists between nanoparticle concentration and oil recovery, mostly due to the negligible oil recoveries obtained for all concentration comparison tests. • Core aging for > 10 weeks with flooding at 20°C results in more oil recovery; aging for 4 weeks with flooding at 60°C results in negligible oil recovery. • An increase in core flooding temperature decreases oil recovery.	• All Berea sandstone cores were similar enough to compare results. • Core flooding is an appropriate representation of how much oil a nanofluid could produce from a petroleum reservoir. • All oil produced during nanoparticle flooding is solely a result of the nanoparticles' effect on residual oil and would not be produced if water flooding was continued without nanoparticles. • The core aging process resulted in intermediate-wet initial wettability (the original wettability state was not confirmed with Amott cell tests). • Tertiary nanoparticle flooding is a more appropriate method of analysis than secondary nanoparticle flooding. • The tests conducted at 60°C produced less oil because of the temperature alone.
RQ3: What are the EOR mechanisms contributing to nanoparticle-induced oil recovery?	***Fluid-fluid interactions*** • There is no significant reduction in IFT, so it is not a primary EOR mechanism. • Oil-in-water emulsions are present in the nanofluid effluent for Part 2 core flooding tests (Nsp_1b, 2b and 3b). ***Fluid-rock interactions*** • No significant changes in contact angle. ***Mechanical displacement*** • Differential pressure increase (dP) correlates to oil recovery for unmodified nanoparticles. • The unmodified nano-structured particles are retained in the core. • The silanized nano-structured particles have better core propagation; retention is possibly reversible. • PSD analysis in nanofluid effluent for Part 4 follows stability trends (agglomeration occurs over time for the same nanoparticles).	***Fluid-fluid interactions*** • Tests conducted at ambient conditions. • Pendant drop tests run < 30 min; adequate time for IFT reactions to take place? • The emulsions are a direct result of the nanoparticles. • The emulsions improve the mobility ratio and enhance oil recovery. ***Fluid-rock interactions*** • The cleaning procedure removed all crude oil components and nanoparticles (it likely did not and should be checked with SEM). • 8, 10 or 24 hours is long enough for the contact angle to be stable. • The glass substrate and polished quartz plate are appropriate analogs for core wettability (they are not). ***Mechanical displacement*** • The dP increase is a result of nanoparticle retention for the unmodified nanoparticles. • The nanoparticle concentrations in the effluent are representative of a proper mass balance for the system.

None of the unmodified nanoparticles were stable in SSW, even at ambient conditions. Initial surface modifications of nano-structured particles rendered them stable at ambient conditions but not at the assumed threshold reservoir temperature (60°C). A further iteration of surface modification (Nsp_3c) resulted in stability at 60°C for at least 16 weeks at a concentration of 0.50 wt%. This was a positive outcome from the research.

However, the advancements in nanoparticle stability resulted in decreased oil production for each subsequent modification. The initial EOR mechanisms for the unmodified particles were never fully researched and understood, so the surface chemistry was not optimized for EOR mechanisms. This was an unfortunate backwards-approach. Instead, the nanoparticles should have been modified for stability with a specific EOR mechanism as a target such as wettability alteration. This would have set more constraints on the nanoparticle development, but it could have given more positive results for oil recovery.

Even for the unmodified nanoparticles that resulted in oil production, there was no positive correlation between nanoparticle surface area and nanofluid flooding recovery factor. If nanoparticles truly contribute to EOR by exploiting their large surface area for enhanced chemical reactivity in the reservoir, then a positive correlation would be visible. Instead, there was a negative relationship for the nano-structured particles, and the driving EOR mechanism appears to be microscopic flow diversion as a result of increased pressure to the system.

Because the differential pressure increases throughout the nanofluid flooding and was greater than the differential pressure achieved during water flooding, an injection rate bump was added to the end of the water flooding stage for future tests to ensure that any oil produced during nanofluid flooding was a result of chemical reactivity and not from the capillary end effect. Therefore, if additional oil recovery was still achieved, then it would be a result of the chemical nature of the nanoparticles. Instead, this new core flooding scheme resulted in little to no oil production during the first few pore volumes of nanofluid flooding for Parts 1, 2 and 3.

None of the modified nanoparticles met the criteria to be viable EOR candidates. The proposed EOR mechanism for oil production during Part 2 core flooding (nanoparticle Nsp_1b, Nsp_2b and Nsp_3b) is the in-situ creation of oil in water. This can be further exploited by tuning the surface of the nanoparticles to better interact with the oil globules.

Most of the experiments with nanoparticles Nsp_3c and Nsp_3d had no significant oil recovery (< 3 %OOIP incremental oil), so no EOR mechanism is proposed. However, tests #22 and #23, with Nsp_3c dispersed at 0.05 wt% and flooded at 20°C through cores aged for more than 10 weeks, showed significant oil recovery (8.8% and 10% OOIP incremental oil). It is unclear whether this oil recovery is from the nanoparticles or from additional flooding in general, but it presents a promising scenario for additional EOR tests.

7.2 Recommendations for future work

If nanoparticles are surface-modified such as they were in this work, then they should be modified in such a way as to target a specific EOR mechanism. There is growing evidence that combining nanoparticles with other EOR additives, such as polymers or surfactants, will produce the greatest oil recovery. A balance must be made between developing a product that can be applied in the field (using field / reservoir conditions) and between using simple systems to thoroughly evaluate the nanoparticles that are already available to better understand the relationship between adjustable parameters such as concentration and oil recovery. Ideally, a faster test is developed to replace core flooding as a screening method for new nanoparticles. Micromodel flooding coupled with contact angle experiments on appropriate mineral surfaces could be the best tool for assessing nanoparticles displaying wettability altering properties. All experiments should eventually be conducted at reservoir conditions to ensure that the same effects will occur in a petroleum field.

7.2.1 Nanofluid stability

The nanoparticle development in this thesis was motivated purely by the issue of sea water stability. Additional surface modifications need to be made to achieve nanofluid stability at 0.05 wt% in seawater. Once a stable nanofluid is identified, the stability tests should be conducted over at least one year. Additional tests should also be conducted at 80°C and 100°C and at reservoir pressures (> 100 bar). The composition of the dispersing fluid could be adjusted to identify the effects of the different cations to evaluate the sensitivity to each component. The

zeta potential can be analyzed as another predictor of nanofluid stability. Stabilizing components such as PVP can be added to the nanofluid to prevent agglomeration.

7.2.2 Oil recovery

Many additional parameters can be investigated with core flooding, but because core flooding inherently has many variations between replicated tests in unique core plugs, other experimental methods such as micromodel flooding can be used to determine oil recovery. The following recommendations can be applied for either core flooding or micromodel flooding.

The nanofluids should be evaluated with a secondary flooding procedure. The injection scheme can also be adjusted to try high concentration slugs of nanofluids followed by extensive chase water flooding. Then a larger nanoparticle concentration can provide a stronger EOR effect, but a short injection period keeps the material cost low. Larger concentrations of nanoparticles can be evaluated in general to have a more pronounced effect when comparing oil recovery to nanoparticle concentration.

Comparable aged cores should be tested with the Amott cell test to confirm initial wettability states. Future work should include a longer aging process of cores before performing nanofluid flooding experiments with surface modified nano-structured particles to be able to significantly increase oil recovery. All aged cores should include S_{wi} that is ideally produced and replicated by using the porous plate method. This would simultaneously produce capillary pressure vs. water saturation curves to better model the capillary end effect. This process is time-consuming so should only be attempted for the most promising nanofluids.

7.2.3 EOR mechanisms

The primary focus for future research should be focused on the EOR mechanisms in coordination with nanofluid stability improvement.

Fluid-fluid. More research is needed to study the behavior at the nanofluid – oil interface, especially over time, to determine the chemical mechanisms leading to increased oil recovery.

Parameters such as crude oil composition, nanofluid dispersing fluid composition and nanoparticle concentration should be routinely varied and compared.

Interfacial tension tests should be conducted at reservoir conditions and for different nanoparticle concentrations. They should also be conducted over days or weeks to see if the nanoparticles need time to find the oil/water interface.

If in-situ emulsion generation is occurring, the system can be analyzed with micromodel flooding. Oil-in-water emulsion stabilization can best be improved by adding cationic surfactants to the nanoparticles because the hydrophilic silica nanoparticles naturally have a negative surface charge (Binks and Whitby, 2005). The addition of surfactants improves stability due to the surfactants' absorption to both the nanoparticle-liquid interface and the oil-liquid interface. Decreasing the surface charge on particles should reduce its hydrophilicity (Binks and Whitby, 2005).

Nanoparticle emulsions should be thoroughly investigated by mixing with an Ultra-Turrax[®] and observing the droplet size over time. Additionally, emulsion droplets can be frozen and investigated with a Cryo-SEM to see where the nanoparticles are distributed in the sample.

Fluid-rock. Additional contact angle tests with varied minerals and therefore varied initial wettability states should be conducted. Repeated tests are needed for the unmodified nanoparticles. A more appropriate substrate should be used than glass, and the substrate should be evaluated with a SEM to ensure that cleaning procedures remove all oil components (especially asphaltenes) and nanoparticles from the mineral surface. There could be additional reactions that need longer than 8 or 24 hours to take place, so the tests should be conducted over days or weeks.

Additional tests with Amott cells should be done to see how the modified nanofluids affect the overall wettability of sandstone. Nanoparticle adsorption should be investigated.

Mechanical displacement. CT scans should be conducted on the core plugs to see where the oil production is taking place. Intermediate pressure sensors should be placed in many locations along the core plug length to better pinpoint where the differential pressure increase is occurring. A mass balance should be conducted for each nanofluid with and without oil saturation. Tracers should be added to the nanofluid phase in coordination with in-line nanoparticle concentration evaluation to compare the dispersion phase break through with nanoparticle transport. Particle size distribution analysis should be added in-line to the effluent to produce continuous analysis.

The microscopic flow diversion mechanism could be physically modeled to better understand how an increase in differential pressure causes redistribution of the fluids in the pore space.

References

Abdallah, W., Buckley, J.S., Carnegie, A., Edwards, J., Herold, B., Fordham, E., Graue, A., Habashy, T., Seleznev, N., Signer, C., Hussain, H., Montaron, B., Ziauddin, M., 2007. Fundamentals of Wettability. Oilfield Rev. 19, 44–61.

Alagic, E., Spildo, K., Skauge, A., Solbakken, J., 2011. Effect of crude oil ageing on low salinity and low salinity surfactant flooding. J. Pet. Sci. Eng. 78, 220–227. doi:10.1016/j.petrol.2011.06.021

Alomair, O.A., Matar, K.M., Alsaeed, Y.H., 2014. Nanofluids Application for Heavy Oil Recovery. Presented at the SPE Asia Pacific Oil & Gas Conference and Exhibition, Society of Petroleum Engineers. doi:10.2118/171539-MS

Alvarado, V., Manrique, E., 2010. Enhanced Oil Recovery: An Update Review. Energies 3, 1529–1575. doi:10.3390/en3091529

Amott, E., 1959. Observations Relating to the Wettability of Porous Rock. Pet. Trans. AIME 216, 156–162.

Anderson, W.G., 1987. Wettability Literature Survey Part 5: The Effects of Wettability on Relative Permeability. J. Pet. Technol. 39, 1,453-1,468. doi:10.2118/16323-PA

Anderson, W.G., 1986. Wettability Literature Survey- Part 1: Rock/Oil/Brine Interactions and the Effects of Core Handling on Wettability. J. Pet. Technol. 38, 1,125-1,144. doi:10.2118/13932-PA

Arce, P.E., 2010. Nanomaterials. Encycl. Nanosci. Soc.

Benner, F.C., Riches, W.W., Bartell, F.E., 1938. Nature and Importance of Surface Forces in Production of Petroleum. Presented at the Drilling and Production Practice 1938, American Petroleum Institute.

Bennetzen, M.V., Mogensen, K., 2014. Novel Applications of Nanoparticles for Future Enhanced Oil Recovery. Presented at the International Petroleum Technology Conference, International Petroleum Technology Conference. doi:10.2523/IPTC-17857-MS

Bera, A., Belhaj, H., 2016. Application of nanotechnology by means of nanoparticles and nanodispersions in oil recovery - A comprehensive review. J. Nat. Gas Sci. Eng. 34, 1284–1309. doi:10.1016/j.jngse.2016.08.023

Binks, B.P., Fletcher, P.D.I., 2001. Particles Adsorbed at the Oil−Water Interface: A Theoretical Comparison between Spheres of Uniform Wettability and "Janus" Particles. Langmuir 17, 4708–4710. doi:10.1021/la0103315

Binks, B.P., Lumsdon, S.O., 2000. Influence of Particle Wettability on the Type and Stability of Surfactant-Free Emulsions. Langmuir 16, 8622–8631. doi:10.1021/la000189s

References

Binks, B.P., Whitby, C.P., 2005. Nanoparticle silica-stabilised oil-in-water emulsions: improving emulsion stability. Colloids Surf. Physicochem. Eng. Asp. 253, 105–115. doi:10.1016/j.colsurfa.2004.10.116

Bolandtaba, A.F., Skauge, A., MacKay, E., 2009. Pore scale modeling of linked polymer solution (LPS) – A new EOR process. Presented at the 15th European Symposium on Improved Oil Recovery, Paris, France, p. 17.

Buckley, J.S., 1995. Asphaltene Precipitation and Crude Oil Wetting. SPE Adv. Technol. Ser. 3, 53–59. doi:10.2118/26675-PA

Buckley, J.S., Liu, Y., Monsterleet, S., 1998. Mechanisms of Wetting Alteration by Crude Oils. SPE J. 3, 54–61. doi:10.2118/37230-PA

Byrne, M., Patey, I., 2004. Core sample preparation - An insight in to new procedures. Presented at the International Symposium of the Society of Core Analysts, Society of Core Analysts, Abu Dhabi, UAE, p. 6.

Cebrián, V., Yagüe, C., Arruebo, M., Martín-Saavedra, F.M., Santamaría, J., Vilaboa, N., 2011. On the role of the colloidal stability of mesoporous silica nanoparticles as gene delivery vectors. J. Nanoparticle Res. 13, 4097–4108. doi:10.1007/s11051-011-0353-8

Chen, K.L., Smith, B.A., Ball, W.P., Fairbrother, D.H., 2010. Assessing the colloidal properties of engineered nanoparticles in water: case studies from fullerene C60 nanoparticles and carbon nanotubes. Environ. Chem. 7, 10–27. doi:10.1071/EN09112

Chengara, A., Nikolov, A.D., Wasan, D.T., Trokhymchuk, A., Henderson, D., 2004. Spreading of nanofluids driven by the structural disjoining pressure gradient. J. Colloid Interface Sci. 280, 192–201. doi:10.1016/j.jcis.2004.07.005

Cheraghian, G., 2016. Application of nano-fumed silica in heavy oil recovery. Pet. Sci. Technol. 34, 12–18. doi:10.1080/10916466.2015.1114497

Churcher, P.L., French, P.R., Shaw, J.C., Schramm, L.L., 1991. Rock Properties of Berea Sandstone, Baker Dolomite, and Indiana Limestone. Presented at the SPE International Symposium on Oilfield Chemistry, Society of Petroleum Engineers. doi:10.2118/21044-MS

Craig, F., 1971. The Reservoir Engineering Aspects of Waterflooding, SPE Monograph. Society of Petroleum Engineers, Richardson, TX.

Cuiec, L., 1984. Rock/Crude-Oil Interactions and Wettability: An Attempt To Understand Their Interrelation. Presented at the SPE Annual Technical Conference and Exhibition, Society of Petroleum Engineers. doi:10.2118/13211-MS

Cuiec, L., 1977. Study of Problems Related to the Restoration Of the Natural State of Core Samples. J. Can. Pet. Technol. 16. doi:10.2118/77-04-09

Dake, L.P., 1998. Fundamentals of Reservoir Engineering. Elsevier.

Dandekar, A.Y., 2013. Petroleum Reservoir Rock and Fluid Properties, 2nd ed. Taylor & Francis.

Derjaguin, B.V., Landau, L., 1941. Theory of the stability of strongly charged lyophobic sols and of the adhesion of strongly charged particles in solutions of electrolytes. Acta Phys Chim URSS 14, 633–662.

Donaldson, E.C., Thomas, R.D., Lorenz, P.B., 1969. Wettability Determination and Its Effect on Recovery Efficiency. Soc. Pet. Eng. J. 9, 13–20. doi:10.2118/2338-PA

Eijkel, J.C.T., Berg, A. van den, 2005. Nanofluidics: what is it and what can we expect from it? Microfluid. Nanofluidics 1, 249–267. doi:10.1007/s10404-004-0012-9

El-Diasty, A.I., 2015. The Potential of Nanoparticles to Improve Oil Recovery in Bahariya Formation, Egypt: An Experimental Study. Presented at the SPE Asia Pacific Enhanced Oil Recovery Conference, Society of Petroleum Engineers. doi:10.2118/174599-MS

Evonik Industries, 2015. AEROSIL® - Fumed Silica: Technical Overview 8th Ed.

Eykens, L., De Sitter, K., Dotremont, C., De Schepper, W., Pinoy, L., Van Der Bruggen, B., 2017. Wetting Resistance of Commercial Membrane Distillation Membranes in Waste Streams Containing Surfactants and Oil. Appl. Sci. 7, 118. doi:10.3390/app7020118

Faust, S.D., Aly, O.M., 1998. Chemistry of Water Treatment, Second Edition. CRC Press.

Fletcher, A., Davis, J., 2010. How EOR Can be Transformed by Nanotechnology. Presented at the SPE Improved Oil Recovery Symposium, Society of Petroleum Engineers. doi:10.2118/129531-MS

Frijters, S., Günther, F., Harting, J., 2012. Effects of nanoparticles and surfactant on droplets in shear flow. Soft Matter 8, 6542. doi:10.1039/C2SM25209K

Frisken, B.J., 2001. Revisiting the method of cumulants for the analysis of dynamic light-scattering data. Appl. Opt. 40, 4087–4091. doi:10.1364/AO.40.004087

Ghosh, S.K., Alargova, R.G., Deguchi, S., Tsujii, K., 2006. Dispersion Stability of Colloids in Sub- and Supercritical Water. J. Phys. Chem. B 110, 25901–25907. doi:10.1021/jp0656328

Grate, J.W., Warner, M.G., Pittman, J.W., Dehoff, K.J., Wietsma, T.W., Zhang, C., Oostrom, M., 2013. Silane modification of glass and silica surfaces to obtain equally oil-wet surfaces in glass-covered silicon micromodel applications. Water Resour. Res. 49, 4724–4729. doi:10.1002/wrcr.20367

Hamon, G., 2015. Low Salinity Water Flooding: Facts, Inconsistencies and Way Forward. Presented at the International Symposium of the Society of Core Analysts, St. John's, Newfoundland and Labrador, Canada, p. 12.

References

Han, D.-K., Yang, C.-Z., Zhang, Z.-Q., Lou, Z.-H., Chang, Y.-I., 1999. Recent development of enhanced oil recovery in China. J. Pet. Sci. Eng. 22, 181–188. doi:10.1016/S0920-4105(98)00067-9

Hannisdal, A., Ese, M.-H., Hemmingsen, P.V., Sjöblom, J., 2006. Particle-stabilized emulsions: Effect of heavy crude oil components pre-adsorbed onto stabilizing solids. Colloids Surf. Physicochem. Eng. Asp. 276, 45–58. doi:10.1016/j.colsurfa.2005.10.011

Hendraningrat, L., Engeset, B., Suwarno, S., Li, S., Torsæter, O., 2013a. Laboratory investigation of porosity and permeability impairments in Berea sandstones due to hydrophilic nanoparticle retention. Presented at the International Symposium of the Society of Core Analysts, Napa Valley, California, USA, p. 6.

Hendraningrat, L., Engeset, B., Suwarno, S., Torsæter, O., 2012a. Improved Oil Recovery by Nanofluids Flooding: An Experimental Study. Presented at the SPE Kuwait International Petroleum Conference and Exhibition, Society of Petroleum Engineers. doi:10.2118/163335-MS

Hendraningrat, L., Li, S., Suwarno, Torsæter, O., 2012b. A Glass Micromodel Experimental Study of Hydrophilic Nanoparticles Retention for EOR Project. Presented at the SPE Russian Oil and Gas Exploration and Production Technical Conference and Exhibition, Society of Petroleum Engineers. doi:10.2118/159161-MS

Hendraningrat, L., Li, S., Torsæter, O., 2013b. A coreflood investigation of nanofluid enhanced oil recovery. J. Pet. Sci. Eng. 111, 128–138. doi:10.1016/j.petrol.2013.07.003

Hendraningrat, L., Li, S., Torsaeter, O., 2013c. Enhancing Oil Recovery of Low-Permeability Berea Sandstone through Optimised Nanofluids Concentration. Presented at the SPE Enhanced Oil Recovery Conference, Society of Petroleum Engineers. doi:10.2118/165283-MS

Hendraningrat, L., Li, S., Torsater, O., 2013d. Effect of Some Parameters Influencing Enhanced Oil Recovery Process using Silica Nanoparticles: An Experimental Investigation. Presented at the SPE Reservoir Characterization and Simulation Conference and Exhibition, Society of Petroleum Engineers. doi:10.2118/165955-MS

Hendraningrat, L., Li, S., Torsater, O., 2013e. A Coreflood Investigation of Nanofluid Enhanced Oil Recovery in Low-Medium Permeability Berea Sandstone. Presented at the SPE International Symposium on Oilfield Chemistry, Society of Petroleum Engineers. doi:10.2118/164106-MS

Hendraningrat, L., Torsæter, O., 2016. A study of water chemistry extends the benefits of using silica-based nanoparticles on enhanced oil recovery. Appl. Nanosci. 6, 83–95. doi:10.1007/s13204-015-0411-0

Hendraningrat, L., Torsæter, O., 2015a. A Stabilizer that Enhances the Oil Recovery Process Using Silica-Based Nanofluids. Transp. Porous Media 108, 679–696. doi:10.1007/s11242-015-0495-8

Hendraningrat, L., Torsæter, O., 2015b. Metal oxide-based nanoparticles: revealing their potential to enhance oil recovery in different wettability systems. Appl. Nanosci. 5, 181–199. doi:10.1007/s13204-014-0305-6

Hendraningrat, L., Torsæter, O., 2014a. Effects of the Initial Rock Wettability on Silica-Based Nanofluid-Enhanced Oil Recovery Processes at Reservoir Temperatures. Energy Fuels 28, 6228–6241. doi:10.1021/ef5014049

Hendraningrat, L., Torsæter, O., 2014b. Understanding Fluid-Fluid and Fluid-Rock Interactions in the Presence of Hydrophilic Nanoparticles at Various Conditions. Presented at the SPE Asia Pacific Oil & Gas Conference and Exhibition, Society of Petroleum Engineers. doi:10.2118/171407-MS

Hendraningrat, L., Zhang, J., 2015. Polymeric nanospheres as a displacement fluid in enhanced oil recovery. Appl. Nanosci. 5, 1009–1016. doi:10.1007/s13204-014-0399-x

Hotze, E.M., Phenrat, T., Lowry, G.V., 2010. Nanoparticle aggregation: challenges to understanding transport and reactivity in the environment. J. Environ. Qual. 39, 1909–1924.

Huang, D.D., Honarpour, M.M., 1998. Capillary end effects in coreflood calculations. J. Pet. Sci. Eng. 19, 103–117. doi:10.1016/S0920-4105(97)00040-5

Huh, C., Lange, E.A., Cannella, W.J., 1990. Polymer Retention in Porous Media. Presented at the SPE/DOE Enhanced Oil Recovery Symposium, Society of Petroleum Engineers. doi:10.2118/20235-MS

Huh, C., Pope, G.A., 2008. Residual Oil Saturation from Polymer Floods: Laboratory Measurements and Theoretical Interpretation. Presented at the SPE Symposium on Improved Oil Recovery, Society of Petroleum Engineers. doi:10.2118/113417-MS

ISO 22412:2017 - Particle size analysis -- Dynamic light scattering (DLS) [WWW Document], n.d. URL https://www.iso.org/standard/65410.html (accessed 3.30.17).

Jadhunandan, P.P., Morrow, N.R., 1995. Effect of Wettability on Waterflood Recovery for Crude-Oil/Brine/Rock Systems. SPE Reserv. Eng. 10, 40–46. doi:10.2118/22597-PA

Jia, D., Buckley, J.S., Morrow, N.R., 1991. Control of Core Wettability With Crude Oil. Presented at the SPE International Symposium on Oilfield Chemistry, Society of Petroleum Engineers. doi:10.2118/21041-MS

Ju, B., Dai, S., Luan, Z., Zhu, T., Su, X., Qiu, X., 2002. A Study of Wettability and Permeability Change Caused by Adsorption of Nanometer Structured Polysilicon on the Surface of Porous Media. Presented at the SPE Asia Pacific Oil and Gas Conference and Exhibition, Society of Petroleum Engineers. doi:10.2118/77938-MS

Ju, B., Fan, T., Ma, M., 2006. Enhanced oil recovery by flooding with hydrophilic nanoparticles. China Particuology 4, 41–46. doi:10.1016/S1672-2515(07)60232-2

References

Kanicky, J.R., Lopez-montilla, J., P, S., Shah, D.O., 2001. Chapter 11: Surface Chemistry in the Petroleum Industry, in: Handbook of Applied Surface and Colloid Chemistry. John Wiley & Sons, New York.

Klinkenberg, L.J., 1941. The Permeability Of Porous Media To Liquids And Gases. Presented at the Drilling and Production Practice, American Petroleum Institute.

Kondiparty, K., Nikolov, A., Wu, S., Wasan, D., 2011. Wetting and Spreading of Nanofluids on Solid Surfaces Driven by the Structural Disjoining Pressure: Statics Analysis and Experiments. Langmuir 27, 3324–3335. doi:10.1021/la104204b

Lai, P., Moulton, K., Krevor, S., 2015. Pore-scale heterogeneity in the mineral distribution and reactive surface area of porous rocks. Chem. Geol. 411, 260–273. doi:10.1016/j.chemgeo.2015.07.010

Lake, L.W., 1989. Enhanced oil recovery. Prentice Hall.

Li, S., Genys, M., Wang, K., Torsæter, O., 2015. Experimental Study of Wettability Alteration during Nanofluid Enhanced Oil Recovery Process and Its Effect on Oil Recovery. Presented at the SPE Reservoir Characterisation and Simulation Conference and Exhibition, Society of Petroleum Engineers. doi:10.2118/175610-MS

Li, S., Hendraningrat, L., Torsaeter, O., 2013. Improved Oil Recovery by Hydrophilic Silica Nanoparticles Suspension: 2-Phase Flow Experimental Studies. Presented at the International Petroleum Technology Conference, International Petroleum Technology Conference. doi:10.2523/IPTC-16707-MS

Li, S., Torsæter, O., 2015. The Impact of Nanoparticles Adsorption and Transport on Wettability Alteration of Intermediate Wet Berea Sandstone. Presented at the SPE Middle East Unconventional Resources Conference and Exhibition, Society of Petroleum Engineers. doi:10.2118/172943-MS

Li, S., Torsæter, O., 2014. An experimental investigation of EOR mechanisms for nanoparticles fluid in glass micromodel. Presented at the International Symposium of the Society of Core Analysts, Avignon, France, p. 12.

Maghzi, A., Mohebbi, A., Kharrat, R., Ghazanfari, M.H., 2013. An Experimental Investigation of Silica Nanoparticles Effect on the Rheological Behavior of Polyacrylamide Solution to Enhance Heavy Oil Recovery. Pet. Sci. Technol. 31, 500–508. doi:10.1080/10916466.2010.518191

Malvern Instruments, 2017. Zetasizer Nano Series: Research Performance, Operational SImplicity, Application Versatility. Malvern Instruments Limited, Worcestershire, UK.

McElfresh, P.M., Holcomb, D.L., Ector, D., 2012. Application of Nanofluid Technology to Improve Recovery in Oil and Gas Wells. Presented at the SPE International Oilfield Nanotechnology Conference and Exhibition, Society of Petroleum Engineers. doi:10.2118/154827-MS

McPhee, C., Reed, J., Zubizarreta, I., 2015. Chapter 6: Preparation for Special Core Analysis, in: Core Analysis: A Best Practice Guide, Volume 64 - 1st Edition. Elsevier, pp. 269–312.

McPhee, C.A., Arthur, K.G., 1994. Relative Permeability Measurements: An Inter-Laboratory Comparison. Presented at the European Petroleum Conference, Society of Petroleum Engineers. doi:10.2118/28826-MS

Metin, C.O., Lake, L.W., Miranda, C.R., Nguyen, Q.P., 2010. Stability of aqueous silica nanoparticle dispersions. J. Nanoparticle Res. 13, 839–850. doi:10.1007/s11051-010-0085-1

Miranda, C.R., Lara, L.S. de, Tonetto, B.C., 2012. Stability and Mobility of Functionalized Silica Nanoparticles for Enhanced Oil Recovery Applications. Presented at the SPE International Oilfield Nanotechnology Conference and Exhibition, Society of Petroleum Engineers. doi:10.2118/157033-MS

Moore, T., Rodriguez-Lorenzo, L., Hirsch, V., Balog, S., Urban, D., Jud, C., Rothen-Rutishauser, B., Lattuada, M., Petri-Fink, A., 2015. Nanoparticle colloidal stability in cell culture media and impact on cellular interactions. Chem. Soc. Rev. 44, 6287–6305. doi:10.1039/C4CS00487F

Morrow, N.R., 1990. Wettability and Its Effect on Oil Recovery. J. Pet. Technol. 42, 1,476-1,484. doi:10.2118/21621-PA

Muggeridge, A., Cockin, A., Webb, K., Frampton, H., Collins, I., Moulds, T., Salino, P., 2014. Recovery rates, enhanced oil recovery and technological limits. Phil Trans R Soc A 372, 20120320. doi:10.1098/rsta.2012.0320

Negin, C., Ali, S., Xie, Q., 2016. Application of nanotechnology for enhancing oil recovery – A review. Petroleum 2, 324–333. doi:10.1016/j.petlm.2016.10.002

Nichols, G., Byard, S., Bloxham, M.J., Botterill, J., Dawson, N.J., Dennis, A., Diart, V., North, N.C., Sherwood, J.D., 2002. A review of the terms agglomerate and aggregate with a recommendation for nomenclature used in powder and particle characterization. J. Pharm. Sci. 91, 2103–2109. doi:10.1002/jps.10191

Norwegian Petroleum Directorate, 2014a. Facts 2014 (No. Y-0103/15 E).

Norwegian Petroleum Directorate, 2014b. Petroleum resources on the Norwegian continental shelf 2014 - Fields and discoveries. Stavanger, Norway.

Ogolo, N.A., Olafuyi, O.A., Onyekonwu, M.O., 2012. Enhanced Oil Recovery Using Nanoparticles. Presented at the SPE Saudi Arabia Section Technical Symposium and Exhibition, Society of Petroleum Engineers. doi:10.2118/160847-MS

Pepper, J.F., DeWitt, W., Demarest, D.F., 1954. Geology of the Bedford Shale and Berea Sandstone in the Appalachian Basin (Geological Survey Professional Paper No. 259). United States Geological Survey.

References

Peters, R., Kramer, E., Oomen, A.G., Herrera Rivera, Z.E., Oegema, G., Tromp, P.C., Fokkink, R., Rietveld, A., Marvin, H.J.P., Weigel, S., Peijnenburg, A.A.C.M., Bouwmeester, H., 2012. Presence of Nano-Sized Silica during In Vitro Digestion of Foods Containing Silica as a Food Additive. ACS Nano 6, 2441–2451. doi:10.1021/nn204728k

Prats, M., 1982. Thermal recovery. SPE Monograph Series Vol. 7. 283 p.

Ragab, A.M.S., Hannora, A.E., 2015. An Experimental Investigation of Silica Nano Particles for Enhanced Oil Recovery Applications. Presented at the SPE North Africa Technical Conference and Exhibition, Society of Petroleum Engineers. doi:10.2118/175829-MS

Ragab, S., M, A., Hannora, A.E., 2015. A Comparative Investigation of Nano Particle Effects for Improved Oil Recovery – Experimental Work. Presented at the SPE Kuwait Oil and Gas Show and Conference, Society of Petroleum Engineers. doi:10.2118/175395-MS

Rahimi, K., Adibifard, M., 2015. Experimental Study of the Nanoparticles Effect on Surfactant Absorption and Oil Recovery in One of the Iranian Oil Reservoirs. Pet. Sci. Technol. 33, 79–85. doi:10.1080/10916466.2014.950382

Rao, D.N., Girard, M., Sayegh, S.G., 1992. The Influence Of Reservoir Wettability On Waterflood And Miscible Flood Performance. J. Can. Pet. Technol. 31. doi:10.2118/92-06-05

Ravina, L., Moramarco, N., 1993. Everything you want to know about coagulation and flocculation. Zeta-Meter, Inc., Staunton, Virginia.

Raza, S.H., Treiber, L.E., Archer, D.L., 1968. Wettability of Reservoir Rocks and Its Evaluation. Prod Mon U. S. 32:4.

Rezaei, N., Firoozabadi, A., 2014. Macro- and Microscale Waterflooding Performances of Crudes which form w/o Emulsions upon Mixing with Brines. Energy Fuels 28, 2092–2103. doi:10.1021/ef402223d

Roustaei, A., Bagherzadeh, H., 2015. Experimental investigation of SiO2 nanoparticles on enhanced oil recovery of carbonate reservoirs. J. Pet. Explor. Prod. Technol. 5, 27–33. doi:10.1007/s13202-014-0120-3

Roustaei, A., Saffarzadeh, S., Mohammadi, M., 2013. An evaluation of modified silica nanoparticles' efficiency in enhancing oil recovery of light and intermediate oil reservoirs. Egypt. J. Pet. 22, 427–433. doi:10.1016/j.ejpe.2013.06.010

Sandengen, K., Kristoffersen, A., Melhuus, K., Jøsang, L.O., 2016. Osmosis as Mechanism for Low-Salinity Enhanced Oil Recovery. SPE J. 21, 1,227-1,235. doi:10.2118/179741-PA

Sen, P.N., Straley, C., Kenyon, W.E., Whittingham, M.S., 1990. Surface-to-volume ratio, charge density, nuclear magnetic relaxation, and permeability in clay-bearing sandstones. Geophysics 55, 61–69. doi:10.1190/1.1442772

Sheng, J.J., 2015. Status of surfactant EOR technology. Petroleum 1, 97–105. doi:10.1016/j.petlm.2015.07.003

Skauge, T., Spildo, K., Skauge, A., 2010. Nano-sized Particles For EOR. Presented at the SPE Improved Oil Recovery Symposium, Society of Petroleum Engineers. doi:10.2118/129933-MS

Smalley, P.C., Ross, A.W., Brown, C., Moulds, T.P., Smith, M.J., 2009. Reservoir Technical Limits: A Framework for Maximizing Recovery From Oil Fields. SPE Reserv. Eval. Eng. 12, 610–629. doi:10.2118/109555-PA

Sparreboom, W., van den Berg, A., Eijkel, J.C.T., 2009. Principles and applications of nanofluidic transport. Nat. Nanotechnol. 4, 713–720. doi:10.1038/nnano.2009.332

Spildo, K., Skauge, A., Aarra, M.G., Tweheyo, M.T., 2009. A New Polymer Application for North Sea Reservoirs. SPE Reserv. Eval. Eng. 12, 427–432. doi:10.2118/113460-PA

Standing, M.B., 1975. Notes on relative permeability relationships.

Sullivan, A.P., Kilpatrick, P.K., 2002. The Effects of Inorganic Solid Particles on Water and Crude Oil Emulsion Stability. Ind. Eng. Chem. Res. 41, 3389–3404. doi:10.1021/ie010927n

Sun, X., Zhang, Y., Chen, G., Gai, Z., 2017. Application of Nanoparticles in Enhanced Oil Recovery: A Critical Review of Recent Progress. Energies 10, 345. doi:10.3390/en10030345

Taber, J.J., Martin, F.D., Seright, R.S., 1997. EOR Screening Criteria Revisited - Part 1: Introduction to Screening Criteria and Enhanced Recovery Field Projects. SPE Reserv. Eng. 12, 189–198. doi:10.2118/35385-PA

Tang, G.Q., Morrow, N.R., 1997. Salinity, Temperature, Oil Composition, and Oil Recovery by Waterflooding. SPE Reserv. Eng. 12, 269–276. doi:10.2118/36680-PA

Tarek, M., El-Banbi, A.H., 2015. Comprehensive Investigation of Effects of Nano-Fluid Mixtures to Enhance Oil Recovery. Presented at the SPE North Africa Technical Conference and Exhibition, Society of Petroleum Engineers. doi:10.2118/175835-MS

Thomas, M., 2013. Improving the oil recovery factor. BP Mag. 31–35.

Tian, Q.Y., Wang, L., Tang, Y., Liu, C., Ma, C., Wang, T., 2012. Research and Application of Nano Polymer Microspheres Diversion Technique of Deep Fluid. Presented at the SPE International Oilfield Nanotechnology Conference and Exhibition, Society of Petroleum Engineers. doi:10.2118/156999-MS

Tichelkamp, T., Vu, Y., Nourani, M., Øye, G., 2014. Interfacial Tension between Low Salinity Solutions of Sulfonate Surfactants and Crude and Model Oils. Energy Fuels 28, 2408–2414. doi:10.1021/ef4024959

Verwey, E., Overbeek, J., van Nes, K., 1948. The theory of the stability of liophobic colloids: The interaction of sol particles having an electric double layer. Elsevier.

Wang, C., Bobba, A.D., Attinti, R., Shen, C., Lazouskaya, V., Wang, L.-P., Jin, Y., 2012. Retention and Transport of Silica Nanoparticles in Saturated Porous Media: Effect of Concentration and Particle Size. Environ. Sci. Technol. 46, 7151–7158. doi:10.1021/es300314n

Wasan, D.T., Nikolov, A.D., 2003. Spreading of nanofluids on solids. Nature 423, 156–159. doi:10.1038/nature01591

Wasan, D.T., Shah, S.M., Aderangi, N., Chan, M.S., McNamara, J.J., 1978. Observations on the Coalescence Behavior of Oil Droplets and Emulsion Stability in Enhanced Oil Recovery. Soc. Pet. Eng. J. 18, 409–417. doi:10.2118/6846-PA

Weir, A., Westerhoff, P., Fabricius, L., von Goetz, N., 2012. Titanium Dioxide Nanoparticles in Food and Personal Care Products. Environ. Sci. Technol. 46, 2242–2250. doi:10.1021/es204168d

Wu, J., He, J., Torsater, O., Zhang, Z., 2012. Effect of Nanoparticles on Oil-Water Flow in a Confined Nanochannel: a Molecular Dynamics Study. Presented at the SPE International Oilfield Nanotechnology Conference and Exhibition, Society of Petroleum Engineers. doi:10.2118/156995-MS

Yousefvand, H., Jafari, A., 2015. Enhanced Oil Recovery Using Polymer/nanosilica. Procedia Mater. Sci., 5th International Biennial Conference on Ultrafine Grained and Nanostructured Materials, UFGNSM15 11, 565–570. doi:10.1016/j.mspro.2015.11.068

Youssif, M.I., El-Maghraby, R.M., Saleh, S.M., Elgibaly, A., 2017. Silica nanofluid flooding for enhanced oil recovery in sandstone rocks. Egypt. J. Pet. doi:10.1016/j.ejpe.2017.01.006

Yuan, C.-D., Pu, W.-F., Wang, X.-C., Sun, L., Zhang, Y.-C., Cheng, S., 2015. Effects of Interfacial Tension, Emulsification, and Surfactant Concentration on Oil Recovery in Surfactant Flooding Process for High Temperature and High Salinity Reservoirs. Energy Fuels 29, 6165–6176. doi:10.1021/acs.energyfuels.5b01393

Zargartalebi, M., Kharrat, R., Barati, N., 2015. Enhancement of surfactant flooding performance by the use of silica nanoparticles. Fuel 143, 21–27. doi:10.1016/j.fuel.2014.11.040

Zhang, H., Nikolov, A., Wasan, D., 2014. Enhanced Oil Recovery (EOR) Using Nanoparticle Dispersions: Underlying Mechanism and Imbibition Experiments. Energy Fuels 28, 3002–3009. doi:10.1021/ef500272r

Zhang, T., Davidson, D., Bryant, S.L., Huh, C., 2010. Nanoparticle-Stabilized Emulsions for Applications in Enhanced Oil Recovery. Presented at the SPE Improved Oil Recovery Symposium, Society of Petroleum Engineers. doi:10.2118/129885-MS

Zhang, T., Murphy, M.J., Yu, H., Bagaria, H.G., Yoon, K.Y., Nielson, B.M., Bielawski, C.W., Johnston, K.P., Huh, C., Bryant, S.L., 2014. Investigation of Nanoparticle Adsorption During Transport in Porous Media. SPE J. doi:10.2118/166346-PA

Zhang, X., Servos, M.R., Liu, J., 2012. Ultrahigh Nanoparticle Stability against Salt, pH, and Solvent with Retained Surface Accessibility via Depletion Stabilization. J. Am. Chem. Soc. 134, 9910–9913. doi:10.1021/ja303787e

Zhang, Y., Morrow, N.R., 2006. Comparison of Secondary and Tertiary Recovery With Change in Injection Brine Composition for Crude-Oil/Sandstone Combinations. Presented at the SPE/DOE Symposium on Improved Oil Recovery, Society of Petroleum Engineers. doi:10.2118/99757-MS

Zhou, X., Morrow, N.R., Ma, S., 1996. Interrelationship of Wettability, Initial Water Saturation, Aging Time, and Oil Recovery by Spontaneous Imbibition and Waterflooding. Presented at the SPE/DOE Improved Oil Recovery Symposium, Society of Petroleum Engineers. doi:10.2118/35436-MS

References

184

Appendix A: Silica nanofluid flooding tests from literature

Table A.1. Summary of silica nanoparticle flooding tests from literature.

Ref.	Rock type	Dispersing fluid	Oil type	Nanoparticles Type	Avg. D (nm)	Conc.	Nanoparticle oil recovery (% OOIP)	Flooding scheme[*]	Q_{inj} (ml/min)
Alomair et al., 2014	Berea	Formation water filtered to 3 wt%	Heavy crude	N/A	15	0.01 0.05 0.1	5.9 -4.1[‡] -2.3[‡]	2[†]	0.2
El-Diasty, 2015	Egyptian sst	Unspecified	Mineral oil	In-house	5	0.01 0.5 3	10.4 7.4 4.4	2[†]	0.2
					20	0.01 0.5 3	26.4 29.4 34.4		
					40	0.01 0.5 3	12.4 15.4 22.4		
					60	0.01 0.5 3	5.4 2.4 -4.6[‡]		
Hend-raningrat et al., 2012a	Berea sst	3 wt% NaCl	Mineral oil	Nsp_3a	7	0.01	3.9 -0.4[‡] 7.9	2	0.5
Hend-raningrat et al., 2013b	Berea sst Low K	3 wt% NaCl	Light crude	Nsp_3a	7	0.01 0.01 0.05 0.05 0.1 0.1	2.6 1.9 6.1 3.0 0.0 0.0	3	0.2
	High K					0.01 0.05 0.05 0.1	4.7 5.3 4.7 4.3		
Hend-raningrat et al., 2013c	Berea sst Low K	3 wt% NaCl	Light crude	Nsp_3a	7	0.02 0.02 0.03 0.03 0.04 0.04 0.05 0.05 0.06 0.06 0.07 0.07 0.08 0.08 0.09 0.09	2.9 0.4 2.7 4.4 1.7 1.1 7.0 9.9 2.7 1.6 2.1 2.5 1.0 0.5 0.7 0.6	3	0.2
Hend-raningrat et al., 2013d	Berea sst	3 wt% NaCl	Light crude	Elkem AS	40	0.05	1.0 1.0	3	0.2
				Nsp_1a	16	0.05	2.0 1.8		

Table A.1. (cont'd) Summary of silica nanoparticle flooding tests from literature.

| Ref. | Rock type | Dispersing fluid | Oil type | Nanoparticles | | | Nanoparticle oil recovery (% OOIP) | Flooding scheme[*] | Q_{inj} (ml/min) |
				Type	Avg. D (nm)	Conc.			
Hend-raningrat et al., 2013d	Berea sst	3 wt% NaCl	Light crude	Nsp_3a	7	0.05	3.5 5.0 7.6	3	0.2
							0.0 1.0		0.4
							0.0 0.9		0.8
Ogolo et al., 2012	Sandpack	Distilled water 3 wt% unspecified	Medium crude	Skyspring Nano-materials, Inc.	10-30	0.3	0.8 4.2	2[†]	N/A
Ragab et al., 2015	Egyptian sst	Unspecified brine	Mineral oil	In-house	87	0.1 0.5 1.0	11 14 9	2[†]	N/A
Ragab and Hannora, 2015	Egyptian sst	Unspecified brine	Light crude	In-house	140	0.1	1.0	3	N/A
					140	0.1	-1.6[‡]	2[†]	
					120	0.1	5.9		
					100	0.1	8.4		
Youssif et al., 2017	Un-specified sst	3 wt% NaCl	Light crude	Un-specified commercial	22	0.01 0.05 0.1 0.5	1.6 9.1 13.3 0.7	3	0.5
						0.05 0.1 0.2 0.5	8.4 12.6 6.6 -2.4[‡]	2[†]	

[*] Flooding scheme is coded as "2" if nanoparticle flooding was conducted as a secondary process. "3" denotes tertiary nanoparticle flooding (conducted after water flooding).

[†] Secondary nanoparticle flooding results compared to only one water flooding test (one control variable).

[‡] A negative oil recovery for some secondary core flooding tests is a result of the nanofluid flooding producing a smaller total oil recovery that the water flooding test with which it is compared.

Appendix B: Nanofluid stability

Table B.1. Overview of nanofluid stability tests and appendix location.

Nanoparticle / nanofluid					Temp. (°C)	Figure #
Type	**Name**	**Modification**	**Surface area (m²/g)**	**Concentration (wt%)**		
Colloidal	Cnp_1	None	65	0.05	20	B.1
	Cnp_2	None	150	0.05	20	
	Cnp_3	None	350	0.05	20	
Nano-structured	Nsp_1a	None	130	0.05	20	B.2
	Nsp_2a	None	200	0.05	20	
	Nsp_3a	None	300	0.05	20	
	Nsp_1b	Silanization	-	0.05	20, 40, 60	B.3
	Nsp_2b		-	0.05	20, 40, 60	B.4
	Nsp_3b		-	0.05	20, 40, 60	B.5
	Nsp_3c	PEG	-	0.05	20, 40, 60	B.6
	Nsp_3c		-	0.10	20, 40, 60	B.7
	Nsp_3c		-	0.50	20, 40, 60	B.8
	Nsp_3d	Epoxy	-	0.05	20, 40, 60	B.9

187

Unmodified colloidal nanoparticles

Nanoparticle	Concentration in SSW (wt%)	Temperature (°C)
Cnp_1	0.05	20
Cnp_2	0.05	20
Cnp_3	0.05	20

Table B.2. Average particle size and polydispersity index for nanofluids with colloidal nanoparticles. Each value is an average of three measurements. The standard deviation is also reported.

		Distilled water	Synthetic Sea water (SSW)		
		0 hours	0 hours	8 hours	24 hours
D_{avg}	Cnp_1	81.0 (± 0.4)	1446 (± 341)[*]	1993 (± 276)[*]	2338 (± 168)
	Cnp_2	38.6 (± 0.3)	38.8 (± 0.5)	51.6 (± 0.1)	66.5 (± 1.1)
	Cnp_3	17.6 (± 0.1)	44.4 (± 1.9)	101.7 (± 1.4)[†]	250.8 (± 5.3)
PdI	Cnp_1	0.030 (± 0.012)	0.449 (± 0.079)[*]	0.246 (± 0.027)[*]	0.140 (± 0.101)
	Cnp_2	0.154 (± 0.026)	0.150 (± 0.006)	0.286 (± 0.001)	0.201 (± 0.003)
	Cnp_3	0.323 (± 0.035)	0.415 (± 0.015)	1.003 (± 1.288)[†]	0.351 (± 0.048)

[*] These samples were too polydisperse for proper cumulant analysis, but the data are reported here to illustrate how quickly agglomeration occurs.
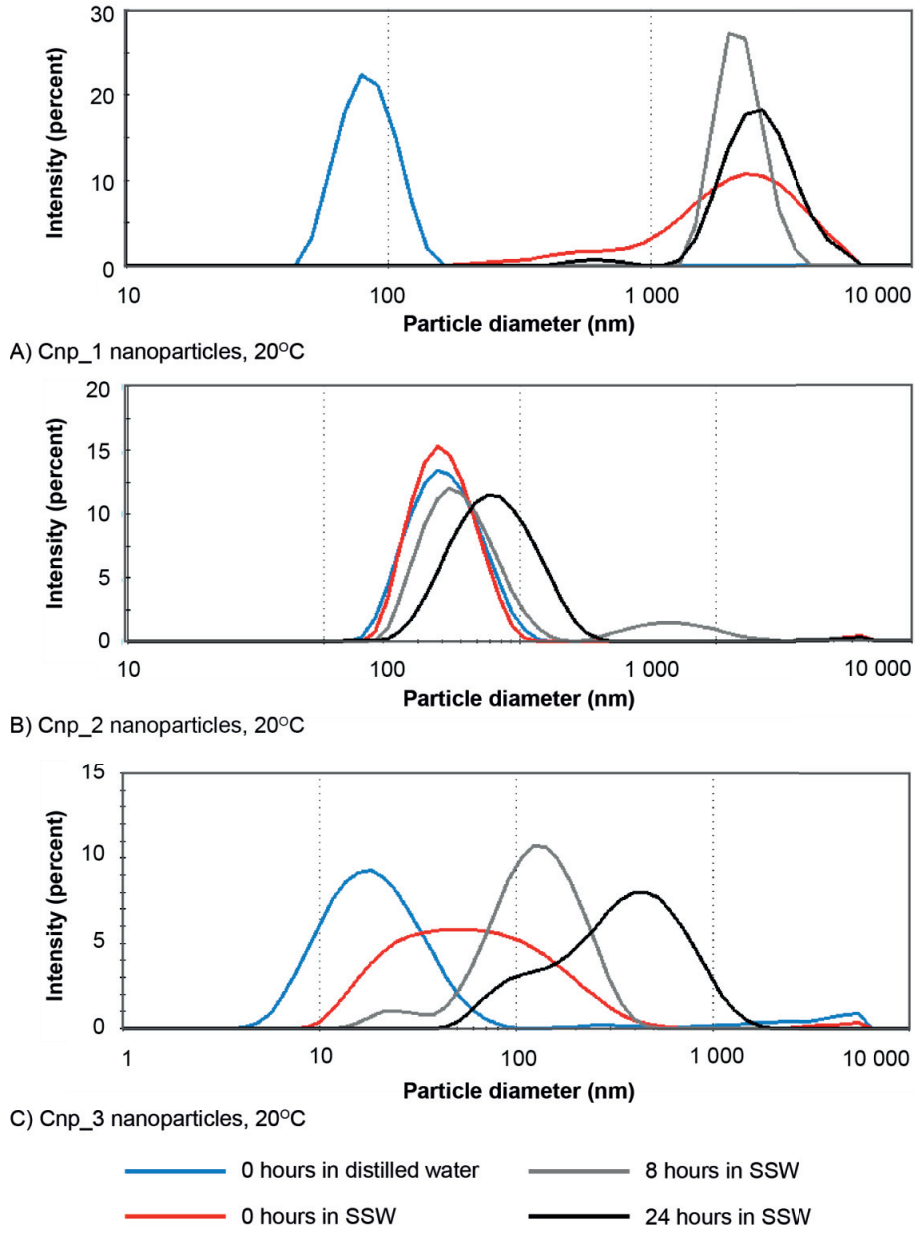[†] This value is an average of two measurements.

A) Cnp_1 nanoparticles, 20°C

B) Cnp_2 nanoparticles, 20°C

C) Cnp_3 nanoparticles, 20°C

—— 0 hours in distilled water	—— 8 hours in SSW
—— 0 hours in SSW	—— 24 hours in SSW

Figure B.1. Particle size distribution by intensity (frequency curves) for A) Cnp_1, B) Cnp_2 and C) Cnp_3 in dispersed at 0.05 wt% and 20°C.

189

Unmodified nano-structured particles

Nanoparticle	Concentration in SSW (wt%)	Temperature (°C)
Nsp_1a	0.05	20
Nsp_2a	0.05	20
Nsp_3a	0.05	20

Table B.3. Average particle size and polydispersity index for nanofluids with unmodified nano-structured particles. Each value is an average of three measurements. The standard deviation is also reported.

		Distilled water	Synthetic Sea water (SSW)	
		0 hours	0 hours	24 hours
D_{avg}	Nsp_1a	144 (± 0.4)	199 (± 4.2)	304 (± 14.5)
	Nsp_2a	95.7 (± 0.2)	190 (± 3.6)	311 (± 9.4)[*]
	Nsp_3a	133 (± 1.5)	138 (± 0.6)	180 (± 1.7)
PdI	Nsp_1a	0.118 (± 0.020)	0.289 (± 0.029)	0.625 (± 0.145)
	Nsp_2a	0.108 (± 0.008)	0.343 (± 0.027)	0.556 (± 0.024)[*]
	Nsp_3a	0.119 (± 0.008)	0.127 (± 0.016)	0.204 (± 0.010)

[*] These samples were too polydisperse for proper cumulant analysis, but the data are reported here to illustrate how quickly agglomeration occurs.
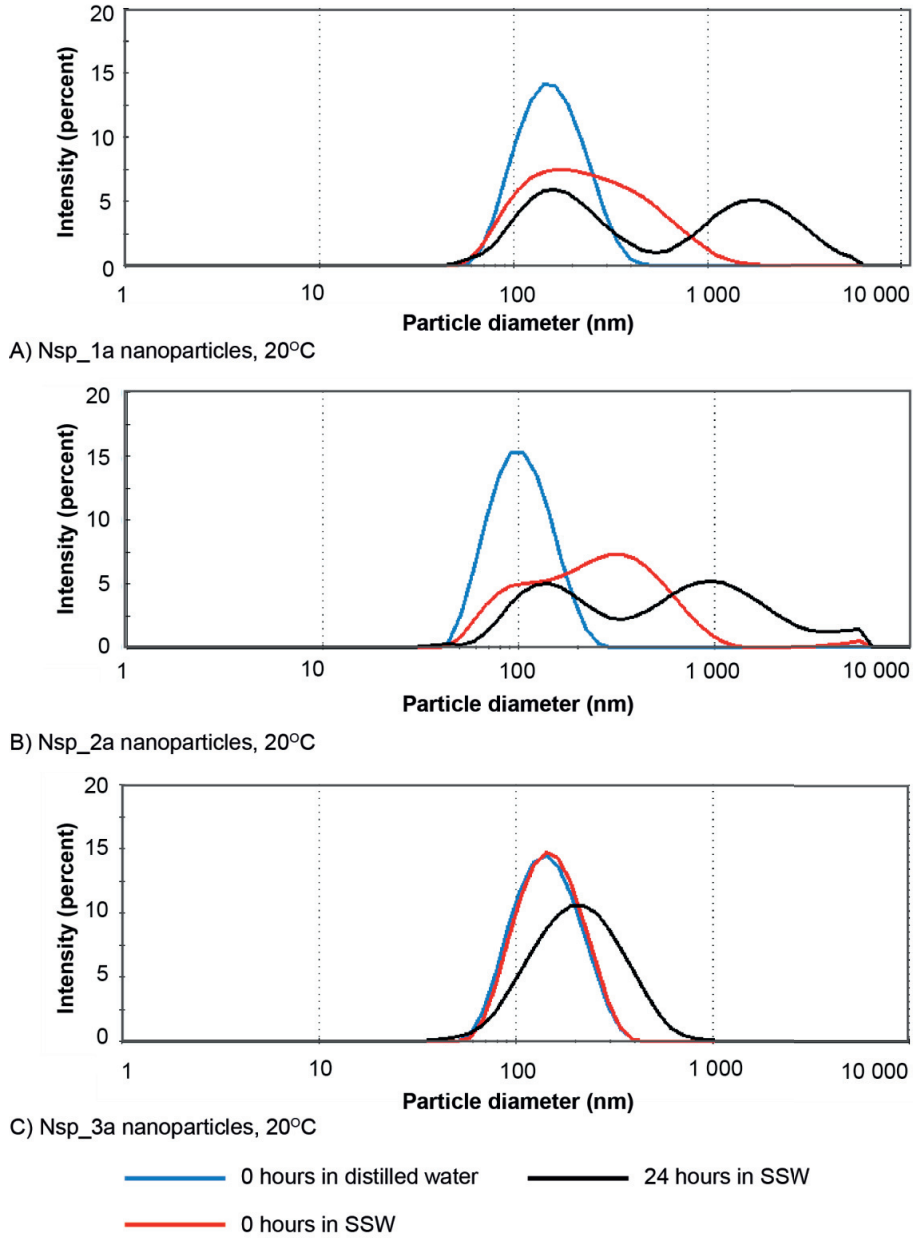[†] This value is an average of two measurements.
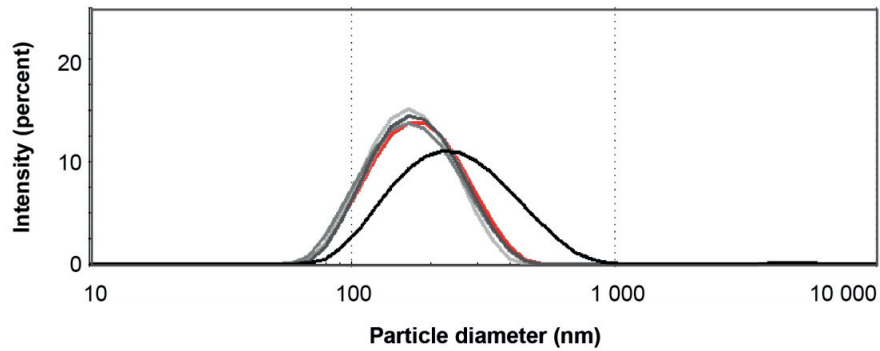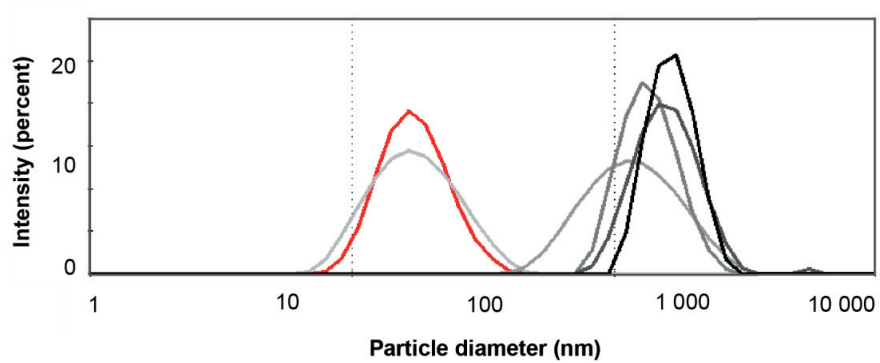
A) Nsp_1a nanoparticles, 20°C

B) Nsp_2a nanoparticles, 20°C

C) Nsp_3a nanoparticles, 20°C

Figure B.2. Particle size distribution by intensity (frequency curves) for A) Nsp_1a, B) Nsp_2a and C) Nsp_3a dispersed at 0.05 wt% and 20°C.

Silanized nano-structured particle Nsp_1b

Nanoparticle	Concentration in SSW (wt%)	Temperature (°C)
Nsp_1b	0.05	20, 40 and 60

A) Nsp_1b nanoparticles, 40°C

B) Nsp_1b nanoparticles, 60°C

Figure B.3. Particle size distribution by intensity (frequency curves) for Nsp_1b dispersed at 0.05 wt% at A) 40°C and B) 60°C.

Silanized nano-structured particle Nsp_2b

Nanoparticle	Concentration in SSW (wt%)	Temperature (°C)
Nsp_2b	0.05	20, 40 and 60

A) Nsp_2b nanoparticles, 20°C

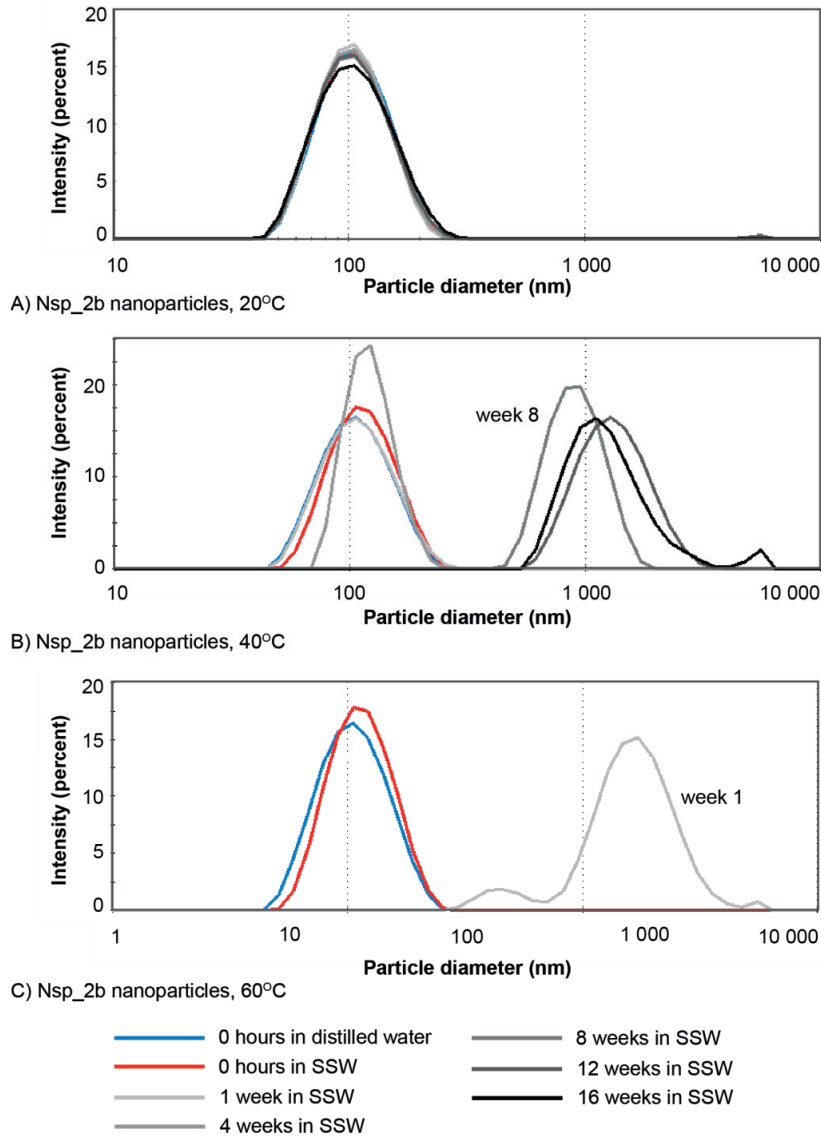B) Nsp_2b nanoparticles, 40°C

C) Nsp_2b nanoparticles, 60°C

Figure B.4. Particle size distribution by intensity (frequency curves) for Nsp_2b at A) 20°C, B) 40°C and C) 60°C. The values at 60°C from week 4 through 16 were too polydisperse to provide accurate particle dispersions.

Silanized nano-structured particle Nsp_3b

Nanoparticle	Concentration in SSW (wt%)	Temperature (°C)
Nsp_3b	0.05	20, 40 and 60

A) Nsp_3b nanoparticles, 20°C

B) Nsp_3b nanoparticles, 40°C

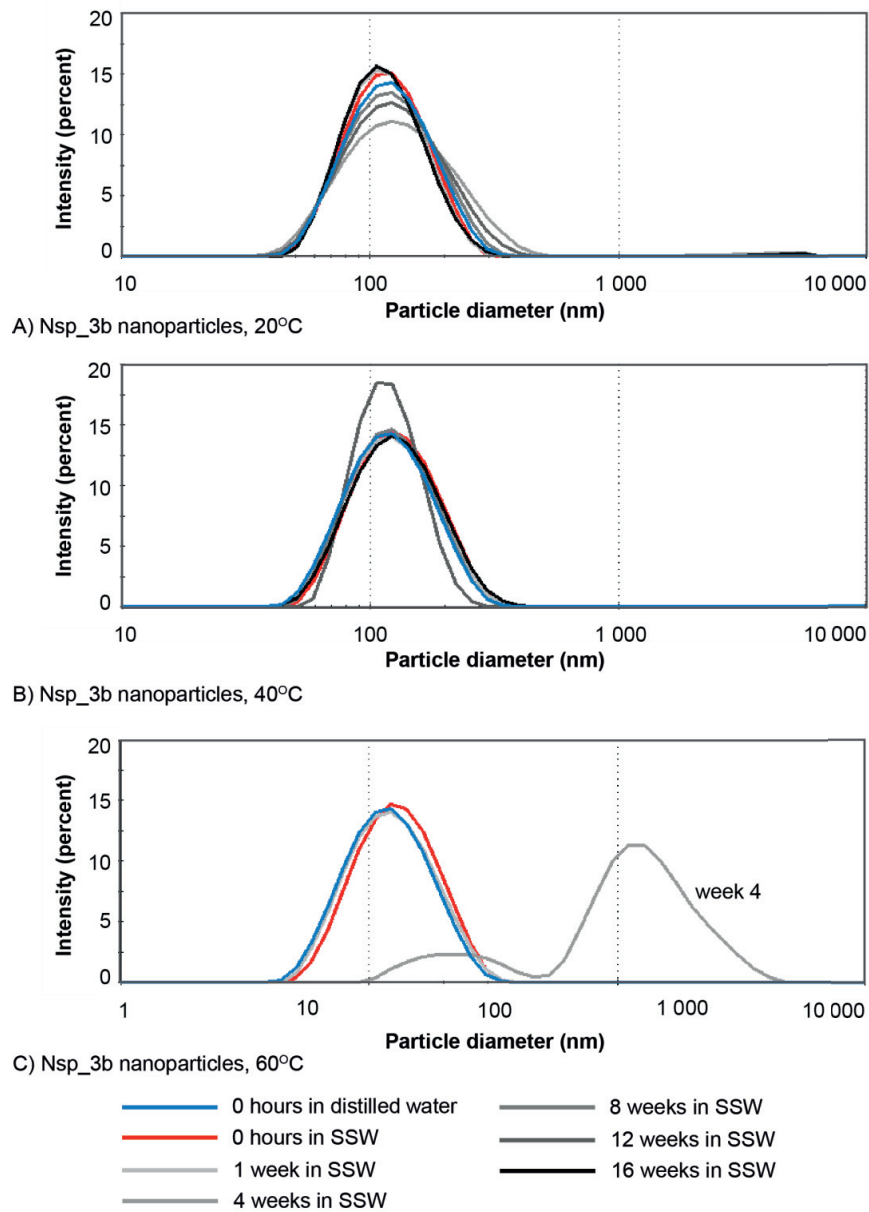C) Nsp_3b nanoparticles, 60°C

Figure B.5. Particle size distribution curves for Nsp_3b at A) 20°C, B) 40°C and C) 60°C.

194

PEG-modified Nsp_3c at 0.05 wt%

Nanoparticle	Concentration in SSW (wt%)	Temperature (°C)
Nsp_3c	0.05	20, 40 and 60
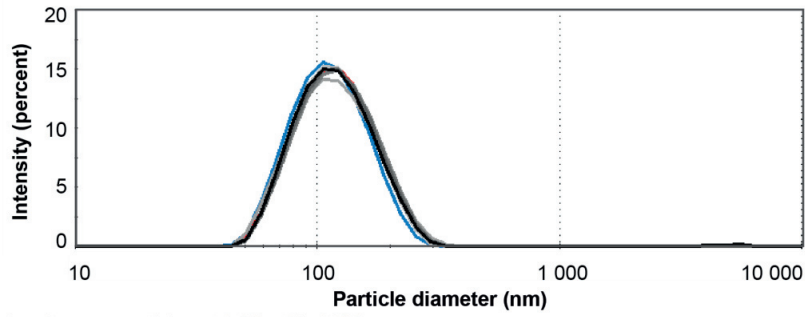
A) Nsp_3c nanoparticles at 0.05 wt%, 20°C
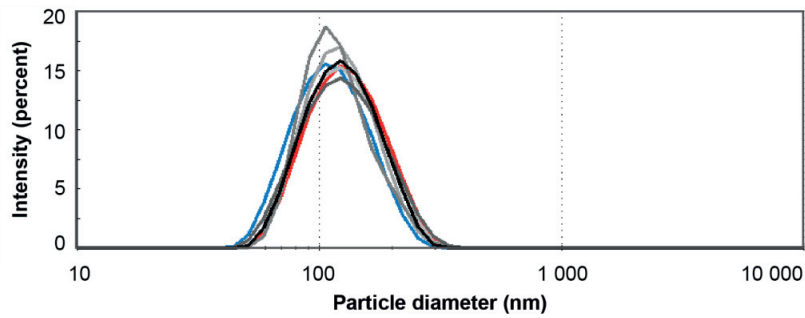
B) Nsp_3c nanoparticles at 0.05 wt%, 40°C

C) Nsp_3c nanoparticles at 0.05 wt%, 60°C

Figure B.6. Particle size distribution curves for Nsp_3c dispersed at 0.05 wt% at A) 20°C, B) 40°C and C) 60°C.

PEG-modified Nsp_3c at 0.10 wt%

Nanoparticle	Concentration in SSW (wt%)	Temperature (°C)
Nsp_3c	0.10	20, 40 and 60

A) Nsp_3c nanoparticles at 0.10 wt%, 20°C

B) Nsp_3c nanoparticles at 0.10 wt%, 40°C

C) Nsp_3c nanoparticles at 0.10 wt%, 60°C

Figure B.7. Particle size distribution curves for Nsp_3c dispersed at 0.10 wt% at A) 20°C, B) 40°C and C) 60°C.

PEG-modified Nsp_3c at 0.50 wt%

Nanoparticle	Concentration in SSW (wt%)	Temperature (°C)
Nsp_3c	0.50	20, 40 and 60
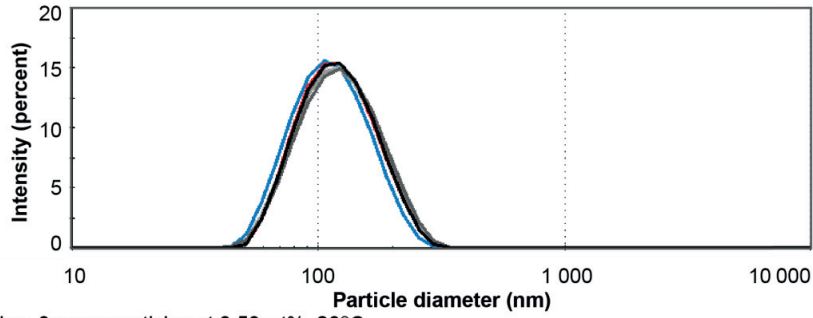
A) Nsp_3c nanoparticles at 0.50 wt%, 20°C
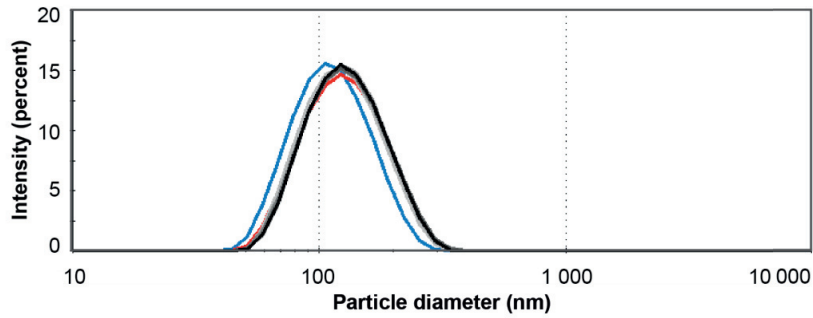
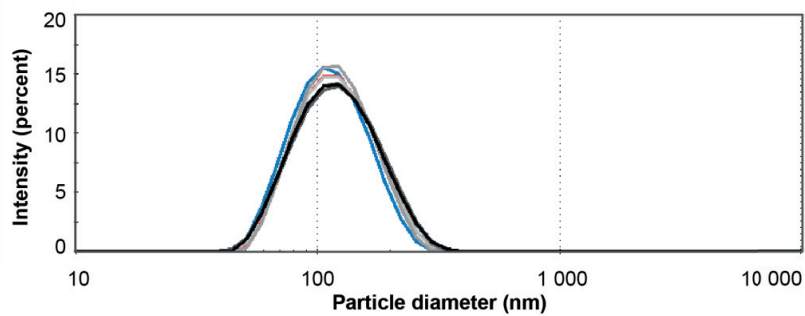B) Nsp_3c nanoparticles at 0.50 wt%, 40°C
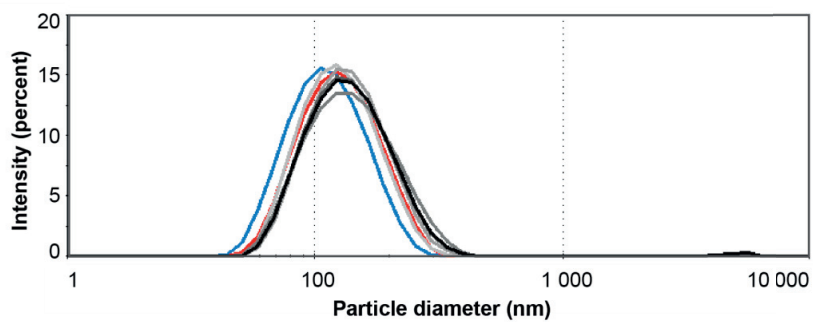
C) Nsp_3c nanoparticles at 0.50 wt%, 60°C

- 0 hours in distilled water
- 0 hours in SSW
- 1 week in SSW
- 4 weeks in SSW
- 8 weeks in SSW
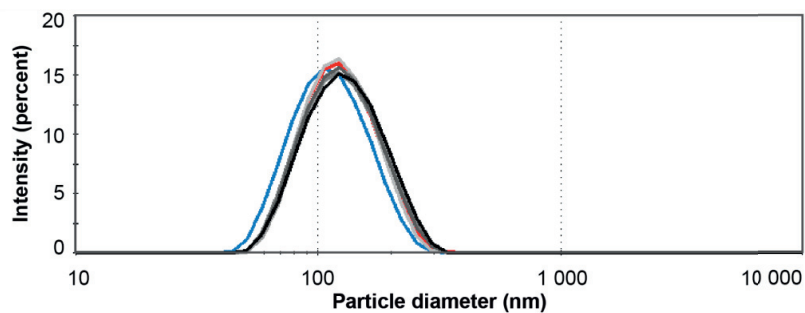- 12 weeks in SSW
- 16 weeks in SSW

Figure B.8. Particle size distribution curves for Nsp_3c dispersed at 0.50 wt% at A) 20°C, B) 40°C and C) 60°C.

197

Epoxy-modified Nsp_3d at 0.05 wt%

Nanoparticle	Concentration in SSW (wt%)	Temperature (°C)
Nsp_3d	0.05	20, 40 and 60
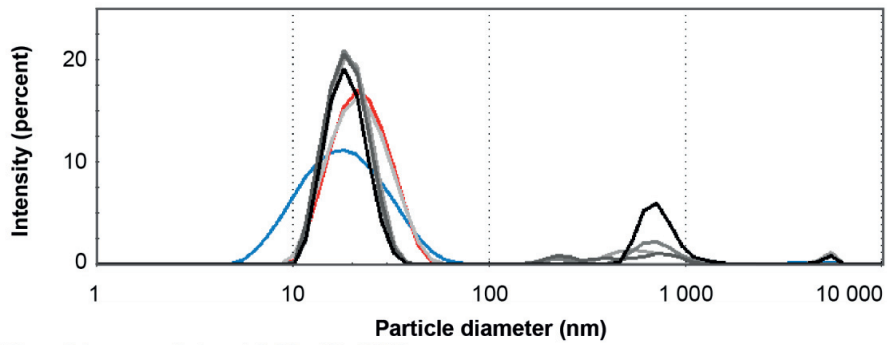
A) Nsp_3d nanoparticles at 0.05 wt%, 20°C
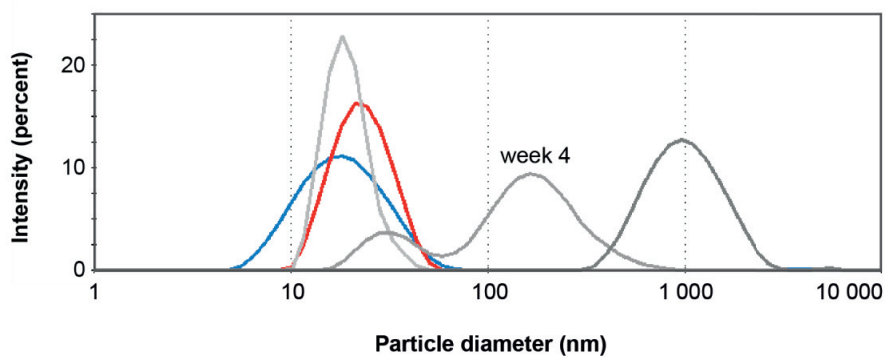
B) Nsp_3d nanoparticles at 0.05 wt%, 60°C

—— 0 hours in distilled water	—— 8 weeks in SSW
—— 0 hours in SSW	—— 12 weeks in SSW
—— 1 week in SSW	—— 16 weeks in SSW
—— 4 weeks in SSW	

Figure B.9. Particle size distribution curves for Nsp_3d dispersed at 0.05 wt% at A) 20°C and B) 60°C.

198

Appendix C: Water flooding comparison
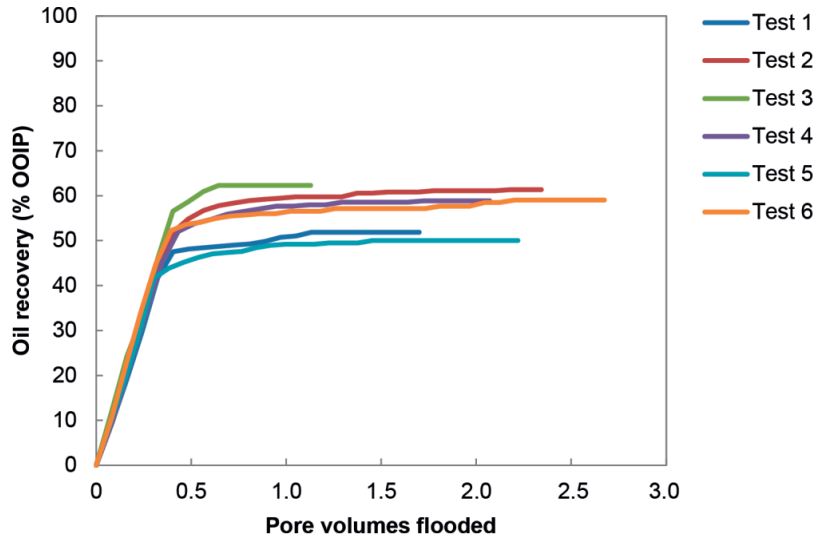
Figure C.1. Oil recovery curves for Part 1 core flooding tests with water flooding occurring at an injection rate of 0.4 ml/min.
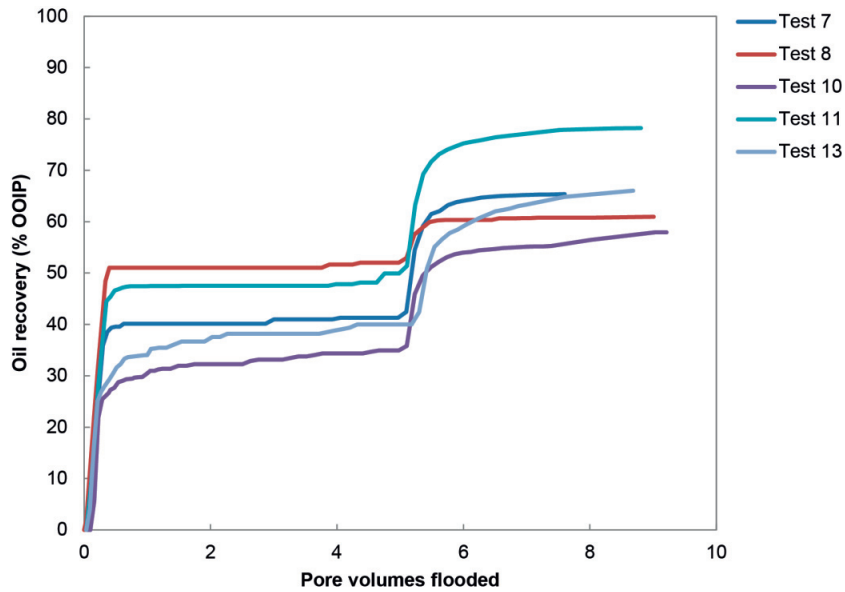
Figure C.2. Oil recovery curves for Part 2 core flooding tests conducted with crude oil. Water flooding was injected at 0.3 ml/min for 5 PV followed by injection at 3.0 ml/min for 2.5 to 4 PV.
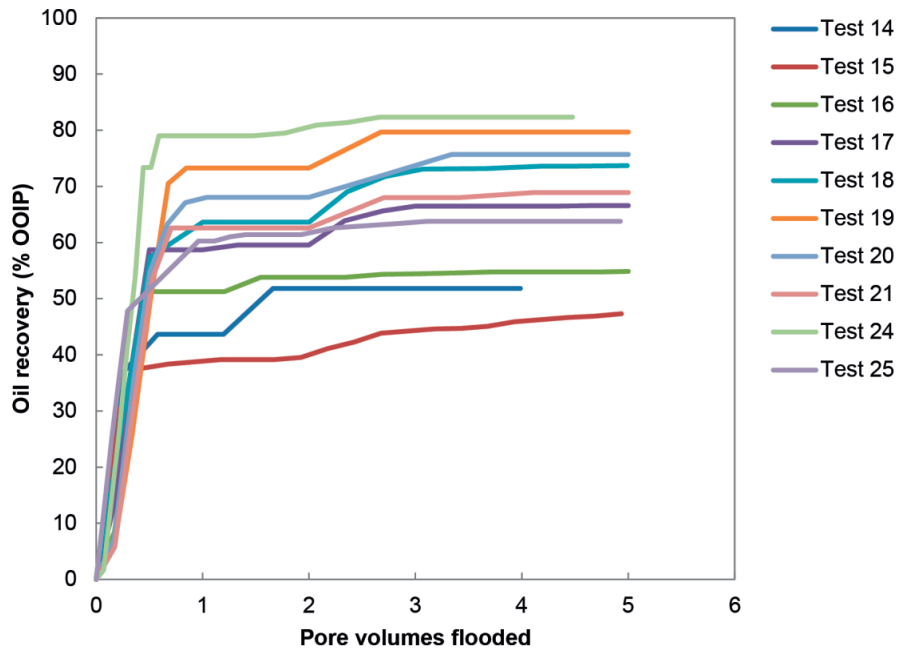
Figure C.3. Oil recovery curves for Part 3 core flooding tests conducted without aging and including initial water saturation (tests #14 through #21). The two tests from Part 4 (#24 and #25) that had similar core plug conditions and water flooding schemes are also shown here. Water flooding was conducted at 0.3 ml/min for 1.2 to 2.0 PV before it was increased to 3.0 ml/min for 2.8 to 3.0 PV.
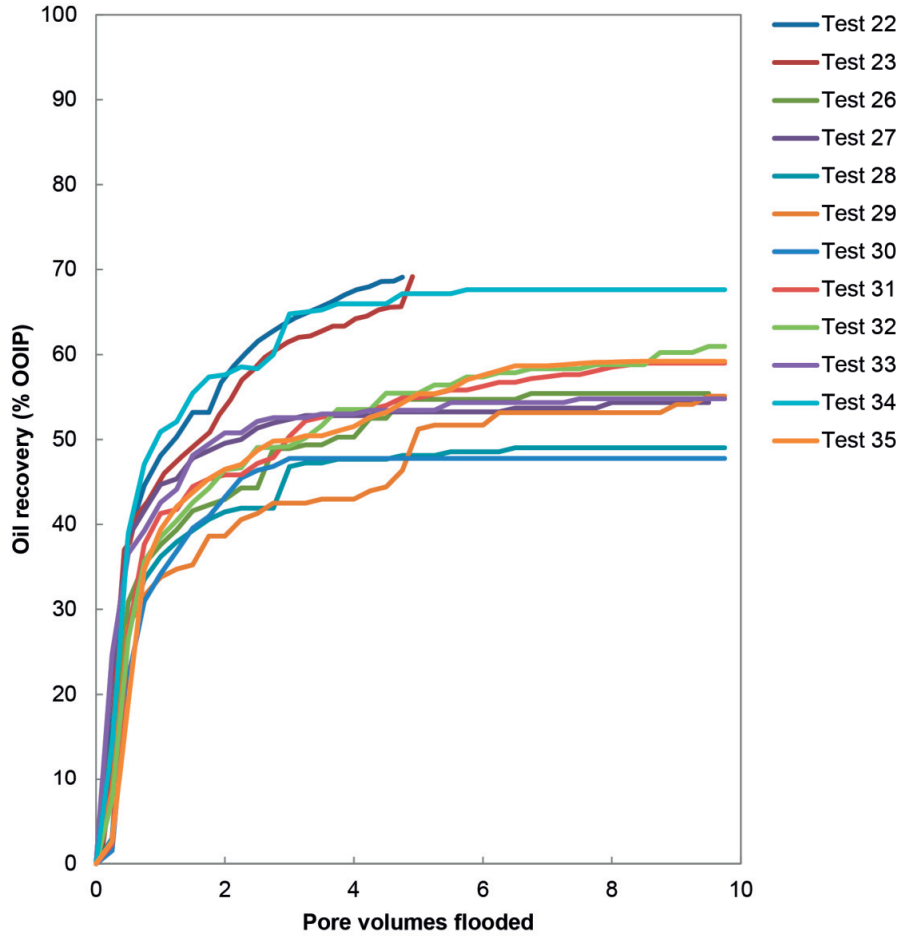
Figure C.4. Oil recovery curves for all core plugs that were aged and had no initial water saturation. That includes the final two tests from Part 3 (#22 and #23) that were aged for 11.5 and 10.5 weeks, respectively, and all the tests from Part 4 that were aged for four weeks (tests #26 through #35). Water flooding was conducted at 0.3 ml/min for 1.75 to 2.75 PV followed by injection at 3.0 ml/min for 3 PV (tests #22 and #23) or 9.5 to 9.75 PV (tests #26 to #35).
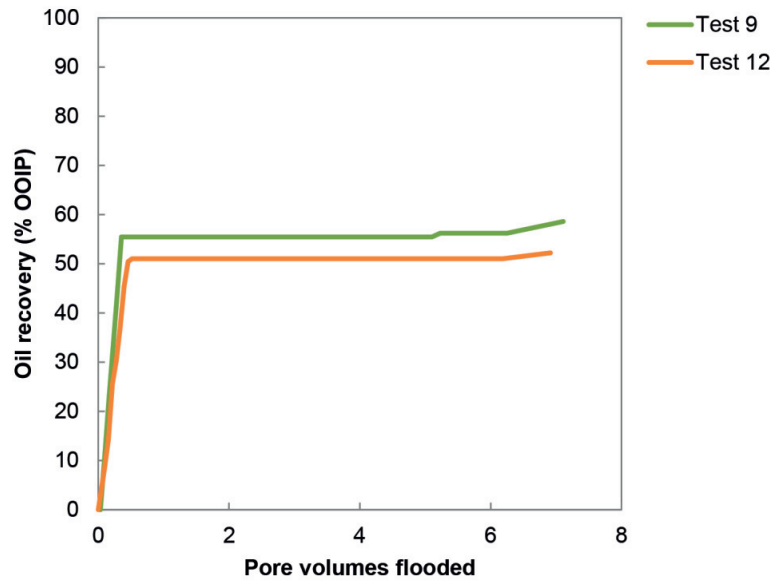
Figure C.5. Oil recovery curves for tests #9 and #12 that were conducted with n-decane. The water flooding was conducted at 0.3 ml/min for 5 PV followed by 3.0 ml/min for 2 PV.

Appendix D: Part 1 core flooding tests – Screening of unmodified nanoparticles

Table D.1. Overview of Part 1 core flooding tests in Appendix D.

| Test # | Nanofluid | | | Oleic phase | Temp. (°C) | Aging |
	Type	Surface modification	Conc. (wt%)			
1	Cnp_1	-	0.05	Crude oil	20	No
2	Cnp_2	-	0.05	Crude oil	20	No
3	Cnp_3	-	0.05	Crude oil	20	No
4	Nsp_1a	-	0.05	Crude oil	20	No
5	Nsp_2a	-	0.05	Crude oil	20	No
6	Nsp_3a	-	0.05	Crude oil	20	No
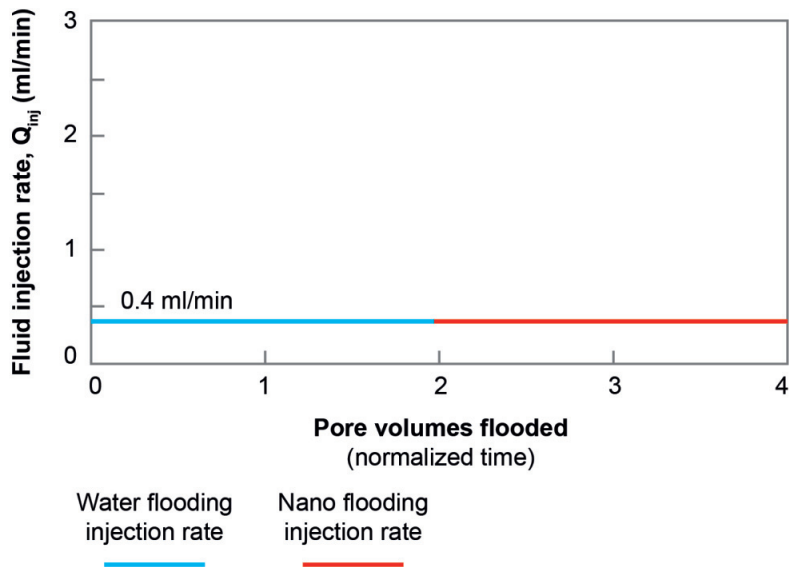
Figure D.1. Core flooding injection scheme for Part 1 tests. There are some exceptions to the injection scheme. See the detailed procedure in Section 5.4 for more information.

Test #1

Nanoparticle	Concentration	Oleic phase	Temperature	Aging
Cnp_1	0.05 wt%	Crude oil	20° C	None

Core plug length (cm)	Porosity (%)	Permeability (mD)	Pore volume (ml)	S_{wi}
13.0	20.8	285	24.8	0.26
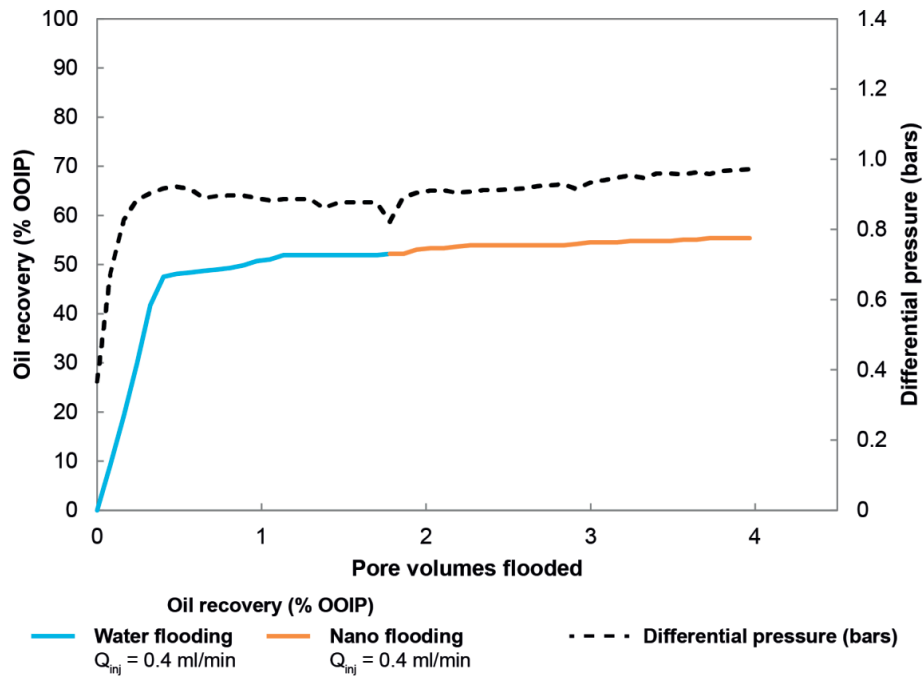
Figure D.1. Oil recovery and differential pressure for test #1. The primary oil bank from nanofluid flooding was produced after 0.2 PV. The nanofluid flooding recovery factor after 1 PV was 2.0%.

Recovery factor, RF (% OOIP)		
Water flood	Nano flood	Total
51.9	3.5	55.4

Residual oil saturation, S_{or}		Capillary number, N_c	
Water flooding	Nanofluid flooding	Water flooding	Nanofluid flooding
0.34	0.31	2.95×10^{-6}	3.90×10^{-6}

Test #2

Nanoparticle	Concentration	Oleic phase	Temperature	Aging
Cnp_2	0.05 wt%	Crude oil	20° C	None

Core plug length (cm)	Porosity (%)	Permeability (mD)	Pore volume (ml)	S_{wi}
13.0	18.5	363	24.8	0.40
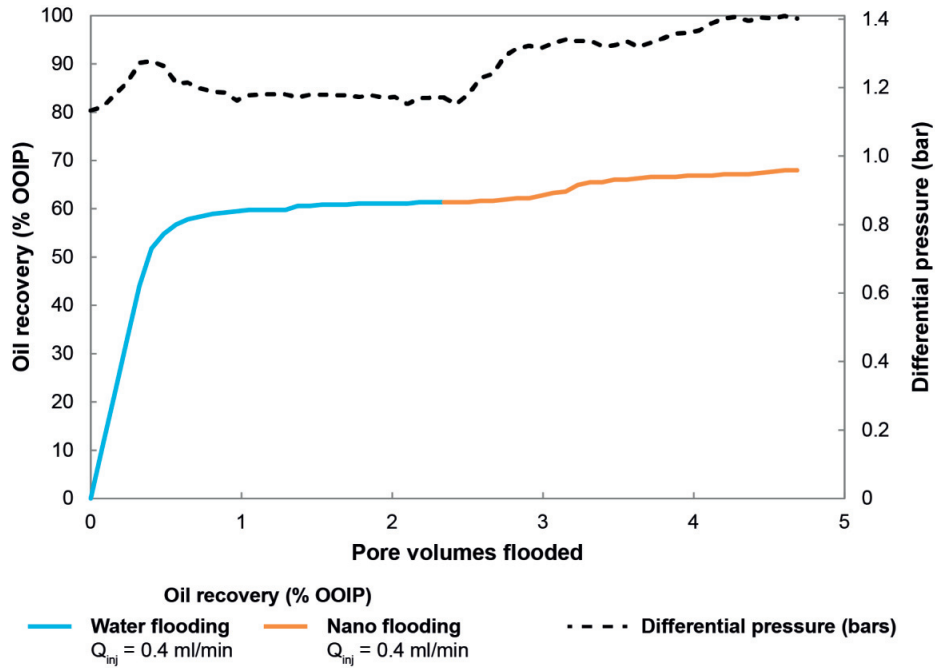
Figure D.2. Oil recovery and differential pressure for test #2. The primary oil bank from nanofluid flooding was produced after 0.6 PV. The nanofluid flooding recovery factor after 1 PV was 4.11%.

Recovery factor, RF (% OOIP)		
Water flood	Nano flood	Total
61.4	6.6	68.0

Residual oil saturation, S_{or}	
Water flooding	Nanofluid flooding
0.29	0.24

Capillary number, N_c	
Water flooding	Nanofluid flooding
3.32×10^{-6}	3.53×10^{-6}

Test #3

Nanoparticle	Concentration	Oleic phase	Temperature	Aging
Cnp_3	0.05 wt%	Crude oil	20° C	None

Core plug length (cm)	Porosity (%)	Permeability (mD)	Pore volume (ml)	S_{wi}
13.0	18.4	438	26.1	0.28

Oil recovery (% OOIP)

— **Water flooding** Q_{inj} = 0.4 ml/min   — **Nano flooding** Q_{inj} = 0.4 ml/min   - - - **Differential pressure (bars)**

Figure D.3. Oil recovery and differential pressure for test #3. The primary oil bank from nanofluid flooding was produced after 0.6 PV. The nanofluid flooding recovery factor after 1 PV was 2.36%, and no additional oil was produced after the initial oil bank.

Recovery factor, RF (% OOIP)		
Water flood	Nano flood	Total
62.3	2.4	64.7

Residual oil saturation, S_{or}	
Water flooding	Nanofluid flooding
0.23	0.21

Capillary number, N_c	
Water flooding	Nanofluid flooding
3.33×10^{-6}	3.98×10^{-6}

Test #4

Nanoparticle	Concentration	Oleic phase	Temperature	Aging
Nsp_1a	0.05 wt%	Crude oil	20° C	None

| Core plug length (cm)	Porosity (%)	Permeability (mD)	Pore volume (ml)	S_{wi}
13.0	17.8	337	24.7	0.30
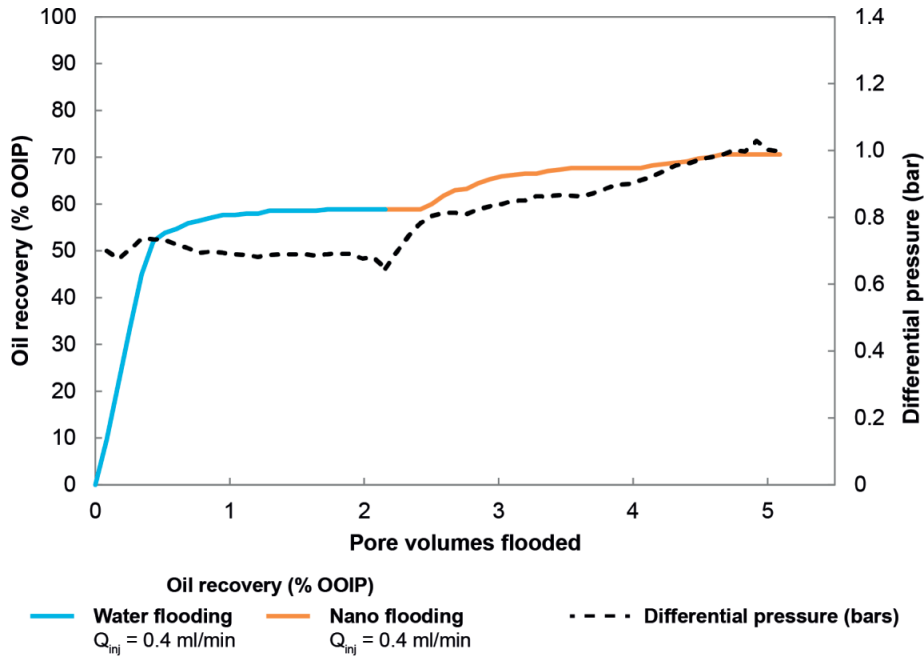
Figure D.4. Oil recovery and differential pressure for test #4. The primary oil bank from nanofluid flooding was produced after 0.4 PV. The nanofluid flooding recovery factor after 1 PV was 7.06%.

Recovery factor, RF (% OOIP)		
Water flood	Nano flood	Total
58.8	11.8	70.6

Residual oil saturation, S_{or}		Capillary number, N_c	
Water flooding	Nanofluid flooding	Water flooding	Nanofluid flooding
0.30	0.22	3.45×10^{-6}	3.65×10^{-6}

207

Test #5

Nanoparticle	Concentration	Oleic phase	Temperature	Aging
Nsp_2a	0.05 wt%	Crude oil	20° C	None

Core plug length (cm)	Porosity (%)	Permeability (mD)	Pore volume (ml)	S_{wi}
13.0	18.1	394	23.2	0.27
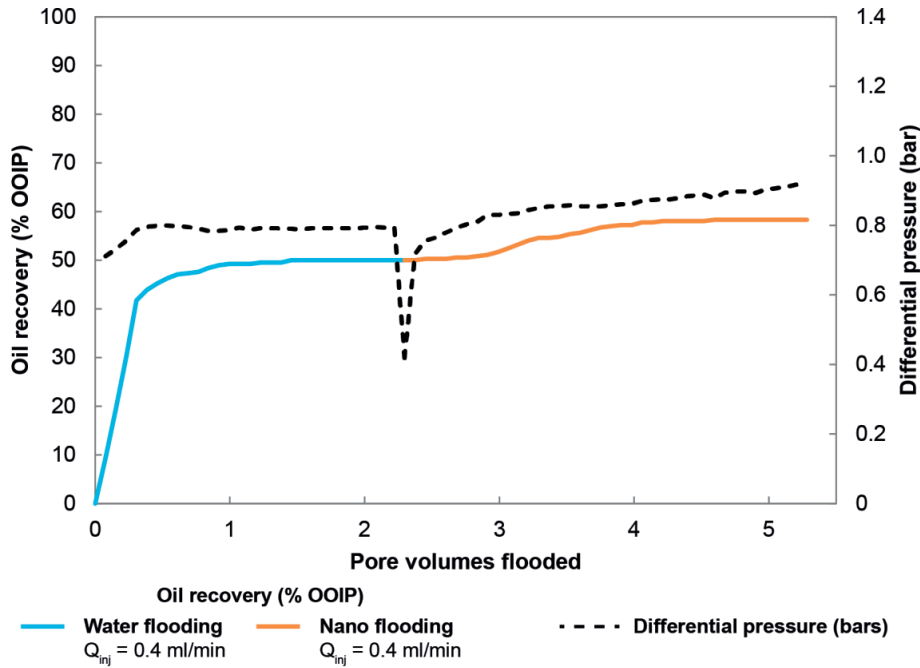
Figure D.5. Oil recovery and differential pressure for test #5. The decrease in pressure at the fluid switch was because the outflow from the nanofluid cylinder was lower than 0.4 ml/min while pressure built up again. The primary oil bank from nanofluid flooding was produced after 0.5 PV. The nanofluid flooding recovery factor after 1 PV was 4.01%.

Recovery factor, RF (% OOIP)		
Water flood	Nano flood	Total
50.0	8.3	58.3

Residual oil saturation, S_{or}		Capillary number, N_c	
Water flooding	Nanofluid flooding	Water flooding	Nanofluid flooding
0.36	0.30	3.39×10^{-6}	3.51×10^{-6}

Test #6

Nanoparticle	Concentration	Oleic phase	Temperature	Aging
Nsp_3a	0.05 wt%	Crude oil	20° C	None

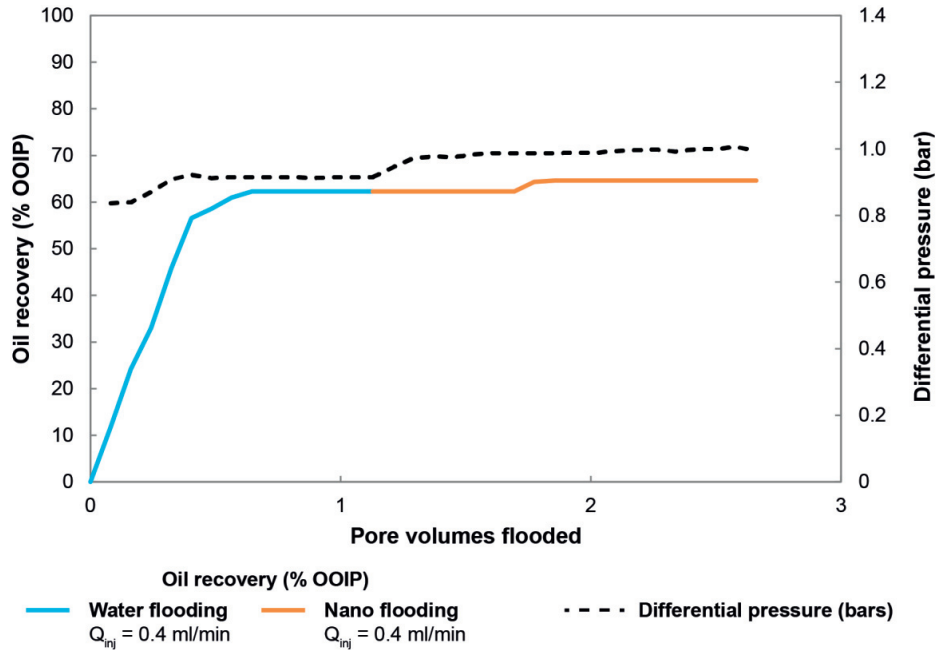| Core plug length (cm)	Porosity (%)	Permeability (mD)	Pore volume (ml)	S_{wi}
13.0	18.2	358	25.4	0.28
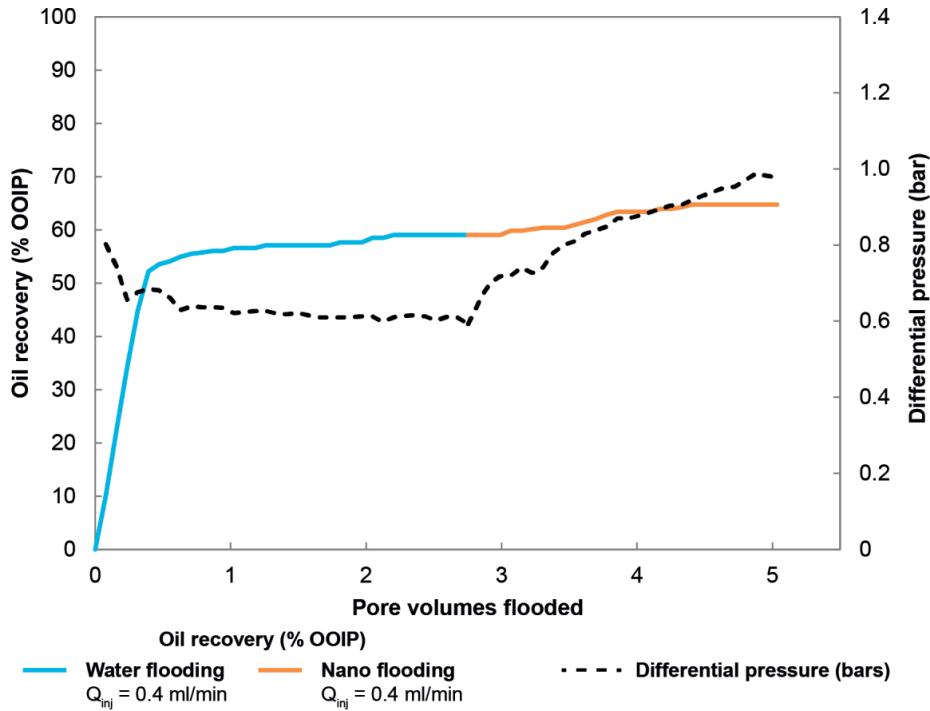
Figure D.6 Oil recovery and differential pressure for test #6. The primary oil bank from nanofluid flooding was produced after 0.3 PV. The nanofluid flooding recovery factor after 1 PV was 3.01%.

Recovery factor, RF (% OOIP)		
Water flood	**Nano flood**	**Total**
59.0	5.7	64.7

Residual oil saturation, S_{or}		Capillary number, N_c	
Water flooding	**Nanofluid flooding**	**Water flooding**	**Nanofluid flooding**
0.29	0.25	3.38×10^{-6}	3.60×10^{-6}

Appendix E: Part 2 core flooding tests – Screening of silanized nanoparticles

Table E.1. Overview of Part 2 core flooding tests in Appendix E.

| Test # | Nanofluid | | | Oleic phase | Temp. (°C) | Aging |
	Type	Surface modification	Conc. (wt%)			
7 8	Nsp_1b	Silanization	0.05	Crude oil	20	No
9	Nsp_1b	Silanization	0.05	n-Decane	20	No
10 11	Nsp_2b	Silanization	0.05	Crude oil	20	No
12	Nsp_2b	Silanization	0.05	n-Decane	20	No
13	Nsp_3b	Silanization	0.05	Crude oil	20	No

☐ Single test
▨ Duplicate test
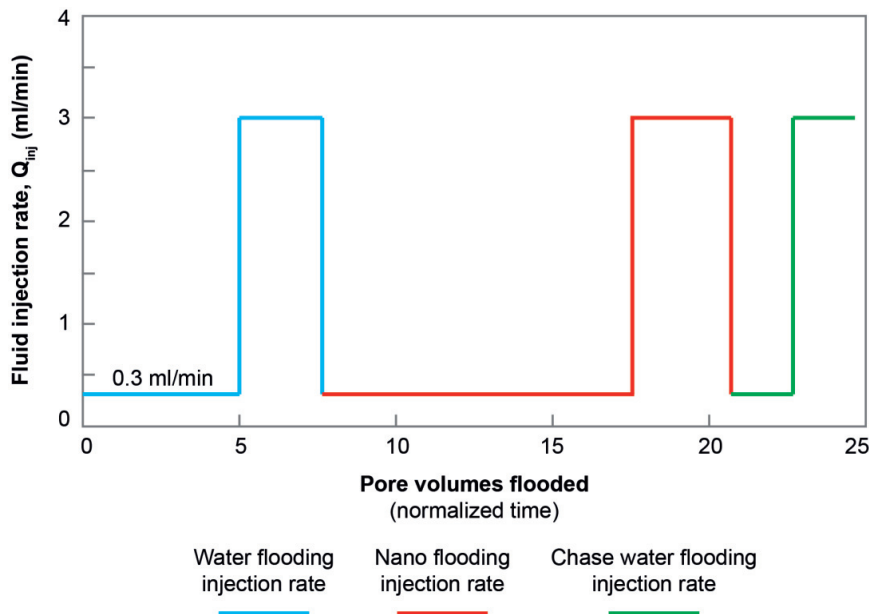
Figure E.1. Core flooding injection scheme for Part 2 tests. There are some exceptions to the injection scheme. See the detailed procedure in Section 5.4 for more information.

Test #7

Nanoparticle	Concentration	Oleic phase	Temperature	Aging
Nsp_1b	0.05 wt%	Crude oil	20° C	None

Core plug length (cm)	Porosity (%)	Permeability (mD)	Pore volume (ml)	S_{wi}
13.0	15.1	327	22.8	0.24

Oil recovery (% OOIP)

Water flooding Q_{inj} = 0.3 ml/min	Nano flooding Q_{inj} = 0.3 ml/min	Differential pressure (bar)
Water flooding Q_{inj} = 3.0 ml/min	Nano flooding Q_{inj} = 3.0 ml/min	

Figure E.2. Oil recovery and differential pressure for test #7. The primary oil bank from nanofluid flooding was produced after 3 PV, but it represented less than 0.1% of OOIP. The recovery factor from NF-Q_{high} was 6%, and production occurred immediately after the injection rate increase. The oil was produced continuously during this stage.

	Recovery factor, RF (% OOIP)				
	Water flooding		Nanofluid flooding		Total
Q_{inj} =	0.3 ml/min	3.0 ml/min	0.3 ml/min	3.0 ml/min	
	41.3	24.1	0.1	6.0	71.5

Residual oil saturation, S_{or}			Capillary number, N_c			
Water flooding	Nanofluid flooding		Water flooding		Nanofluid flooding	
		Q_{inj} =	0.3 ml/min	3.0 ml/min	0.3 ml/min	3.0 ml/min
0.26	0.22		3.05×10^{-6}	3.05×10^{-5}	3.31×10^{-6}	3.31×10^{-5}

Test #8

Nanoparticle	Concentration	Oleic phase	Temperature	Aging
Nsp_1b	0.05 wt%	Crude oil	20° C	None

| Core plug length (cm)	Porosity (%)	Permeability (mD)	Pore volume (ml)	S_{wi}
13.0	16.3	276	24.6	0.37
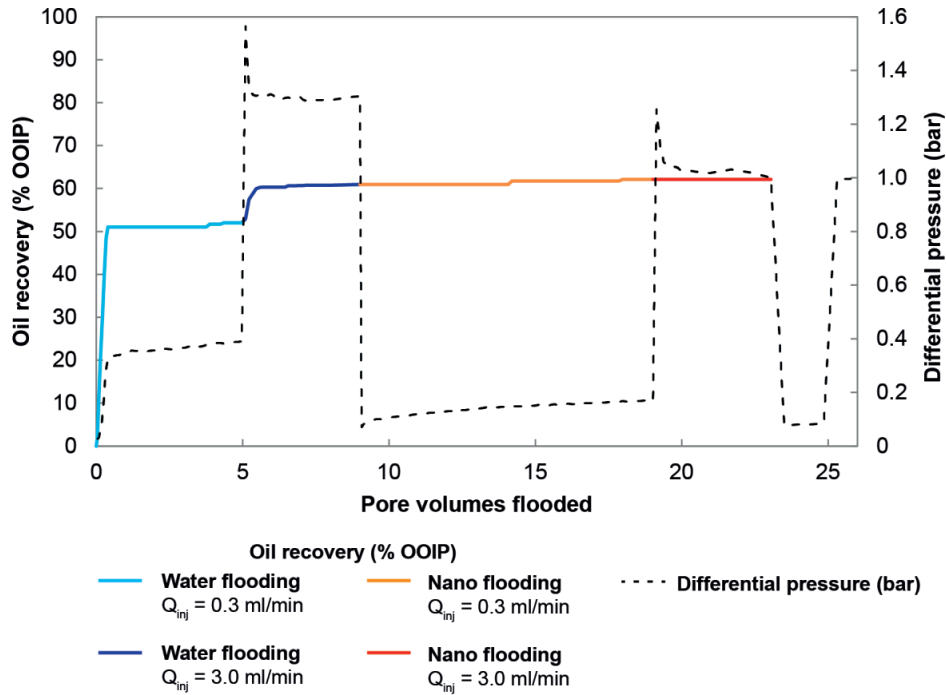
Figure E.3. Oil recovery and differential pressure for test #8. The primary oil bank from nanofluid flooding was produced after 5.2 PV, and it represented slightly less than 1% of OOIP. There was no additional oil recovery from the nanofluid flooding after the injection rate increase.

	Recovery factor, RF (% OOIP)				
	Water flooding		Nanofluid flooding		Total
$Q_{inj} =$	0.3 ml/min	3.0 ml/min	0.3 ml/min	3.0 ml/min	
	52.0	9.0	1.1	0.0	62.1

Residual oil saturation, S_{or}			Capillary number, N_c			
Water flooding	Nanofluid flooding		Water flooding		Nanofluid flooding	
		$Q_{inj} =$	0.3 ml/min	3.0 ml/min	0.3 ml/min	3.0 ml/min
0.25	0.24		2.82×10^{-6}	3.82×10^{-5}	3.06×10^{-6}	3.06×10^{-5}

Test #9

Nanoparticle	Concentration	Oleic phase	Temperature	Aging
Nsp_1b	0.05 wt%	n-decane	20° C	None

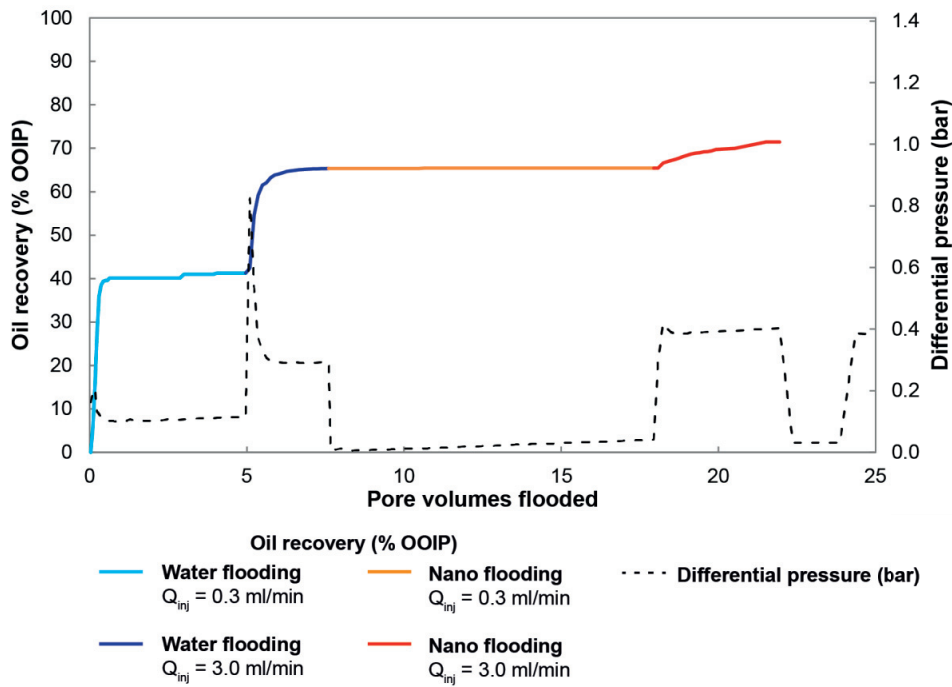| Core plug length (cm)	Porosity (%)	Permeability (mD)	Pore volume (ml)	S_{wi}
13.0	15.6	394	23.5	0.46
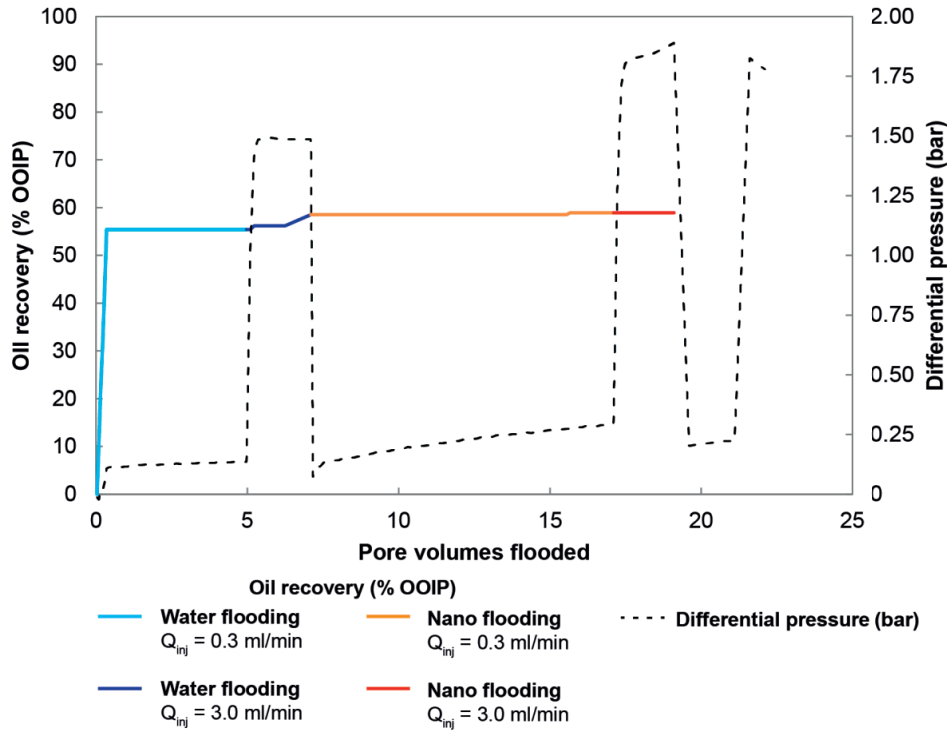
Figure E.4. Oil recovery and differential pressure for test #9. The primary oil bank from nanofluid flooding was produced after 8.5 PV, and it was < 0.5% of OOIP. There was no additional oil recovery from the nanofluid flooding after the injection rate increase.

	Recovery factor, RF (% OOIP)				
	Water flooding		Nanofluid flooding		Total
Q_{inj} =	0.3 ml/min	3.0 ml/min	0.3 ml/min	3.0 ml/min	
	55.4	3.1	0.4	0.0	58.9

Residual oil saturation, S_{or}			Capillary number, N_c			
Water flooding	Nanofluid flooding		Water flooding		Nanofluid flooding	
		Q_{inj} =	0.3 ml/min	3.0 ml/min	0.3 ml/min	3.0 ml/min
0.24	0.22		2.95×10^{-6}	2.95×10^{-5}	3.20×10^{-6}	3.20×10^{-5}

Test #10

Nanoparticle	Concentration	Oleic phase	Temperature	Aging
Nsp_2b	0.05 wt%	Crude oil	20° C	None

| Core plug length (cm)	Porosity (%)	Permeability (mD)	Pore volume (ml)	S_{wi}
13.0	15.5	224	23.7	0.29
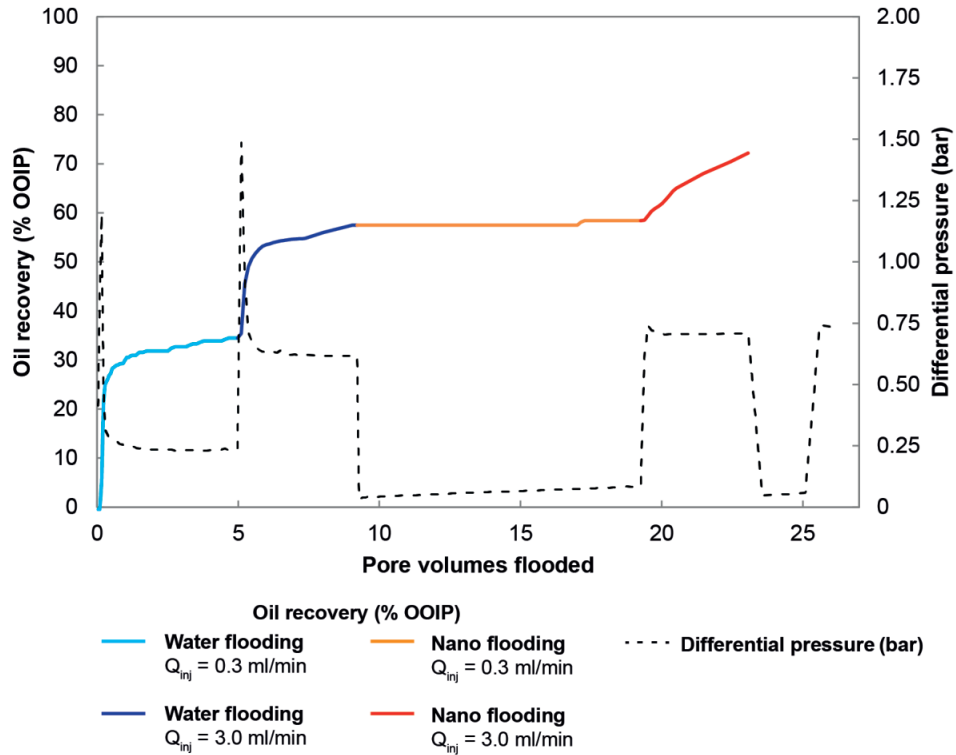
Figure E.5. Oil recovery and differential pressure for test #10. The primary oil bank from nanofluid flooding was produced after 8 PV, and it was about 0.5% of OOIP. The recovery factor from NF-Q_{high} was 13.8%, and production occurred immediately after the injection rate increase. The oil was produced continuously during this stage.

	Recovery factor, RF (% OOIP)				
	Water flooding		Nanofluid flooding		Total
Q_{inj} =	0.3 ml/min	3.0 ml/min	0.3 ml/min	3.0 ml/min	
	34.9	23.0	0.9	13.8	72.6

Residual oil saturation, S_{or}			Capillary number, N_c			
Water flooding	Nanofluid flooding		Water flooding		Nanofluid flooding	
		Q_{inj} =	0.3 ml/min	3.0 ml/min	0.3 ml/min	3.0 ml/min
0.30	0.19		$2.97{\times}10^{-6}$	$2.97{\times}10^{-5}$	$3.19{\times}10^{-6}$	$3.19{\times}10^{-5}$

Test #11

Nanoparticle	Concentration	Oleic phase	Temperature	Aging
Nsp_2b	0.05 wt%	Crude oil	20° C	None

| Core plug length (cm)	Porosity (%)	Permeability (mD)	Pore volume (ml)	S_{wi}
13.0	15.5	363	23.5	0.29
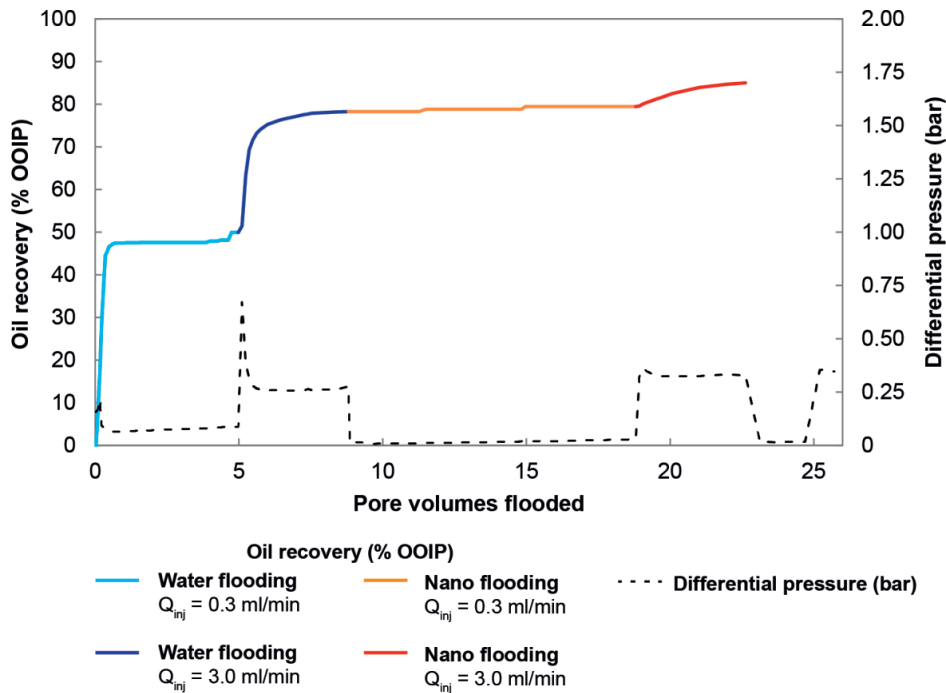
Figure E.6. Oil recovery and differential pressure for test #11. The primary oil bank from nanofluid flooding was produced after 2.5 PV, and it was 0.6% of OOIP. An additional oil bank was produced after 6.15 PV of nanofluid flooding, and it was also 0.6% of OOIP. The oil recovery from NF-Q_{high} was 5.6%, and production occurred immediately after the injection rate increase. The oil was produced continuously during this stage.

	Recovery factor, RF (% OOIP)				
	Water flooding		Nanofluid flooding		Total
Q_{inj} =	0.3 ml/min	3.0 ml/min	0.3 ml/min	3.0 ml/min	
	49.9	28.3	1.2	5.6	85.0

Residual oil saturation, S_{or}			Capillary number, N_c			
Water flooding	Nanofluid flooding		Water flooding		Nanofluid flooding	
		Q_{inj} =	0.3 ml/min	3.0 ml/min	0.3 ml/min	3.0 ml/min
0.16	0.11		2.96×10^{-6}	2.96×10^{-5}	3.18×10^{-6}	3.18×10^{-5}

Test #12

Nanoparticle	Concentration	Oleic phase	Temperature	Aging
Nsp_2b	0.05 wt%	n-decane	20° C	None

Core plug length (cm)	Porosity (%)	Permeability (mD)	Pore volume (ml)	S_{wi}
13.0	16.3	453	24.7	0.32
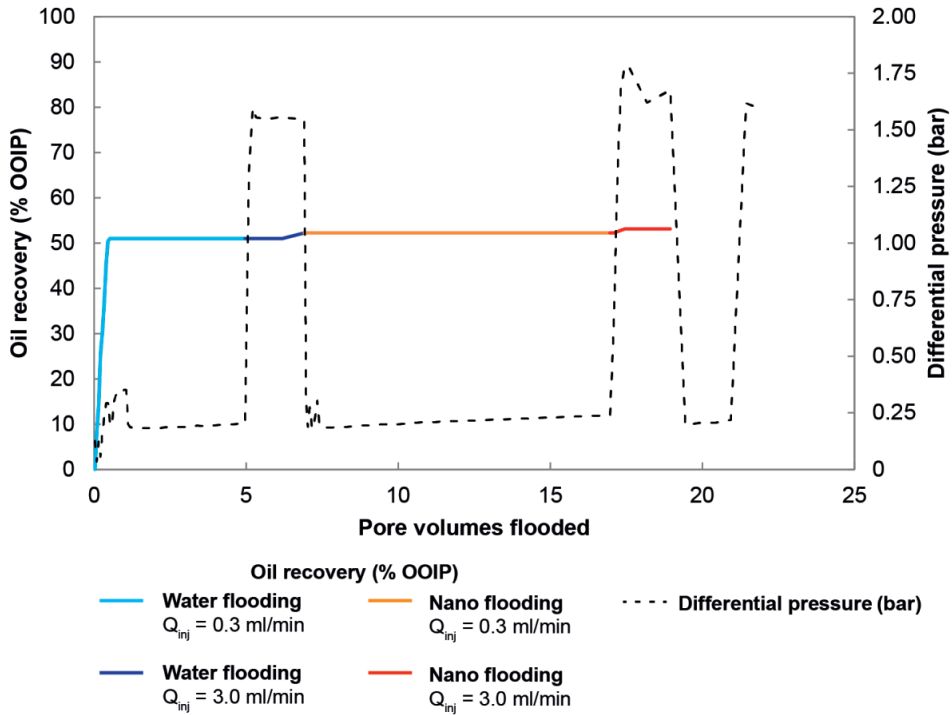
Figure E.7. Oil recovery and differential pressure for test #12. No oil was produced during the nanofluid flooding stage with the low injection rate. A recovery factor of 0.9% was achieved during nanofluid flooding after the injection rate increase. Additional recovery occurred 0.25 PV after the rate increased.

	Recovery factor, RF (% OOIP)				
	Water flooding		Nanofluid flooding		Total
Q_{inj} =	0.3 ml/min	3.0 ml/min	0.3 ml/min	3.0 ml/min	
	51.0	1.2	0.0	0.9	53.1

Residual oil saturation, S_{or}			Capillary number, N_c			
Water flooding	Nanofluid flooding		Water flooding		Nanofluid flooding	
		Q_{inj} =	0.3 ml/min	3.0 ml/min	0.3 ml/min	3.0 ml/min
0.32	0.32		2.82×10^{-6}	2.82×10^{-5}	3.03×10^{-6}	3.03×10^{-5}

Test #13

Nanoparticle	Concentration	Oleic phase	Temperature	Aging
Nsp_3b	0.05 wt%	Crude oil	20° C	None

| Core plug length (cm)	Porosity (%)	Permeability (mD)	Pore volume (ml)	S_{wi}
13.0	15.7	332	23.7	0.33
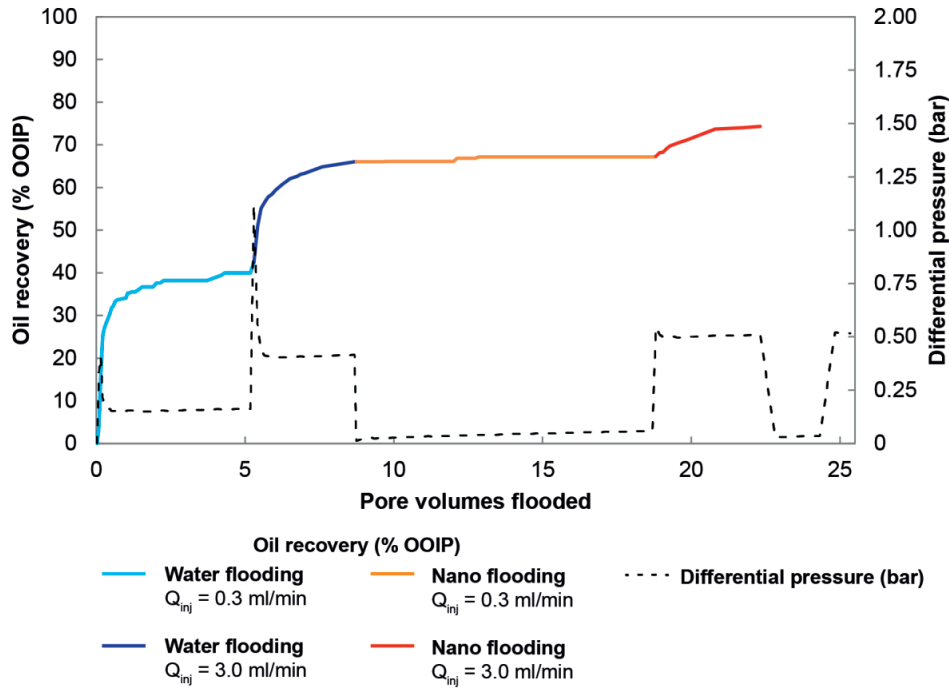
Figure E.8. Oil recovery and differential pressure for test #13. The primary oil bank from nanofluid flooding was produced after 3.45 PV, and it was 0.75% of OOIP. Trace oil (0.03% OOIP) was produced at 1 PV of nanofluid flooding, and an additional oil bank was produced at 4 PV amounting to 0.3 % of OOIP. The recovery factor from NF-Q_{high} was 7.2%, and production occurred immediately after the injection rate increase. The oil was produced continuously during this stage.

	Recovery factor, RF (% OOIP)				
	Water flooding		Nanofluid flooding		Total
Q_{inj} =	0.3 ml/min	3.0 ml/min	0.3 ml/min	3.0 ml/min	
	40.0	26.0	1.1	7.2	74.3

Residual oil saturation, S_{or}			Capillary number, N_c			
Water flooding	Nanofluid flooding		Water flooding		Nanofluid flooding	
		Q_{inj} =	0.3 ml/min	3.0 ml/min	0.3 ml/min	3.0 ml/min
0.23	0.17		2.92×10^{-6}	2.92×10^{-5}	2.83×10^{-6}	2.83×10^{-5}

Appendix F: Part 3 core flooding tests – Evaluation of surface-modified Nsp_3a

Table F.1. Overview of Part 3 core flooding tests in Appendix F.

Test #	Nanofluid			Oleic phase	Temp. (°C)	Aging
	Type	Surface modification	Conc. (wt%)			
14	Nsp_3c	PEG	0.05	Crude oil	20	No
15						
16	Nsp_3c	PEG	0.05	Crude oil	20	No
17	Nsp_3c	PEG	0.025	Crude oil	20	No
18	Nsp_3c	PEG	0.01	Crude oil	20	No
19	Nsp_3c	PEG	0.05	Crude oil	20	No
20	Nsp_3c	PEG	0.10	Crude oil	20	No
21	Nsp_3d	Epoxy	0.05	Crude oil	20	No
22	Nsp_3c	PEG	0.05	Crude oil	20	11.5 weeks at 60°C
23	Nsp_3c	PEG	0.05	Crude oil	20	10.5 weeks at 60°C

☐ Single test
▨ Duplicate test

Figure F.1. Core flooding injection scheme for Part 3 tests. There are some exceptions to the injection scheme. See the detailed procedure in Section 5.4 for more information.

Test #14

Nanoparticle	Concentration	Oleic phase	Temperature	Aging
Nsp_3c	0.05 wt%	Crude oil	20° C	None

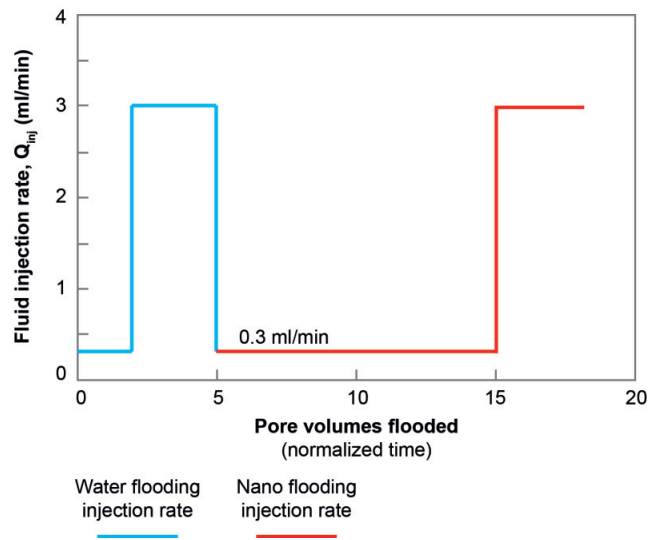| Core plug length (cm)	Porosity (%)	Permeability (mD)	Pore volume (ml)	S_{wi}
10.0	16.9	320	19.4	0.37

Oil recovery (% OOIP)

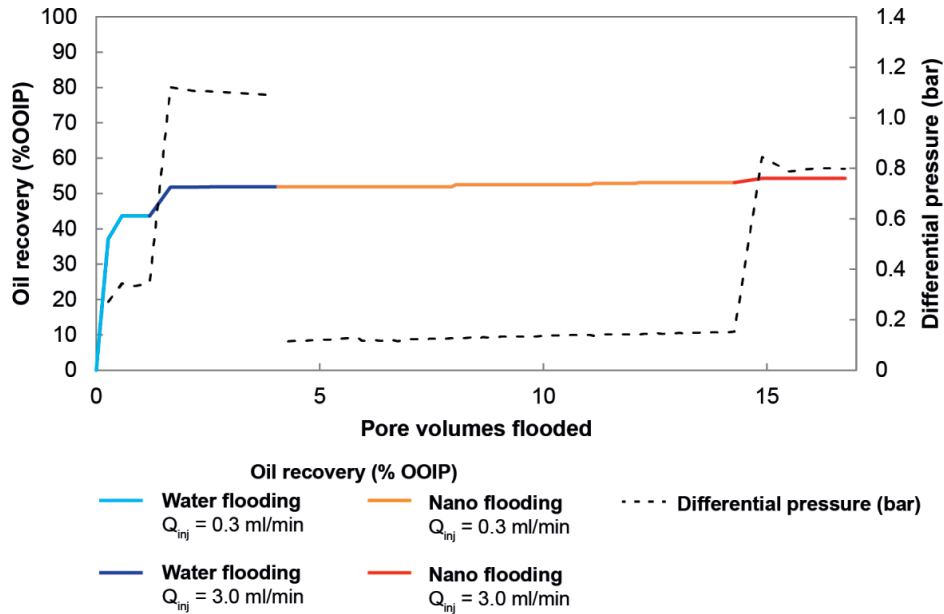|		
Water flooding Q_{inj} = 0.3 ml/min	**Nano flooding** Q_{inj} = 0.3 ml/min	**Differential pressure (bar)**
Water flooding Q_{inj} = 3.0 ml/min	**Nano flooding** Q_{inj} = 3.0 ml/min	

Figure F.2. Oil recovery and differential pressure for test #14. The primary oil bank from nanofluid flooding at 0.3 ml/min was produced after 4 PV, but it represented less than 1% of OOIP. Two other small oil banks were produced after 7 and 8 PV of nanofluid flooding. The recovery factor from NF-Q_{high} was 1.2%, and production occurred immediately after the injection rate increase.

	Recovery factor, RF (% OOIP)				
	Water flooding		**Nanofluid flooding**		**Total**
Q_{inj} =	**0.3 ml/min**	**3.0 ml/min**	**0.3 ml/min**	**3.0 ml/min**	
	43.6	8.2	1.2	1.2	54.2

Residual oil saturation, S_{or}			Capillary number, N_c			
Water flooding	**Nanofluid flooding**		**Water flooding**		**Nanofluid flooding**	
		Q_{inj} =	**0.3 ml/min**	**3.0 ml/min**	**0.3 ml/min**	**3.0 ml/min**
0.31	0.29		2.72×10^{-6}	2.72×10^{-5}	2.87×10^{-6}	2.87×10^{-5}

Test #15

Nanoparticle	Concentration	Oleic phase	Temperature	Aging
Nsp_3c	0.05 wt%	Crude oil	20° C	None

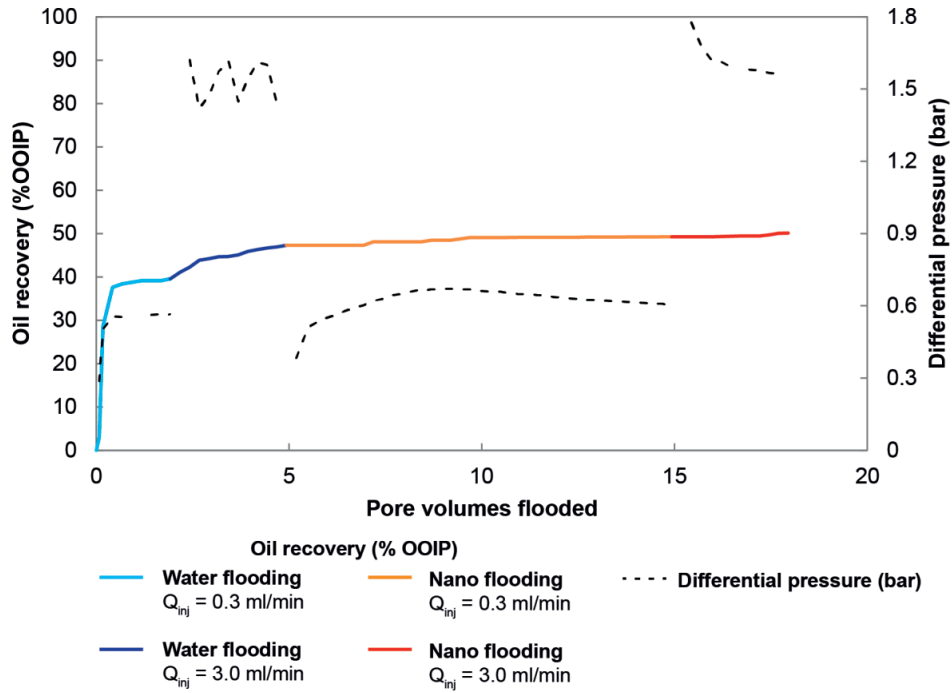| Core plug length (cm)	Porosity (%)	Permeability (mD)	Pore volume (ml)	S_{wi}
10.0	17.7	396	20.1	0.37

Figure F.3. Oil recovery and differential pressure for test #15. The primary oil bank from nanofluid flooding was produced after 2PV, and it represented slightly less than 1% of OOIP. There was intermittent production throughout the rest of the low rate nanofluid flooding, totally slightly less than 2% RF in total. Recovery from high rate did not occur until after 1 PV, and it was sporadic production totaling less than 1%.

	Recovery factor, RF (% OOIP)				
	Water flooding		**Nanofluid flooding**		**Total**
$Q_{inj} =$	0.3 ml/min	3.0 ml/min	0.3 ml/min	3.0 ml/min	
	39.5	7.8	1.9	0.9	50.1

Residual oil saturation, S_{or}			Capillary number, N_c			
Water flooding	**Nanofluid flooding**		**Water flooding**		**Nanofluid flooding**	
		$Q_{inj} =$	0.3 ml/min	3.0 ml/min	0.3 ml/min	3.0 ml/min
0.33	0.32		2.60×10^{-6}	2.60×10^{-5}	2.74×10^{-6}	2.74×10^{-5}

Test #16

Nanoparticle	Concentration	Oleic phase	Temperature	Aging
Nsp_3c	0.05 wt%	Crude oil	20° C	None

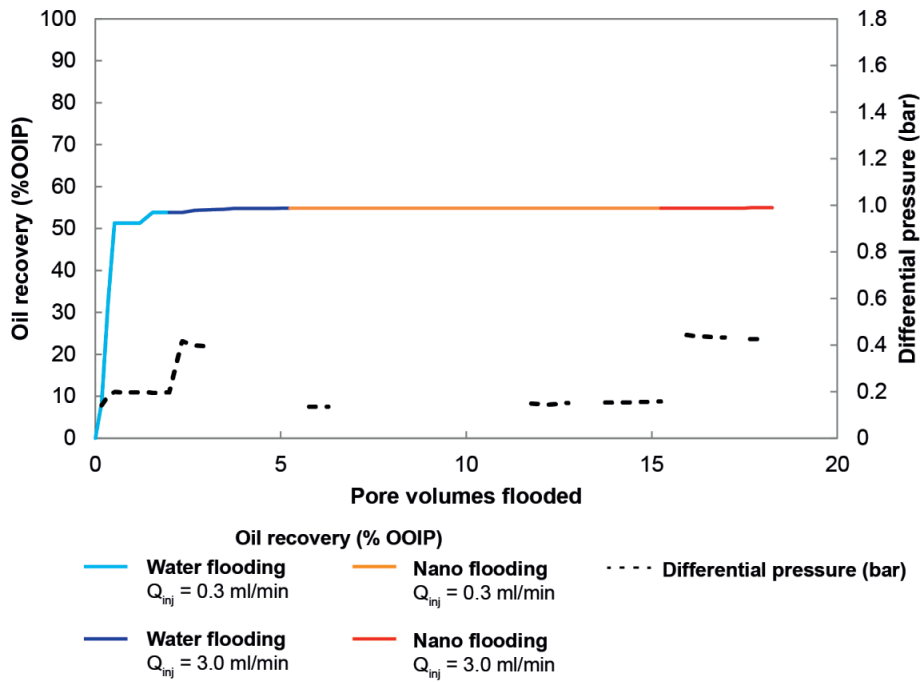| Core plug length (cm)	Porosity (%)	Permeability (mD)	Pore volume (ml)	S_{wi}
4.5	17.8	322	8.7	0.33

Figure F.4. Oil recovery and differential pressure for test #16. The nanofluid flooding was paused overnight after 5 PV and resumed for 5 PV more after shut-in. No oil was produced during the nanofluid flooding. The little bit of oil produced during the increased rate (nanofluid flooding) was after 2.25 PV.

	Recovery factor, RF (% OOIP)				
	Water flooding		Nanofluid flooding		Total
$Q_{inj} =$	0.3 ml/min	3.0 ml/min	0.3 ml/min	3.0 ml/min	
	53.8	1.0	0	0.1	54.9

Residual oil saturation, S_{or}			Capillary number, N_c			
Water flooding	Nanofluid flooding		Water flooding		Nanofluid flooding	
		$Q_{inj} =$	0.3 ml/min	3.0 ml/min	0.3 ml/min	3.0 ml/min
0.30	0.30		2.58×10^{-6}	2.58×10^{-5}	2.73×10^{-6}	2.73×10^{-5}

Test #17

Nanoparticle	Concentration	Oleic phase	Temperature	Aging
Nsp_3c	0.025 wt%	Crude oil	20° C	None

Core plug length (cm)	Porosity (%)	Permeability (mD)	Pore volume (ml)	S_{wi}
4.5	17.5	300	9.0	0.36

Oil recovery (% OOIP)

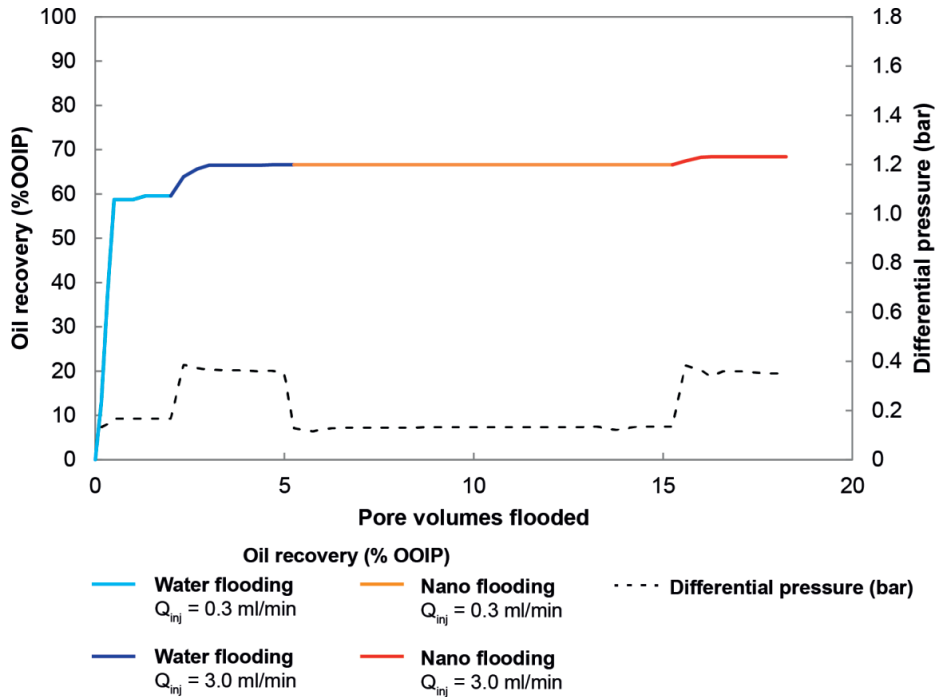| Water flooding Q_{inj} = 0.3 ml/min	Nano flooding Q_{inj} = 0.3 ml/min	- - - - Differential pressure (bar)
Water flooding Q_{inj} = 3.0 ml/min	Nano flooding Q_{inj} = 3.0 ml/min	

Figure F.5. Oil recovery and differential pressure for test #17. Nanofluid flooding was continuous, and no oil was produced. The oil produced during the rate increase was produced right away (at the beginning, within the first 1 PV).

	Recovery factor, RF (% OOIP)				
	Water flooding		Nanofluid flooding		Total
Q_{inj} =	0.3 ml/min	3.0 ml/min	0.3 ml/min	3.0 ml/min	
	59.6	7.0	0.0	1.8	68.4

Residual oil saturation, S_{or}			Capillary number, N_c			
Water flooding	Nanofluid flooding		Water flooding		Nanofluid flooding	
		Q_{inj} =	0.3 ml/min	3.0 ml/min	0.3 ml/min	3.0 ml/min
0.22	0.20		2.62×10^{-6}	2.62×10^{-5}	2.77×10^{-6}	2.77×10^{-5}

Test #18

Nanoparticle	Concentration	Oleic phase	Temperature	Aging
Nsp_3c	0.01 wt%	Crude oil	20° C	None

Core plug length (cm)	Porosity (%)	Permeability (mD)	Pore volume (ml)	S_{wi}
4.5	17.2	264	8.5	0.34

Oil recovery (% OOIP)

Water flooding Q_{inj} = 0.3 ml/min	**Nano flooding** Q_{inj} = 0.3 ml/min	···· **Differential pressure (bar)**
Water flooding Q_{inj} = 3.0 ml/min	**Nano flooding** Q_{inj} = 3.0 ml/min	
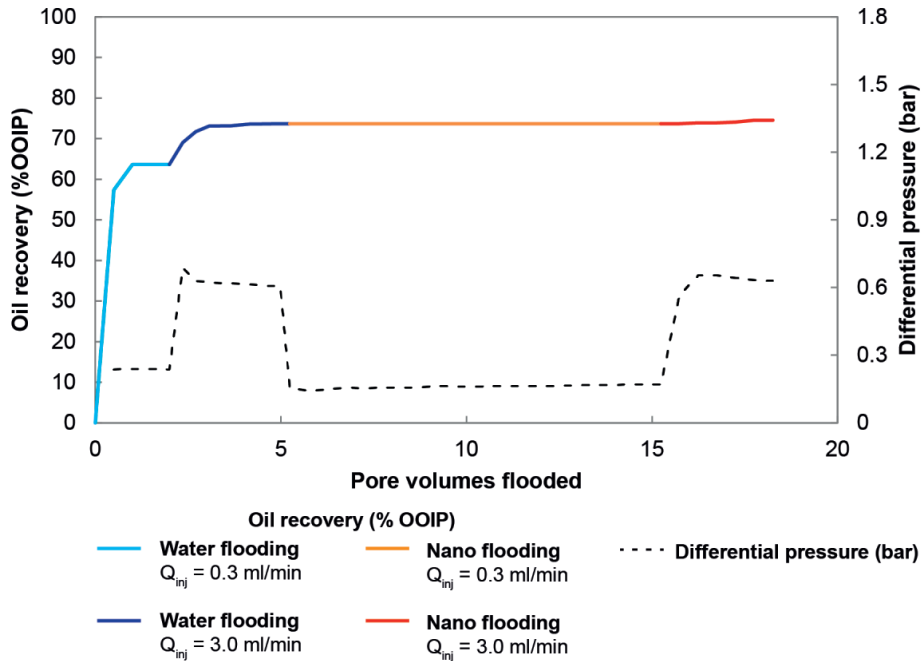
Figure F.6. Oil recovery and differential pressure for test #18. No oil was produced during the 10 PV of nanofluid flooding. The little bit of oil produced when the rate was increased was not immediate; there was some production at 1 PV and then the rest at 2 PV. Nevertheless, total oil production from nanofluid flooding was less than 1% OOIP.

	Recovery factor, RF (% OOIP)				
	Water flooding		**Nanofluid flooding**		**Total**
Q_{inj} =	**0.3 ml/min**	**3.0 ml/min**	**0.3 ml/min**	**3.0 ml/min**	
	63.7	10.0	0.0	0.8	74.5

Residual oil saturation, S_{or}			Capillary number, N_c			
Water flooding	**Nanofluid flooding**		**Water flooding**		**Nanofluid flooding**	
		Q_{inj} =	**0.3 ml/min**	**3.0 ml/min**	**0.3 ml/min**	**3.0 ml/min**
0.17	0.17		2.68×10^{-6}	2.68×10^{-5}	2.82×10^{-6}	2.82×10^{-5}

Test #19

Nanoparticle	Concentration	Oleic phase	Temperature	Aging
Nsp_3c	0.05 wt%	Crude oil	20° C	None

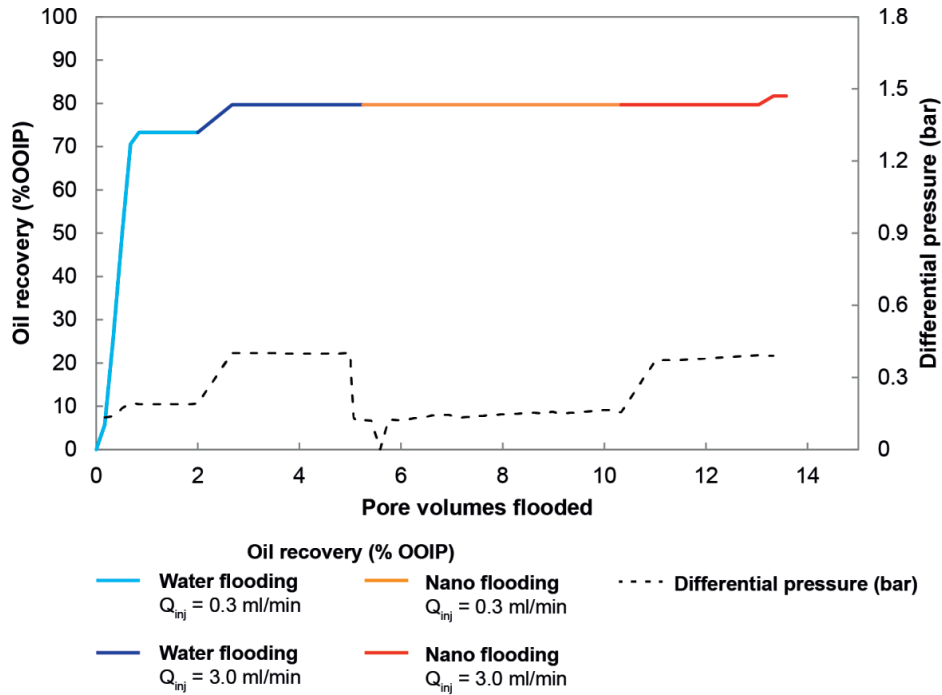| Core plug length (cm)	Porosity (%)	Permeability (mD)	Pore volume (ml)	S_{wi}
4.5	17.3	364	8.9	0.38

Figure F.7. Oil recovery and differential pressure for test #19. Nanofluid flooding was for 5 PV instead of 10 PV. No oil was produced. The little bit of oil produced during rate increase was at the very end (close to 3 PV).

	Recovery factor, RF (% OOIP)				
	Water flooding		Nanofluid flooding		Total
Q_{inj} =	0.3 ml/min	3.0 ml/min	0.3 ml/min	3.0 ml/min	
	73.3	6.4	0.0	2.1	81.8

Residual oil saturation, S_{or}			Capillary number, N_c			
Water flooding	Nanofluid flooding		Water flooding		Nanofluid flooding	
		Q_{inj} =	0.3 ml/min	3.0 ml/min	0.3 ml/min	3.0 ml/min
0.13	0.11		2.67×10^{-6}	2.67×10^{-5}	2.81×10^{-6}	2.81×10^{-5}

Test #20

Nanoparticle	Concentration	Oleic phase	Temperature	Aging
Nsp_3c	0.10 wt%	Crude oil	20° C	None

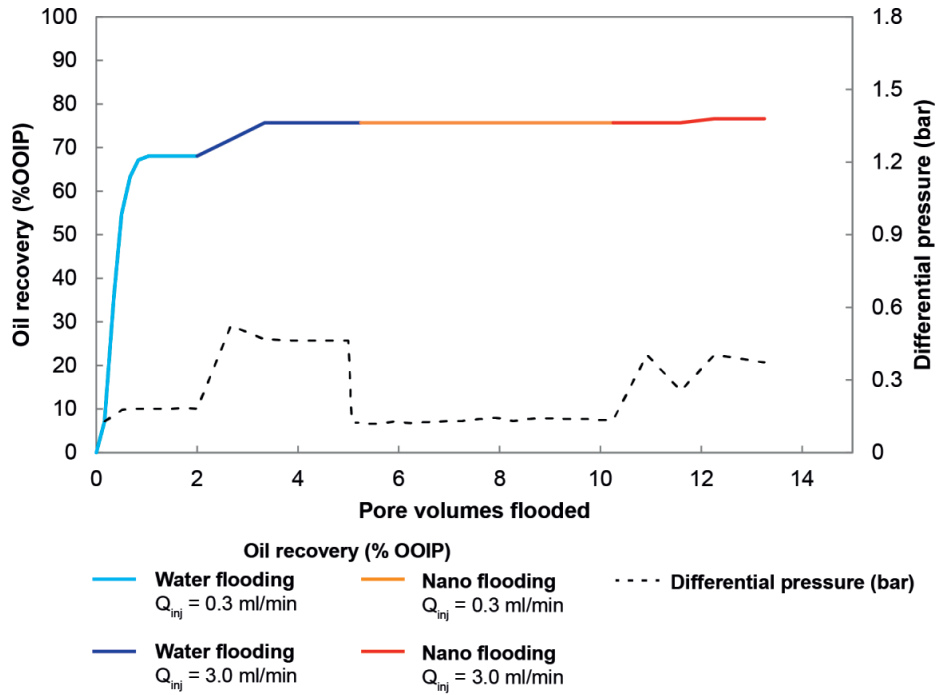| Core plug length (cm)	Porosity (%)	Permeability (mD)	Pore volume (ml)	S_{wi}
4.5	17.7	304	9.0	0.41

Figure F.8. Oil recovery and differential pressure for test #20. The nanofluid flooding was also only conducted for 5 PV instead of 10 PV here, and no oil was produced. The bit of oil produced during the high rate was at 2 PV, and it represented less than 1% OOIP.

	Recovery factor, RF (% OOIP)				
	Water flooding		Nanofluid flooding		Total
Q_{inj} =	0.3 ml/min	3.0 ml/min	0.3 ml/min	3.0 ml/min	
	68.1	7.6	0.0	1.0	76.7

Residual oil saturation, S_{or}			Capillary number, N_c			
Water flooding	Nanofluid flooding		Water flooding		Nanofluid flooding	
		Q_{inj} =	0.3 ml/min	3.0 ml/min	0.3 ml/min	3.0 ml/min
0.14	0.14		2.60×10^{-6}	2.60×10^{-5}	2.75×10^{-6}	2.75×10^{-5}

Test #21

Nanoparticle	Concentration	Oleic phase	Temperature	Aging
Nsp_3d	0.05 wt%	Crude oil	20° C	None

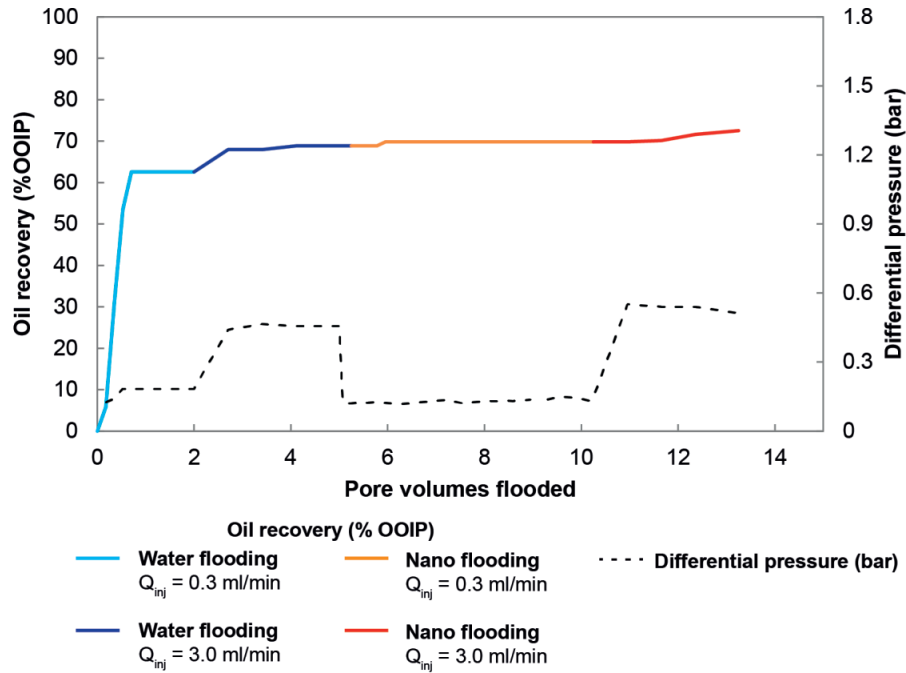| Core plug length (cm)	Porosity (%)	Permeability (mD)	Pore volume (ml)	S_{wi}
4.5	17.3	353	8.5	0.35

Figure F.9. Oil recovery and differential pressure for test #21. Some oil (0.9% OOIP) was produced after 0.5 PV. No more oil was produced until the nanofluid flooding rate increase, and that oil came after 1 PV. A total of 2.7% OOIP was produced from the increased rate nanofluid flooding.

	Recovery factor, RF (% OOIP)				
	Water flooding		Nanofluid flooding		Total
$Q_{inj} =$	0.3 ml/min	3.0 ml/min	0.3 ml/min	3.0 ml/min	
	62.6	6.3	0.0	2.7	71.6

Residual oil saturation, S_{or}			Capillary number, N_c			
Water flooding	Nanofluid flooding		Water flooding		Nanofluid flooding	
		$Q_{inj} =$	0.3 ml/min	3.0 ml/min	0.3 ml/min	3.0 ml/min
0.20	0.18		2.66×10^{-6}	2.66×10^{-5}	2.64×10^{-6}	2.64×10^{-5}

Test #22

Nanoparticle	Concentration	Oleic phase	Temperature	Aging
Nsp_3c	0.05 wt%	Crude oil	20° C	11.5 weeks at 60° C

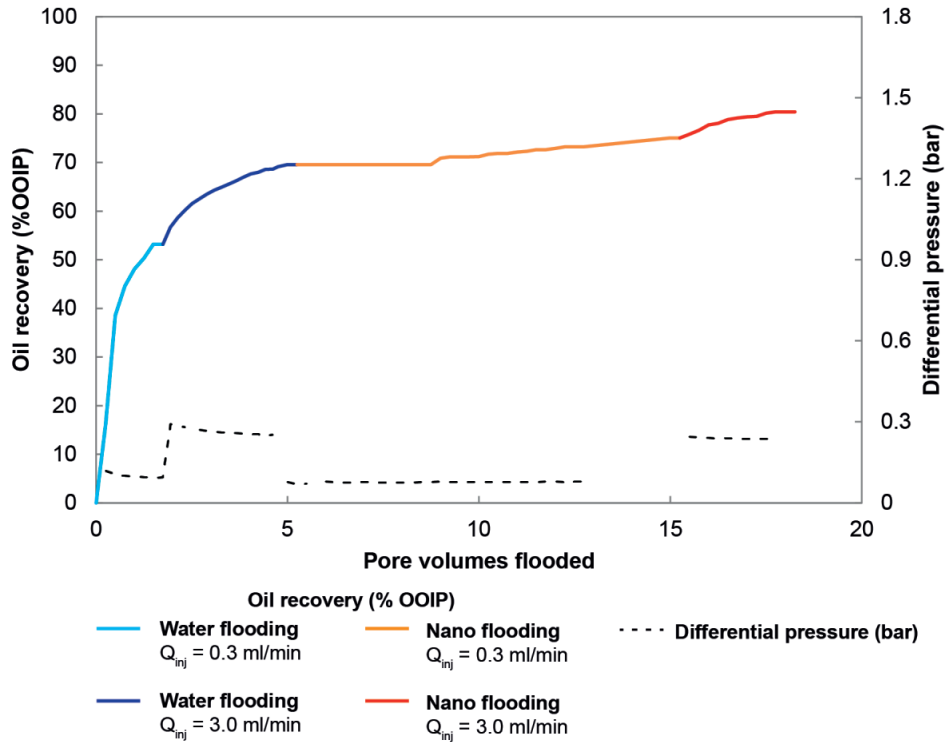| Core plug length (cm)	Porosity (%)	Permeability (mD)	Pore volume (ml)	S_{wi}
10.0	13.8	382	15.7	0

Figure F.10. Oil recovery and differential pressure for test #22. Oil production began after 3.75 PV, with intermittent production occurring throughout the remainder of nanofluid flooding. Additional recovery was achieved after the inejciton rate bump, and it produced steadily throughout most of the rate bump.

	Recovery factor, RF (% OOIP)				
	Water flooding		Nanofluid flooding		Total
Q_{inj} =	0.3 ml/min	3.0 ml/min	0.3 ml/min	3.0 ml/min	
	53.2	16.4	5.4	5.4	80.4

Residual oil saturation, S_{or}			Capillary number, N_c			
Water flooding	Nanofluid flooding		Water flooding		Nanofluid flooding	
		Q_{inj} =	0.3 ml/min	3.0 ml/min	0.3 ml/min	3.0 ml/min
0.30	0.20		3.32×10^{-6}	3.32×10^{-5}	3.51×10^{-6}	3.51×10^{-5}

Test #23

Nanoparticle	Concentration	Oleic phase	Temperature	Aging
Nsp_3c	0.05 wt%	Crude oil	20° C	10.5 weeks at 60° C

Core plug length (cm)	Porosity (%)	Permeability (mD)	Pore volume (ml)	S_{wi}
10.0	14.9	357	17.0	0

Oil recovery (% OOIP)

- **Water flooding** Q_{inj} = 0.3 ml/min
- **Water flooding** Q_{inj} = 3.0 ml/min
- **Nano flooding** Q_{inj} = 0.3 ml/min
- **Nano flooding** Q_{inj} = 3.0 ml/min
- - - - **Differential pressure (bar)**
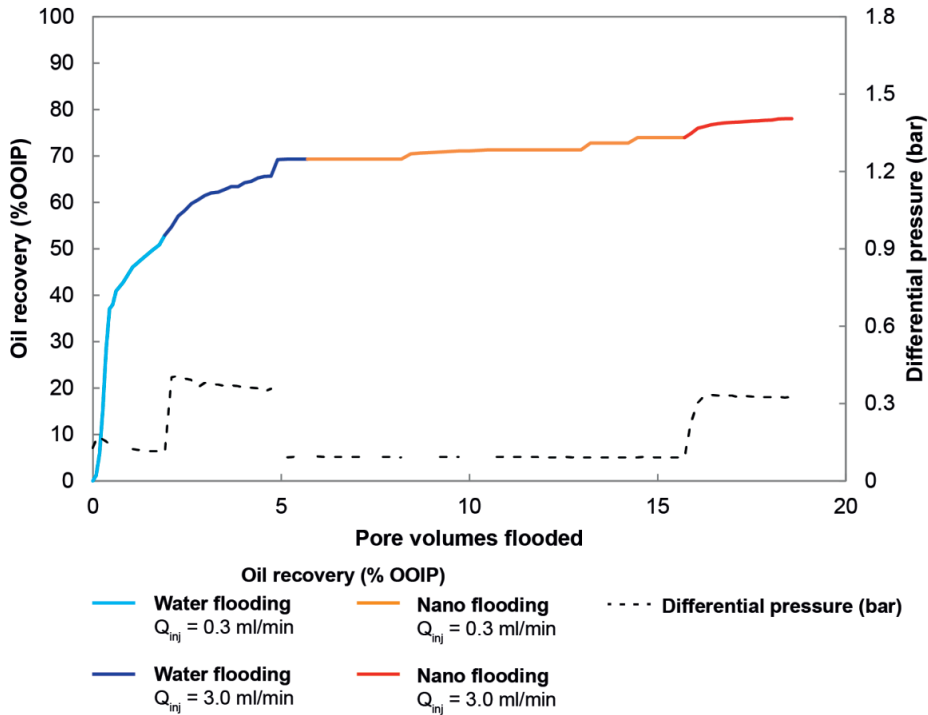
Figure F.11. Oil recovery and differential pressure for test #23. The nanofluid flooding was stopped after 5 PV for an overnight shut-in period. About 2% OOIP was produced before shut-in, with the oil bank starting at about 2.75 PV after nanofluid flooding. An additional 2.5% OOIP was produced during the remaining 5 PV after the shut-in. This oil was primarily from oil slugs at 2.5 and 3.75 PV after shut-in. The injection rate increase brought an additional 4% OOIP.

	Recovery factor, RF (% OOIP)				
	Water flooding		Nanofluid flooding		Total
Q_{inj} =	0.3 ml/min	3.0 ml/min	0.3 ml/min	3.0 ml/min	
	52.9	16.3	4.7	4.1	78.0

Residual oil saturation, S_{or}			Capillary number, N_c			
Water flooding	Nanofluid flooding		Water flooding		Nanofluid flooding	
		Q_{inj} =	0.3 ml/min	3.0 ml/min	0.3 ml/min	3.0 ml/min
0.31	0.22		3.10×10^{-6}	3.10×10^{-5}	3.27×10^{-6}	3.27×10^{-5}

Appendix G: Part 4 core flooding tests – Testing with aged cores and elevated temperature

Table G.1. Overview of Part 4 core flooding tests in Appendix G.

| Test # | Nanofluid | | | Oleic phase | Temp. (°C) | Aging |
	Type	Surface modification	Conc. (wt%)			
24	Nsp_3c	PEG	0.05	Crude oil	60	No
25	Nsp_3d	Epoxy	0.05	Crude oil	60	No
26	Nsp_3a	-	0.05	Crude oil	60	4 weeks at 60°C
27						
28	Nsp_3c	PEG	0.01	Crude oil	60	4 weeks at 60°C
29	Nsp_3c	PEG	0.05	Crude oil	60	4 weeks at 60°C
30						
31	Nsp_3c	PEG	0.15	Crude oil	60	4 weeks at 60°C
32						
33						
34	Nsp_3d	Epoxy	0.05	Crude oil	60	4 weeks at 60°C
35						

Single test
Duplicate test
Triplicate tests

Figure G.1. Core flooding injection scheme for Part 4 tests. This does not show the relative permeability test injection scheme run after water flooding and after nanofluid flooding. There are also some exceptions to the injection scheme. See the detailed procedure in Section 5.4 for more information.

Test #24

Nanoparticle	Concentration	Oleic phase	Temperature	Aging
Nsp_3c	0.05 wt%	Crude oil	60° C	None

Core plug length (cm)	Porosity (%)	Permeability (mD)	Pore volume (ml)	S_{wi}
10.0	17.7	339	20.2	0.47

Oil recovery (% OOIP)

| Water flooding Q_{inj} = 0.3 ml/min	Nano flooding Q_{inj} = 0.3 ml/min	---- Differential pressure (bar)
Water flooding Q_{inj} = 3.0 ml/min	Nano flooding Q_{inj} = 3.0 ml/min	
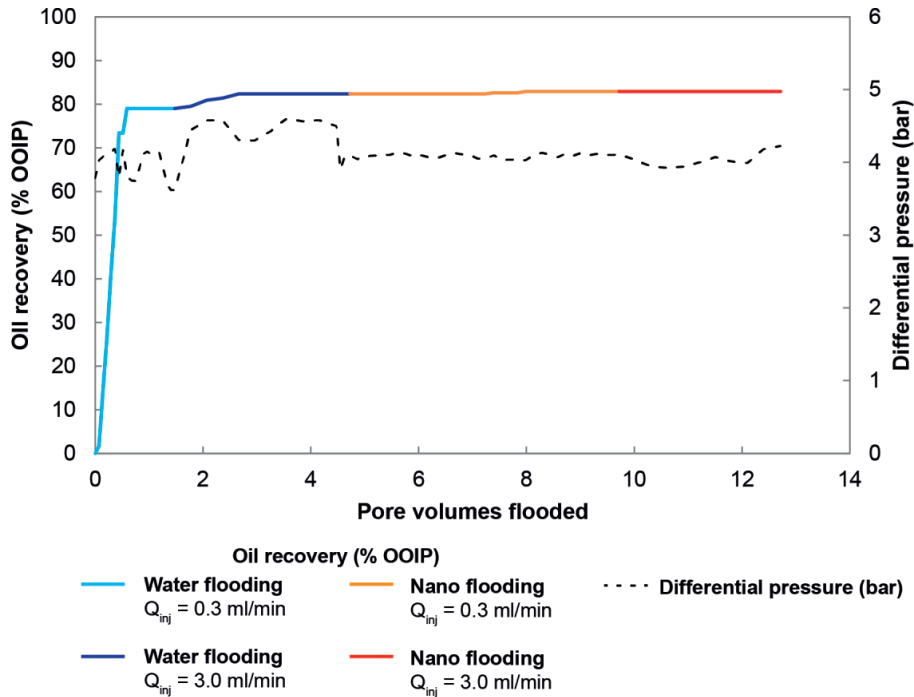
Figure G.2. Oil recovery and differential pressure for test #24. The first occurrence of oil production during nanofluid flooding occurred after 2.5 PV, and it represented less than 0.3% OOIP. More oil was produced about 0.5 PV later, resulting in the final nanofluid flooding recovery factor of 0.57% OOIP for the low rate injection. No oil was produced when the injection rate was increased.

Residual oil saturation, S_{or}			Recovery factor, RF (% OOIP)				
Water flooding	Nanofluid flooding		Water flooding		Nanofluid flooding		Total
		Q_{inj} =	0.3 ml/min	3.0 ml/min	0.3 ml/min	3.0 ml/min	
0.09	0.09		79.0	3.3	0.6	0.0	82.9

Test #25

Nanoparticle	Concentration	Oleic phase	Temperature	Aging
Nsp_3d	0.05 wt%	Crude oil	60° C	None

Core plug length (cm)	Porosity (%)	Permeability (mD)	Pore volume (ml)	S_{wi}
10.0	17.2	632	20.2	0.36
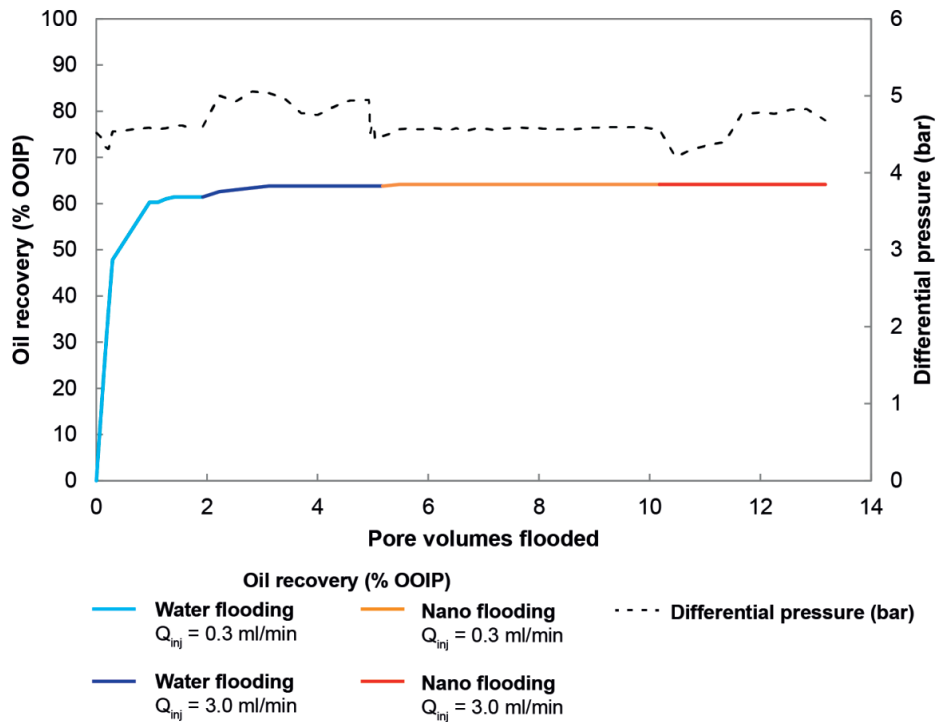
Figure G.3. Oil recovery and differential pressure for test #25. The first occurrence of oil production during nanofluid flooding occurred right after nanofluid flooding was initiated, but it represented less than 0.4% OOIP. No more oil was produced during either the remainder of the low rate injection or high rate injection for nanofluid flooding.

Residual oil saturation, S_{or}			Recovery factor, RF (% OOIP)				
Water flooding	Nanofluid flooding		Water flooding		Nanofluid flooding		Total
		$Q_{inj} =$	0.3 ml/min	3.0 ml/min	0.3 ml/min	3.0 ml/min	
0.23	0.23		61.4	2.3	0.4	0.0	64.1

Test #26

Nanoparticle	Concentration	Oleic phase	Temperature	Aging
Nsp_3a	0.05 wt%	Crude oil	60° C	4 weeks at 60° C

Core plug length (cm)	Porosity (%)	Permeability (mD)	Pore volume (ml)	S_{wi}
10.0	19.3	393	22.3	0
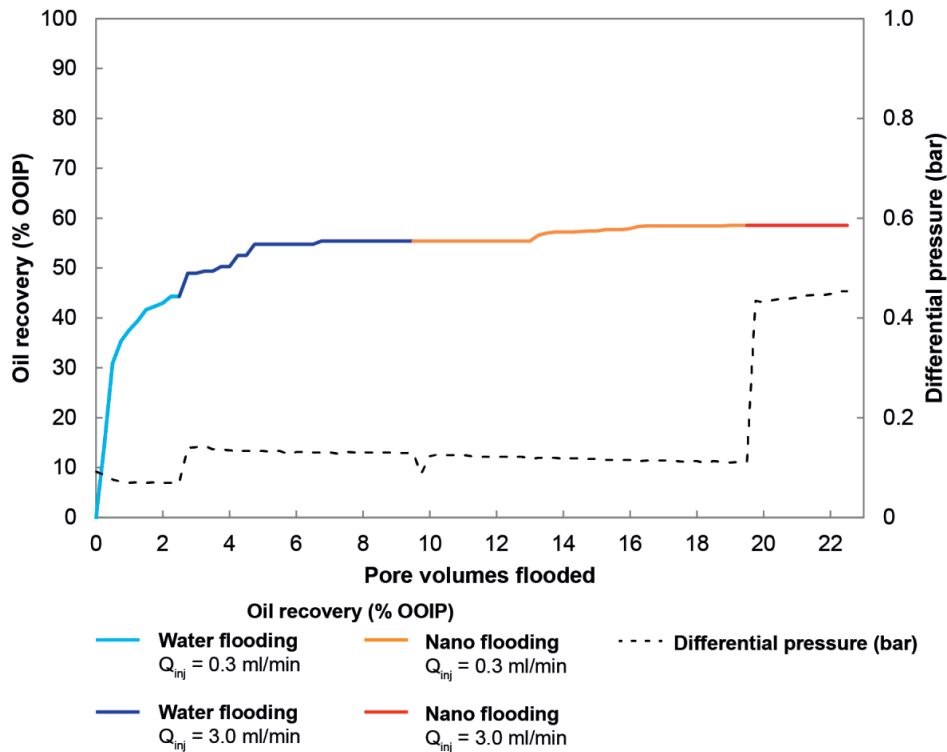
Figure G.4. Oil recovery and differential pressure for test #26. The first occurrence of oil production during nanofluid flooding occurred after 3 PV. Sporadic production occurred throughout the remainder of the nanofluid flooding at the low rate, resulting in a total recovery of 3.11% OOIP. No oil was produced when the injection rate was increased.

Residual oil saturation, S_{or}			Recovery factor, RF (% OOIP)				
Water flooding	Nanofluid flooding	Q_{inj} =	Water flooding		Nanofluid flooding		Total
			0.3 ml/min	3.0 ml/min	0.3 ml/min	3.0 ml/min	
0.48	0.41		44.3	11.1	3.1	0.0	58.5
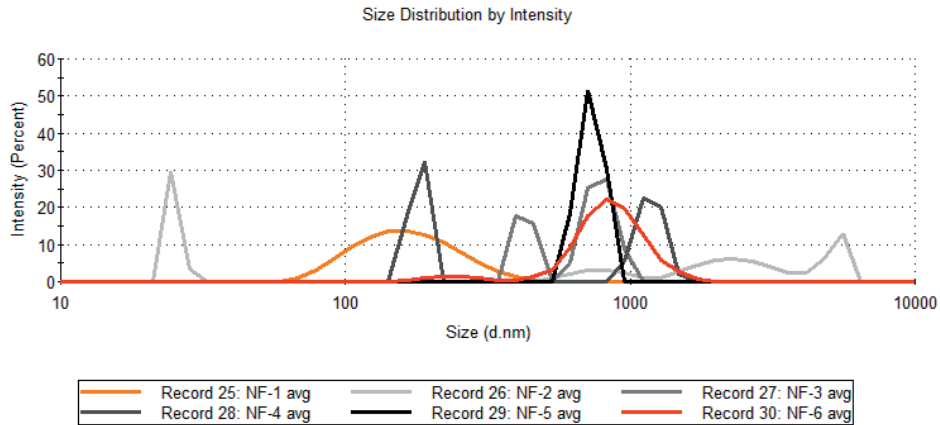
Figure G.5. Test #26 revealed that the nanoparticles aggregate in the reservoir throughout the duration of the test (NF-1 < NF-6). The particle size distributions from the core effluent exhibit a lot of scatter and erroneous results.

NF-1 = Nanofluid influent particle size distribution.

NF-2 = Effluent sample taken at the end of the nanofluid flooding at the low injection rate (0.3 ml/min). It was collected during from the effluent emerging during 9.5 to 10 PV of nanofluid flooding.

NF-3 = Effluent sample taken at the end of the high injection rate (3 ml/min) during the last half pore volume (from 2.5 to 3 PV flooding).

NF-4 = Effluent sample taken during the relative permeability flooding and collected during the 10 minutes when the injection rate was 1.0 ml/min.

NF-5 = Effluent sample taken immediately after NF-4, when the injection rate was 0.5 ml/min for 10 min.

NF-6 = Sample taken from the outlet of the nanofluid reservoir after the test was completed to see what the particle size distribution was before the nanofluid entered the core plug.

Test #27

Nanoparticle	Concentration	Oleic phase	Temperature	Aging
Nsp_3a	0.05 wt%	Crude oil	60° C	4 weeks at 60° C

Core plug length (cm)	Porosity (%)	Permeability (mD)	Pore volume (ml)	S_{wi}
10.0	20.7	389	22.6	0
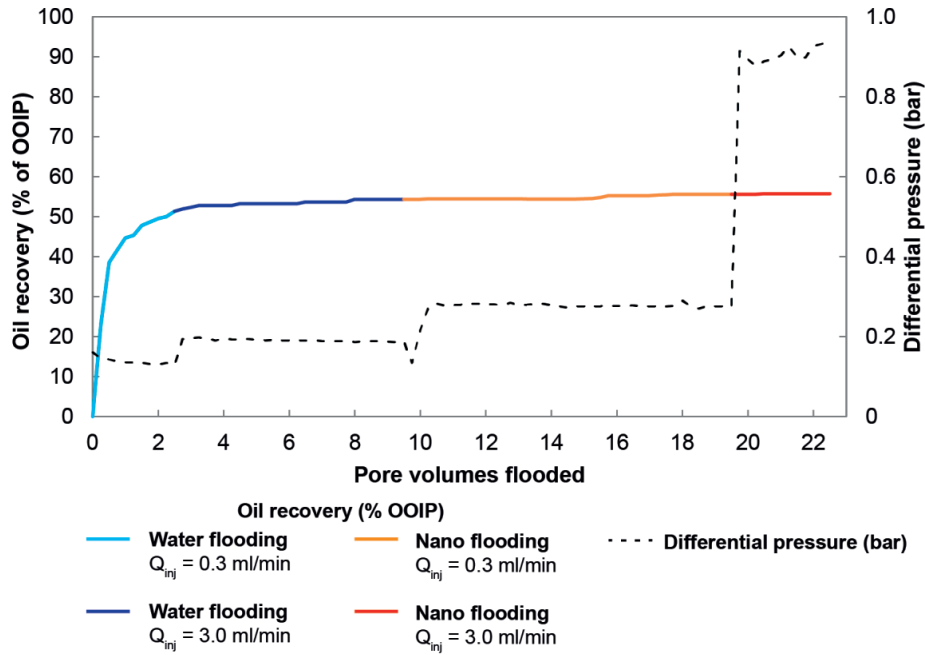
Figure G.6. Oil recovery and differential pressure for test #27. After 0.5 PV of nanofluid flooding, 0.1% OOIP was produced. But the primary oil bank occurred around 5.75 PV. The total recovery factor for low rate nanofluid flooding was 1.25% OOIP. An additiona 0.15 wt% was produced after the injection rate was increased.

Residual oil saturation, S_{or}			Recovery factor, RF (% OOIP)				
Water flooding	Nano flooding		Water flooding		Nanofluid flooding		Total
		Q_{inj} =	0.3 ml/min	3.0 ml/min	0.3 ml/min	3.0 ml/min	
0.48	0.44		51.3	3.0	1.3	0.2	55.8

Test #28

Nanoparticle	Concentration	Oleic phase	Temperature	Aging
Nsp_3c	0.01 wt%	Crude oil	60° C	4 weeks at 60° C

| Core plug length (cm)	Porosity (%)	Permeability (mD)	Pore volume (ml)	S_{wi}
10.0	20.6	319	22.6	0

Figure G.7. Oil recovery and differential pressure for test #28. The first occurrence of oil production during nanofluid flooding occurred between 1.75 and 2 PV, but it produced only 0.02 wt%. The main oil bank was produced around 7.5 PV, resulting in a total recovery of 1.78% OOIP. A negligible amount (0.08 wt%) was produced when the injection rate was increased.

| Residual oil saturation, S_{or}			Recovery factor, RF (% OOIP)				
Water flooding	Nanofluid flooding		Water flooding		Nanofluid flooding		Total
		Q_{inj} =	0.3 ml/min	3.0 ml/min	0.3 ml/min	3.0 ml/min	
0.51	0.49		41.9	7.1	1.8	0.1	50.9
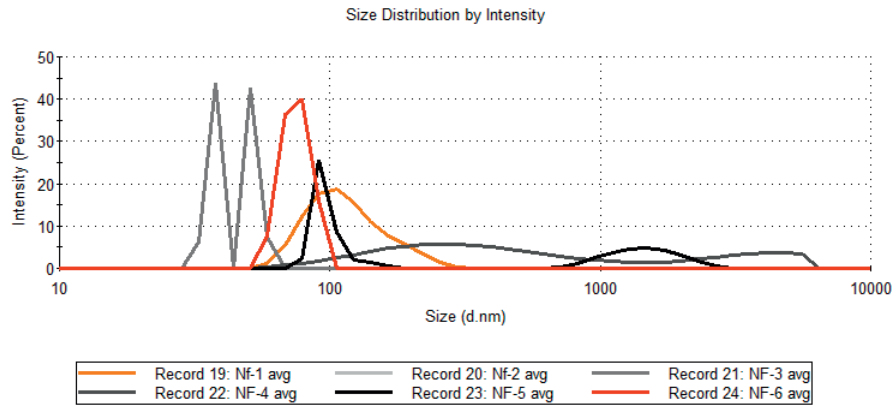
Figure G.8. Test #28 revealed that the composition of the nanofluid did not substantially change throughout the duration of the test (NF-1 ≈ NF-6). However, large particles are detected at the end of nanofluid flooding (NF-4 and NF-5).

NF-1 = Nanofluid influent particle size distribution.

NF-2 = Effluent sample taken at the end of the nanofluid flooding at the low injection rate (0.3 ml/min). It was collected during from the effluent emerging during 9.5 to 10 PV of nanofluid flooding.

NF-3 = Effluent sample taken at the end of the high injection rate (3 ml/min) during the last half pore volume (from 2.5 to 3 PV flooding).

NF-4 = Effluent sample taken during the relative permeability flooding and collected during the 10 minutes when the injection rate was 1.0 ml/min.

NF-5 = Effluent sample taken immediately after NF-4, when the injection rate was 0.5 ml/min for 10 min.

NF-6 = Sample taken from the outlet of the nanofluid reservoir after the test was completed to see what the particle size distribution was before the nanofluid entered the core plug.

Test #29

Nanoparticle	Concentration	Oleic phase	Temperature	Aging
Nsp_3c	0.05 wt%	Crude oil	60° C	4 weeks at 60° C

Core plug length (cm)	Porosity (%)	Permeability (mD)	Pore volume (ml)	S_{wi}
10.0	18.0	279	22.6	0
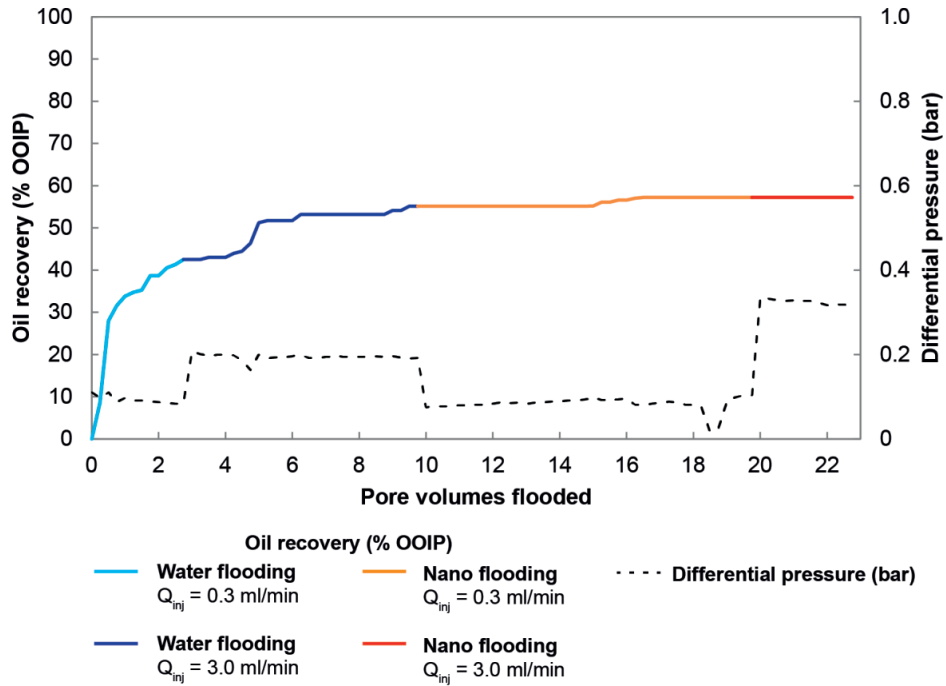
Figure G.9. Oil recovery and differential pressure for test #29. The first occurrence of oil production during nanofluid flooding occurred between 5 to 5.25 PV (0.1 wt%) with production occurring over the next 1.5 PV. The total recovery factor from the nanofluid flooding at low rate was 2.14%. No oil was produced when the injection rate was increased.

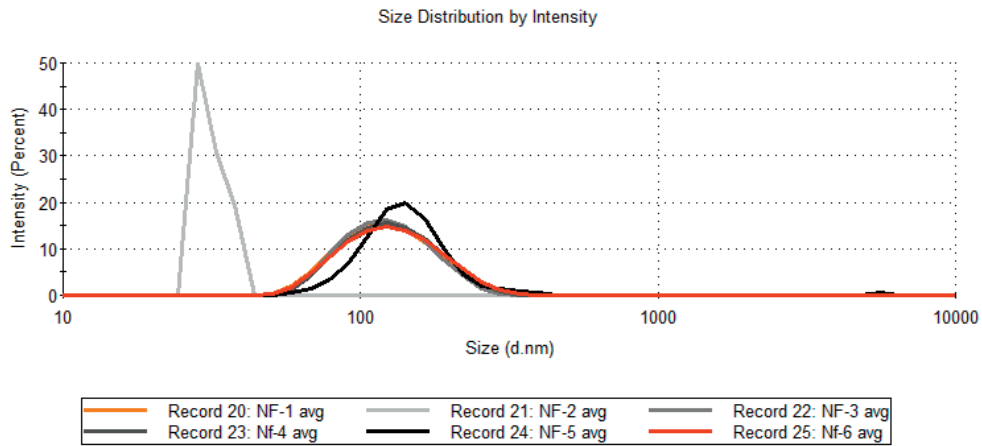| Residual oil saturation, S_{or}			Recovery factor, RF (% OOIP)				
Water flooding	Nanofluid flooding		Water flooding		Nanofluid flooding		Total
		Q_{inj} =	0.3 ml/min	3.0 ml/min	0.3 ml/min	3.0 ml/min	
0.45	0.43		42.5	12.6	2.1	0.0	57.2
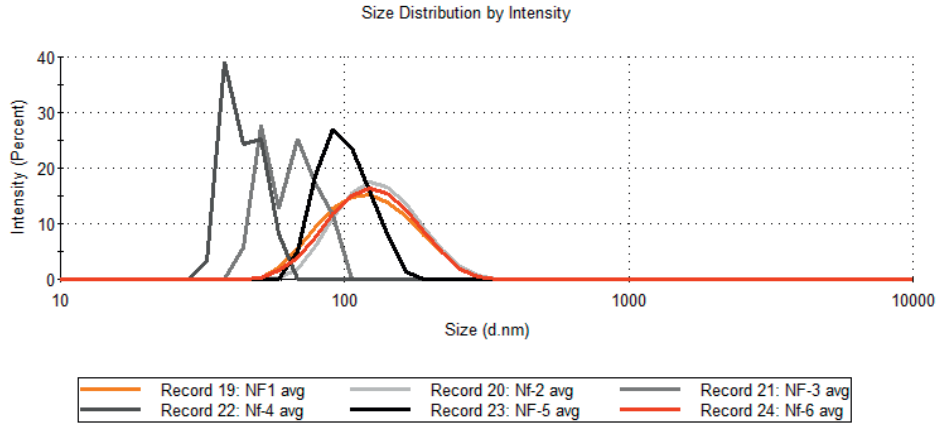
Figure G.10. Test #29 revealed that the composition of the nanofluid did not change throughout the duration of the test (NF-1 = NF-6). It appears that smaller nanoparticles are the ones propagating through the core for NF-3 through NF-5.

NF-1 = Nanofluid influent particle size distribution.

NF-2 = Effluent sample taken at the end of the nanofluid flooding at the low injection rate (0.3 ml/min). It was collected during from the effluent emerging during 9.5 to 10 PV of nanofluid flooding.

NF-3 = Effluent sample taken at the end of the high injection rate (3 ml/min) during the last half pore volume (from 2.5 to 3 PV flooding).

NF-4 = Effluent sample taken during the relative permeability flooding and collected during the 10 minutes when the injection rate was 1.0 ml/min.

NF-5 = Effluent sample taken immediately after NF-4, when the injection rate was 0.5 ml/min for 10 min.

NF-6 = Sample taken from the outlet of the nanofluid reservoir after the test was completed to see what the particle size distribution was before the nanofluid entered the core plug.

Test #30

Nanoparticle	Concentration	Oleic phase	Temperature	Aging
Nsp_3c	0.05 wt%	Crude oil	60° C	4 weeks at 60° C

Core plug length (cm)	Porosity (%)	Permeability (mD)	Pore volume (ml)	S_{wi}
10.0	20.2	301	22.1	0

Oil recovery (% OOIP)

— Water flooding Q_{inj} = 0.3 ml/min   — Nano flooding Q_{inj} = 0.3 ml/min   - - - - Differential pressure (bar)

— Water flooding Q_{inj} = 3.0 ml/min   — Nano flooding Q_{inj} = 3.0 ml/min
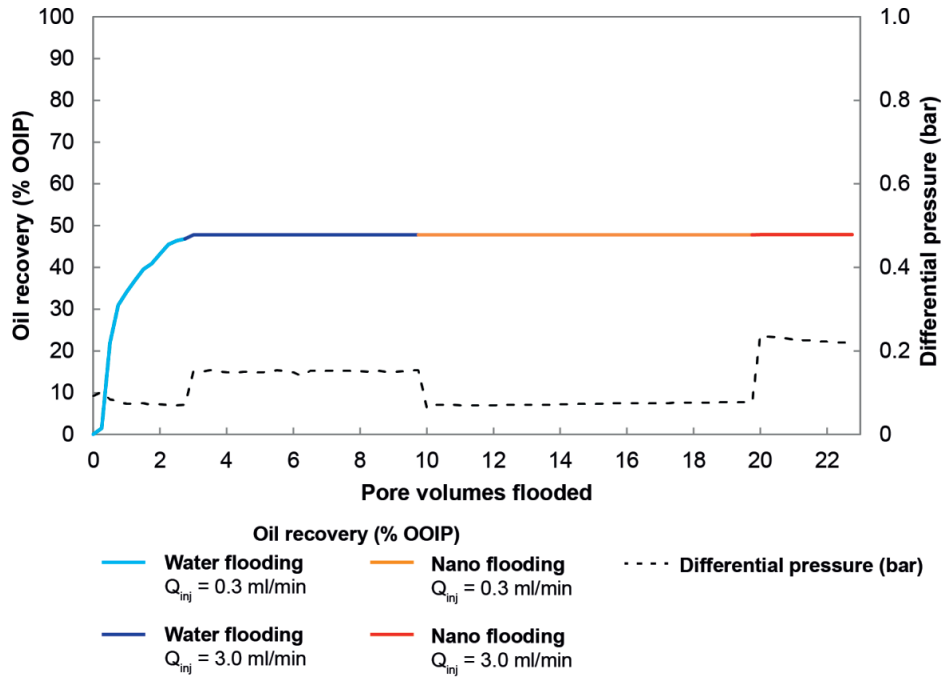
Figure G.11. Oil recovery and differential pressure for test #30. No oil was produced during the nanofluid flooding at the low injection rate. A negligible amount of oil (0.09% OOIP) was produced right away when the injection rate was increased.

| Residual oil saturation, S_{or}			Recovery factor, RF (% OOIP)				
Water flooding	Nanofluid flooding		Water flooding		Nanofluid flooding		Total
		Q_{inj} =	0.3 ml/min	3.0 ml/min	0.3 ml/min	3.0 ml/min	
0.52	0.52		46.8	0.9	0.0	0.1	47.8

Figure G.12. Test #30 revealed that the composition of the nanofluid did not change throughout the duration of the test (NF-1 = NF-6). It appears that smaller nanoparticles are the ones propagating through the core for NF-2. Otherwise, the nanoparticles propagated throughout the core while retaining their particle size distribution.

NF-1 = Nanofluid influent particle size distribution.

NF-2 = Effluent sample taken at the end of the nanofluid flooding at the low injection rate (0.3 ml/min). It was collected during from the effluent emerging during 9.5 to 10 PV of nanofluid flooding.

NF-3 = Effluent sample taken at the end of the high injection rate (3 ml/min) during the last half pore volume (from 2.5 to 3 PV flooding).

NF-4 = Effluent sample taken during the relative permeability flooding and collected during the 10 minutes when the injection rate was 1.0 ml/min.

NF-5 = Effluent sample taken immediately after NF-4, when the injection rate was 0.5 ml/min for 10 min.

NF-6 = Sample taken from the outlet of the nanofluid reservoir after the test was completed to see what the particle size distribution was before the nanofluid entered the core plug.

Test #31

Nanoparticle	Concentration	Oleic phase	Temperature	Aging
Nsp_3c	0.15 wt%	Crude oil	60° C	4 weeks at 60° C

| Core plug length (cm)	Porosity (%)	Permeability (mD)	Pore volume (ml)	S_{wi}
10.0	19.2	328	22.0	0
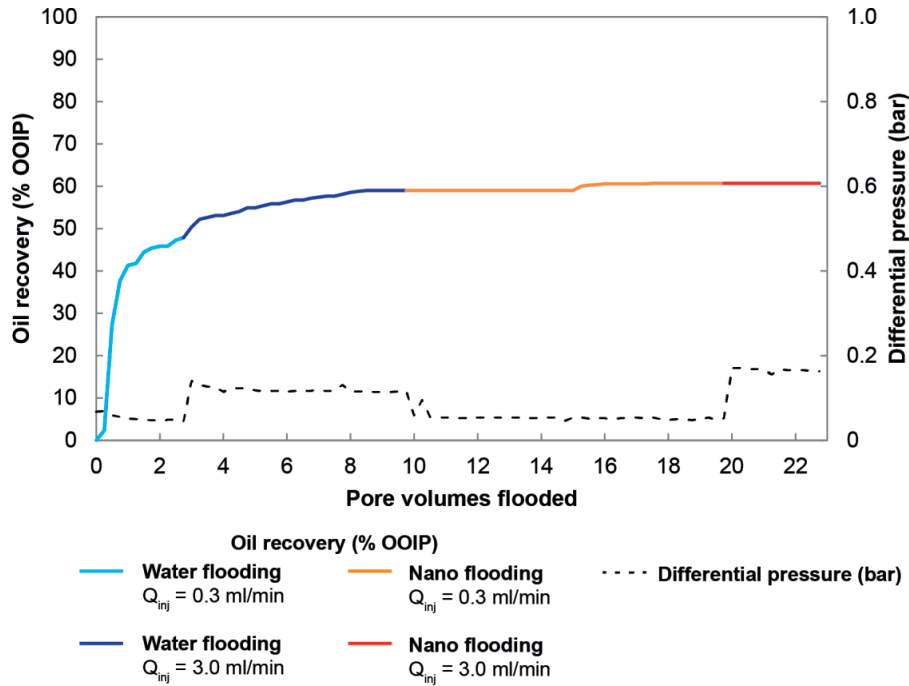
Figure G.13. Oil recovery and differential pressure for test #31. The first occurrence of oil production during nanofluid flooding occurred between 5.25 and 5.5 PV, with production occurring for a short time thereafter. The total recovery from nanofluid flooding at the low rate was 1.68%. No oil was produced when the injection rate was increased.

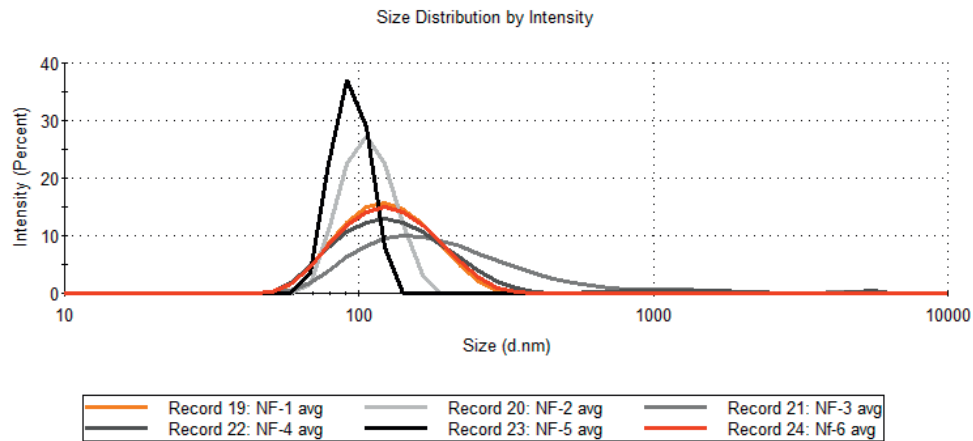| Residual oil saturation, S_{or}			Recovery factor, RF (% OOIP)				
Water flooding	Nanofluid flooding		Water flooding		Nanofluid flooding		Total
		Q_{inj} =	0.3 ml/min	3.0 ml/min	0.3 ml/min	3.0 ml/min	
0.41	0.39		47.9	11.1	1.7	0.0	60.7
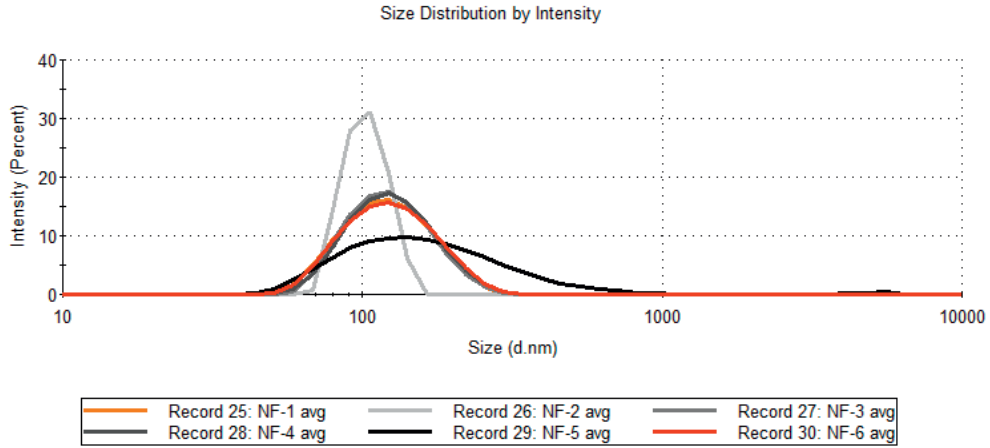
Figure G.14. Test #31 revealed that the composition of the nanofluid did not change throughout the duration of the test (NF-1 = NF-6). The nanoparticles have a more disperse particle size distribution at the end (NF-5).

NF-1 = Nanofluid influent particle size distribution.

NF-2 = Effluent sample taken at the end of the nanofluid flooding at the low injection rate (0.3 ml/min). It was collected during from the effluent emerging during 9.5 to 10 PV of nanofluid flooding.

NF-3 = Effluent sample taken at the end of the high injection rate (3 ml/min) during the last half pore volume (from 2.5 to 3 PV flooding).

NF-4 = Effluent sample taken during the relative permeability flooding and collected during the 10 minutes when the injection rate was 1.0 ml/min.

NF-5 = Effluent sample taken immediately after NF-4, when the injection rate was 0.5 ml/min for 10 min.

NF-6 = Sample taken from the outlet of the nanofluid reservoir after the test was completed to see what the particle size distribution was before the nanofluid entered the core plug.

Test #32

Nanoparticle	Concentration	Oleic phase	Temperature	Aging
Nsp_3c	0.15 wt%	Crude oil	60° C	4 weeks at 60° C

Core plug length (cm)	Porosity (%)	Permeability (mD)	Pore volume (ml)	S_{wi}
10.0	18.1	379	20.9	0
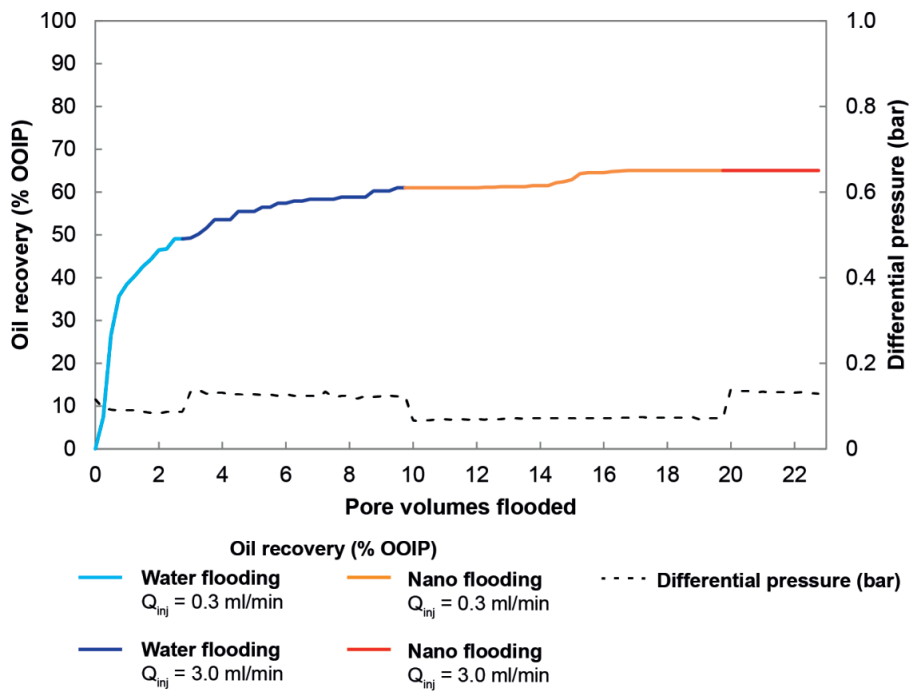
Figure G.15. Oil recovery and differential pressure for test #32. The first occurrence of oil production during nanofluid flooding occurred between 2.25 and 2.5 PV (0.14%). Sporadic production occurred throughout the next 4.5 PV, resulting in a total recovery of 4.02% OOIP. 0.04 wt% was produced immediately after the injection rate was increased.

| Residual oil saturation, S_{or}			Recovery factor, RF (% OOIP)				
Water flooding	Nanofluid flooding	Q_{inj} =	Water flooding		Nanofluid flooding		Total
			0.3 ml/min	3.0 ml/min	0.3 ml/min	3.0 ml/min	
0.39	0.35		49.1	11.9	4.0	0.0	65.0

Figure G.16. Test #32 revealed that the composition of the nanofluid did not change throughout the duration of the test (NF-1 = NF-6). The nanoparticles propagated throughout the core while retaining their particle size distribution.

NF-1   =   Nanofluid influent particle size distribution.

NF-2   =   Effluent sample taken at the end of the nanofluid flooding at the low injection rate (0.3 ml/min). It was collected during from the effluent emerging during 9.5 to 10 PV of nanofluid flooding.

NF-3   =   Effluent sample taken at the end of the high injection rate (3 ml/min) during the last half pore volume (from 2.5 to 3 PV flooding).

NF-4   =   Effluent sample taken during the relative permeability flooding and collected during the 10 minutes when the injection rate was 1.0 ml/min.

NF-5   =   Effluent sample taken immediately after NF-4, when the injection rate was 0.5 ml/min for 10 min.

NF-6   =   Sample taken from the outlet of the nanofluid reservoir after the test was completed to see what the particle size distribution was before the nanofluid entered the core plug.

Test #33

Nanoparticle	Concentration	Oleic phase	Temperature	Aging
Nsp_3c	0.15 wt%	Crude oil	60° C	4 weeks at 60° C

Core plug length (cm)	Porosity (%)	Permeability (mD)	Pore volume (ml)	S_{wi}
10.0	20.8	466	22.5	0
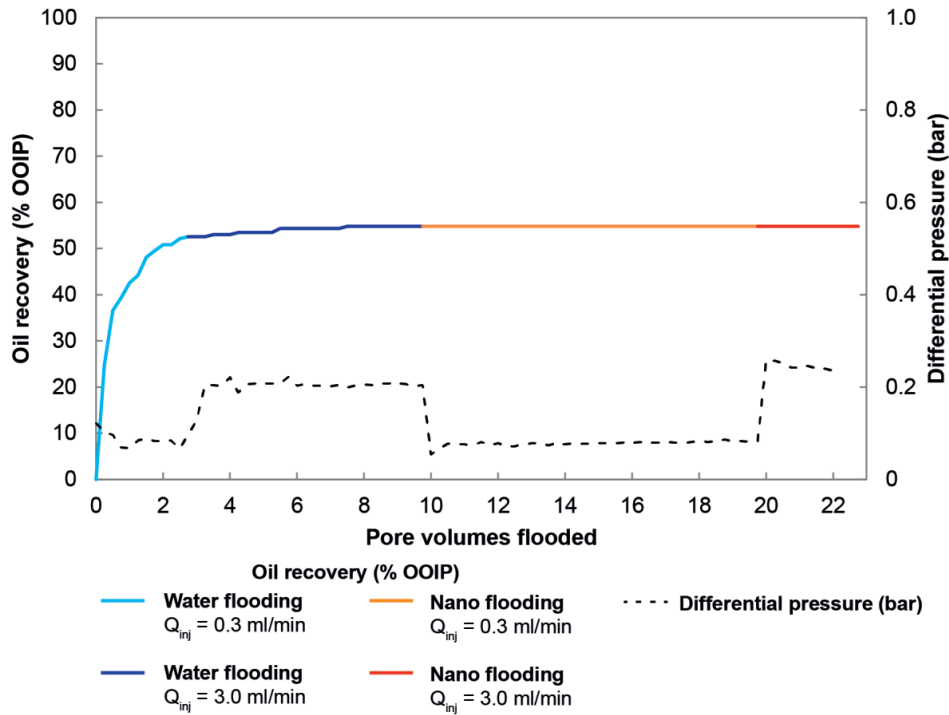
Figure G.17. Oil recovery and differential pressure for test #33. No oil was produced during nanofluid flooding.

Residual oil saturation, S_{or}			Recovery factor, RF (% OOIP)				
Water flooding	Nanofluid flooding		Water flooding		Nanofluid flooding		Total
		Q_{inj} =	0.3 ml/min	3.0 ml/min	0.3 ml/min	3.0 ml/min	
0.45	0.45		52.6	2.2	0.0	0.0	54.8
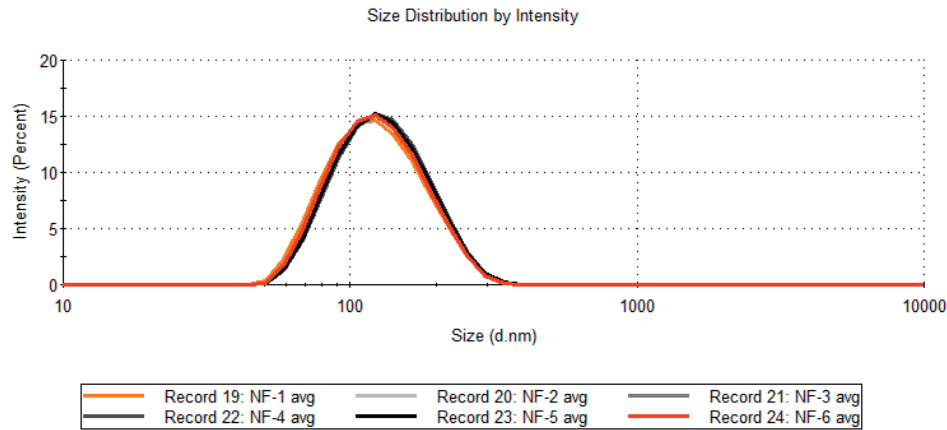
Figure G.18. Test #33 revealed that the composition of the nanofluid did not change throughout the duration of the test (NF-1 = NF-6). The nanoparticles propagated throughout the core while retaining their particle size distribution.

NF-1 = Nanofluid influent particle size distribution.

NF-2 = Effluent sample taken at the end of the nanofluid flooding at the low injection rate (0.3 ml/min). It was collected during from the effluent emerging during 9.5 to 10 PV of nanofluid flooding.

NF-3 = Effluent sample taken at the end of the high injection rate (3 ml/min) during the last half pore volume (from 2.5 to 3 PV flooding).

NF-4 = Effluent sample taken during the relative permeability flooding and collected during the 10 minutes when the injection rate was 1.0 ml/min.

NF-5 = Effluent sample taken immediately after NF-4, when the injection rate was 0.5 ml/min for 10 min.

NF-6 = Sample taken from the outlet of the nanofluid reservoir after the test was completed to see what the particle size distribution was before the nanofluid entered the core plug.

Test #34

Nanoparticle	Concentration	Oleic phase	Temperature	Aging
Nsp_3d	0.05 wt%	Crude oil	60° C	4 weeks at 60° C

Core plug length (cm)	Porosity (%)	Permeability (mD)	Pore volume (ml)	S_{wi}
10.0	18.2	270	20.9	0
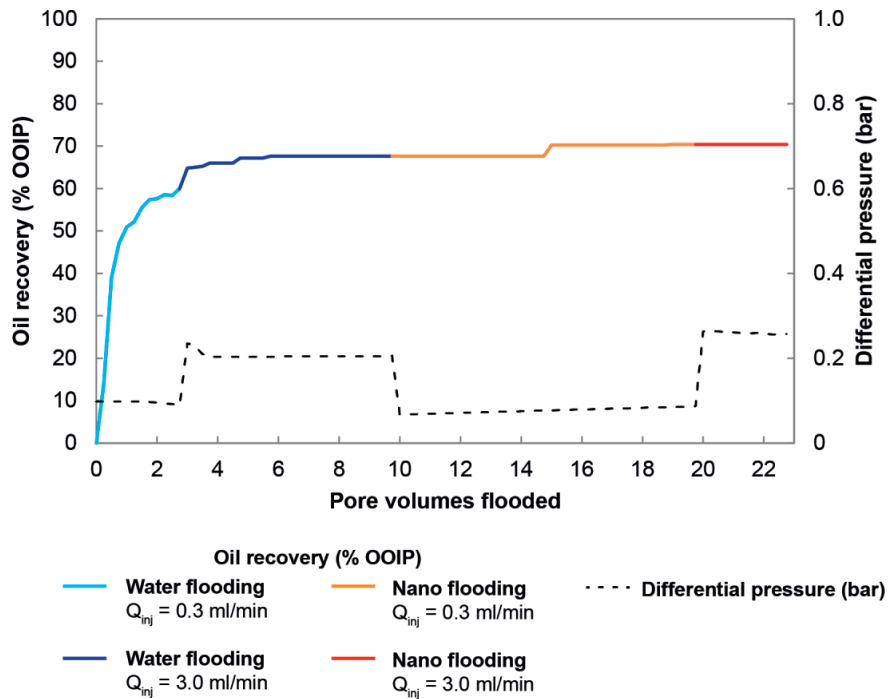
Figure G.19. Oil recovery and differential pressure for test #34. The first occurrence of oil production during nanofluid flooding occurred after 5 PV (2.65%). A bit more was produced after 9 PV, resulting in a total recovery of 2.74%. No oil was produced when the injection rate was increased.

Residual oil saturation, S_{or}			Recovery factor, RF (% OOIP)				
Water flooding	**Nanofluid flooding**	$Q_{inj}=$	**Water flooding**		**Nanofluid flooding**		**Total**
			0.3 ml/min	**3.0 ml/min**	**0.3 ml/min**	**3.0 ml/min**	
0.32	0.30		60.0	7.6	2.7	0.0	70.4
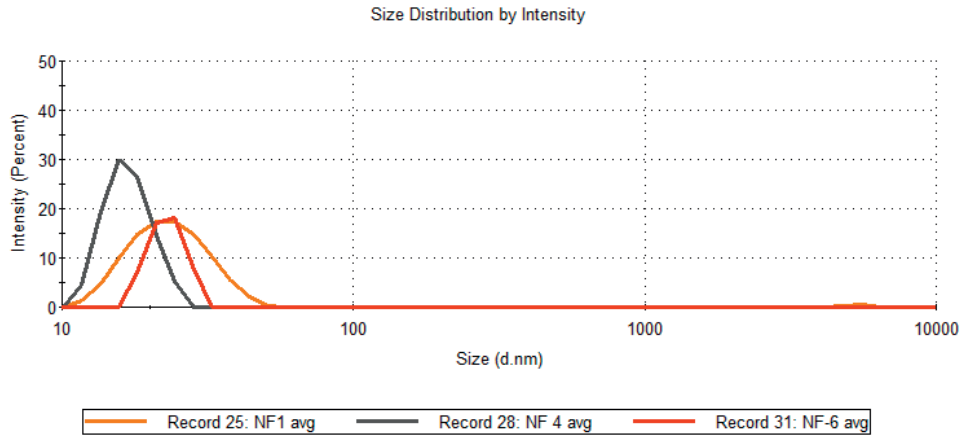
Figure G.20. Test #34 had inaccurate readings for NF-2, NF-3 and NF-5. The composition of the nanofluid did not change throughout the duration of the test (NF-1 = NF-6). Slightly smaller nanoparticles appear to be propagating through the core (NF-4).

NF-1 = Nanofluid influent particle size distribution.

NF-2 = Effluent sample taken at the end of the nanofluid flooding at the low injection rate (0.3 ml/min). It was collected during from the effluent emerging during 9.5 to 10 PV of nanofluid flooding.

NF-3 = Effluent sample taken at the end of the high injection rate (3 ml/min) during the last half pore volume (from 2.5 to 3 PV flooding).

NF-4 = Effluent sample taken during the relative permeability flooding and collected during the 10 minutes when the injection rate was 1.0 ml/min.

NF-5 = Effluent sample taken immediately after NF-4, when the injection rate was 0.5 ml/min for 10 min.

NF-6 = Sample taken from the outlet of the nanofluid reservoir after the test was completed to see what the particle size distribution was before the nanofluid entered the core plug.

Test #35

Nanoparticle	Concentration	Oleic phase	Temperature	Aging
Nsp_3d	0.05 wt%	Crude oil	60° C	4 weeks at 60° C

Core plug length (cm)	Porosity (%)	Permeability (mD)	Pore volume (ml)	S_{wi}
10.0	15.9	489	18.2	0
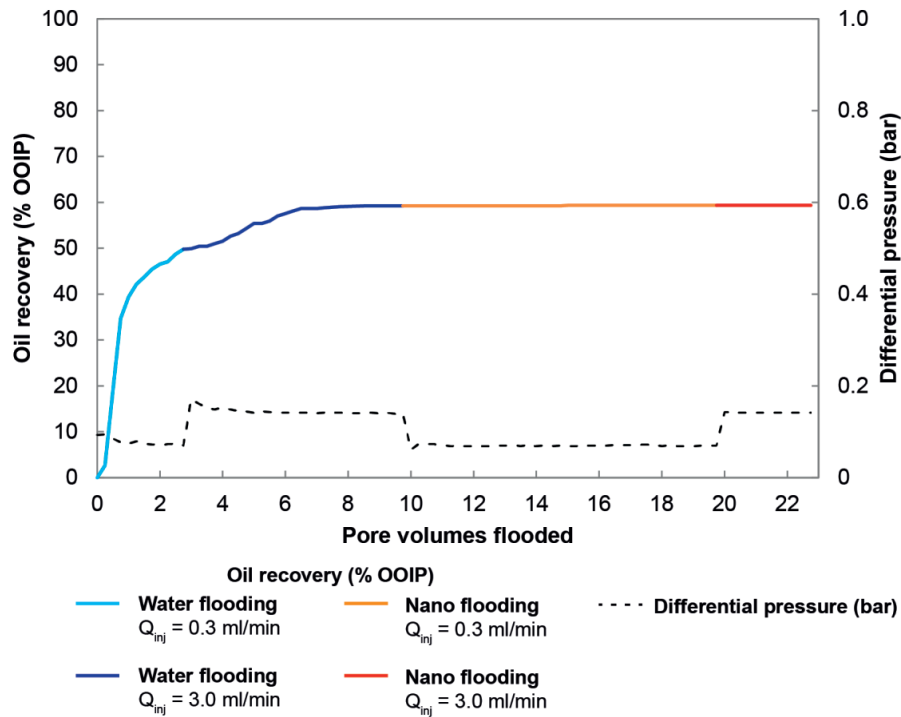
Figure G.21. Oil recovery and differential pressure for test #35. A negligible amount of oil was produced after 5 PV (0.15 wt%), with no more oil production occurring after that.

Residual oil saturation, S_{or}			Recovery factor, RF (% OOIP)				
Water flooding	Nanofluid flooding		Water flooding		Nanofluid flooding		Total
		$Q_{inj} =$	0.3 ml/min	3.0 ml/min	0.3 ml/min	3.0 ml/min	
0.41	0.41		49.8	9.4	0.1	0.0	59.3

Figure G.22. Test #35 revealed that Nsp_3d remained stable in the nanofluid flooding reservoir throughout the duration of the test, and that nanoparticles propagated throughout the core while retaining their particle size distribution.

NF-1   =   Nanofluid influent particle size distribution.

NF-2   =   Effluent sample taken at the end of the nanofluid flooding at the low injection rate (0.3 ml/min). It was collected during from the effluent emerging during 9.5 to 10 PV of nanofluid flooding.

NF-3   =   Effluent sample taken at the end of the high injection rate (3 ml/min) during the last half pore volume (from 2.5 to 3 PV flooding).

NF-4   =   Effluent   sample taken during the relative permeability flooding and collected during the 10 minutes when the injection rate was 1.0 ml/min.

NF-5   =   Effluent sample taken immediately after NF-4, when the injection rate was 0.5 ml/min for 10 min.

NF-6   =   Sample taken from the outlet of the nanofluid reservoir after the test was completed to see what the particle size distribution was before the nanofluid entered the core plug.

Appendix H: Micromodel flooding experiments

Note that the scale bars and magnification are incorrect on all the pictures. This is an artifact from the computer program used to take the pictures.

The nodes / pore walls in the glass micromodels appear as evenly-spaced white circles in the figures. Refer to Figure 3-5 and Figure 3-6 for a close-up of the pore throat geometry.

In the figures below, the crude oil in the pore space is shown in dark gray. The SSW and nanofluid are shown in white. The amount of dark gray in each figure is therefore representative of the oil saturation distribution.

Table H.1. Summary of photos from the micromodel experiments.

| Test #	Figures
36 (water-wet model)	H.1 to H.5
37 (water-wet model)	H.6 to H.10
38 (oil-wet model)	H.11 to H.15
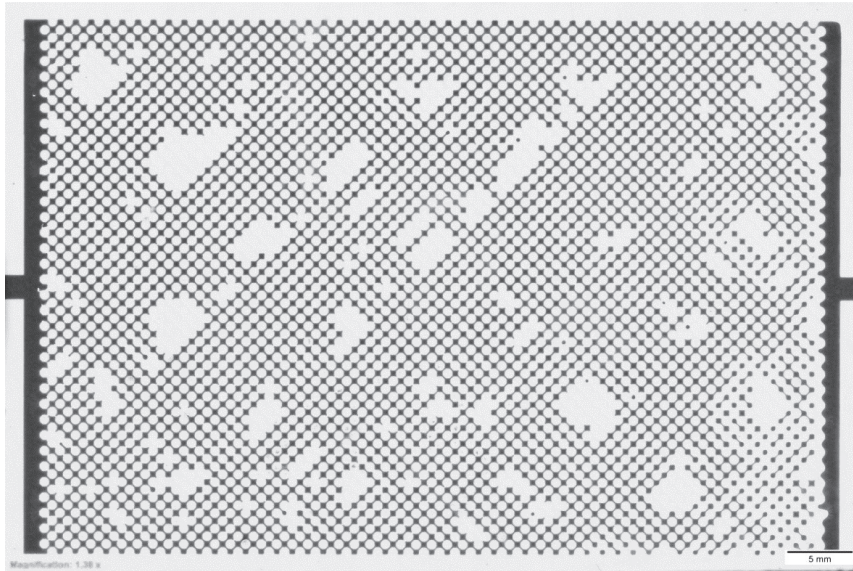
Figure H.1. Swi established after 3 PV of oil flooding. Swi is 17.4 %. Flow is from left to right.
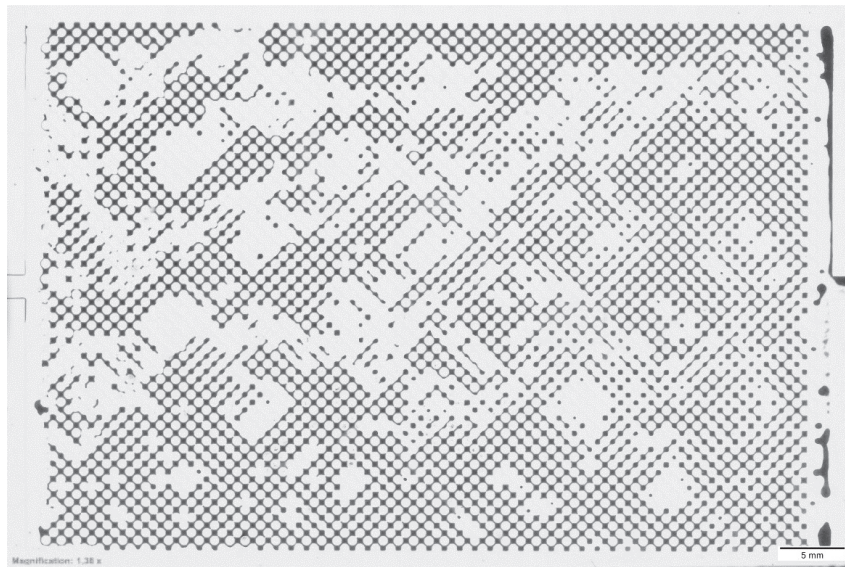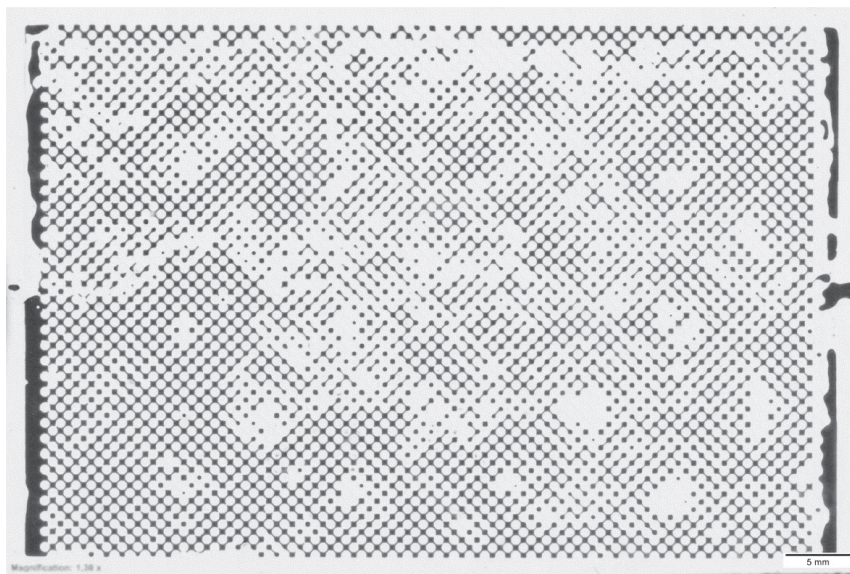

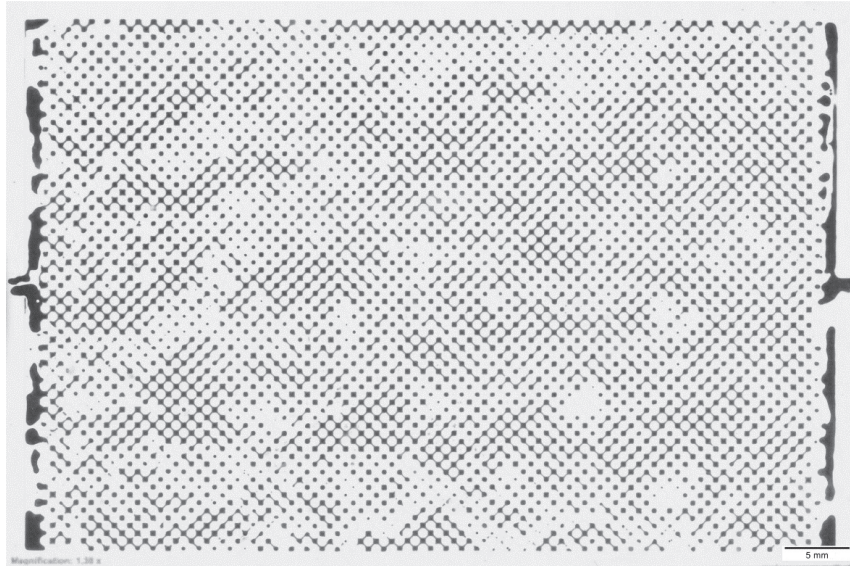**Figure H.2.** After 1 PV of water flooding at 0.0025 ml/min. Oil saturation is 62.8%.
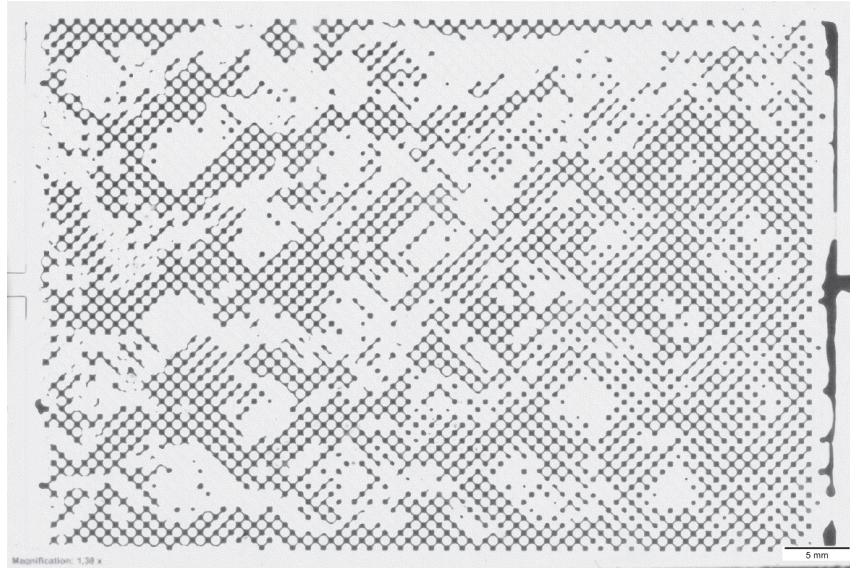
Figure H.3. Sor$_1$ after 6.5 PV of water flooding at various flow rates. Sor$_1$ is 55.8 %.
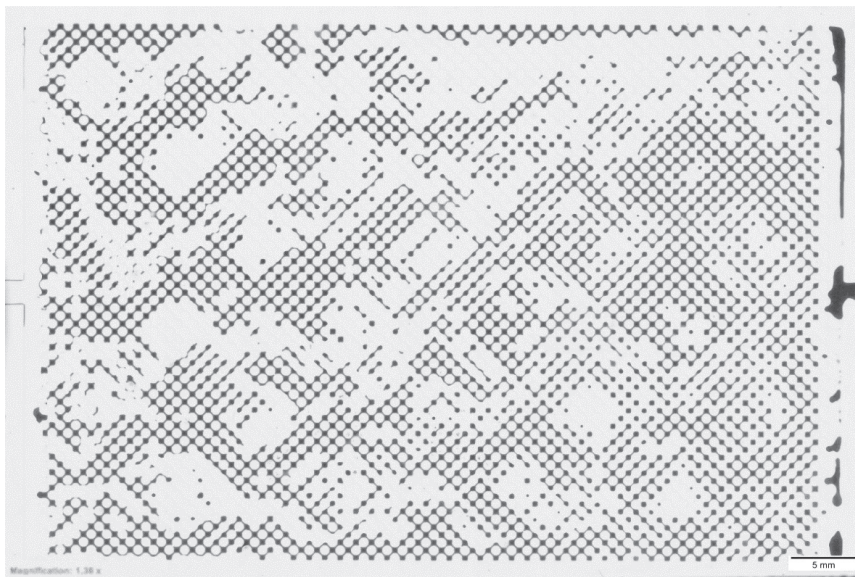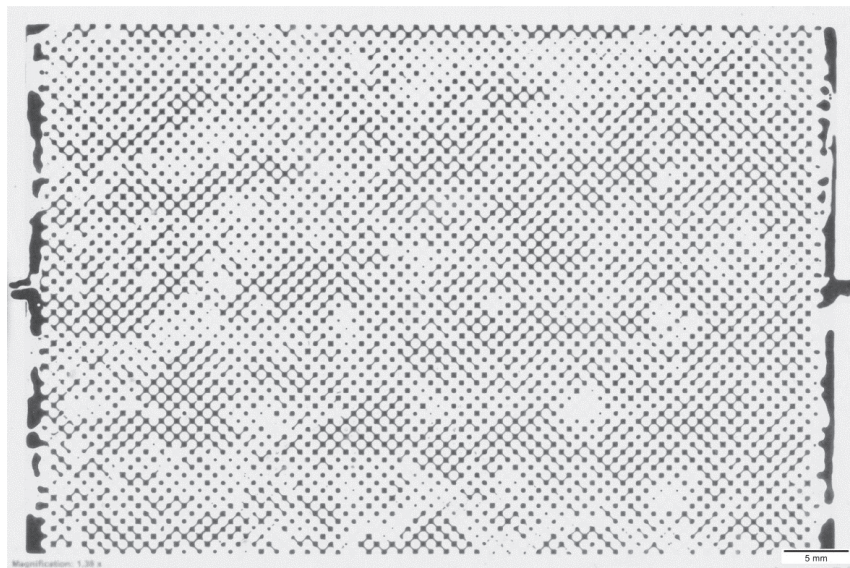

Figure H.4. After 1 PV of nanofluid flooding at 0.0025 ml/min. Oil saturation is 55.8%.
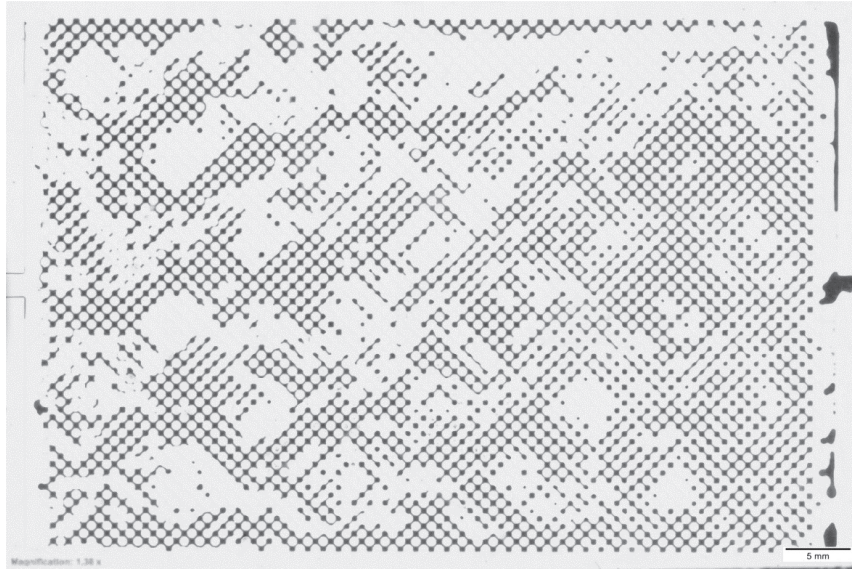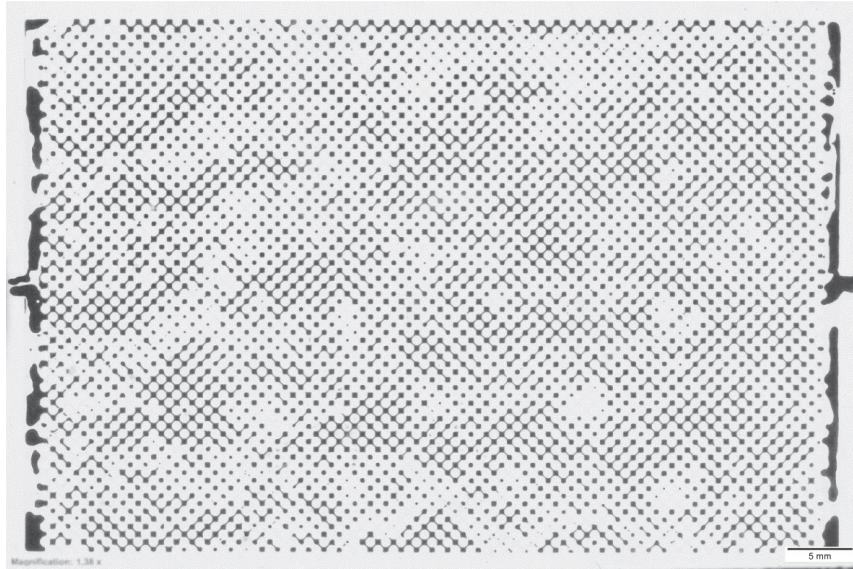
Figure H.5. Sor_2 after 4 PV of nanofluid flooding at various flow rates, including a period of over 16 hours where the nanofluid was allowed to statically react with the oil. Sor_2 is 55.8 %.
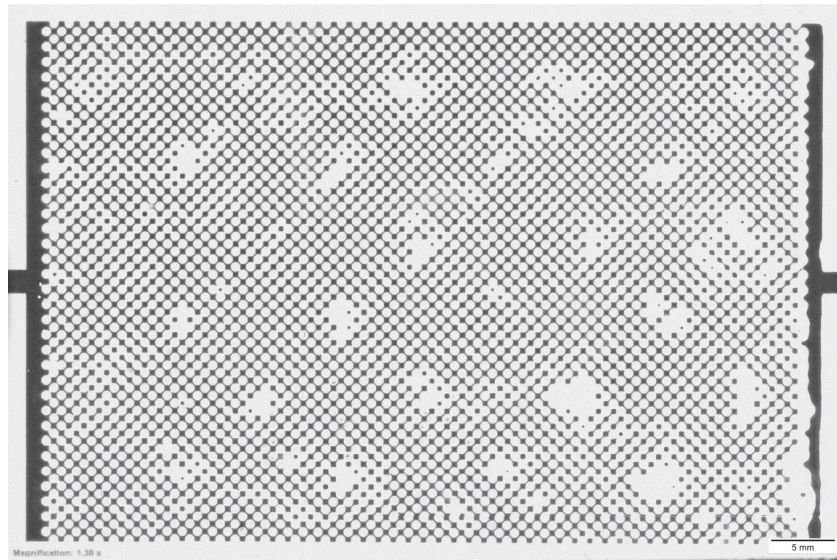
Figure H.6. Swi established after 3 PV of oil flooding. Swi is 16.0%. Flow is from left to right.

Figure H.7. After 1 PV of water flooding at 0.0025 ml/min. Oil saturation is 68.0%

Figure H.8. Sor_1 after 8.5 PV of water flooding at various flow rates. Sor_1 is 59.7%.

Figure H.9. After 1 PV of nanofluid flooding at 0.0025 ml/min. Oil saturation is 59.7%.

Figure H.10. Sor$_2$ after 10 PV of nanofluid flooding at various flow rates, including a period of over 16 hours where the nanofluid was allowed to statically react with the oil. Sor$_2$ is 59.7 %.

Figure H.11. Swi established after 3 PV of oil flooding. Swi is 38.7%. Flow is from left to right.

Figure H.12. After 1 PV of water flooding at 0.0025 ml/min. Oil saturation is 34.1%.

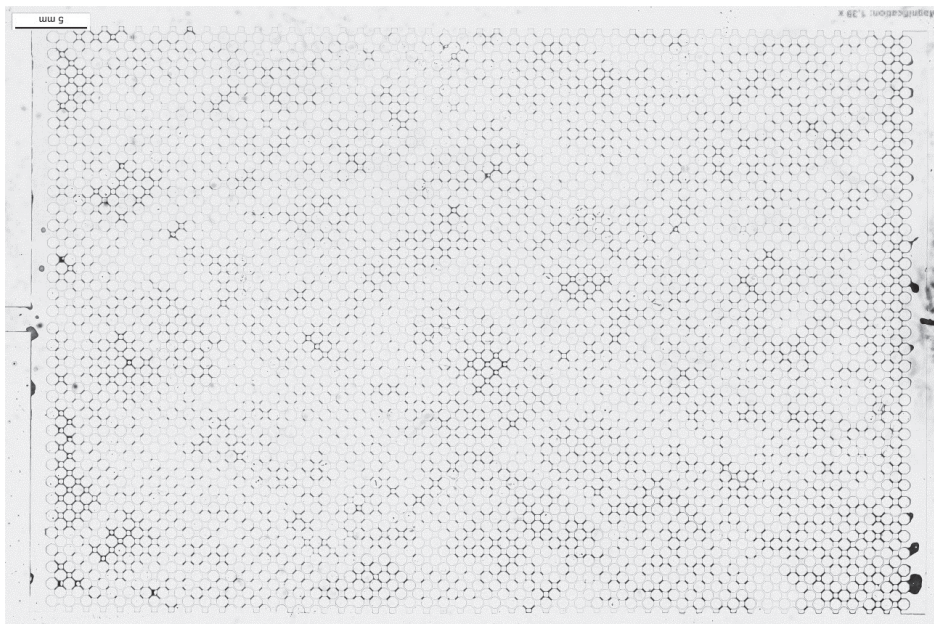**Figure H.13.** Sor$_1$ after 7.5 PV of water flooding at various flow rates. Sor$_1$ is 28.3%.

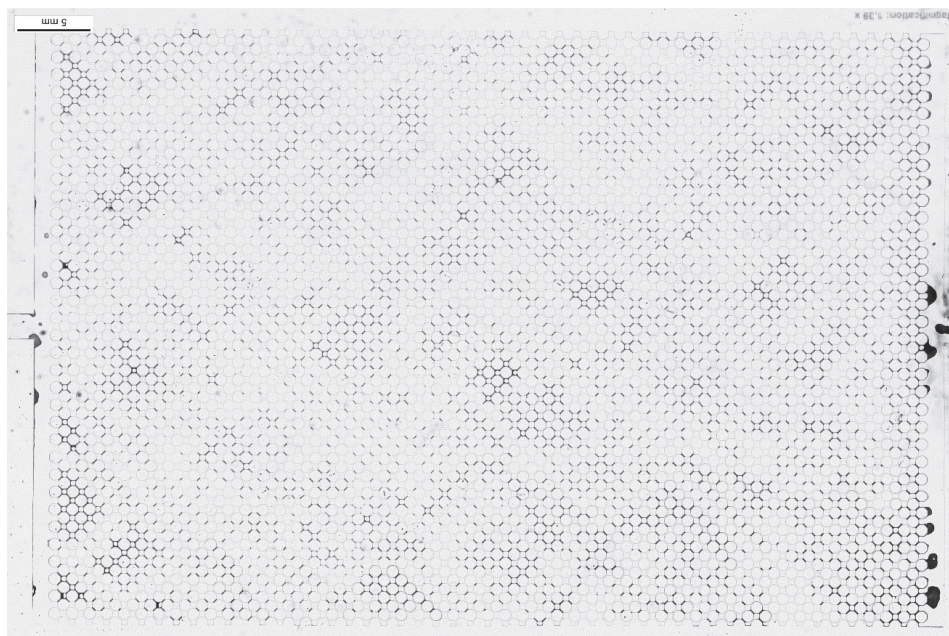**Figure H.14.** After 1 PV of nanofluid flooding at 0.0025 ml/min. Oil saturation is 28.0%.

Figure H.15. Sor$_2$ after 4.5 PV of nanofluid flooding at various flow rates. Sor$_2$ is 27.6 %.